

# University of Alberta

Geology, geochronology, thermobarometry, and tectonic evolution of the Queen Maud block, Churchill craton, Nunavut, Canada

by

Daniel B. Tersmette

A thesis submitted to the Faculty of Graduate Studies and Research  
in partial fulfillment of the requirements for the degree of

Master of Science

Department of Earth and Atmospheric Sciences

©Daniel B. Tersmette  
Spring 2012  
Edmonton, Alberta

Permission is hereby granted to the University of Alberta Libraries to reproduce single copies of this thesis and to lend or sell such copies for private, scholarly or scientific research purposes only. Where the thesis is converted to, or otherwise made available in digital form, the University of Alberta will advise potential users of the thesis of these terms.

The author reserves all other publication and other rights in association with the copyright in the thesis and, except as herein before provided, neither the thesis nor any substantial portion thereof may be printed or otherwise reproduced in any material form whatsoever without the author's prior written permission.

## **Dedication**

For Tawny

## **Abstract**

The Queen Maud block is divided into two crustal belts. The western Perry River belt is dominated by Mesoarchean to Neoproterozoic granitic gneisses and supracrustal rocks; it was incorporated into the Rae domain by at least 2.46 Ga. The eastern Paalliq belt is dominated by the 2.52-2.45 Ga Queen Maud granitoids and the 2.45-2.39 Ga Sherman supracrustal sequence, both of which were formed on Neoproterozoic crust of the Rae domain. Slave-Churchill collision and convergence occurred ca. 2.43-2.35 Ga resulting in granulite-facies metamorphism, regional scale N-S trending strike-slip shearing, and minor crustal melting in the Queen Maud block. Post-collisional magmatism occurred ca. 2.32 Ga. Between 2.3 and 2.1 Ga mafic magmatism and monazite growth occurred in the western Queen Maud block, possibly as a result of continental rifting. The 2.01-1.91 Ga Thelon Orogeny affects only the western-most Queen Maud block, where 1.93 Ga metamorphism and very weak deformation are preserved.

## Acknowledgements

Funding for this thesis was provided by the Polar Continental Shelf Project and an NSERC discovery grant to Dr. Tom Chacko. The University of Alberta funded the author through a teaching assistantship.

There are many people to thank for their support in preparing this thesis. My supervisor, Tom Chacko, deserves huge thanks for his ceaseless enthusiasm, constructive feedback, and constant support over the last two years. I would also like to thank Tom for simply allowing me to be part of such an exciting project. It is not every Master's student who has the opportunity to participate in such thrilling, discovery-style research as was provided by the Queen Maud block. I also thank Larry Heaman, not only for his efforts as a member of my supervisory committee but also for discussions throughout the course of the research and for assistance with zircon grain mount preparation. Thank you to Claire Currie for her review of this thesis as the external examiner on the supervisory committee.

Field work was greatly aided by the staff at The Arctic Islands Lodge in Cambridge Bay; in particular, Jane Cunningham, who unknowingly became our field manager. I would also like to thank our trustworthy helicopter pilot, Guy Fisher for ensuring our safety during field activities. Rameses D'Souza, Mark Labbe, and David Pirie all assisted in thin-section preparation and rock crushing. Zircon separation and grain mount preparation were made possible with the assistance of Barry Herchuck, Judy Schultz, and Angus Duncan. Thank you also to Sergei Matveev and De-Ann Rollings for their assistance with microprobe analysis and BSE imaging. A thank you to Rob Creasar for his work on the Sm-Nd isotopic analyses (also thank you to Tom for not making me write an additional chapter when these data became available in December, 2011). Without the assistance of Andy DuFrane, the U-Pb dating conducted for this study would not have been possible; I offer Andy a sincere thank you for his assistance during our many long days on the laser.

Behind the scenes there are many more people to thank. I would like to thank Benoit Beauchamp, Dave Pattison, and Jerry Osborn from the University of Calgary. Though they may not know, their teaching and enthusiasm inspired me to further my education at the University of Alberta. My family, who have supported me and acted as a sounding board over the last two years, helped me to maintain my sanity. My fiancée, who somehow did not get tired of hearing about the Queen Maud block and who stuck with me while I lived away from home, deserves the greatest thanks.



# Table of Contents

Title

Dedication

Abstract

Acknowledgements

Table of Contents

List of Tables

List of Figures

List of Abbreviations

<b>CHAPTER 1 – Introduction .....</b>	<b>1</b>
<b>1.1 – Objectives.....</b>	<b>2</b>
<b>1.2 – Geology of the Churchill Province.....</b>	<b>3</b>
<b>1.3 – The Queen Maud block .....</b>	<b>5</b>
<i>1.3.1 – Defining the Queen Maud block .....</i>	<i>5</i>
<i>1.3.2 – Previous research in the Queen Maud block .....</i>	<i>6</i>
<i>1.3.3 – Economic geology of the Queen Maud block.....</i>	<i>8</i>
<b>CHAPTER 2 – Field relationships and petrography.....</b>	<b>11</b>
<b>2.1 – Methodology .....</b>	<b>11</b>
<b>2.2 – Geology of the Queen Maud block .....</b>	<b>12</b>
<i>2.2.1 – Lithology .....</i>	<i>12</i>
<i>2.2.2 – Tectono-metamorphism.....</i>	<i>13</i>
<b>CHAPTER 3 – U-Pb geochronology .....</b>	<b>26</b>
<b>3.1 – Methodology .....</b>	<b>26</b>
<b>3.2 – U-Pb age dating results.....</b>	<b>28</b>
<b>3.3 – Detrital zircon results .....</b>	<b>43</b>
<b>CHAPTER 4 – Geothermobarometry.....</b>	<b>64</b>
<b>4.1 – Methodology .....</b>	<b>64</b>
<i>4.1.1 – Net-transfer and Fe-Mg exchange geothermobarometry.....</i>	<i>64</i>
<i>4.1.2 – Reintegrated feldspar thermometry.....</i>	<i>66</i>
<b>4.2 – Results .....</b>	<b>67</b>
<b>CHAPTER 5 – Evolution of the Queen Maud Block.....</b>	<b>82</b>
<b>5.1 – A geological map of the Queen Maud block .....</b>	<b>82</b>
<b>5.2 – Metamorphic history of the Queen Maud block .....</b>	<b>89</b>

5.2.1 – Archean metamorphism .....	89
5.2.2 – Metamorphism: ca. 2.52-2.45 Ga .....	89
5.2.3 – Metamorphism: ca. 2.43-2.42 Ga .....	90
5.2.4 – Regional metamorphism: 2.39-2.35 Ga Arrowsmith Orogeny .....	91
5.2.5 – Post Arrowsmith metamorphism: 2.35-2.10 Ga .....	92
5.2.6 – Thelon Orogeny: 2.01-1.91 Ga .....	93
5.2.7 – The Trans-Hudson Orogen: ca. 1.9-1.8 Ga metamorphism .....	94
<b>5.3 – A review of previous models for the Slave-Churchill relationship .....</b>	<b>95</b>
5.3.1 – 2.01-1.91 Ga collision of the Slave and Churchill cratons .....	95
5.3.2 – 2.01-1.91 Ga intracontinental orogenesis .....	97
<b>5.4 – A new model for the evolution of northwestern Laurentia .....</b>	<b>99</b>
5.4.1 – The Archean .....	99
5.4.2 – Pre-collisional tectono-magmatism: 2.52-2.45 Ga .....	102
5.4.3 – Slave-Churchill collision and convergence: 2.43-2.35 Ga .....	103
5.4.4 – Post-collision magmatism: 2.32 Ga .....	105
5.4.5 – Continental rifting ca. 2.3-2.1 Ga .....	106
5.4.6 – Thelon Orogeny: 2.01-1.91 Ga .....	106
<b>CHAPTER 6 – Conclusion .....</b>	<b>113</b>
6.1 – Summary .....	113
6.2 – Further Research .....	114
6.3 – Final Remarks .....	115
<b>References .....</b>	<b>117</b>
<b>APPENDIX A – Geological Notes .....</b>	<b>129</b>
<b>APPENDIX B – U-Pb Geochronological Data .....</b>	<b>145</b>
<b>APPENDIX C – Official sample collection .....</b>	<b>160</b>

## List of Tables

Table 3-1: Summary of U-Pb age dating .....	46
Table 4-1: Standards used in EPMA .....	66
Table 4-2: (2 pages) Net-transfer and Fe-Mg exchange mineral compositions .....	79
Table 4-3: Reintegrated feldspar mineral compositions .....	81

## List of Figures

Figure 1-1: Tectonic map of the northwestern Canadian Shield.....	10
Figure 2-1: Map of the Queen Maud block area showing field locations.....	16
Figure 2-2: (7 pages) Outcrop photographs .....	17
Figure 2-3: (2 pages) Thin section photographs .....	24
Figure 3-1: (2 pages) Location QM-1 geochronology summary .....	47
Figure 3-2: Location QM-2 geochronology summary .....	49
Figure 3-3: Locations QM-4 & QM-5 geochronology summary.....	50
Figure 3-4: Location QM-6 geochronology summary .....	51
Figure 3-5: Location QM-7 geochronology summary .....	52
Figure 3-6: Location QM-8 geochronology summary .....	53
Figure 3-7: Location QM-9 geochronology summary .....	54
Figure 3-8: (2 pages) Location QM-10 geochronology summary .....	55
Figure 3-9: (2 pages) Location QM-13 geochronology summary .....	57
Figure 3-10: Locations QM-14 and QM-15 geochronology summary .....	59
Figure 3-11: Location QM-16 geochronology summary .....	60
Figure 3-12: Location QM-17 geochronology summary .....	61
Figure 3-13: QM-1H detrital zircon analysis summary .....	62
Figure 3-14: QM-10C detrital zircon analysis summary .....	63
Figure 4-1: (2 pages) Thin section photographs .....	74
Figure 4-2: BSE images .....	76
Figure 4-3: P-T graphs .....	77
Figure 4-4: Ternary feldspar plots .....	78
Figure 5-1: Geological map of the northern Queen Maud block. ....	108
Figure 5-2: Summarized results of monazite dating .....	109
Figure 5-3: Map showing the spatial distribution of metamorphic events.....	110
Figure 5-4: Cartoon cross-sections illustrating tectonic evolution of QMB .....	111
Figure 5-5: Cartoon comparing Slave-Churchill with India-Asia collision.....	112

## List of Abbreviations

BSE	backscatter electron
ca.	circa
DDH	diamond drill hole
EDS	energy dispersive spectroscopy
EMPA	Electron Probe Microanalyser
Ga	billion years ago
GASP	garnet-sillimanite-quartz-plagioclase geobarometer
GSC	Geological Survey of Canada
LA-MC-ICP-MS	laser ablation-multi collector-inductively coupled plasma-mass spectrometry
Ma	million years ago
MSWD	mean square weighted deviation
P	pressure
PRB	Perry River belt
QMB	Queen Maud block
T	temperature
TTZ	Thelon tectonic zone
WDS	wavelength dispersive spectroscopy

### Elements

Al	aluminum
Ar	argon
Ca	calcium
Cu	copper
Fe	iron
K	potassium
Nb	niobium
Nd	neodymium
Ni	nickle
Mg	magnesium
O	oxygen
Pb	lead
Si	silicon
Sm	samarium
Th	thorium
Ti	titanium
U	uranium
V	vanadium

### Minerals

Bt	biotite
Crd	cordierite
Cpx	clinopyroxene
Grt	garnet
Kspar	K-feldspar
Opx	orthopyroxene
Plag	plagioclase
Qtz	quartz
Sil	sillimanite

## CHAPTER 1 – Introduction

The Canadian Arctic is a remote, vast, and poorly understood land. These characteristics have captured the interest and imagination of scientists, prospectors, and artists for over 400 years since early European explorers, such as Martin Frobisher and Henry Hudson, first began searching this land for the Northwest Passage. While the Arctic Grail that is the ice-locked Northwest Passage (Berton, 1988) remains commercially unviable, interest in this land is growing. The ever-depleting resource base in more accessible areas of the world is the main driving force behind this increased interest. As economic interest shifts to the Arctic, so too does scientific interest. Naturalists, anthropologists, climatologists, and geologists actively research the vast Canadian Arctic, testing old hypotheses and formulating new ones.

In addition to examining rocks from the Arctic frontier, this thesis investigates the topical frontier of Precambrian geology. One of the primary questions currently driving research in geoscience asks: how did the early continental crust form and stabilise? By studying the oldest rocks available—the Precambrian shields—scientists can most directly and effectively address this problem. Within the Canadian borders lies the largest Precambrian shield in the world, much of which is present in the relatively unstudied Canadian Arctic. The Queen Maud block (QMB) is a large portion of the Canadian Shield located in the Kitikmeot region of Nunavut. By investigating the QMB, this study addresses questions encompassed by the much broader topic of how the early continental crust formed.

Prior to the present study, only four direct geological studies of the QMB have been published. It is astonishing how little researched the area is compared to any area south of the 60<sup>th</sup> parallel. Two of these studies are geological reconnaissance investigations conducted by the Geological Survey of Canada (GSC) in the 1960's (Fraser, 1964; Heywood, 1961). These studies discovered that the QMB is dominated by high-grade metamorphosed granitoids with subordinate mafic and metasedimentary rocks; however, they were conducted at a time when the understanding of Precambrian shields and the analytical methods used to study them were in their infancy. A third publication provides Nd depleted mantle model ages for rocks from the southwestern QMB (Theriault et al, 1994). While useful, this study was limited in its scope.

A former master's student at the University of Alberta conducted what is by far the most detailed investigation of the QMB (Schultz, 2007; Schultz et al., 2007). This study discovered that the early Paleoproterozoic (2.5-2.0 Ga) geologic history of the

northeastern QMB is distinct from that of adjacent areas. During this investigation the 2.50-2.46 Ga Queen Maud granitoids and the 2.45-2.39 Ga Sherman sedimentary basin were discovered, both of which are unique to the QMB. It was also found that metamorphism of these rocks occurred *ca.* 2.39 Ga, concurrent with the Arrowsmith Orogeny documented elsewhere in the western Canadian Shield. In most areas where evidence for this orogeny has been found there is extensive overprinting by younger (*ca.* 2.0-1.8 Ga) tectonic events. A unique feature of the QMB is that there is very little overprinting of the Arrowsmith Orogeny, making it the ideal location to study this orogeny.

Creating additional interest in the QMB is the fact that it occupies a unique tectonic position in the Canadian Shield. The Canadian Shield has been divided into several geological provinces, including but not limited to, the Slave and Churchill provinces (Figure 1-1; Stockwell, 1961). The QMB is located at the northwestern boundary of the Churchill Province and is separated from the Slave Province by the 2.01-1.91 Ga Thelon tectonic zone (TTZ). Several models currently exist regarding the relationship between the Slave Province, Churchill Province, and the TTZ. One commonly held belief is that the TTZ represents the boundary between two Archean crustal blocks—the Slave and Churchill provinces—that were formerly separated by an ocean basin, but which collided at *ca.* 1.97 Ga (e.g., Hoffman, 1987; Theriault, 1992). An alternative hypothesis is that the TTZ is an area of intracontinental reworking and that the Slave and Churchill provinces may have collided earlier, during the 2.4-2.3 Ga Arrowsmith Orogeny (e.g., Chacko et al., 2000; Schultz et al., 2007). A growing body of literature, including this study, provides insight into the relationship between the Slave and Churchill provinces.

## **1.1 – Objectives**

There are two primary goals of this thesis. The first is to investigate the geology and geochronology of the northwestern and central QMB at a reconnaissance scale. Prior to the present study, no robust geochronologic data from this area has been published. Secondly, this thesis investigates the metamorphic history of the QMB including the timing and pressure-temperature (P-T) conditions of metamorphism. In doing so, the understanding of the enigmatic Arrowsmith Orogeny is improved. The findings of this study are summarized in a modified geological map of the QMB and provide new insight

into the relationship between the Slave and Churchill provinces as well as the Paleoproterozoic evolution of the western Churchill Province.

In order to accomplish these objectives, a variety of methods commonly used for studying Precambrian geology were employed. Fundamental to this study was three days of helicopter-supported fieldwork along the south coast of the Queen Maud Gulf. This was followed by petrographic analysis of the 60 rock samples collected during fieldwork. In addition to geological observation, several analytical methods were used throughout this study. Quantitative geothermobarometric calculations were carried out on seven samples using mineral composition data generated by electron microprobe analysis. Uranium-lead (U-Pb) age dates of zircon and monazite grains from 30 samples were obtained using laser ablation-multi collector-inductively coupled plasma mass spectrometry (LA-MC-ICP-MS). Finally, following mineral separation, detrital zircon studies were conducted on two metasedimentary samples, also using LA-MC-ICP-MS.

## **1.2 – Geology of the Churchill Province**

The North American craton, known as Laurentia, includes the exposed parts of the Canadian and American shields as well as platform areas, which are covered by Phanerozoic rocks. The Canadian Shield was first divided into the Churchill, Slave, Bear, Superior, Southern, and Grenville provinces by Stockwell (1961). These subdivisions were made based on varying lithology, metamorphism, and structural style between the provinces. The boundaries dividing these Archean provinces are areas of Proterozoic deformation.

The Churchill Province is separated from the Slave and Buffalo Head terranes to the west by the 2.01-1.91 Ga Taltson-Thelon magmatic zone, and from the Superior Province to the southeast by the 1.9-1.8 Ga Trans-Hudson Orogeny (Figure 1-1; Hoffman, 1988; Hoffman, 1989). The Churchill Province is commonly divided into three sub-regions: the Rae and Hearne domains, which are separated by the Snowbird tectonic zone, and the QMB, which is characterized by its relatively high metamorphic grade and is separated from the Rae domain by prominent fault zones.

The Rae domain is underlain predominantly by Archean gneisses of variable age and lithology. The oldest gneisses are found in a belt along the western boundary of the Rae domain and exhibit Nd depleted mantle model ages ranging from 3.9-3.0 Ga (Hartlaub et al., 2005). Prior to the present study, little direct U-Pb dating of these Mesoarchean rocks had been conducted (Hartlaub et al., 2005). To the east of this belt,



gneisses exhibit predominantly Neoproterozoic ages. Archean aged greenstone belts are common throughout the Rae domain and include the Prince Albert Group, Woodburn Group, Mary River Group, and possibly the Murmac Bay Group, which were deposited around 2.7 Ga (Hartlaub et al., 2004). Widespread intrusion of tonalite-trondhjemite-granodiorite (TTG) plutons occurred throughout much of the Rae domain between 2.7 and 2.6 Ga (LeCheminant and Roddick, 1991).

Evidence that a 2.4-2.3 Ga tectonic event affected the western margin of the Rae domain and the QMB has been found from a relatively recent body of literature (e.g., Berman et al., 2005; Bostock and van Breemen, 1994; Hartlaub et al., 2007; McNicoll et al., 2000; Schutz et al., 2007). This event, dubbed the Arrowsmith Orogeny (Berman et al., 2005), has associated metamorphism and plutonism. The cause of this orogeny continues to be debated and interestingly, the time period between 2.45-2.20 Ga is often regarded as a prolonged episode of global tectonic quiescence (e.g., Condie et al., 2009)

The Taltson-Thelon zone is a north-south trending curvilinear belt of magmatic and high grade metamorphic rocks along the western boundary of the Churchill Province. The northern portion of this belt, the Thelon tectonic zone (TTZ) divides the Slave and Churchill Provinces. At the southern limit of the TTZ, near Great Slave Lake, the belt is dextrally offset 300-700 kilometres by the Great Slave Lake shear zone (Hoffman, 1987). The Taltson-Thelon zone continues south into northern Alberta and Saskatchewan where it is referred to as the Taltson magmatic zone. The Taltson magmatic zone is bound to the west, not by the Slave province, but by the Buffalo Head terrane. Two generations of magmatic rocks have been found within the belt. The dominant age of magmatism and metamorphism has been dated between 2.01 and 1.91 Ga (van Breemen et al., 1987a; van Breemen et al., 1987b; van Breemen and Henderson, 1988), while an older, more cryptic event has been dated between 2.4 and 2.3 Ga, concurrent with the Arrowsmith Orogeny (Bostock and van Breemen, 1994; van Breemen et al., 1991; McNicoll et al., 2000). This belt extends from as far south as northern Alberta and Saskatchewan to possibly as far north as Somerset Island (Hoffman, 1987; Ross et al., 1991; Kitsul et al., 2000). Due to its location at the boundary between the Churchill Province and the Slave and Buffalo Head terranes, the Taltson-Thelon belt has been the subject of a large amount of research (e.g., James, 1989 and references therein). In spite of this, the origin of the belt remains controversial and it has been interpreted as both a collisional orogeny as well as an intracratonic mountain belt (Hoffman, 1987; Chacko et al., 2000).

The enigmatic 1800 km long SW-NE trending mylonite zone known as the Snowbird tectonic zone not only divides the Churchill Province into the Rae and Hearne domains, but also divides the scientific community. This feature has been interpreted as both a Paleoproterozoic continental suture, and an Archean strike-slip fault system (e.g., Berman et al., 2007; Mahan and Williams, 2005).

The most recent major orogenic event to affect the Churchill Province is the Trans-Hudson Orogeny, also known as the Hudsonian Orogeny (Hoffman, 1990). Metamorphism and plutonism associated with this orogeny is found throughout much of the Churchill Province and has been dated between roughly 1.9 and 1.8 Ga (Hoffman, 1990; Peterson et al., 2002). The prevailing view is that this tectonic event was the result of the Himalayan style collision between the Churchill and the Superior Provinces following northward dipping subduction along the southeast margin of the Churchill Province (Hoffman, 1990).

### **1.3 – The Queen Maud block**

#### ***1.3.1 – Defining the Queen Maud block***

The QMB also known as the Queen Maud uplift, is a ~75000 km<sup>2</sup> triangular shaped portion of the Canadian Shield approximately 500 km long by 300 km wide located in the Kitikmeot region of Nunavut, Canada. The QMB is named for the adjacent Queen Maud Gulf, which was named by Norwegian explorer Roald Amundsen for the Englishwoman, Queen Maud of Norway. Upon her marriage to King Haakon in 1905, Queen Maud was crowned; she remained Queen of Norway until her death in 1938. The remains of Amundsen's ship, *The Queen Maud*, can still be seen near the town of Cambridge Bay in Nunavut.

The original defining of the QMB was by Heywood and Schau (1978), who divided the northern Churchill Province into the QMB, the Committee Bay block, and the Armit Lake block. These subdivisions were made based on the metamorphic grade of each area and boundaries were drawn along well defined mylonite zones. The metamorphic grade of the QMB is significantly higher than in the adjacent Committee Bay and Armit Lake blocks.

Currently, the most commonly used subdivisions of the Churchill Province include the Rae domain, the Hearne domain, and the QMB, as defined by Hoffman (1988). In this thesis the geographic limits of the QMB are those defined by Schultz (2007), who slightly modified the original limits of Heywood and Schau (1978), and

those used by Hoffman (1988). The QMB is bounded to the west by the TTZ, to the southeast by the Slave-Chantrey mylonite zone (Heywood and Schau, 1978), and to the east by an easily recognizable magnetic lineament, which constrains the 2.50-2.46 Ga Queen Maud granitoids within the QMB (Schultz et al., 2007). The northern limit of the QMB is unknown due to the fact that it is submerged in the Queen Maud Gulf and farther north is covered by younger Paleozoic rocks.

It is possible that rocks of a similar affinity to QMB can be found along Boothia Peninsula and as far north as Somerset Island. This is based on aeromagnetic data that suggests the northward continuation of the TTZ for 700 km beyond the Queen Maud Gulf (Geological Survey of Canada, 2010). Moreover, it has been postulated that the Boothia-Somerset granulite terrane represents an extension of the TTZ based on similar metamorphic grade and age (Kitsul et al., 2000). If indeed these rocks are equivalent to the TTZ, it is possible that QMB-like rocks are to be found east (or south) of this area.

The validity of the QMB as a subdivision of the Churchill Province was called into question by Jackson and Berman (2000), due to the overlapping Nd depleted mantle model ages between the southwest QMB and the southwest and northwest Committee Bay belt. However, the findings by Schultz et al. (2007) reinforce the legitimacy of the subdivision, due to the presence of the uniquely aged Queen Maud granitoids within the QMB.

### 1.3.2 – Previous research in the Queen Maud block

As mentioned, the quantity of research pertaining to the QMB is limited to four direct geological studies. The first two studies of the QMB were mapping projects conducted by the GSC in the 1960's. The first study (Heywood, 1961), mapped the eastern portion of the QMB at the 1:1,000,000 scale whereas the second study, (Fraser, 1964) mapped the western portion of the block. Released in conjunction with these studies, were several K-Ar air furnace fusion radiometric age dates (Lowdon, 1960; Lowdon et al., 1963; Wanless et al., 1965; Wanless et al., 1966; Wanless et al., 1968). Although these studies provide useful information regarding the lithology, structure, and metamorphism of the QMB, they do not address the tectonic evolution of the area. In particular, the K-Ar dates for the area are of limited use in understanding the original tectonic evolution of the QMB. The main shortcoming of these dates is that the K-Ar system has a relatively low closure temperature and is highly susceptible to resetting in polymetamorphosed terranes such as the QMB. As such, the age dates, which range from

1.37-1.97 Ga, do not provide evidence for the Paleoproterozoic metamorphic events to which the QMB was subjected, but reflect the latest time at which the rocks cooled through the closure temperature of the K-Ar system.

The GSC has supplemented these geological and geochronological studies with geophysical data. An aeromagnetic survey of the Thelon River area, which includes the entire QMB, was published in 1982 (Geological Survey of Canada, 1982). In addition, Bouguer gravity anomaly surveys covering the QMB and adjacent areas were released in the 1970's (Hornal and Boyd, 1972; Gibb and Halliday, 1974; Gibb and Halliday, 1975).

Theriault et al. (1994) reported Nd depleted mantle model ages of several samples from the southwestern QMB. The ages vary from 3.1 to 3.6 Ga. Schultz et al., (2007) determined model ages from between 2.9 and 3.1 Ga for rocks from the northeastern QMB. These findings are consistent with the observations made by Hartlaub et al. (2005) that a belt of Mesoarchean rocks is present along the western margin of the Churchill Province with younger gneisses found further east.

The most comprehensive and modern study of the QMB was conducted by a graduate student at the University of Alberta (Schultz, 2007; Schultz et al., 2007). This study focused on intrusive granitoids and a supracrustal sequence in the northeastern part of the block. Schultz et al. (2007) identified two generations of granitoid rocks in the QMB area. First, are the 2.6-2.7 Ga granitoids present within and to the east of the block; granites of this age are widespread throughout the Rae domain (LeCheminant and Roddick, 1991). Second, are the Queen Maud granitoids, unique to the QMB, which crystallized from 2.50-2.46 Ga and were derived from Neoproterozoic to latest Mesoarchean source rocks. Also newly identified, using detrital zircon U-Pb analysis, was the extensive NE trending belt of supracrustal rocks, known as the Sherman Basin, which was deposited between 2.45 and 2.39 Ga and is dominated by 2.45-2.50 Ga detritus. The Sherman Basin and Queen Maud granitoids underwent granulite facies metamorphism at 2.39 Ga. Schultz et al. (2007) interpreted that the Queen Maud granitoids and the Sherman Basin formed in response to continental rifting. Evidence supporting this interpretation is the bimodal nature of the 2.50-2.46 Ga magmatism as well as the low Th/Nb ratios and high Ti and V contents of mafic igneous rocks from this suite (Schultz, 2007). According to Schultz et al. (2007), this crustal extension was followed shortly after by compression, resulting in the tectonic burial of the Sherman Basin and 2.39 Ga granulite-facies metamorphism.

Previous research has documented little evidence for tectonic activity in the QMB after these early Paleoproterozoic events. The findings by Schultz et al. (2007) indicate that the northeastern QMB did not undergo any significant reworking during the 2.01-1.91 Ga Thelon Orogeny. Evidence for very minor reworking during the Trans-Hudson Orogeny has been documented and includes local pegmatitic dykes dated at ca. 1.8 Ga (Schultz and Chacko, unpublished data). The southernmost QMB is unconformably overlain by the Paleoproterozoic quartz-dominated Thelon Basin (Palmer et al., 2004). The age of deposition of the Thelon Basin is constrained between 1.85 and 1.70 Ga; it is interpreted that basin formation was in response to the Trans-Hudson Orogen (Rainbird et al., 2003).

The tectonic significance of the QMB has been discussed in several papers. In the late 1980's P. F. Hoffman, an influential expert on the Canadian Shield, released a series of publications describing the amalgamation of the Canadian Shield in Proterozoic time (Hoffman, 1987; Hoffman, 1988; Hoffman, 1989; Hoffman, 1990). In his model, Hoffman hypothesizes that the QMB occupies a Tibetan Plateau-like tectonic setting formed in response to the collision of the Slave and Churchill provinces during the 2.01-1.91 Ga Thelon Orogen. This analogue predicts that the QMB should have undergone extensive deformation and reworking at this time, much like is currently occurring in the Tibetan Plateau (e.g., Zhang et al., 2004). An alternative model proposed by Chacko et al. (2000) and De et al. (2000), asserts that the Thelon Orogen is intraplate in nature. In this model the QMB will not necessarily exhibit Thelon aged deformation, but rather, should preserve evidence of earlier deformation events.

### 1.3.3 – Economic geology of the Queen Maud block

Economic activity in the QMB has been nearly as sparse as academic activity. The former is probably due in part to the latter, but also due to the presence of the Queen Maud Gulf Migratory Bird Sanctuary. Whereas areas adjacent to the QMB have been extensively and successfully explored for gold, base metals, and uranium, the QMB itself is largely unexplored for ore deposits.

In the early 1970's several exploration companies prospected the northwestern QMB along the Perry River for Ni-Cu mineralization (Canada-Nunavut Geoscience Office, 2008). This prospecting led to the acquisition of geophysical data in the area as well as the drilling of several DDH cores. The deposit of interest, referred to as the Perry River showing, is hosted by mafic to ultramafic rocks. Sulphide minerals present in the

Perry River showing are pyrite, pyrrhotite, chalcophyrite, and pentlandite. Grab samples from boulder trains as well as assay samples from diamond drill holes provide Ni grades typically in the 0.5-1.0% range and Cu grades around 1%. After the Perry River deposit was deemed uneconomic at 1970's metal prices, exploration activities were halted.

Although not technically part of the QMB due to the fact that it is an overlying sedimentary basin, the unconformity-type uranium deposits of the Thelon Basin are worth mentioning due to their proximity to the QMB. Exploration for U in the Thelon basin began in 1968 after discoveries in the geologically similar Athabasca Basin (Davidson and Gandhi, 1989). By 1989 two U discoveries had been made in the Thelon Basin, and by comparison 20 had been made in the Athabasca Basin (Davidson and Gandhi, 1989). This is not to say that the Thelon Basin is deprived of U, but is more likely due to the fact that the remote Thelon Basin has seen much less exploration activity than the more accessible Athabasca Basin. Unlike the Perry River showing, U exploration in the Thelon Basin is thriving. As an example, Uravan Minerals Inc. is actively exploring the Boomerang Lake and Garry Lake properties in the southwest and northeast Thelon Basin, respectively.

Land use complications in the QMB include the presence of both the Queen Maud Gulf Migratory Bird Sanctuary as well as several parcels of Inuit owned lands. The Queen Maud Gulf Migratory Bird Sanctuary was established in 1961 and is 63655km<sup>2</sup> in area; it is the nesting ground for a large population of snow goose, and nearly the entire population of Ross' goose (Didiuk and Ferguson, 2005). This environmentally sensitive area is protected under the Migratory Birds Convention Act (1994). Further land use complications are the several small parcels of Inuit owned lands located near the mouths of the Perry and McNaughton rivers along the southern coastline of the Queen Maud Gulf.

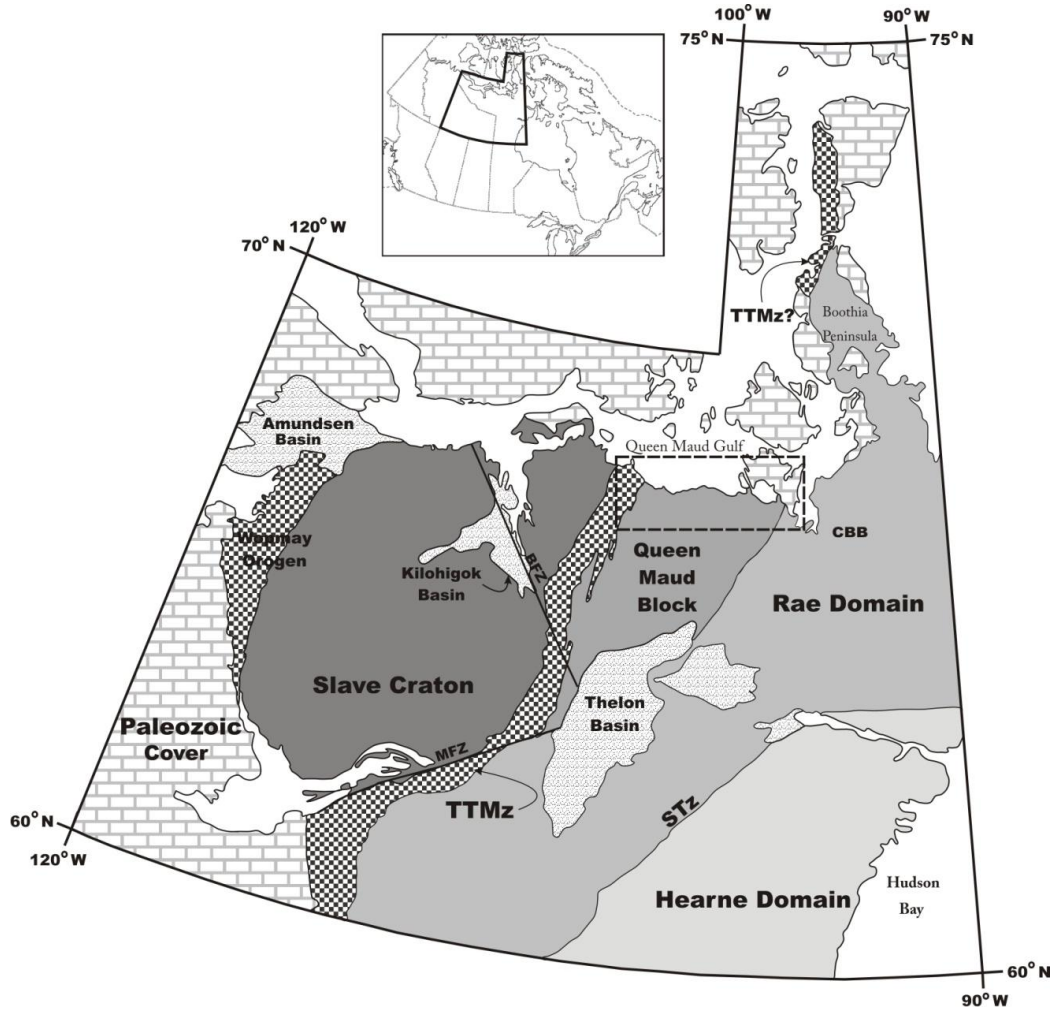


Figure 1-1: Tectonic map of the northwestern Canadian Shield showing the location of the Queen Maud block and adjacent tectonic elements (modified after Hoffman, 1989; Schultz et al., 2007). The Queen Maud block, Rae domain, and Hearne domain combine to form the Churchill Craton. The study area is outlined and shown in detail in later figures. CBB = Committee Bay belt. TTMZ = Talston-Thelon magmatic zone. STz = Snowbird tectonic zone. BFZ = Bathurst fault zone. MFZ = McDonald Fault Zone.

## **CHAPTER 2 – Field relationships and petrography**

The presence of a rocky coastline and thousands of small wave washed islands along the southern coast of the Queen Maud Gulf provides a magnificent natural laboratory for studying the QMB. These islands contain pristine, lichen-free rock outcroppings; lichen being a problem that plagues any geologist studying the Canadian Shield. Furthermore, this coastline trends east to west, almost perpendicular to strike of the main fabrics in the rocks of the QMB. Exposures such as these provide the opportunity to fully comprehend the generally complex relationships between the different rock types present at any given outcrop, as well as variations between outcrops. Moreover, it enables one to accurately collect representative samples of each of these rocks within this contextual understanding. Although the scientific value of this is incontrovertible, it is the beauty of these outcrops, with their swirling gneissic textures and myriad of colors that excite geologist and layman alike. This chapter describes the lithology, metamorphism, and structural geology of the QMB. These descriptions and interpretations are based on observations made in the field and through petrographic analysis. Coordinates of outcrop locations and a set of edited geological notes for each outcrop and sample collected are provided in Appendix A.

### **2.1 – Methodology**

Helicopter assisted field-work for this project was based out of Cambridge Bay, Nunavut and conducted over a span of three days from July 28<sup>th</sup> to July 30<sup>th</sup>, 2010. The field party, consisting of the author and Dr. Tom Chacko, was flown by helicopter from Cambridge Bay across the Queen Maud Gulf to the field area, a distance of about 200 kilometres, each day.

A total of seventeen outcrops were studied over the three days of field work. Outcrops selected for study were chosen with the aid of existing geological maps and aeromagnetic data. Areas that exhibit unique aeromagnetic signatures or are present within different map units were targeted for study. The outcrops chosen for study are located in a west-to-east transect along the southern coastline of the Queen Maud Gulf, and are separated from each other by approximately 10-20 kilometres (Figure 2-1). The western-most stop is located near the eastern edge of the TTZ and the eastern-most stop is located approximately 170 km east of this point, in the QMB.

A representative sample of most of the main lithologies present at every outcrop was collected, resulting in a total of 60 samples from the seventeen outcrops. Samples



range from fist- to head-sized depending on the anticipated use of the sample as well as the ease of extracting the sample from the outcrop. Samples were collected such that they contain as few weathered surfaces as possible. Thin-sections from 53 of the 60 samples were prepared at Vancouver GeoTech Labs as well as ‘in house’ using the University of Alberta’s Thin-Section Laboratory housed in the Department of Earth and Atmospheric Sciences (hereafter referred to as the Department). Petrographic study of the thin-sections was done using a standard transmitted light polarizing microscope.

## **2.2 – Geology of the Queen Maud block**

The QMB is dominated by a lithologically diverse suite of variably strained gneisses and migmatites. These rocks are primarily metamorphosed granitoids with subordinate metamorphosed sedimentary and mafic rocks. The widespread occurrence of orthopyroxene in these rocks indicates that the majority of the northern QMB is metamorphosed at granulite-facies. There is evidence for no less than three deformation and three metamorphic events having affected the QMB. Rare undeformed and unmetamorphosed granitoids and mafic dykes are also present locally. Figure 2-2 is a collection of field photographs illustrating the various geological characteristics discussed, and Figure 2-3 is a supporting collection of photographs of petrographic thin-sections.

### 2.2.1 – Lithology

Gneissic granitoid rocks vary in composition from granitic to tonalitic, with the majority being granitic to granodioritic in composition. In addition to quartz, plagioclase, and K-feldspar, minerals such as biotite, hornblende, orthopyroxene, magnetite, and other minor accessory phases are common (Figure 2-3b; 2-3c). U-Pb dating indicates that these granitic gneisses belong to several generations. Archean aged granitic gneisses, dated between 3.2 and 2.7 Ga, display grey to pinkish-grey weathering, have well developed relatively straight gneissosity, and locally contain plagioclase-poor, highly deformed mafic inclusions and dykes (Figure 2-2a). Paleoproterozoic granitic gneisses, dated between 2.52 and 2.45 Ga, are restricted to the eastern QMB. These rocks are slightly more pinkish-orange weathering than the Archean gneisses, have less well defined gneissosity (except in local zones of very high strain), and are distinctly bimodal, in that they commonly contain numerous plagioclase-rich mafic inclusions (Figure 2-2b).

Supracrustal rocks within the QMB are quartzitic, psammitic, semi-pelitic and pelitic in bulk composition and also include iron formations and mafic igneous rocks (Figure 2-2c; 2-2d, 2-2e; 2-2f). Supracrustal packages are typically intercalated with granitoid rocks in highly-strained areas making it difficult to establish relative ages in the field. Metamorphic minerals such as garnet, spinel, cordierite, sillimanite, orthopyroxene, K-feldspar, and biotite are common throughout pelitic and semi-pelitic rocks (Figure 2-3a). Mafic rocks believed to be supracrustal in origin commonly contain orthopyroxene, clinopyroxene, hornblende, plagioclase, and garnet.

Multiple generations of mafic magmatism have been identified in the QMB on the basis of cross-cutting relationships and U-Pb dating. Mafic rocks occur as inclusions in granitoids, gneissosity-parallel dykes, cross-cutting dykes, and undeformed gabbroic plutons. Some of these mafic rocks are metamorphosed at granulite-facies and conformable with the gneissosity of the host rocks (Figure 2-2a; 2-3d); others are clearly cross-cutting yet still metamorphosed (Figure 2-2g; 2-3e; 2-3f), others still are cross-cutting and completely unaltered (Figure 2-2h; 2-3g). Well-defined chilled-margins are preserved in many of the cross-cutting dykes. Depending on their metamorphic grade, the mafic rocks contain some combination of metamorphic garnet, clinopyroxene, orthopyroxene, and hornblende (Figure 2-3d/e/f). The metamorphosed, cross-cutting mafic dykes exhibit highly variable trends between 330° and 080°. The undeformed, unmetamorphosed dykes consistently trend 355°.

Additional lithologies that are present in relatively minor abundance include the following: undeformed and unmetamorphosed felsic and mafic plutons, pegmatite dykes, syenite sheets, and S-type granites. The undeformed plutons were only encountered at location QM-8 (Figure 2-2i; 2-3k; 2-3l). Rare syenite and garnet bearing S-type granites are locally encountered. These crustally derived magmas are observed intruding the aforementioned granitic gneisses, yet themselves are deformed (Figure 2-2j). Cross-cutting granitic pegmatite dykes were encountered at nearly every outcrop studied. Some of these dykes appear completely unstrained and unmetamorphosed, whereas others are boudinaged, folded, or contain elongated quartz grains.

### 2.2.2 – Tectono-metamorphism

As mentioned, the majority of the northern QMB is metamorphosed at granulite-facies. In addition to the minor effects of retrogression there is clear evidence for no less

than three episodes of metamorphism. The QMB also preserves evidence for at least three distinct deformation events.

The primary tectono-metamorphic event to affect the QMB resulted in formation of the dominant gneissic fabrics (D1) and the granulite-facies mineral assemblages (M1) observed throughout the QMB (Figures 2-2a, 2-2b, and 2-2c illustrate examples of D1 gneissosity). It is possible that earlier tectono-metamorphic events affected the QMB, but if that is the case, evidence for these events has been completely overprinted by the widespread D1/M1 event. D1 fabrics exhibit a high degree of local variation, but in general trend N to NE and dip steeply to the east. The granulite-facies mineral assemblages associated with M1 metamorphism are generally well preserved. Rocks with pelitic and semi-pelitic bulk-composition contain stable mineral assemblages of garnet, sillimanite, cordierite, K-feldspar, and biotite (Figure 2-3a). Orthopyroxene is widespread in rocks of granitic bulk composition (Figure 2-3b). Mafic bulk-composition rocks exhibit stable mineral assemblages of plagioclase, clinopyroxene, and orthopyroxene (Figure 2-3d).

A NNE-SSW trending high-strain shear zone was observed at location QM-13 (Figure 2-2j). This high-strain zone parallels a prominent topographic depression (Figure 2-2k). Mineral lineations within this area are horizontal indicating strike-slip displacement occurred along this shear zone. This shear zone also forms the contact between the Sherman group supracrustal rocks to the east, described by Shultz et al. (2007), and the Queen Maud granitoids to the west. A rock of granitic bulk-composition collected from this high strain zone contains a stable mineral assemblage of hornblende, biotite, clinopyroxene, plagioclase, quartz, and K-feldspar (sample QM-13D). Orthopyroxene is preserved in many granitoid samples throughout this outcrop. The metamorphic grade indicated by the minerals preserved here is similar to those found throughout much of the QMB, suggesting this shearing must have occurred before or during M1/D1 tectono-metamorphism. Interestingly, location QM-13 contains syenite sheets which locally truncate the gneissic banding preserved in this high-strain zone, but are themselves deformed (Figure 2-2j). This observation indicates these sheets may have intruded syntectonically with shearing.

A second metamorphic event, M2, affects cross-cutting mafic and pegmatite dykes in the western QMB. For example, the mafic dyke from which sample QM-1C was collected clearly truncates the M1/D1 gneissosity, but contains a granoblastic texture and a metamorphic mineral assemblage plagioclase, garnet, clinopyroxene, and hornblende

(Figures 2.2g; 2.3e). Similarly trending dykes to the one encountered at location QM-1 are present at locations QM-2 and QM-9 further east, and also exhibit varying degrees of metamorphic recrystallization (Figure 2-3f). Additional evidence for M2 metamorphism is found in granitic gneisses from locations QM-3, QM-4, and QM-5. In these samples, actinolite rims form coronitic haloes around orthopyroxene cores (Figure 2-3c). There is no evidence that M2 metamorphism is associated with any significant deformation, nor is any evidence for this event observed east of location QM-9.

Evidence for a relatively minor deformation event, expressed as southwest plunging folds, is preserved locally in the QMB. Within these D2 folds, which have wavelengths of a few ten of meters, the gneissic fabrics characteristic of the QMB are clearly folded (Figure 2-2l). At location QM-9 a pegmatite dyke that cross-cuts the M1/D1 gneissosity is folded about this D2 fold. This provides further evidence that D2 post-dates D1; however the relative timing of D2 compared with M2 is uncertain, and the relative timing of D2 with D3/M3 remains somewhat speculative, and is discussed in the following paragraph.

A third metamorphic event (M3) is expressed as the recrystallization and re-equilibration of rocks within locally occurring shear zones (D3). While it is not entirely certain if D2 folding pre-dates, post-dates, or is synchronous with D3/M3 shearing, the relatively low grade conditions preserved within this shear zone indicate movement occurred relatively recently, after much of the overlying rock in the QMB had been eroded. One such D3/M3 shear zone is found at location QM-7. Here, a NNE-SSW striking, vertically dipping high-strain zone deforms rocks of mafic and granitic bulk composition (Figure 2-2m). This zone exhibits a strong mylonite texture with horizontal mineral lineations, indicating that strike-slip motion occurred (Figure 2-3i; 2-3j). The M3 mineral assemblage in sample QM-7B, collected from within this mylonite zone, is that of typical upper greenschist- to lower amphibolite-facies basalts. Actonilite (or possibly hornblende), chlorite, epidote, calcite, plagioclase, quartz, and biotite are the stable minerals in this specimen (Figure 2-3h). Outside of the 2 to 5 meter wide anastomosing mylonite zone, rocks contain the granulite-facies mineral assemblages typical of M1 metamorphism.

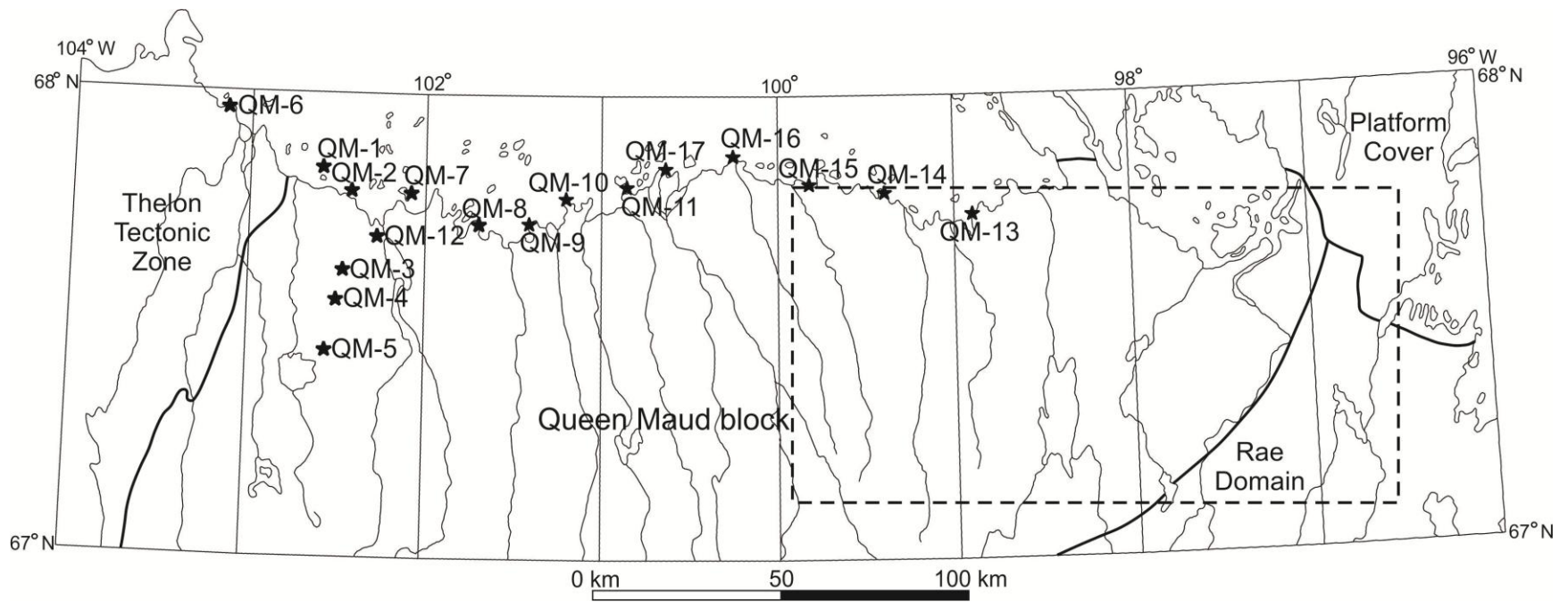


Figure 2-1: Map of the Queen Maud block area showing location of outcrops visited. Area outlined in dashed box is the area studied by Schultz et al. (2007) and Schultz (2007).





Figure 2-2 (1 of 7): a) Typical grey to pink weathering Archean granitic gneiss with gneissosity conformable mafic dyke (Location QM-2). b) Typical orange-pink weathering Paleoproterozoic granitic gneiss (Location QM-15).



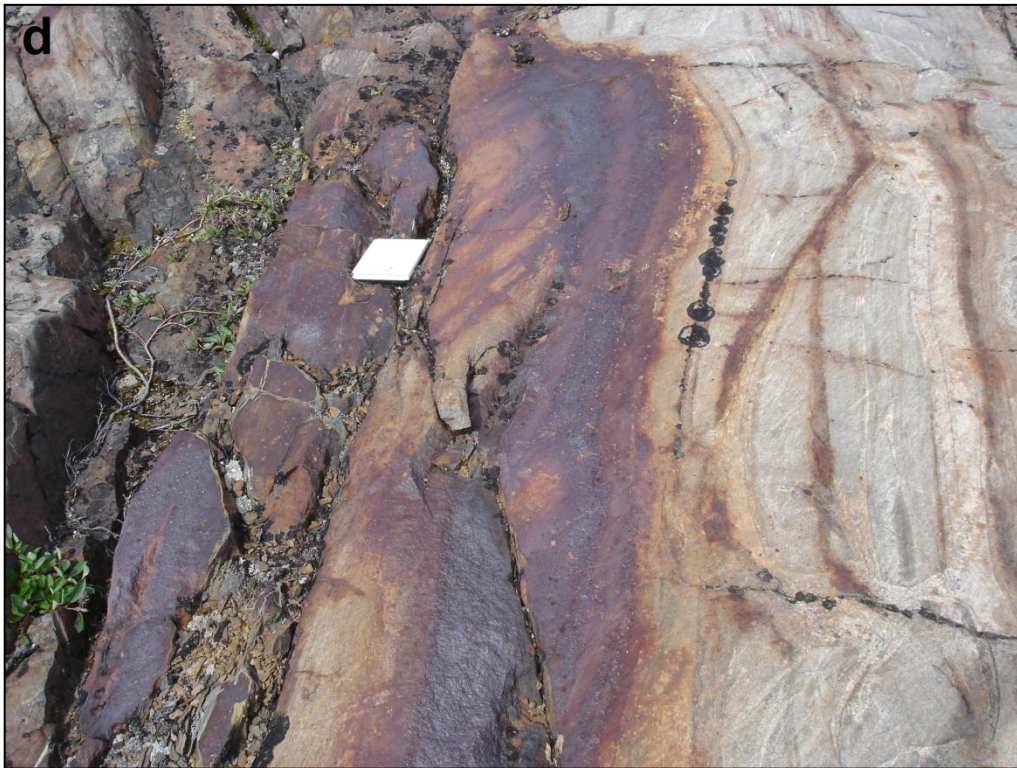


Figure 2-2 (2 of 7): Supracrustal rocks of the QMB. c) Quartzite (Location QM-1) d) Iron formation (Location QM-1)





Figure 2-2 (3 of 7): e) Garnet bearing mafic rock (supracrustal? Location QM-1). f) Orthopyroxene dominated mafic rock (supracrustal? Location QM-10).



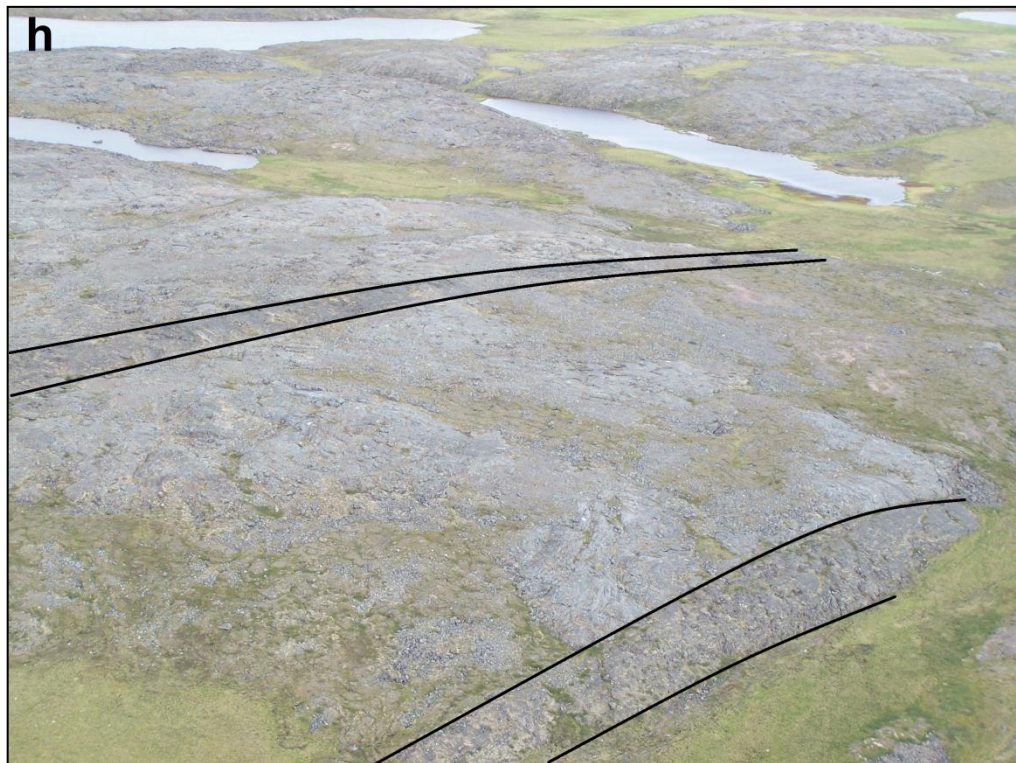


Figure 2-2 (4 of 7): g) Cross-cutting metamorphosed mafic dyke and host metasedimentary paragneiss (Location QM-1). h) Undeformed, unmetamorphosed cross-cutting mafic dykes (outlined) seen from air (Location QM-5).





Figure 2-2 (5 of 7): i) Undeformed and unmetamorphosed gabbro and granitic plutons (Location QM-8). j) Possibly syn-tectonic syenite sheet (outlined) cross-cutting gneissosity at low angle, yet still deformed (Location QM-13).





Figure 2-2 (6 of 7): k) Aerial view of topographic depression parallel to high-strain shear zone (Location QM-13). l) Aerial view of southwest plunging D2 fold (Location QM-9).





Figure 2-2 (7 of 7): m) D3/M3 high-strain mylonite shear zone containing an upper greenschist- to lower amphibolite-facies mineral assemblage (Location QM-7).



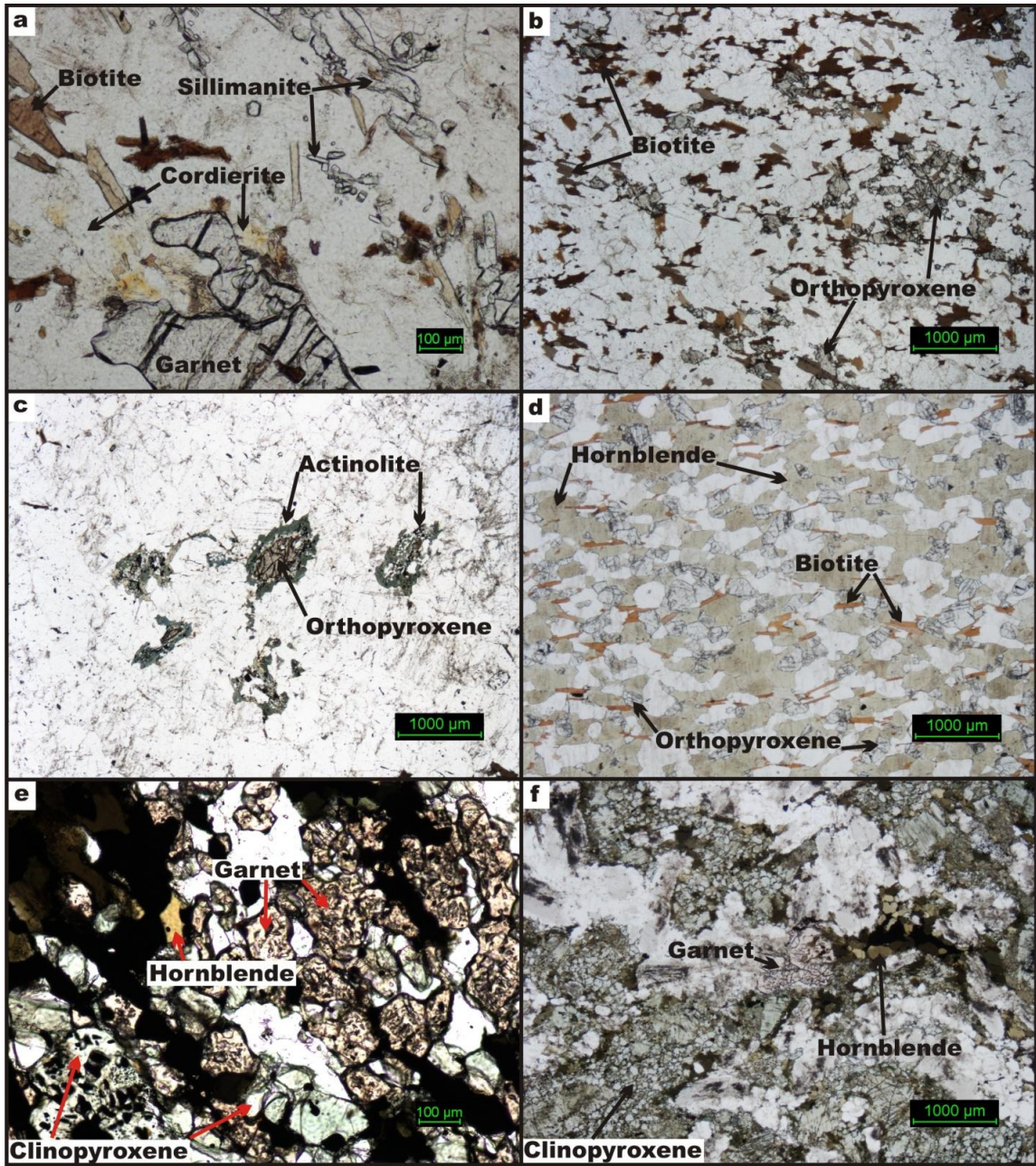


Figure 2-3 (1 of 2): a) Typical granulite-facies M1 mineral assemblage found in pelitic rocks (sample QM-15C). b) Typical granulite-facies M1 mineral assemblage found in granitic rocks (sample QM-14B). c) Actinolite haloes around orthopyroxene, as evidence for M2 metamorphism (sample QM-4B). d) M1 metamorphosed, gneissosity parallel mafic dyke (sample QM-2B). e) Cross-cutting mafic dyke metamorphosed during M2 (sample QM-1C). f) Cross-cutting mafic dyke metamorphosed during M2 (sample QM-9A).



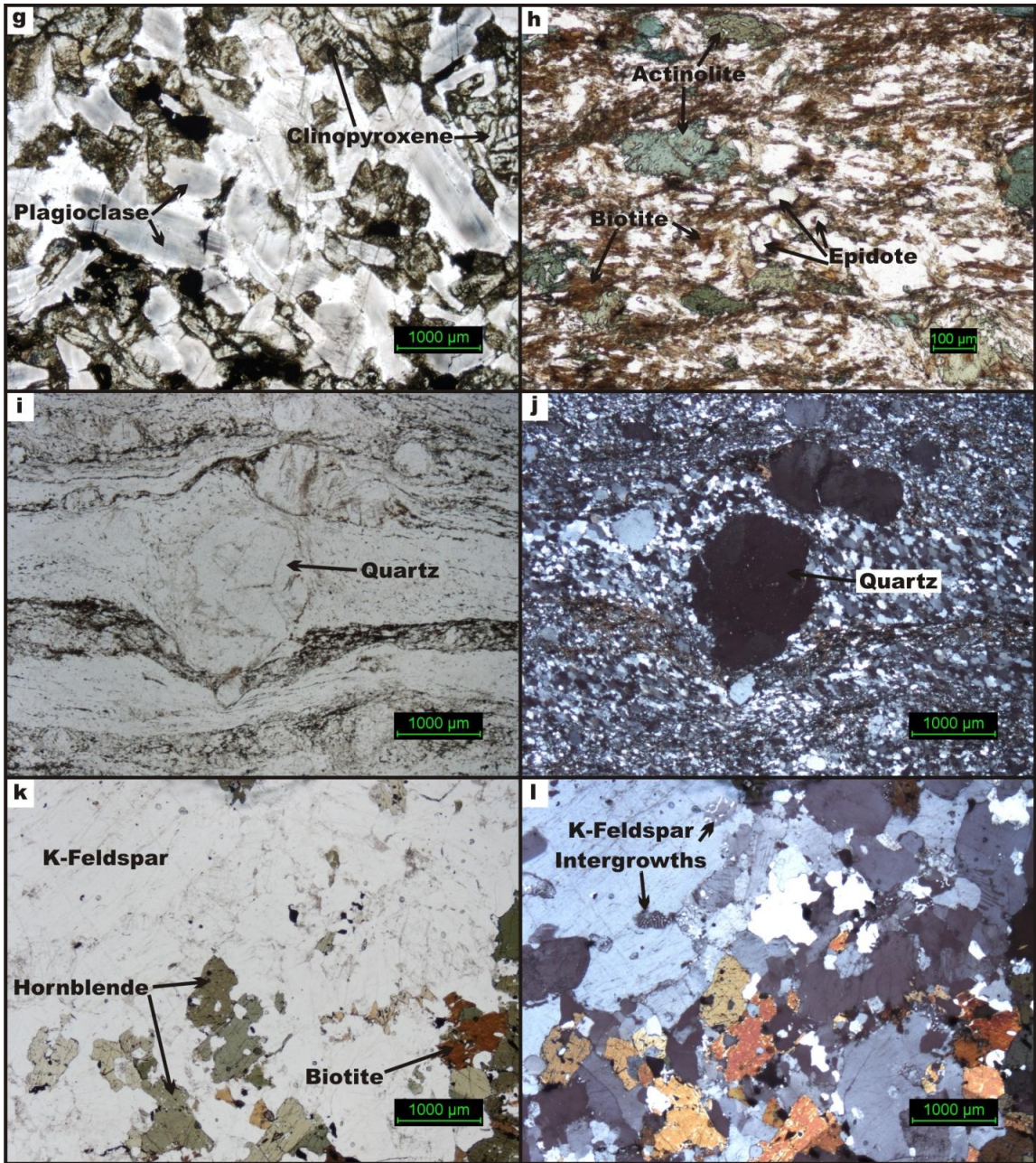


Figure 2-3 (2 of 2): g) Undeformed, unmetamorphosed mafic dyke (sample QM-3B). h) Greenschist-facies mineral assemblage from D3/M3 high-strain mylonite zone (sample QM-7B). i) Strongly developed mylonite texture in D3/M3 high-strain zone in plane-polarized light (sample QM-7B). j) Same as previous in cross-polarized light. k) Undeformed and unmetamorphosed granite in plane-polarized light (sample QM-8B). l) Same as previous in cross-polarized light; note the preservation of intergrowths in K-feldspar grain as evidence for this rock being unmetamorphosed.

## **CHAPTER 3 – U-Pb geochronology**

U-Pb dating of zircon and monazite grains is one of the key tools used in the study of Precambrian areas and is an integral part of this thesis. Dating of these mineral grains provides insight into the timing of metamorphism, igneous crystallization, and sedimentary basin formation. Concordia plots, histograms, select backscatter electron images, and a brief discussion of ages from each sample analysed are included in this chapter. The results of U-Pb dating are synthesized and further discussed in Chapter 5 and the full U-Pb data set is provided in Appendix B.

### **3.1 – Methodology**

Zircon and monazite grains from a total of 31 unique samples were dated at the Department's Radiogenic Isotope Facility. Dating was done on a NuPlasma multi collector - inductively coupled plasma - mass spectrometer (MC-ICP-MS) attached to a New Wave Research UP-213 laser ablation system. U-Pb dating of zircon and monazite grains was performed in-situ in petrographic thin-section and in grain mount following a method slightly modified from the one pioneered by Simonetti et al. (2005; 2006).

Samples chosen for in-situ U-Pb dating in petrographic thin-section contain multiple zircon or monazite grains with a large enough diameter (over 16  $\mu\text{m}$  for monazite and over 30  $\mu\text{m}$  for zircon) to analyse without ablating surrounding mineral grains. 19 zircon-bearing and 10 monazite-bearing samples were identified as suitable for in-situ dating.

Mineral separations were conducted on five key samples in which the required number or size of mineral grains were not found in petrographic thin-section. Mineral separations for grain mounts were conducted by the author using Department mineral separation facilities. Samples were first crushed in a shatter box. Powdered samples were then separated into a heavy and light component using a Wilfley Table. A series of Frantz magnetic separations were conducted on the heavy component in order to remove magnetic mineral phases. Following Frantz magnetic separations, a heavy liquids separation was conducted in order to remove any residual light mineral phases. Zircon grains were picked from the remaining sample and were mounted on epoxy mounts.

After appropriate mineral grains were mounted and identified in thin-section, backscatter electron (BSE) images of these grains were obtained using the Department's JEOL 8900 Microprobe or Zeiss EVO MA 15 scanning electron microscope. BSE images were obtained for two purposes: first, to determine which grains were suitable for dating

based on their size as well as lack of fracturing and inclusions, and second, to identify any radiation damage or internal structure in the zircon grains.

Monazite analyses were typically conducted using a 12  $\mu\text{m}$  diameter laser spot size; however in samples QM-1A and QM-9D a 16  $\mu\text{m}$  spot size was used to compensate for low radiogenic Pb contents. Most zircon analyses were conducted using a 30  $\mu\text{m}$  spot size; however zircons in samples QM-10C and QM-17C contained exceptionally high quantities of  $^{206}\text{Pb}$ , so a 20  $\mu\text{m}$  spot was used. Data collection consisted of one-second integrations carried out over 30 seconds. Rare analyses characterized by noticeable changes in radiogenic Pb counts throughout the 30 integrations were omitted in the age calculations. Common lead ( $^{204}\text{Pb}$ ) contents were measured, however no common Pb correction was made to either standard or sample analyses due to the large uncertainties in applying this correction.  $^{204}\text{Pb}$  counts in standard and sample analyses were comparable and generally quite low (i.e., <100 cps). In rare instances, sample analyses exhibit anomalously high  $^{204}\text{Pb}$  counts when compared to standard analyses; where this is the case, these analyses are omitted from age calculations. Monazite ages were standardized using an in-house Western Australia standard (Simonetti et al., 2006). Zircon standardization was done using the in-house LH94-15 zircon (Ashton et al., 1999) as a primary standard and the accuracy of zircon analyses were tested using the OG-1 zircon (Stern et al., 2009) as a secondary standard. Weighted mean  $^{207}\text{Pb}/^{206}\text{Pb}$  age calculations of the OG-1 secondary standard were accurate within  $\pm 10$  Ma of the expected  $3465.4 \pm 0.6$  Ma age calculated from TIMS analysis (Stern et al., 2009).

Data analysis, including constructing concordia plots and calculating ages, was conducted using Isoplot 3.0 (Ludwig, 2003). All quoted ages and error ellipses in concordia plots are at the two sigma level of uncertainty. Results of in-situ and grain mount dating are presented in Section 3.2 in numeric order based on outcrop location and sample number. Results of detrital zircon analyses are presented in Section 3.3. Concordia plots, age calculations, and probability density plots as well as supporting outcrop photographs, grain mount photographs, and select BSE images from each sample dated in-situ and in grain mount are presented in Figures 3-1 through to 3-12. Photographs, select BSE images, grain mount photographs, and probability density plots from detrital zircon analyses are shown in Figures 3-13 and 3-14. Table 3-1 summarizes the results of all U-Pb ages acquired for this study.



### 3.2 – U-Pb age dating results

#### Location QM-1

Location QM-1 is moderately to highly deformed and composed of a lithologically diverse suite of gneisses that occur in distinct layers. Due to the highly strained nature of this outcrop the relative age of different gneisses was impossible to determine in the field. A large mafic dyke and several smaller pegmatite dykes cross-cut these host gneisses. Although the mafic dyke clearly intruded after the gneissosity forming tectonic event, the dyke itself is metamorphosed. Geochronological data from this location are summarized in Figure 3-1.

Sample QM-1A is an orthopyroxene-bearing granitic gneiss, with trace amounts of biotite, and makes up part of the aforementioned host rock at this outcrop. Eleven analyses from three monazite grains were obtained from this sample. Monazite grains are irregularly shaped, have patchy zoning profiles, and a mottled appearance. One of the monazite grains analyzed contains a zircon inclusion, whereas a second grows partially around a titanite grain. These textural observations suggest that monazite grains grew as a result of secondary crystallization, not magmatic crystallization. Analyses are concordant to moderately discordant and their  $^{207}\text{Pb}/^{206}\text{Pb}$  ages span a range from approximately 2.26-2.09 Ga. One of the BSE images shown in Figure 3-1 reveals possible insight into this spreading of ages. The oldest of the three ages from this monazite grain provides a  $^{207}\text{Pb}/^{206}\text{Pb}$  age of  $2217 \pm 18$  Ma and comes from the lighter patch on the right hand side of the grain. The youngest analysis is from the darker patch on the left hand side of the image and provides a  $^{207}\text{Pb}/^{206}\text{Pb}$  age of  $2117 \pm 18$  Ma. The analysis that straddles the two zones yields a  $^{207}\text{Pb}/^{206}\text{Pb}$  age of  $2145 \pm 18$  Ma. It is possible that monazite grains in this sample contain two distinct age domains (ca. 2117 and 2217 Ma), and the intermediate age reflects a mixed analysis that incorporated material from both age populations.

Sample QM-1C was collected from near the core of a mafic dyke that cross-cuts the gneissosity of the host paragneiss that dominates location QM-1. The dyke exhibits a granoblastic texture and a metamorphic mineral assemblage of garnet, clinopyroxene, hornblende, and plagioclase. In petrographic thin-section, euhedral and elongate zircon grains were identified. Two distinct zircon populations were identified in mineral separate. One of the populations is characterized by somewhat angular, irregularly shaped grains with a beige hue and variably metamict texture. Zircons of this morphology are commonly interpreted as being magmatic in origin (Corfu et al., 2003). The second end-member population is characterized by rounded, irregularly shaped grains that are notably

colorless, consistent with their being metamorphic in origin (Corfu et al., 2003). U-Pb analyses of sample QM-1C were conducted on 38 mineral grains obtained through mineral separation and two additional grains identified in petrographic thin-section. The ages provided by these analyses span a range between 2.10 and 1.91 Ga, with 20 clearly clustered analyses providing a concordia age of  $1928.2 \pm 6.6$  Ma with MSWD = 3.5. 17 analyses are spread between this 1.93 Ga cluster and 2.10 Ga. Generally speaking, the 20 analyses providing the 1.93 Ga age are from clear, unzoned, non-metamict, subrounded zircon grains. This textural observation suggests they grew as a result of metamorphism. The older ages are from beige colored, angular, variably metamict grains, and also from the two elongate partially metamict zircons analysed in petrographic thin-section. The fact that metamict grains provide ages older than non-metamict grains suggests they crystallized earlier and underwent lead loss, likely during 1.93 Ga metamorphism. It is probable that these older metamict grains are magmatic zircons, and therefore the oldest age of 2.10 Ga provides, at best, the approximate age of crystallization of this mafic dyke, and at worst, a minimum crystallization age for the dyke.

Sample QM-1D was collected from the contact between a cross-cutting mafic dyke and a garnet-K-feldspar psammitic gneiss. 15 analyses were conducted on five monazite grains, all of which are found within the psammite, not the mafic dyke. Monazite grains are variable in appearance: some are irregularly shaped and have a mottled appearance, whereas others are more regularly shaped and lack the mottled texture. 14 of the analyses are concordant to moderately discordant and provide  $^{207}\text{Pb}/^{206}\text{Pb}$  ages spanning a range between 2.30 and 2.08 Ga. Analyses at the older end of the spectrum tend to come from the more regularly shaped monazites, while younger analyses are from the more mottled monazite grains. These observations indicate the possibility of two episodes of monazite growth and the subsequent mixing of age domains as being responsible for the range in ages. A single analysis provides a  $^{207}\text{Pb}/^{206}\text{Pb}$  age of  $1843 \pm 21$  Ma.

Sample QM-1I is a quartz-rich semi-pelitic gneiss containing orthopyroxene, garnet, biotite, sillimanite and K-feldspar. Eight analyses were conducted on three monazite grains. In BSE images monazite grains exhibit dark centres with lighter colored, thin and discontinuous rims. Once again, these prominent rims suggest the possibility of at least two distinct phases of monazite growth at this location. Abundant inclusions are visible in these monazite grains. The  $^{207}\text{Pb}/^{206}\text{Pb}$  ages obtained span a similar range as observed in QM-1A and QM-1D, between 2.23 and 2.10 Ga. One analysis revealed a

slightly older  $^{207}\text{Pb}/^{206}\text{Pb}$  age of  $2350 \pm 6$  Ma, consistent with the timing of significant monazite growth elsewhere in the QMB.

U-Pb age dates from monazite grains from location QM-1 reveal interesting results. The oldest  $^{207}\text{Pb}/^{206}\text{Pb}$  age interpreted as being metamorphic in origin is dated at 2.35 Ga. The majority of  $^{207}\text{Pb}/^{206}\text{Pb}$  ages are concordant to moderately discordant and span a range of ages between approximately 2.3 and 2.1 Ga. Textural observations suggest the possibility that this phenomenon could be the result of the mixing of two or possibly several age domains. The age domains may have formed during distinct metamorphic events. A single monazite analysis provides a  $^{207}\text{Pb}/^{206}\text{Pb}$  age of  $1843 \pm 21$  Ma. Zircon grains from a cross-cutting mafic dyke (sample QM-1C) were dated following mineral separation and provide a minimum crystallization age of  $\sim 2.10$  Ga and a metamorphic age of  $\sim 1.93$  Ga for this dyke.

#### Location QM-2

Location QM-2 is composed of intercalated granitoid gneisses, varying in composition from granodioritic to granitic, that are cross-cut by two distinct generations of mafic dykes. An older generation is boudinaged and parallel to the gneissosity of the granitoids. The younger generation cross-cuts this gneissosity, yet is weakly deformed and metamorphosed. Geochronological data from this location are summarized in Figure 3-2.

Sample QM-2C is a magnetite-hornblende-biotite-orthopyroxene granodiorite. 15 analyses were conducted on 7 zircon grains from this sample. Zircon grains are variably metamict yet still preserve prominent oscillatory zoned cores as well as irregularly shaped recrystallized zones that are lighter in color and much more homogenous in BSE image. Eight analyses from within oscillatory zoned cores reveal an upper intercept age of  $3205 \pm 31$  Ma and a lower intercept age of  $463 \pm 450$  Ma with  $\text{MSWD} = 4.9$ . The upper intercept age of approximately 3.2 Ga is interpreted as being the timing of crystallization of this rock. A weighted mean  $^{207}\text{Pb}/^{206}\text{Pb}$  age from four analyses within recrystallized zones is calculated at  $2365.0 \pm 4.6$  Ma with  $\text{MSWD} = 0.16$ . This date is interpreted as being the result of zircon growth or recrystallization during a metamorphic event.

QM-2D is a hornblende-biotite granite. 11 analyses of 7 zircon grains were conducted in this sample. Zircons contain oscillatory zoned cores and irregularly shaped recrystallized zones, similar to zircons from sample QM-2C. Intercept ages from a regression line calculated from five analyses from oscillatory zoned cores are  $3227 \pm 19$

Ma and  $670 \pm 420$  Ma with MSWD = 0.38. The upper intercept age is interpreted as the approximate crystallization age of this granite. Several analyses from recrystallized zones provide Paleoproterozoic  $^{207}\text{Pb}/^{206}\text{Pb}$  ages between  $2308 \pm 10$  Ma and  $2425 \pm 10$  Ma, which are once again interpreted as metamorphic ages.

U-Pb analyses from this location record a geologic history involving early Mesoarchean crystallization of the granitoid rocks, followed by partial metamorphic recrystallization during the Paleoproterozoic. The significance of the two lower intercept ages quoted is uncertain, however, they may simply be the result of Pb loss during Phanerozoic surface weathering.

#### Locations QM-4 & QM-5

These lichen covered outcrops are composed of only two distinct lithologies: granitic gneisses that are cross-cut by  $355^\circ$ -trending undeformed, unmetamorphosed mafic dykes. Geochronological data from these locations are summarized in Figure 3-3.

Sample QM-4B is a representative sample of the magnetite-biotite-hornblende-orthopyroxene granitic gneiss at location QM-4. Ten analyses were conducted on six zircon grains from this sample. Zircons are variable in their appearance. Some are subhedral and display weakly developed oscillatory zoning, whereas others are anhedral, highly fractured, and exhibit little to no patterned zoning. A weighted mean  $^{207}\text{Pb}/^{206}\text{Pb}$  age from four of the analyses is calculated at  $2704 \pm 26$  Ma with MSWD = 11.3. This is interpreted as being the approximate age of crystallization of this rock as these analyses are from the subhedral, slightly zoned zircon grains and from the cores of anhedral grains. A single analysis from a heavily fractured, well defined core of a zircon grain provides a  $^{207}\text{Pb}/^{206}\text{Pb}$  age of  $3123 \pm 10$  Ma, interpreted as being the result of inheritance. The remaining analyses reveal a series of concordant  $^{207}\text{Pb}/^{206}\text{Pb}$  ages spread between 2.65 and 2.34 Ga. These analyses come from nearest the rims of subhedral zircon grains and from the unzoned anhedral zircon grains. These analyses may represent a series of ages related to a Pb loss event at 2.34 Ga, or the mixing of two age domains, one being ca. 2.7 Ga magmatic cores and a second being 2.34 Ga zones that recrystallized during metamorphism.

Sample QM-5B is a sample of the biotite-orthopyroxene-hornblende granitic gneiss that dominates location QM-5. 18 analyses were conducted on ten zircon grains in this specimen. Zircons are euhedral to subhedral and display either no zoning or prominent core-rim zoning. 13 analyses from both cores and rims provide a weighted

mean  $^{207}\text{Pb}/^{206}\text{Pb}$  age of  $2698 \pm 11$  Ma with MSWD = 1.4. This is interpreted as being the best estimate for the crystallization age of this granite. The remaining five analyses are slightly discordant, only partially overlapping the concordia curve, and are from unzoned zircons that appear to have been recrystallized and from near the rims of zircon grains. These analyses are grouped into two clusters at roughly 2.45 and 2.60 Ga. It is uncertain whether these analyses represent Pb loss, recrystallization, or both, during one or more metamorphic events that took place in the Neoproterozoic and Paleoproterozoic.

Locations QM-4 and QM-5 are strikingly similar in terms of both lithology and geochronology. Granitic gneisses from both locations were emplaced ca. 2.7 Ga, there is evidence for inheritance of an early Mesoarchean component, and the U-Pb systematics of the two samples may be complicated by multiple metamorphic events that took place in the Neoproterozoic and Paleoproterozoic.

#### Location QM-6

Location QM-6 is located in what is mapped as the TTZ. The outcrop is dominated by distinctly grey-weathering gneissic granodiorite that is locally porphyritic, strongly magnetic, and contains common mafic inclusions. The highly magnetic nature of these rocks is consistent with the observation that the TTZ is defined by an area of high aeromagnetic signature. No similar looking magmatic rocks were encountered within the QMB. Geochronological data from this location are summarized in Figure 3-4.

Sample QM-6B is a sample of the granodiorite gneiss that dominates this outcrop. 13 analyses were conducted on eight zircon grains in this sample. Zircons often contain well defined oscillatory zoned cores and are generally heavily fractured. Analyses are slightly discordant and cluster around 2.01 Ga. A weighted mean  $^{207}\text{Pb}/^{206}\text{Pb}$  age from eight analyses is calculated at  $2009 \pm 17$  Ma with MSWD = 4.4. This is interpreted as being the approximate age of crystallization of this granodiorite. The remaining analyses exhibit slightly older  $^{207}\text{Pb}/^{206}\text{Pb}$  ages, which are interpreted as being due to zircon inheritance and subsequent Pb loss. The oldest analysis provides a  $^{207}\text{Pb}/^{206}\text{Pb}$  age of  $2347 \pm 52$  from the rim of a heavily fractured zircon that appears to have undergone partial resorption. Core analyses of this grain provide  $^{207}\text{Pb}/^{206}\text{Pb}$  ages of  $2110 \pm 34$  Ma and  $2065 \pm 33$  Ma. It is interpreted that the core of this inherited grain underwent more Pb loss than the rim, resulting in these younger ages.

Location QM-7

This location is dominated by granitoid gneisses of variable composition ranging from tonalitic to granitic. Mafic and metasedimentary enclaves are found within these granitoid rocks. An anastomosing high-strain zone several meters wide trending in a NNE direction with a 70° dip to the SSE cuts through this outcrop. Within this high-strain zone rocks contain greenschist-facies mineral assemblages that contrast sharply with the upper amphibolite- to granulite-facies assemblages outside the shear zone. Geochronological data from this location are summarized in Figure 3-5.

Sample QM-7A is a biotite-magnetite-clinopyroxene-orthopyroxene granodiorite gneiss collected from outside of the high-strain zone. 13 analyses were conducted on six monazite grains. Monazite grains are both irregularly shaped and mottled, or much smaller with regular shapes and uniform textures. Analyses are clearly clustered and are concordant to moderately discordant. A weighted mean  $^{207}\text{Pb}/^{206}\text{Pb}$  age of  $2361.8 \pm 4.9$  Ma with MSWD = 1.01 was calculated from 12 of these analyses. It is interpreted that this age represents the timing of metamorphism of this sample.

Sample QM-7C is a biotite-hornblende tonalitic gneiss. 10 analyses were conducted on six zircon grains from this sample. Zircon grains are euhedral to subhedral and variably metamict. Faint oscillatory zoning and core-rim zoning is visible in some grains. Eight analyses fall along a well defined discordia line with an upper intercept age of  $3107 \pm 40$  Ma and a lower intercept age of  $717 \pm 320$  with MSWD = 2.8. The upper intercept age is interpreted as the approximate age of crystallization, and the lower intercept is likely due to Pb loss during Phanerozoic surface weathering. The two most concordant of these analyses are from the least metamict areas analysed and provide a weighted mean  $^{207}\text{Pb}/^{206}\text{Pb}$  age of  $3104 \pm 13$  Ma with MSWD = 0.17. The remaining analysis has 15.9 % discordance and a  $^{207}\text{Pb}/^{206}\text{Pb}$  age of  $2456 \pm 23$  Ma, which may be related to Paleoproterozoic metamorphism.

Sample QM-7D is a magnetite-garnet-orthopyroxene-biotite semi-pelitic gneiss. The sample was collected from a large enclave within host granitoid rocks. Nine analyses were conducted on four monazite grains. Monazite grains are mottled in their appearance and lack any patterned zoning.  $^{207}\text{Pb}/^{206}\text{Pb}$  ages from this sample span a range from approximately 2.36 to 2.14 Ga. Similar to location QM-1, this spreading of ages could be the result of two or more periods of monazite growth during the earliest Paleoproterozoic, though based on BSE image it is difficult to resolve any potential age domains.

This outcrop is dominated by magmatic rocks that crystallized ca. 3.1 Ga and were metamorphosed in the Paleoproterozoic. A difference in metamorphic monazite ages in samples QM-7A and QM-7D is readily apparent. In the former sample, analyses are clearly clustered and define a weighted mean  $^{207}\text{Pb}/^{206}\text{Pb}$  age of approximately 2.36 Ga, while in the latter  $^{207}\text{Pb}/^{206}\text{Pb}$  ages span a range between 2.36 and 2.14 Ga. Due to the proximity of where the two samples were collected from one must assume that they both underwent the same tectonic events in the Paleoproterozoic. Therefore, the inconsistency in the distribution of their U-Pb ages is attributed to differences in their bulk composition. It is possible that being a semi-pelite, sample QM-7D is more reactive and susceptible to the effects of metamorphism than sample QM-7A, which is a relatively anhydrous granodiorite.

#### Location QM-8

Site QM-8 is composed of an undeformed and unmetamorphosed gabbro and a pink-weathering granite. The gabbro is intruded by, and occurs as xenoliths within the granite. The gabbro is composed of plagioclase as well as biotite, hornblende, and clinopyroxene. The granite contains hornblende, biotite, and plagioclase, as well as abundant K-feldspar and quartz. Geochronological data from this location are summarized in Figure 3-6.

Sample QM-8A was collected from a coarse-grained, leucocratic segregation in the gabbro body, and likely represents a late-stage differentiate of the gabbroic magma. In addition to the clinopyroxene-plagioclase mineralogy that is typical of the gabbro, the segregation also contains hornblende, biotite, alkali feldspar and quartz. Zircon grains obtained after mineral separation are irregularly shaped and have a yellow-brown to colorless hue. In general, the more strongly colored grains have larger proportions of metamict zones than the colorless grains. Aside from small to moderate degrees of radiation damage in some grains, these zircons lack any distinct zoning. U-Pb ages were acquired from 26 zircon grains. The 26 analyses yield a weighted mean  $^{207}\text{Pb}/^{206}\text{Pb}$  age of  $2323.4 \pm 5.5$  Ma age with a MSWD of 4.2. Removal of 3 outlier analyses that are more than  $2\sigma$  off of the mean value yields a weighted mean  $^{207}\text{Pb}/^{206}\text{Pb}$  age of  $2321.8 \pm 3.8$  Ma with a substantially smaller MSWD of 1.8. This date is interpreted as the best estimate of the crystallization age of the gabbro body.

Sample QM-8B is a sample of the hornblende-biotite granite. Two thin-sections were made in order to obtain a well constrained age of this undeformed granite. 14

analyses were conducted on nine zircon grains from one thin-section and an additional 19 analyses from 10 zircon grains were conducted on the second thin-section. Zircons are generally euhedral to subhedral, display prominent oscillatory zoning, and are heavily fractured. There is some variation in the discordance of the analyses but the weighted mean  $^{207}\text{Pb}/^{206}\text{Pb}$  age from 29 of the 33 analyses is calculated at  $2319.0 \pm 4.3$  Ma with  $\text{MSWD} = 2.6$ . This is interpreted as being the crystallization age of this granite. One anomalous analysis reveals a  $^{207}\text{Pb}/^{206}\text{Pb}$  age of  $2997 \pm 12$  Ma. It is interpreted that this analysis is from an inherited zircon.

Geochronological data from this location are consistent with field observations. A 2322 Ma gabbro is intruded by a 2319 Ma granite. The granite preserves evidence for inheritance of Mesoarchean material. The rocks at this location preserve no geochronological or textural evidence for metamorphism.

#### Location QM-9

This outcrop is dominated by orthopyroxene-bearing granitic gneisses, and garnet-biotite psammitic migmatite. A large mafic dyke and several smaller pegmatite dykes cross-cut the gneissosity of the host rocks. One of the most striking features of this outcrop is a prominent southwest plunging fold, wherein gneissosity is folded. Within this fold is a pegmatite dyke that itself is folded but cross-cuts the gneissic fabric of the host rocks. Outside of the folded area, rocks are very highly strained and are deformed into straight gneiss. Heywood (1961) mapped a NNE-SSW trending fault in this area, similar to the direction of gneissosity in the high-strain zone documented at location QM-13. Geochronological data from this location are summarized in Figure 3-7.

Sample QM-9C is a garnet-biotite psammitic migmatite. Two analyses on two zircon grains and 21 analyses on six monazite grains were conducted. The two zircon grains analysed are well rounded with some fracturing and faint zoning, and one occurs as an inclusion in garnet.  $^{207}\text{Pb}/^{206}\text{Pb}$  age dates from the two zircon grains are  $3200 \pm 10$  and  $3201 \pm 12$  Ma. The zircon grains are thought to be detrital in origin. Monazite grains exhibit irregular zoning profiles defined by light and relatively dark areas. 11 of the monazite analyses define a cluster of concordant ages with a weighted mean  $^{207}\text{Pb}/^{206}\text{Pb}$  age of  $2423.7 \pm 7.9$  Ma with  $\text{MSWD} = 18$ . These analyses are from lighter colored areas of monazite grains.  $^{207}\text{Pb}/^{206}\text{Pb}$  ages from the remaining ten analyses are concordant and span a range from 2.42-2.13 Ga.



Sample QM-9D was collected from the pegmatite dyke described above. A total of nine analyses were conducted on three monazite grains. Monazite is found both within fractures of large apatite crystals and partially rimming apatite. This relationship indicates that the monazite is most likely a secondary feature, having grown sometime after the initial crystallization of this pegmatite dyke.  $^{207}\text{Pb}/^{206}\text{Pb}$  ages are concordant to moderately discordant and spread between 2.21 and 1.97 Ga. The oldest analysis of  $2.21 \pm 0.18$  Ga provides a minimum crystallization age for this pegmatite dyke. The ages provided by this sample are younger than most metamorphic ages from the QMB. This, combined with the atypical morphology of these grains, makes interpreting the significance of these ages difficult.

Geochronological analysis of rocks from this location yields interesting results. Evidence for earliest Mesoarchean crust is preserved as detrital zircons in sample QM-9C. A prominent cluster of monazite analyses from this sample provides a ca. 2.42 Ga metamorphic age. Such ages are rare in the QMB, but are also documented at locations QM-13 and ST-4 (Schultz, 2007). Similar to other samples analysed, an array of early Paleoproterozoic monazite ages is preserved in samples from this location. It is thought that this array of ages is due multiple episodes of monazite growth.

#### Location QM-10

Location QM-10 consists of layered gneiss of highly variable lithology. The majority of the location is composed of two distinct varieties of granite. Pelitic and mafic sheets are less common and several cross-cutting mafic dykes roughly 1 m across are present as well. Geochronological data from this location are summarized in Figure 3-8.

Sample QM-10A is a biotite-hornblende-clinopyroxene-orthopyroxene granitic gneiss. 11 analyses were conducted on five zircon grains, all of which are irregularly shaped and fairly well rounded. Zircon grains have patchy, discontinuous zoning patterns. Seven analyses that are well clustered and concordant to moderately discordant define a weighted mean  $^{207}\text{Pb}/^{206}\text{Pb}$  age of  $3159 \pm 13$  Ma with MSWD = 1.8. This is interpreted as being the crystallization age of this granite. The remaining four analyses are all roughly 12% discordant and have  $^{207}\text{Pb}/^{206}\text{Pb}$  ages spread between 2961 and 2685 Ma, possibly the result of Pb loss and recrystallization during Archean or Paleoproterozoic metamorphism.

Sample QM-10B is a biotite-magnetite granitic gneiss containing zircon and monazite grains, both of which were dated. Three zircon grains from this sample were

analyzed a total of five times. Zircon grains are subhedral with rounded edges and exhibit patchy zoning patterns. Analyses are concordant or roughly 15% discordant and provide similar but highly spread  $^{207}\text{Pb}/^{206}\text{Pb}$  ages. The weighted mean  $^{207}\text{Pb}/^{206}\text{Pb}$  age of these analyses is  $3114 \pm 68$  Ma with MSWD = 106. These data indicate that the granitic protolith of the gneiss is Mesoarchean but, given the large MSWD, its exact age remains poorly constrained. 18 analyses were conducted on five monazite grains. Monazite grains are regular in their shape and lack any distinct zoning patterns. A weighted mean  $^{207}\text{Pb}/^{206}\text{Pb}$  age of a distinct cluster of seven monazite analyses is calculated at  $2347.8 \pm 6.5$  Ma with MSWD = 0.46. Nine of the remaining monazite analyses are fairly concordant and exhibit  $^{207}\text{Pb}/^{206}\text{Pb}$  ages spread between approximately 2.35 and 2.20 Ga. Similar to other samples exhibiting monazite ages in this range, it is possible that several discrete age populations exist and some analyses represent the mixing of these age domains.

QM-10C is an orthopyroxene-cordierite-biotite semi-pelite. Thirteen analyses were conducted on three monazite grains. Monazite grains are regularly shaped, laden with inclusions, and lack any clear zoning patterns. Two distinct clusters of ages are recorded in this sample. Whereas two of the monazite grains provide ages from only one of the two populations, the third monazite grain contains ages from both clusters. The older cluster, consisting of seven measurements, exhibits a weighted mean  $^{207}\text{Pb}/^{206}\text{Pb}$  age of  $2459 \pm 13$  Ma with MSWD = 26. The younger cluster, consisting of four measurements, provides a weighted mean  $^{207}\text{Pb}/^{206}\text{Pb}$  age of  $2365 \pm 12$  Ma with MSWD = 13. The older age population has distinctly higher radiogenic Pb contents than the younger population. Taken alone, these results can be interpreted one of two ways. First, is that both populations represent periods of in-situ monazite growth associated with two distinct metamorphic events. Alternatively, the older age could be interpreted as being inherited monazite grains, while the younger age could be the result of metamorphism. A detrital zircon study from this sample supports the interpretation that both monazite populations grew in-situ during metamorphic events, as the youngest detrital zircon is dated in the Mesoarchean (see Section 3.3). Schultz et al. (2007) report a similar pattern in monazite age populations in samples collected from the Sherman basin, but based on their own detrital analysis interpreted the older population as being inherited rather than grown in-situ.

QM-10D is a cordierite-orthopyroxene-garnet-biotite pelite. 14 analyses from four monazite grains were obtained from this sample. Monazite grains are irregularly

shaped and display patchy zoning. 13 of the analyses are concordant to slightly negatively discordant and are clearly clustered. The weighted mean  $^{207}\text{Pb}/^{206}\text{Pb}$  age from these 13 analyses is  $2360.9 \pm 7.5$  Ma with MSWD = 2.0. The remaining analysis provides a  $^{207}\text{Pb}/^{206}\text{Pb}$  age of  $2189 \pm 20$  Ma. The cluster of ages at 2.36 Ga is interpreted to be the result of monazite growth during metamorphism.

This location is dominated by magmatic rocks that crystallized in the earliest Mesoproterozoic (Samples QM-10A, 10B). Several Neoproterozoic ages were acquired from sample QM-10A, indicating the possibility of metamorphic events during this time. Monazite ages from samples QM-10B, 10C, and 10D belong to several populations, all of which are interpreted to be metamorphic in origin. The oldest population is around 2.46 Ga, while the majority of analyses are dated between 2.36 and 2.35 Ga. A spreading of monazite ages from 2.35-2.20 Ga is observed in sample QM-10B, and is likely the result of one or more additional metamorphic events during this time.

#### Location QM-13

Location QM-13 is composed of a lithologically diverse suite of variably strained granitoid gneisses. The site is located along a NNE-SSW trending topographic depression several hundred meters wide that defines a prominent, large-scale shear zone, trending a similar direction to the one mapped by Heywood (1961) near location QM-9. Local zones of highly strained straight gneisses several meters wide are separated from each other by areas of lower strain wherein gneissosity is wavy. There is clear evidence for multiple generations of granitoid rocks at this outcrop. The older generation is strongly gneissic both within and outside of high strain zones and contains abundant dark grey colored, plagioclase-rich mafic inclusions. A younger generation is of alkali feldspar granite composition and intrudes the older generation. These pink alkali feldspar granite sheets locally truncate gneissosity at a low angle; however, within high-strain zones are themselves deformed. These observations suggest that these sheets may be syn-tectonic with the deformation event that formed the shear zones at this locality. Geochronological data from this location are summarized in Figure 3-9.

QM-13A is a biotite-orthopyroxene-hornblende granodioritic gneiss. This sample is moderately gneissic and was collected from outside of the high-strain zones described. Zircon grains are subhedral to anhedral and display poorly preserved oscillatory zoning in BSE image. Five analyses were conducted on two zircon grains. Analyses are concordant to moderately discordant. Three of these analyses are clearly clustered and define a

weighted mean  $^{207}\text{Pb}/^{206}\text{Pb}$  age of  $2455 \pm 17$  Ma with MSWD = 2.9. This is interpreted as being the approximate age of crystallization of this granitoid. The remaining two analyses record younger, slightly discordant  $^{207}\text{Pb}/^{206}\text{Pb}$  ages of  $2421 \pm 9$  and  $2410 \pm 14$  Ma, which may be related to Pb loss associated with one or more metamorphic events.

QM-13D is a clinopyroxene-biotite-hornblende straight gneiss of granitic bulk composition. This specimen was collected from within one of the high-strain zones. Eight analyses were conducted on five zircon grains in this specimen. Zircon grains are heavily fractured, contain numerous inclusions, are euhedral to anhedral, and are variably metamict. Three of these analyses partially overlap the concordia line and define a weighted mean  $^{207}\text{Pb}/^{206}\text{Pb}$  age of  $2488 \pm 55$  Ma with MSWD = 17. The remaining analyses are on average 10% discordant and provide  $^{207}\text{Pb}/^{206}\text{Pb}$  ages spread between 2413 and 2241 Ma. The variable appearance of zircon grains and the difficulty in obtaining ‘clean’ spots for analysis makes interpreting this data-set difficult. Given that this sample was collected from a zone of incredibly high-strain, these results are not surprising. It is possible that this granitoid crystallized at around 2488 Ma, similar to other granitoids from this outcrop, and that the discordance and spread in  $^{207}\text{Pb}/^{206}\text{Pb}$  ages is due to multiple metamorphic events. Alternatively, the data are fit reasonably well along a discordia line with intercepts at  $1401 +320/-260$  Ma and  $2548 +160/-63$  Ma with MSWD = 1.3.

Sample QM-13E is a hornblende-biotite-clinopyroxene-orthopyroxene granodiorite collected from outside the high-strain zones. 15 analyses were conducted on seven zircon grains. Seven of these analyses define a weighted mean  $^{207}\text{Pb}/^{206}\text{Pb}$  age of  $2450.4 \pm 6.6$  Ma with MSWD = 1.9. This is interpreted as being the age of crystallization of this granodiorite. A discordia line through these seven analyses provides intercept ages of  $-41 +240/-44$  Ma and  $2448 +20/-4.8$  Ma with MSWD = 0.52. Note that within error both the weighted mean and upper intercept ages are identical. The remaining analyses are typically around 20% discordant and spread between 2429 Ma to as young as 2291 Ma. These may be the result of Paleoproterozoic metamorphism with subsequent Pb loss related to surface weathering.

Sample QM-13G was collected from an alkali feldspar granite sheet that intrudes the granitic and granodioritic gneisses that dominate location QM-13, but is itself deformed in the high-strain zones. This sample was targeted for a mineral separation in order to determine the crystallization age of this rock, as well as to constrain the timing of the shear event. Zircon grains are generally colorless with local areas of reddish

coloration. In BSE image prominent oscillatory zoned cores surrounded by unzoned rims are visible in some of these grains. Other grains are elongate and subhedral with little to no internal structure. Others still are equant with little to no zoning. 30 zircon grains from this sample were analysed. A weighted mean  $^{207}\text{Pb}/^{206}\text{Pb}$  age from 24 of these analyses (two analyses are omitted due to high common Pb abundance, one due to high discordance and radiogenic Pb content, and three are more than  $2\sigma$  off the mean age) is  $2427.9 \pm 6.7$  Ma with MSWD = 1.8. Observation of spot location and BSE image analysis reveals that the oldest analyses are generally from oscillatory zoned cores of zircon grains and the youngest analyses are from the most equant, anhedral, and unzoned zircon grains. The remaining 18 analyses are generally from unzoned yet subhedral zircon grains and provide a weighted mean  $^{207}\text{Pb}/^{206}\text{Pb}$  age of  $2426.3 \pm 5.4$  Ma with MSWD = 0.45. The data can be interpreted in several ways. One is that the oscillatory zoned cores are inherited,  $2426.3 \pm 5.4$  Ma is the crystallization age of this granitoid, and any younger ages are due to Pb loss and recrystallization associated with metamorphism. Based on zircon morphology and spot location analysis, this is the favoured interpretation. Alternatively the oscillatory zoned cores may be magmatic, and all younger ages due to Pb loss and recrystallization associated with multiple metamorphic events, the primary event being at  $2426.3 \pm 5.4$  Ma. Regardless of which interpretation one favours, either crustal melting or significant metamorphic zircon growth occurred at 2.426 Ga.

Sample QM-13H was collected from one of the plagioclase-rich mafic inclusions found within the granodiorite gneiss in an area of relatively low-strain. 13 analyses were conducted of six zircon grains. Zircon grains in this sample are abundant, euhedral, and weakly zoned. Small, yet distinct zones of recrystallization are visible in BSE image. Ten analyses from outside the zones of recrystallization are concordant to slightly discordant and clearly clustered. These analyses define a weighted mean  $^{207}\text{Pb}/^{206}\text{Pb}$  age of  $2465.6 \pm 9.7$  Ma with MSWD = 8.7. This is interpreted to be the crystallization age of this mafic inclusion. The remaining three analyses come from the zones of recrystallization and provide concordant  $^{207}\text{Pb}/^{206}\text{Pb}$  ages spread between 2.39 and 2.35 Ga. These ages are likely the result of recrystallization during a metamorphic event.

This outcrop is dominated by granitic gneisses dated between 2.50 and 2.45 Ga, roughly the same age as Schultz et al. (2007) report for the Queen Maud granitoids. Numerous discordant ages, younger than the interpreted crystallization ages, are recorded and are attributed to metamorphism. An alkali feldspar granite sheet interpreted to have

intruded syntectonically with high-strain deformation was dated following mineral separation and either crystallized or was metamorphosed at 2.426 Ga.

Location QM-14 & QM-15

Locations QM-14 and QM-15 are dominated by granitic gneisses containing abundant plagioclase-rich mafic inclusions. The rocks present at these outcrops are similar in composition and geochronology to those present at location QM-13; however, they are not as highly strained. Geochronological data from these locations are summarized in Figure 3-10.

Sample QM-14A is a specimen of the orthopyroxene-biotite granitic gneiss that dominates this location. Eight analyses were conducted on five zircon grains in this specimen. Zircon grains are subhedral to anhedral and contain poorly developed oscillatory zoning or patchy zoning patterns. A weighted mean  $^{207}\text{Pb}/^{206}\text{Pb}$  age from four moderately discordant, yet clustered analyses is calculated at  $2532 \pm 29$  Ma with an MSWD = 9.8. These analyses were conducted on the cores of zircons and areas of zircon grains with the best developed oscillatory zoning. Although this age is poorly constrained and the data are discordant, it is interpreted that  $2532 \pm 29$  Ma is the best estimate for the crystallization age of this granitoid. Three of the remaining analyses are scattered near the concordia line and provide  $^{207}\text{Pb}/^{206}\text{Pb}$  ages of 2.46, 2.45, and 2.39 Ga. These analyses are from near the rim of a subhedral zircon, and from an unzoned, partially metamict zircon grain. It is interpreted that these ages are the result of Pb loss or recrystallization during Paleoproterozoic metamorphism.

QM-15A is an orthopyroxene-biotite granitic gneiss. 11 analyses were conducted on eight zircon grains in this specimen. Zircon grains are subhedral to anhedral. In BSE images, oscillatory zoning is faint and most zircon grains exhibit patchy zoning patterns. Six analyses from areas in zircon grains where relatively clear oscillatory zoning is preserved overlap the concordia curve or are slightly discordant. A weighted mean  $^{207}\text{Pb}/^{206}\text{Pb}$  age of  $2516 \pm 13$  Ma with MSWD = 3.1 is calculated from these analyses. This is interpreted as the approximate crystallization age of this granite. Three analyses are moderately discordant, exhibit a range of  $^{207}\text{Pb}/^{206}\text{Pb}$  ages between 2.48 and 2.32 Ga, and may represent partial Pb loss from igneous grains during younger Paleoproterozoic metamorphism.

Although the granitoids at locations QM-14 and QM-15 are similar in appearance to the 2.50-2.46 Ga Queen Maud granitoids described by Schultz et al. (2007) (i.e., they

are orange weathering, and contain large K-feldspar megacrysts), they exhibit slightly older crystallization ages of ~2.52 Ga. This suggests that the Queen Maud granitoid suite may include rocks older than previously thought.

#### Location QM-16

Location QM-16 is composed of orange weathering hornblende-biotite-orthopyroxene granite with large K-feldspar megacrysts. Abundant mafic inclusions are present throughout this granite. These rocks are metamorphosed, yet relatively unstrained, as this location lacks the gneissic textures prominent throughout the QMB. Geochronological data from this location are summarized in Figure 3-11.

Sample QM-16A is a specimen of the granite described above. 13 analyses were conducted on eight zircon grains. Zircon grains are subhedral with well developed oscillatory zoning and rounded edges. Analyses are moderately discordant and occur in two distinct clusters. One group includes eight concordant to ~10% discordant analyses and provides  $^{207}\text{Pb}/^{206}\text{Pb}$  ages from 2.63-2.72 Ga. The second group, which includes four concordant to 10% discordant analyses, provides  $^{207}\text{Pb}/^{206}\text{Pb}$  ages between 2.43 and 2.50 Ga. Both populations include analyses from oscillatory zoned zircon grains and from unzoned zircon grains. Since grains from the younger population exhibit oscillatory zoning, it is likely that crystallization of this granitoid occurred between 2.43 and 2.50 Ga, and that the older population is inherited.

Lithologically, this sample is comparable to QM-15A, which has a relatively well constrained age of  $2516 \pm 13$  Ma. Both granitoids are orange weathering and contain large K-feldspar megacrysts (Figures 3-10 & 3-11). Although the precise crystallization age of this granitoid is only loosely bracketed between 2.43 and 2.50 Ga, it is similar in appearance to other samples belonging to the Queen Maud granitoid suite.

#### Location QM-17

Location QM-17 consists primarily of greyish weathering, strongly gneissic orthopyroxene-biotite granodiorite to tonalite. Abundant lit-par-lit, pink weathering granitic veins intrude the granodiorite gneiss. Two boudinaged and metamorphosed mafic dykes are present as well. Geochronological data from this location are summarized in Figure 3-12.

Sample QM-17B was collected from one of the cross-cutting and boudinaged mafic dykes. Five analyses were conducted on three zircon grains. Zircons are irregularly

shaped and unzoned, except for extremely small cores. A weighted mean  $^{207}\text{Pb}/^{206}\text{Pb}$  age from three fairly concordant analyses is calculated at  $2390.8 \pm 3.2$  Ma with MSWD = 0.6. The remaining analyses are also fairly concordant and reveal slightly younger  $^{207}\text{Pb}/^{206}\text{Pb}$  ages of  $2368 \pm 7$  Ma and  $2321 \pm 12$  Ma. The younger zircon analyses are from a single zircon grain. A core analysis of this grain provides the 2321 Ma age, whereas the 2368 Ma age is from the rim of this grain. Evidently, the core of this grain underwent a relatively high amount of Pb loss compared to the rim. The 2368 Ma age may be a mixing of the 2.39 Ga age recorded in other grains and the younger core age. Due to the irregular shape and unzoned nature of these zircon grains it is interpreted that zircon growth in this sample occurred as a result of metamorphism (e.g., Corfu et al., 2003).

QM-17C is a sample of the host granodiorite gneiss. Eight analyses were conducted on five zircon grains. Zircons are euhedral to subhedral, exhibit poorly developed oscillatory zoning, and are partially metamict. A weighted mean  $^{207}\text{Pb}/^{206}\text{Pb}$  age from five moderately discordant analyses is calculated at  $3071 \pm 27$  Ma with MSWD = 2.4. Two of the remaining analyses are clustered around 2.8 Ga and the final analysis has a  $^{207}\text{Pb}/^{206}\text{Pb}$  age of approximately 2.25 Ga. The oldest  $^{207}\text{Pb}/^{206}\text{Pb}$  ages are from zircon grains exhibiting prominent oscillatory zoning, whereas younger analyses are from variably metamict zircon grains. It is interpreted that 3.07 Ga is the approximate crystallization age of the granodioritic protolith of this gneiss, and that the younger ages are due to Pb loss and recrystallization associated with one or more metamorphic events that took place in the Neoproterozoic and Paleoproterozoic.

The granitoid gneisses that dominate this outcrop crystallized in the earliest Mesoarchean at approximately 3.07 Ga, similar to other granitoids from the QMB analysed for the present study. This location was metamorphosed at approximately 2.39 Ga, based on the dating of metamorphic zircons in a cross-cutting mafic dyke.

### 3.3 – Detrital zircon results

#### Sample QM-1H

Sample QM-1H is a quartzite collected from the host gneiss at location QM-1. A detrital zircon study of this sample was conducted in order to constrain the maximum depositional age of this quartzite. The minimum age of deposition of this rock is approximately 2.35 Ga based on the oldest metamorphic age obtained from monazite analyses in other metasedimentary samples from this location.



Zircon grains are elongate to equant, euhedral to well rounded, and variable in color (Figure 3-13). The high degree of variation in morphology suggests multiple sources for these detrital zircon grains, and for some grains, significant distances of transportation. In BSE image some of these grains display prominent oscillatory zoning, while others are variably metamict or lack any distinct zoning (Figure 3-13).

U-Pb age dates were successfully acquired from 97 zircon grains. A probability density plot of  $^{207}\text{Pb}/^{206}\text{Pb}$  ages within 10% discordance and further culled based on bad spot locations (i.e., those located on inclusions or fractures) and high common Pb counts is shown in Figure 3-13 and includes 75 of these analyses. A similar distribution pattern is obtained when analyses within 5% discordance are plotted; however this probability density plot is not shown, as it only contains 43 analyses. The oldest ages obtained are latest Paleoproterozoic, between 3.2 and 3.3 Ga. A prominent peak in ages occurs between 2.8-3.0 Ga. Several smaller peaks occur around 2.7 and 2.6 Ga, and again from 2.5-2.4 Ga.

The youngest zircon exhibiting oscillatory zoning is dated at  $2576 \pm 28$  Ma. As mentioned, several analyses provide younger ages from 2.5-2.4 Ga. Although these ages are from crystalline zircons, many of which are subhedral, all grains younger than 2576 Ma lack obvious oscillatory zoning and therefore may be zircon grains that recrystallized during metamorphism. In one case, a zircon grain has been partially recrystallized; an analysis of this recrystallized domain provides a  $^{207}\text{Pb}/^{206}\text{Pb}$  age of  $2409 \pm 24$  Ma. These textural observations suggest that these zircons may be detrital grains that experienced significant Pb loss and recrystallization during post-depositional early Paleoproterozoic metamorphism.

The observation that detrital zircon ages span an exceptionally long time period is consistent with the observation that a wide range in zircon morphology was identified in mineral separate. The maximum depositional age of this quartzite is 2576 Ma, based on what is clearly the youngest detrital zircon. The minimum depositional age is approximately 2.35 Ga, based on the oldest metamorphic monazite age from this location (Sample QM-11). The origin of the zircon population dated between 2.5-2.4 Ga is inherently ambiguous. If this population is related to post-depositional metamorphism, then the timing of deposition of this sample remains constrained between 2.6 and 2.35 Ga; alternatively, if this population is in fact detrital, then the timing of deposition is constrained between approximately 2.4 and 2.35 Ga.

Sample QM-10C

Sample QM-10C is an orthopyroxene-biotite-cordierite semi-pelitic gneiss. Two distinct age populations from monazite grains analysed in-situ were identified in this sample. As previously discussed, the two populations are dated at approximately 2.46 and 2.37 Ga. The 2.37 Ga population is inferred to be due to metamorphism, however it is uncertain if the older, 2.46 Ga population, is detrital or metamorphic in origin. A detrital zircon study of this sample was carried out in order to determine: a) the origin of this older monazite population, and b) a maximum age constraint on deposition of this metasedimentary rock.

Zircon grains obtained from mineral separation are slender, elongate, and subrounded, commonly with red or beige hues (Figure 3-14). In BSE image many of these grains exhibit well developed oscillatory zoning, and approximately 10-20% of the grains have zones that are metamict. The subrounded yet elongate shape of these grains suggests a proximal source for these zircon grains.

U-Pb age dates from 105 zircon grains were acquired. A probability density plot of 78  $^{207}\text{Pb}/^{206}\text{Pb}$  ages within 10% discordance, and further screened based on an inferred non-detrital origin, is shown in Figure 3-14. The oldest analyses provide ages of approximately 3.3 Ga. The dominant age of zircon grains in this sample is around 3.2 Ga, similar to the Mesoarchean rocks dated at this outcrop. The youngest zircon dated that exhibits oscillatory zoning provides a  $^{207}\text{Pb}/^{206}\text{Pb}$  age of  $3089 \pm 33$  Ma. This age represents the maximum age of deposition of this sample. Two slightly younger grains provide  $^{207}\text{Pb}/^{206}\text{Pb}$  ages of 3042 and 3010 Ma, and three provide ages between 2404 and 2564 Ma. However, none of these grains display oscillatory zoning and these ages are interpreted to be the result of new zircon growth or extensive Pb loss from Mesoarchean zircons during post-depositional metamorphism.

Since the youngest detrital zircon in this sample is dated at 3089 Ma, it is likely that both the 2.37 and the 2.46 Ga monazite populations are metamorphic in origin. If this is indeed the case, then the depositional age of this sediment is bracketed between 3.09 and 2.46 Ga.

Table 3-1: Summary of U-Pb ages acquired through in-situ and grain mount LA-ICP-MS dating

Sample	Rock Type*	Min**	Age (Ga)	Age Type	Interpretation	n	MSWD
QM-1A	Bt-Opx granitic gneiss	Mnz	2.26-2.09	<sup>207</sup> Pb/ <sup>206</sup> Pb	Metamorphic	11	
QM-1C	Grt-Cpx-Hbl mafic dyke	Zir##	1.928 ± 0.007	<sup>207</sup> Pb/ <sup>206</sup> Pb mean	Metamorphic	20	0.83
		Zir##	2.104 ± 0.014	<sup>207</sup> Pb/ <sup>206</sup> Pb mean	Min. crystallization	6	0.77
QM-1D	Mafic dyke/host gneiss (from contact)	Mnz	2.30-2.08	<sup>207</sup> Pb/ <sup>206</sup> Pb	Metamorphic	14	
		Mnz	1.843 ± 0.021	<sup>207</sup> Pb/ <sup>206</sup> Pb	Metamorphic	1	
QM-1H	Quartzite	Zir##	2.576 ± 0.028	<sup>207</sup> Pb/ <sup>206</sup> Pb	Youngest Detrital	1	
QM-1I	Sil-Opx-Grt-Kspar-Bt semi-pelitic gneiss	Mnz	2.350 ± 0.006	<sup>207</sup> Pb/ <sup>206</sup> Pb	Metamorphic	1	
		Mnz	2.23-2.10	<sup>207</sup> Pb/ <sup>206</sup> Pb	Metamorphic	7	
QM-2C	Hbl-Bt-Opx granodioritic gneiss	Zir	3.205 ± 0.031	Upper Intercept	Crystallization	8	4.9
		Zir	2.365 ± 0.005	<sup>207</sup> Pb/ <sup>206</sup> Pb mean	Metamorphic	4	0.16
QM-2D	Hbl-Bt granitic gneiss	Zir	3.227 ± 0.019	Upper Intercept	Crystallization	5	0.38
		Zir	2.43-2.31	<sup>207</sup> Pb/ <sup>206</sup> Pb	Uncertain	4	
QM-4B	Bt-Hbl-Opx granitic gneiss	Zir	3.123 ± 0.010	<sup>207</sup> Pb/ <sup>206</sup> Pb	Inherited	1	
		Zir	2.704 ± 0.026	<sup>207</sup> Pb/ <sup>206</sup> Pb mean	Crystallization	4	11.3
		Zir	2.65-2.34	<sup>207</sup> Pb/ <sup>206</sup> Pb	Metamorphic	5	
QM-5B	Bt-Opx-Hbl granitic gneiss	Zir	2.698 ± 0.011	<sup>207</sup> Pb/ <sup>206</sup> Pb mean	Crystallization	12	1.4
		Zir	2.60-2.45	<sup>207</sup> Pb/ <sup>206</sup> Pb	Metamorphic	6	
QM-6B	Cpx-Bt-Hbl granitic gneiss	Zir	2.009 ± 0.017	<sup>207</sup> Pb/ <sup>206</sup> Pb mean	Crystallization	8	4.4
		Zir	2.35	<sup>207</sup> Pb/ <sup>206</sup> Pb	Inherited	1	
QM-7A	Cpx-Bt-Opx granodioritic gneiss	Mnz	2.362 ± 0.005	<sup>207</sup> Pb/ <sup>206</sup> Pb mean	Metamorphic	12	1.01
QM-7C	Bt-Hbl tonalitic gneiss	Zir	3.107 ± 0.040	Upper Intercept	Crystallization	8	2.8
		Zir	2.456 ± 0.023	<sup>207</sup> Pb/ <sup>206</sup> Pb	Metamorphic	1	
QM-7D	Grt-Opx-Bt semi-pelitic gneiss	Mnz	2.36-2.14	<sup>207</sup> Pb/ <sup>206</sup> Pb	Metamorphic	9	
QM-8A	Gabbro	Zir##	2.322 ± 0.004	<sup>207</sup> Pb/ <sup>206</sup> Pb mean	Crystallization	23	1.8
QM-8B	Bt-Hbl granite	Zir	2.319 ± 0.004	<sup>207</sup> Pb/ <sup>206</sup> Pb mean	Crystallization	29	2.6
		Zir	2.997 ± 0.012	<sup>207</sup> Pb/ <sup>206</sup> Pb	Inherited	1	
QM-9C	Grt-Bt psammitic migmatite	Mnz	2.424 ± 0.008	<sup>207</sup> Pb/ <sup>206</sup> Pb mean	Metamorphic	11	18
		Mnz	2.42-2.13	<sup>207</sup> Pb/ <sup>206</sup> Pb	Metamorphic	10	
		Zir	~3.2	<sup>207</sup> Pb/ <sup>206</sup> Pb	Inherited	2	
QM-9D	Granitic pegmatite	Mnz	2.205 ± 0.018	<sup>207</sup> Pb/ <sup>206</sup> Pb age	Min. crystallization	1	
		Mnz	2.21-1.97	<sup>207</sup> Pb/ <sup>206</sup> Pb	Uncertain	9	
QM-10A	Bt-Hbl-Opx-Cpx granitic gneiss	Zir	3.159 ± 0.013	<sup>207</sup> Pb/ <sup>206</sup> Pb mean	Crystallization	7	1.8
		Zir	2.96-2.65	<sup>207</sup> Pb/ <sup>206</sup> Pb	Metamorphic	4	
QM-10B	Opx-Bt granitic gneiss	Mnz	2.348 ± 0.007	<sup>207</sup> Pb/ <sup>206</sup> Pb mean	Metamorphic	7	26
		Mnz	2.35-2.20	<sup>207</sup> Pb/ <sup>206</sup> Pb	Metamorphic	9	
		Zir	3.114 ± 0.068	<sup>207</sup> Pb/ <sup>206</sup> Pb mean	~Crystallization	5	106
QM-10C	Opx-Bt-Crd semi-pelitic gneiss	Mnz	2.459 ± 0.013	<sup>207</sup> Pb/ <sup>206</sup> Pb mean	Metamorphic	7	26
		Mnz	2.365 ± 0.012	<sup>207</sup> Pb/ <sup>206</sup> Pb mean	Metamorphic	4	13
		Zir##	3.089 ± 0.033	<sup>207</sup> Pb/ <sup>206</sup> Pb	Youngest Detrital	1	
QM-10D	Sil-Crd-Opx-Grt-Bt pelitic gneiss	Mnz	2.361 ± 0.008	<sup>207</sup> Pb/ <sup>206</sup> Pb mean	Metamorphic	13	2.0
		Mnz	2.189 ± 0.020	<sup>207</sup> Pb/ <sup>206</sup> Pb	Metamorphic	1	
QM-13A	Bt-Opx-Hbl granodioritic gneiss	Zir	2.455 ± 0.017	<sup>207</sup> Pb/ <sup>206</sup> Pb mean	Crystallization	3	2.9
		Zir	2.42-2.41	<sup>207</sup> Pb/ <sup>206</sup> Pb	Metamorphic	2	
QM-13D	Cpx-Bt-Hbl straight gneiss	Zir	2.47-2.24	<sup>207</sup> Pb/ <sup>206</sup> Pb	Uncertain	8	
QM-13E	Hbl-Bt-Cpx-Opx granodioritic gneiss	Zir	2.450 ± 0.007	<sup>207</sup> Pb/ <sup>206</sup> Pb mean	Crystallization	7	1.9
		Zir	2.43-2.29	<sup>207</sup> Pb/ <sup>206</sup> Pb	Metamorphic	8	
QM-13G	Alkali-feldspar granite	Zir##	2.426 ± 0.005	<sup>207</sup> Pb/ <sup>206</sup> Pb mean	Crystallization?	18	0.45
QM-13H	Mafic enclave	Zir	2.466 ± 0.010	<sup>207</sup> Pb/ <sup>206</sup> Pb mean	Crystallization	10	8.7
		Zir	2.39-2.35	<sup>207</sup> Pb/ <sup>206</sup> Pb	Metamorphic	3	
QM-14A	Bt granitic gneiss	Zir	2.532 ± 0.029	<sup>207</sup> Pb/ <sup>206</sup> Pb mean	Crystallization	4	9.8
		Zir	2.46-2.39	<sup>207</sup> Pb/ <sup>206</sup> Pb	Metamorphic	3	
QM-15A	Opx-Bt granitic gneiss	Zir	2.516 ± 0.013	<sup>207</sup> Pb/ <sup>206</sup> Pb mean	Crystallization	6	3.1
		Zir	2.48-2.32	<sup>207</sup> Pb/ <sup>206</sup> Pb	Metamorphic	3	
QM-16A	Hbl-Opx-Bt granite	Zir	2.63-2.72	<sup>207</sup> Pb/ <sup>206</sup> Pb	Inherited	8	
		Zir	2.43-2.50	<sup>207</sup> Pb/ <sup>206</sup> Pb	~Crystallization	4	
QM-17B	Mafic dyke	Zir	2.391 ± 0.003	<sup>207</sup> Pb/ <sup>206</sup> Pb mean	Metamorphic	3	0.6
QM-17C	Opx-Bt granodioritic gneiss	Zir	3.071 ± 0.027	<sup>207</sup> Pb/ <sup>206</sup> Pb mean	Crystallization	5	2.4
		Zir	2.86-2.25	<sup>207</sup> Pb/ <sup>206</sup> Pb	Metamorphic	3	

\*Bt = biotite, Opx = orthopyroxene, Sil = sillimanite, Grt = garnet, Kspar = k-feldspar, Hbl = hornblende, Cpx = clinopyroxene, Crd = cordierite

\*\* Min = mineral, Zir = zircon, Mnz = monazite

##Age acquired through grain mount dating; all others acquired in-situ in petrographic thin-section.

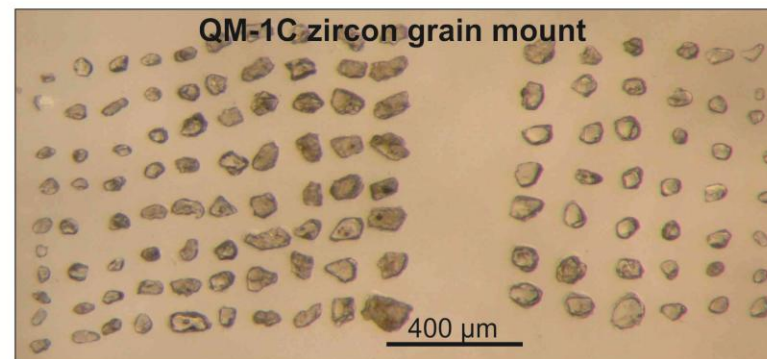
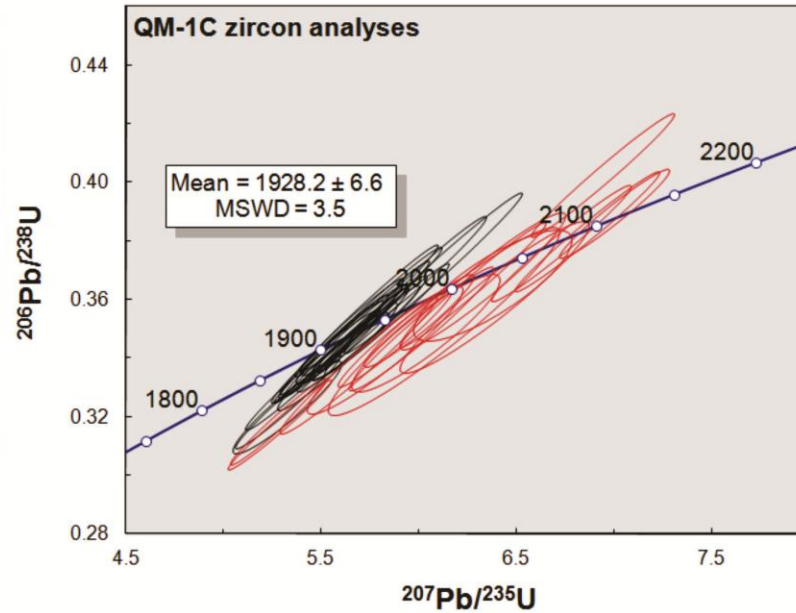
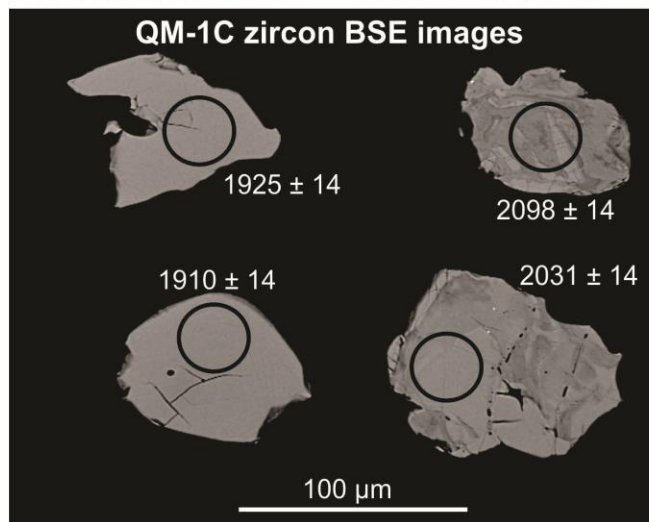
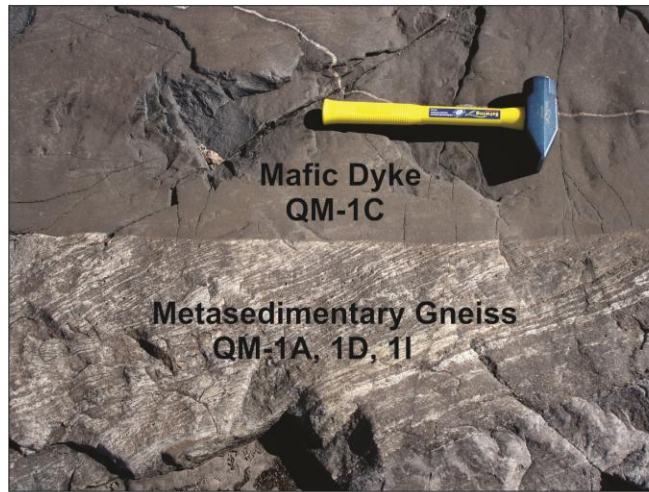


Figure 3-1 (1 of 2): Location QM-1 geochronology summary. Outcrop photograph shows cross-cutting mafic dyke and host metasedimentary gneiss. Concordia plot, BSE images and zircon grain mount photograph from sample QM-1C, the cross-cutting mafic dyke, are shown. Analyses shown as black ellipses are used in calculating the weighted mean  $^{207}\text{Pb}/^{206}\text{Pb}$  age of 1928.2 Ma. Note that metamict zircon grains provide older ages than non metamict grains. This provides evidence for their being magmatic grains that underwent Pb loss during 1928.2 Ma metamorphism.

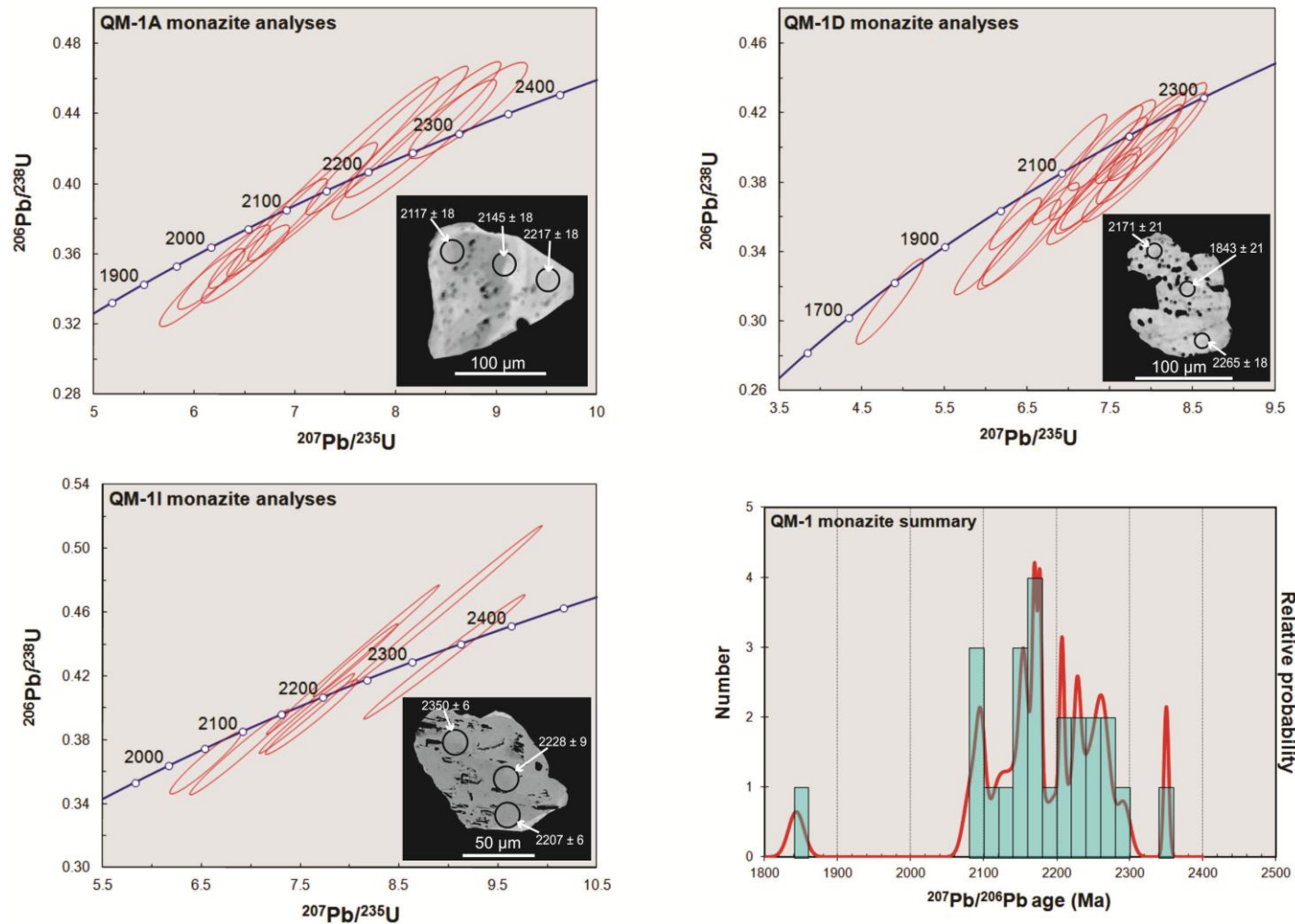


Figure 3-1 (2 of 2): Location QM-1 geochronology summary (continued). Concordia plots and select BSE images of monazite grains from metasedimentary samples QM-1A, QM-1D, and QM-1I. Note that multiple ages are present in individual monazite grains. Also note that monazite ages from all three samples are not evenly spread across the period from 2.3-2.1 Ga, but occur as several distinct peaks, as shown in the probability density plot. This provides evidence for multiple age domains present in these monazite grains.

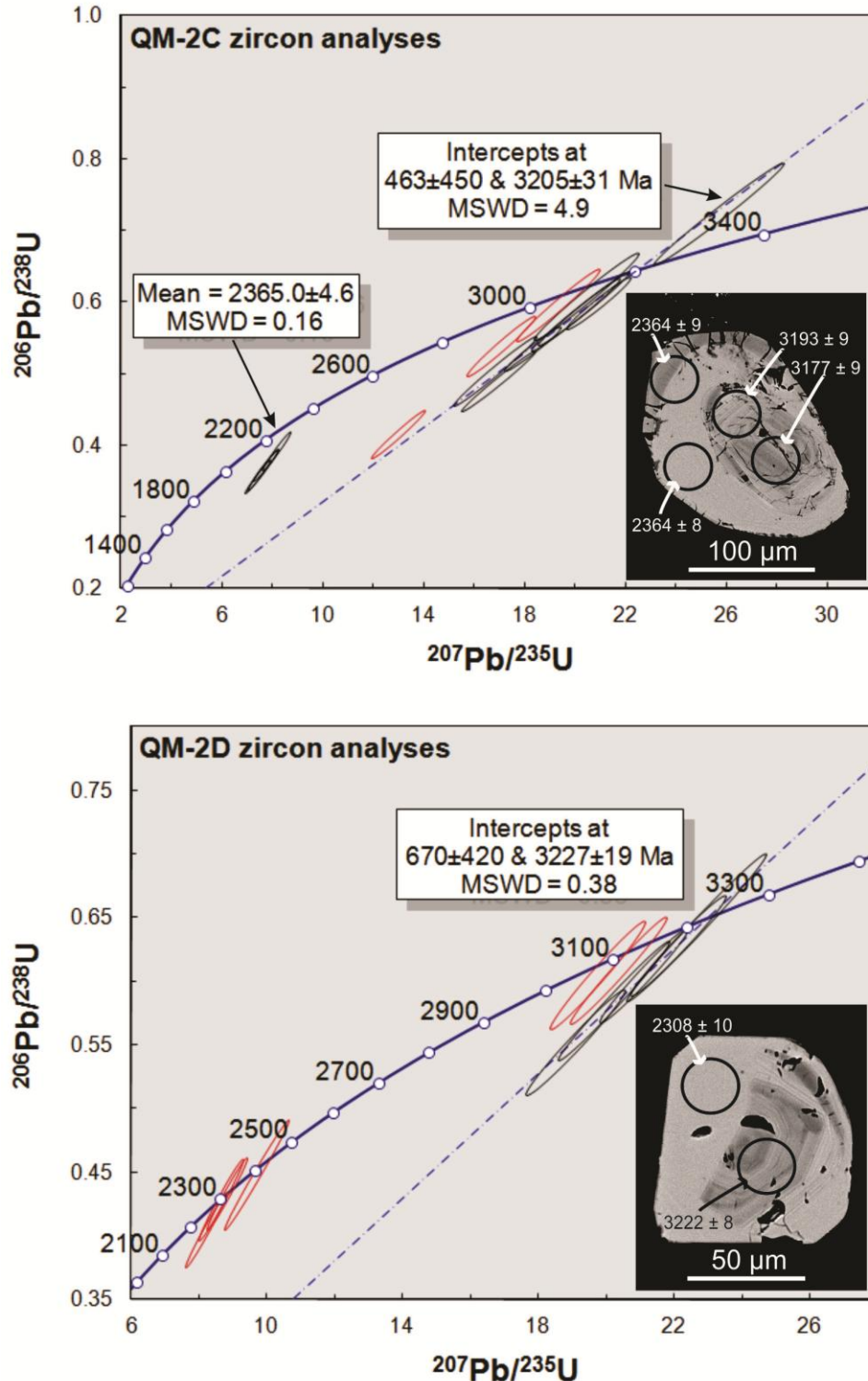


Figure 3-2: Location QM-2 geochronology summary. Concordia plots and select BSE images of zircon grains from samples QM-2C and QM-2D, both granitoid gneisses, are shown. Analyses shown as black ellipses are used in calculating ages quoted in the diagrams. Note that for both samples the younger ages are from spots that analysed unzoned, recrystallized areas of zircon grains, whereas older analyses are from oscillatory zoned areas. This provides evidence for the older, ca. 3.2 Ga, ages being magmatic, and younger ages being metamorphic in origin.



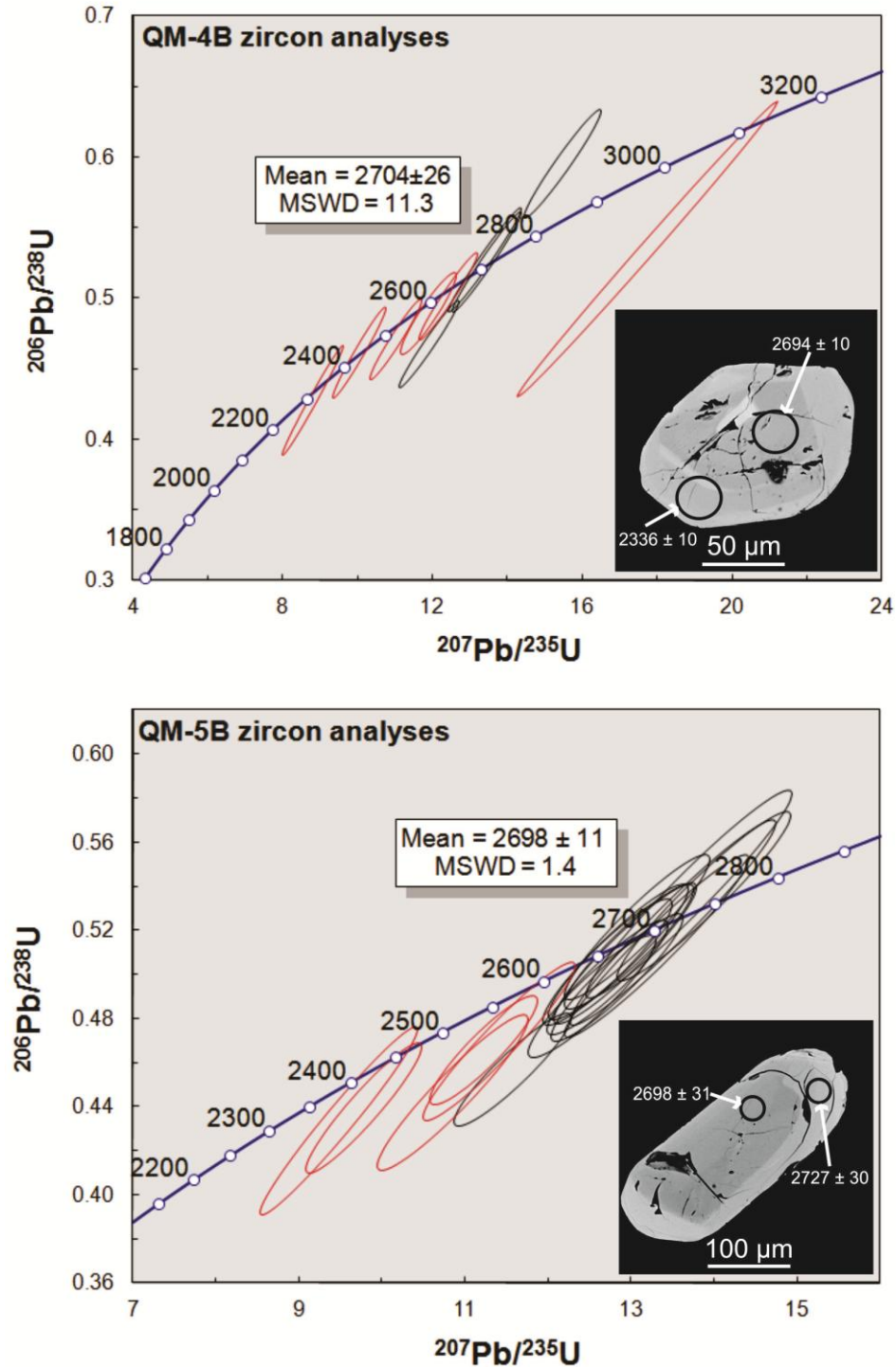


Figure 3-3: Locations QM-4 & QM-5 geochronology summary. Concordia plots and select BSE images of zircon grains from samples QM-4B and QM-5B, both granitoid gneisses, are shown. Analyses shown as black ellipses are used in calculating ages quoted in the diagrams. Quoted ages of approximately 2.7 Ga are crystallization ages of these granitoids. Note the presence of a single older analysis, thought to be an inherited grain, and multiple younger analyses possibly due to Pb loss and recrystallization during multiple Neoproterozoic and Paleoproterozoic metamorphic events.

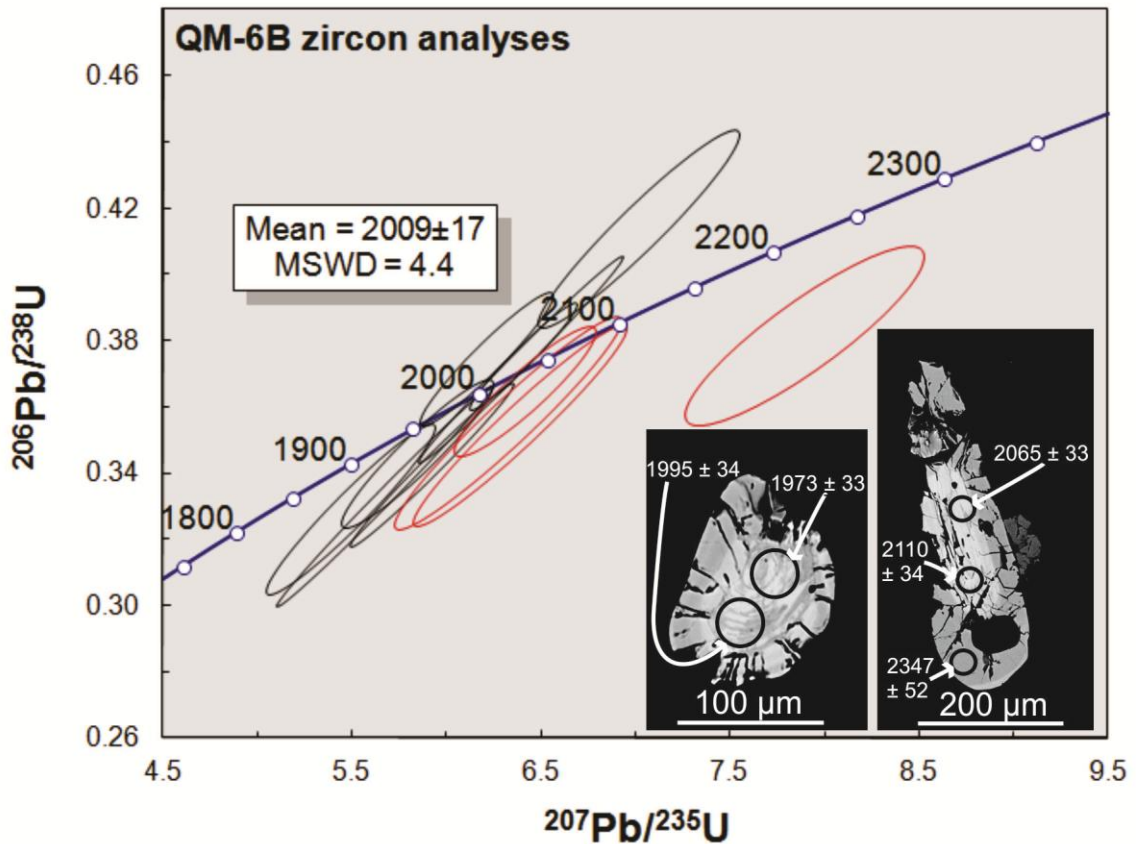


Figure 3-4: Location QM-6 geochronology summary. Concordia plot and select BSE images of zircon grains from sample QM-6B, a granitoid gneiss. Analyses shown as black ellipses are used in calculating the age quoted in the diagram. Analyses from oscillatory zoned grains are clustered at around 2009 Ma, the crystallization age of this granitoid, whereas older analyses are from the zircon grain shown at the right. This is thought to be an inherited zircon grain whose core underwent a high amount of Pb loss relative to its rim, as evidenced by the younger analyses from spots near the core of the grain.



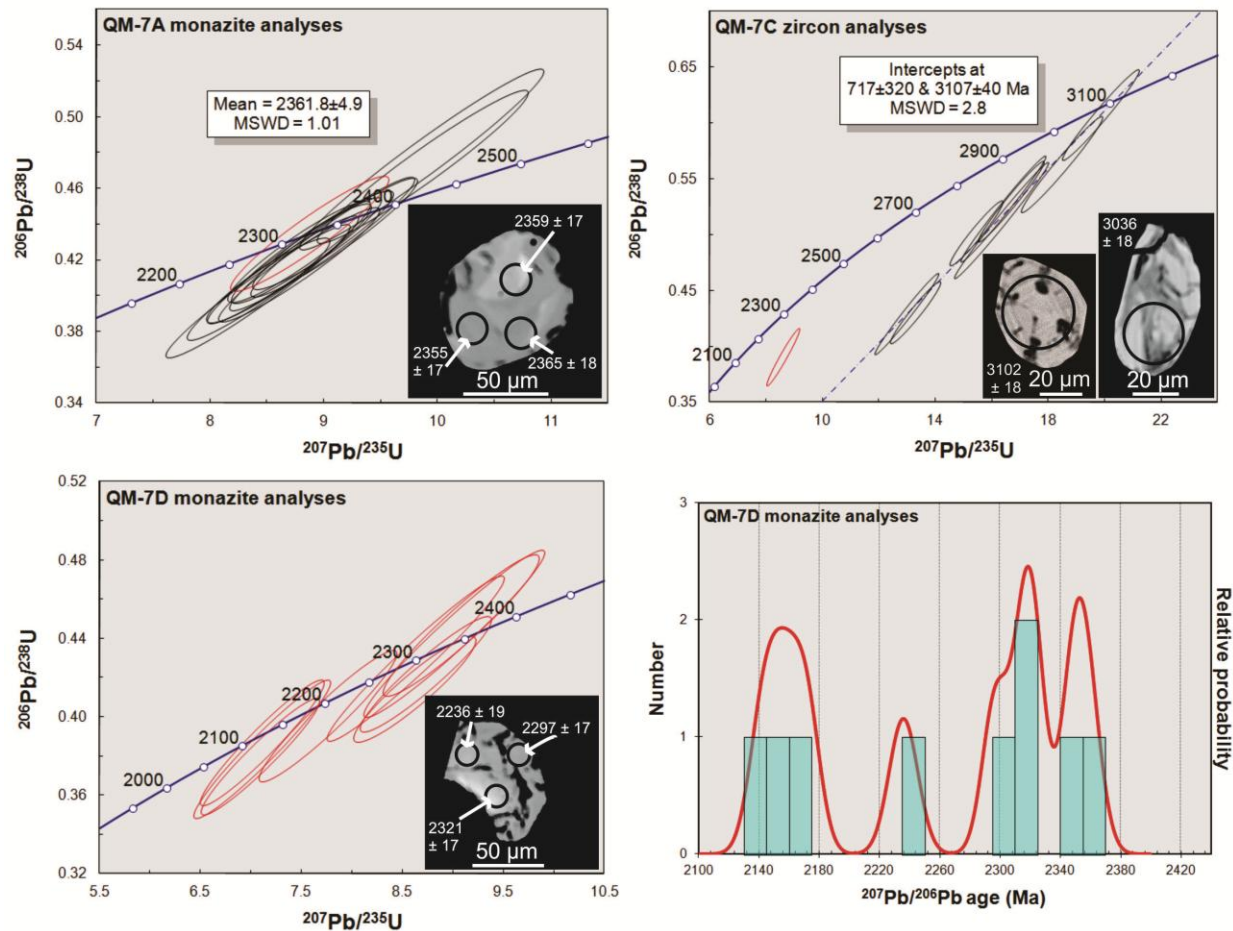


Figure 3-5: Location QM-7 geochronology summary. Concordia plot and select BSE images of zircon and monazite grains from samples QM-7A, QM-7C, and QM-7D are shown. Analyses shown as black ellipses are used in calculating the ages quoted in the diagrams. Sample QM-7A is a granitoid gneiss that contains a metamorphic monazite population yielding a weighted mean  $^{207}\text{Pb}/^{206}\text{Pb}$  age of 2361.8 Ma. Sample QM-7C is a granitoid gneiss containing magmatic zircon grains that provide a crystallization age of approximately 3107 Ma. QM-7D is a semi-pelite containing metamorphic monazite grains dated between ~2.35 and 2.15 Ga. The probability density plot shows monazite analyses from sample QM-7D as being grouped into several distinct clusters, as evidence for multiple episodes of monazite growth throughout this time.

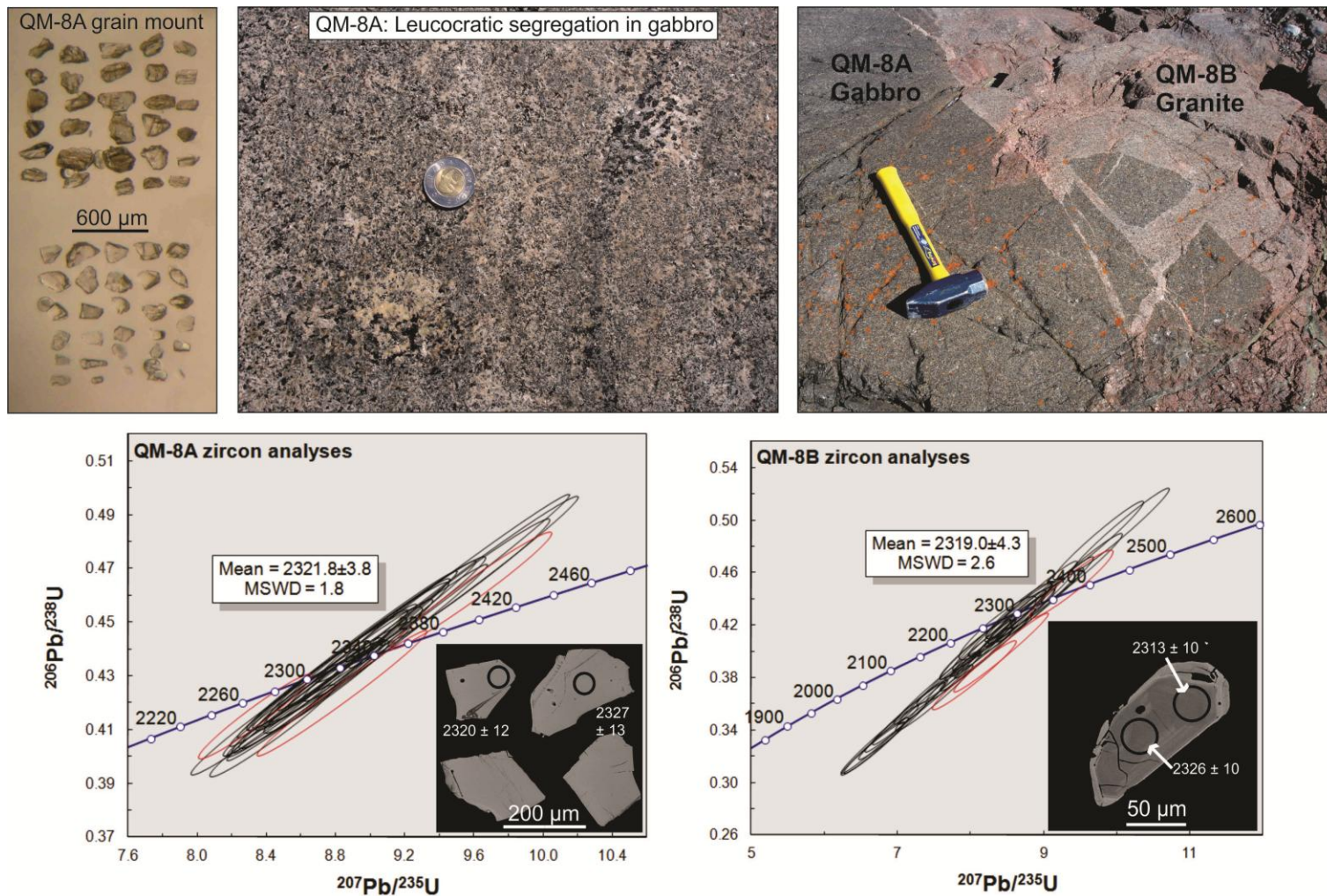


Figure 3-6: Location QM-8 geochronology summary. Outcrop photographs show cross-cutting relationship between QM-8A and QM-8B, and the leucocratic segregation from which sample QM-8A was collected. Concordia plots and select BSE images of zircon grains from samples QM-8A and QM-8B shown, as well as zircon grain mount photograph from sample QM-8A. Analyses shown as black ellipses are used in calculating the ca. 2.32 Ga crystallization ages of these magmatic rocks, as quoted in the diagrams.

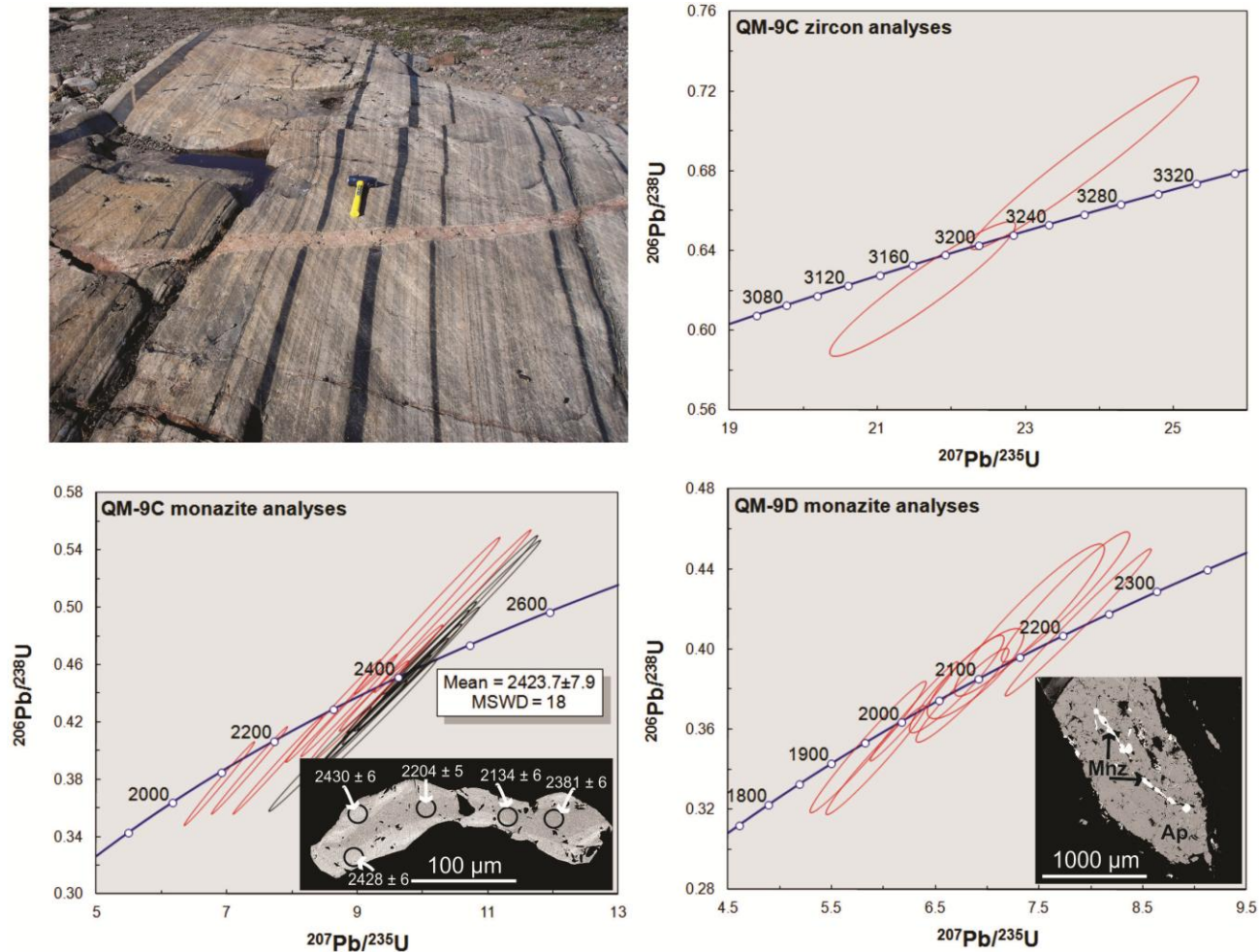


Figure 3-7: Location QM-9 geochronology summary. Outcrop photograph shows high-strain straight gneiss. Concordia plots and select BSE images of zircon and monazite grains from samples QM-9C and QM-9D are shown. Circa 3.2 Ga zircon grains from sample QM-9C, a psammitic migmatite, are inherited. Analyses shown as black ellipses are used in calculating the 2423.7 Ma metamorphic age of sample QM-9C. The peculiar morphology of monazite (i.e., as fracture fill in a large apatite grain) in sample QM-9D makes interpreting the significance of ages difficult; however, the oldest analysis of ~2.2 Ga provides a minimum crystallization age.



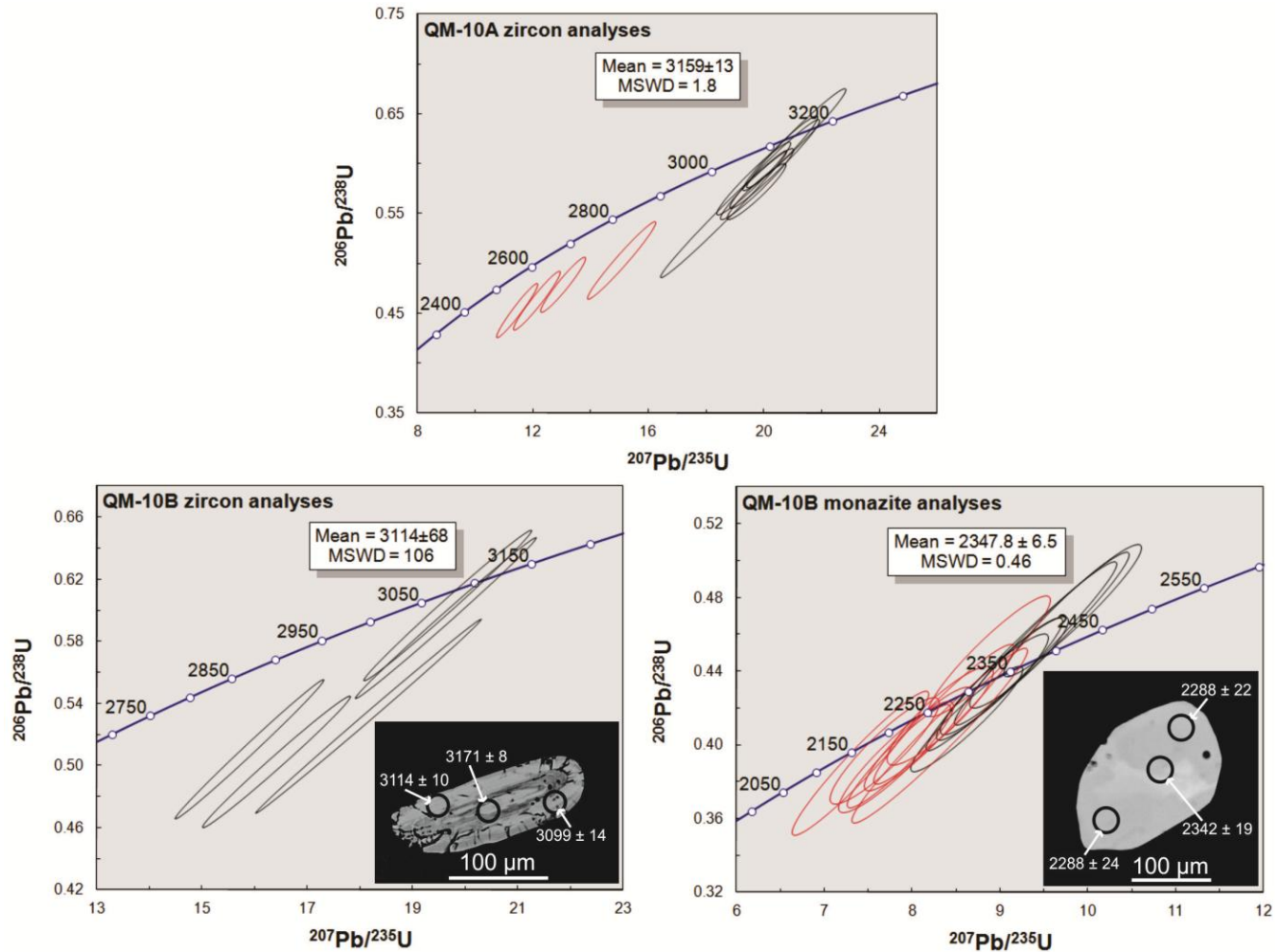


Figure 3-8 (1 of 2): Location QM-10 geochronology summary. Concordia plots and select BSE images of zircon and monazite grains from samples QM-10A and QM-10B are shown. Analyses shown as black ellipses are used in calculating the ages quoted in the diagrams. Zircon analyses from samples QM-10A and QM-10B indicate crystallization ages in the earliest Mesoarchean, between 3.2 and 3.1 Ga. Monazite analyses from sample QM-10B indicate metamorphism between 2.35 and 2.2 Ga.

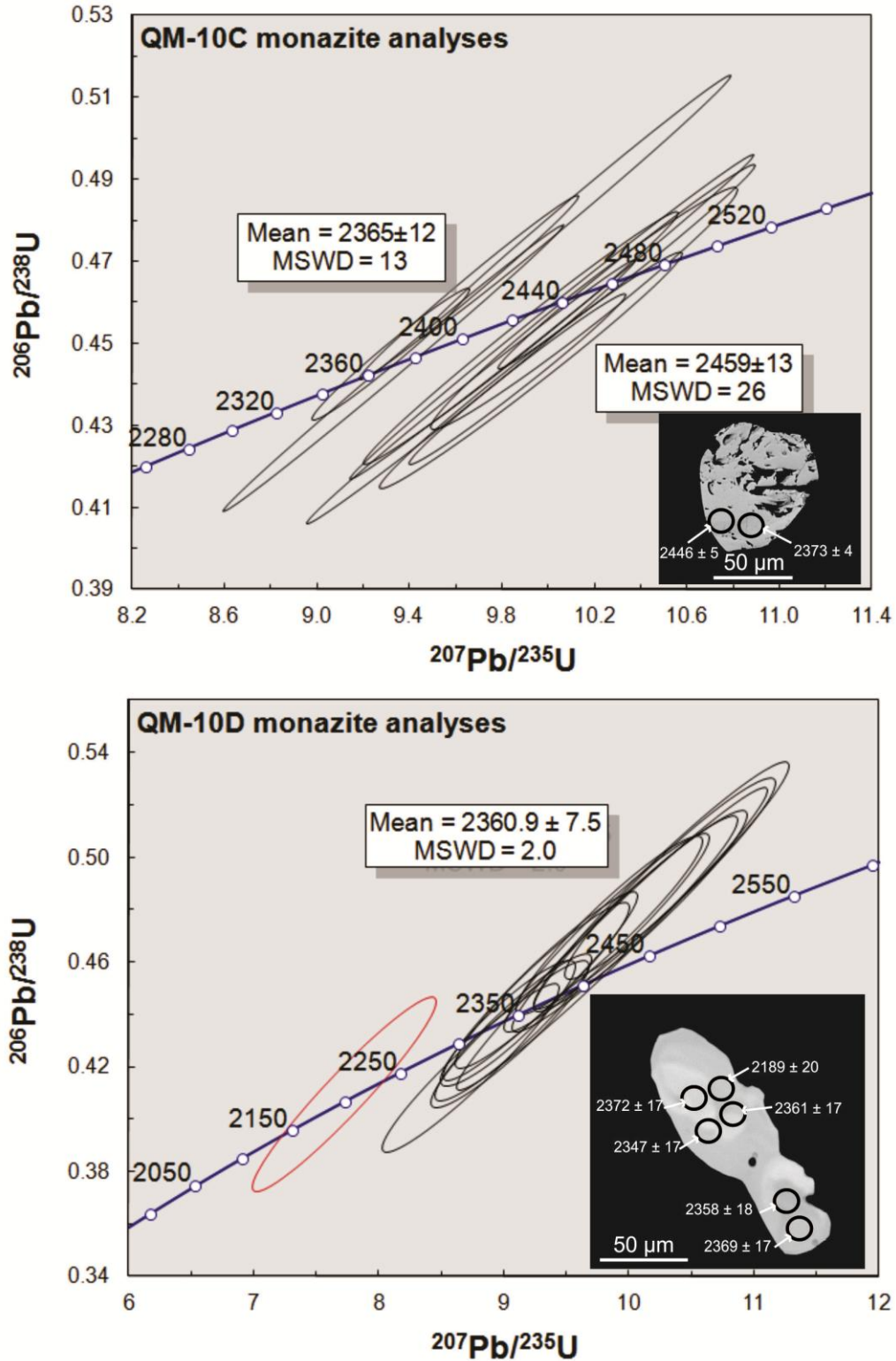


Figure 3-8 (2 of 2): Location QM-10 geochronology summary (continued). Concordia plots and select BSE images of monazite grains from samples QM-10C and QM-10D are shown. Analyses shown as black ellipses are used in calculating the ages quoted in the diagrams. Monazite growth in these samples is interpreted as being the result of multiple metamorphic events that took place in the early Paleoproterozoic.

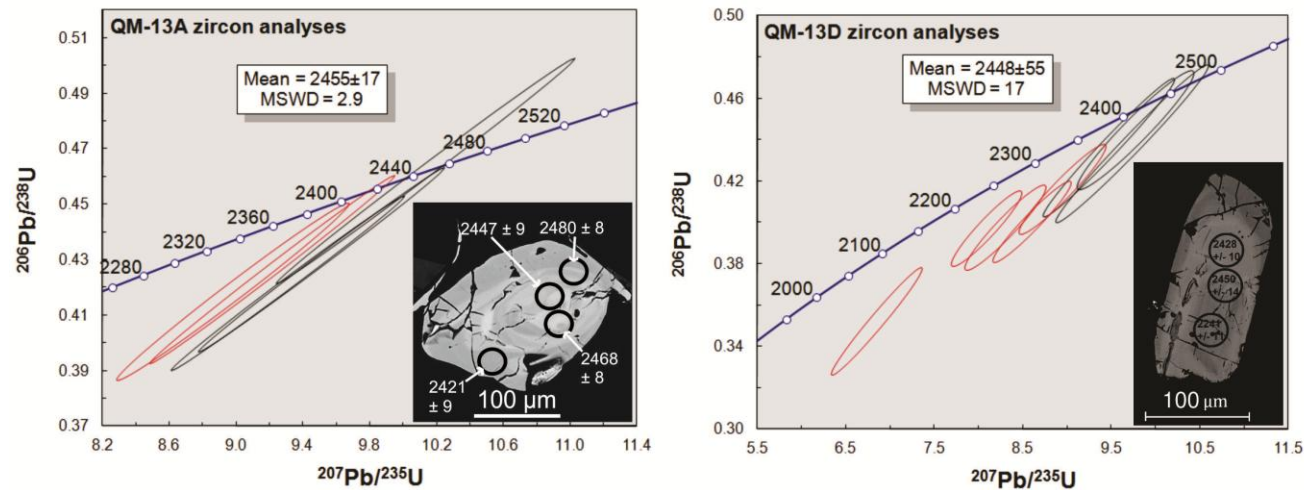
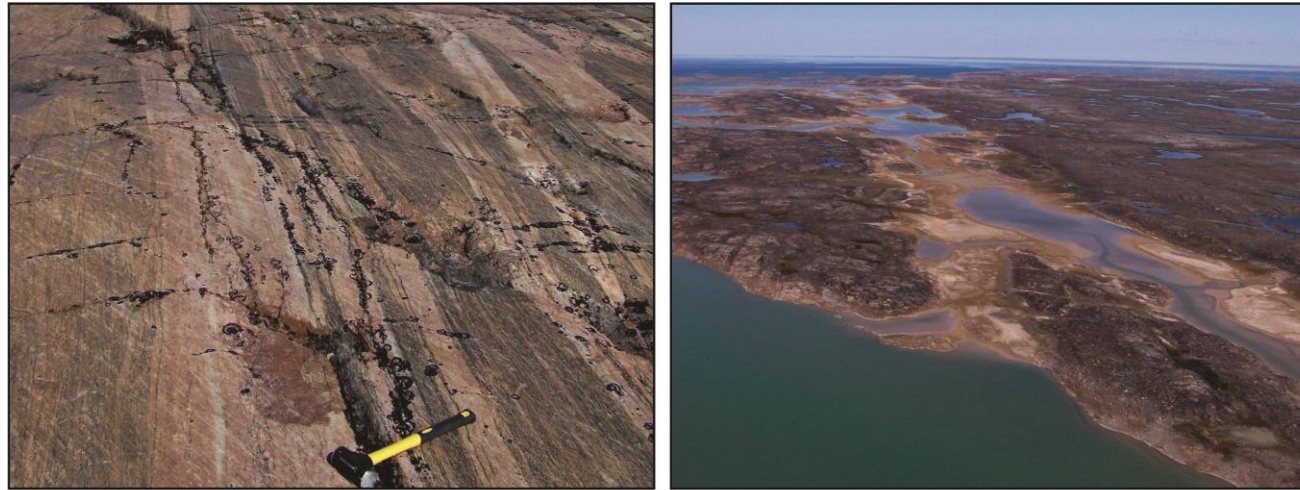


Figure 3-9 (1 of 2): Location QM-13 geochronology summary. Photographs show outcrop and aerial views of  $010^\circ$  striking high-strain zone. Concordia plots and select BSE images of zircon grains from samples QM-13A and QM-13D are shown. Analyses shown as black ellipses are used in calculating the ages quoted in the diagrams. Quoted ages are interpreted as the approximate crystallization ages of these granitoid gneisses, and younger analyses are due to Pb loss or recrystallization during Paleoproterozoic metamorphic events.

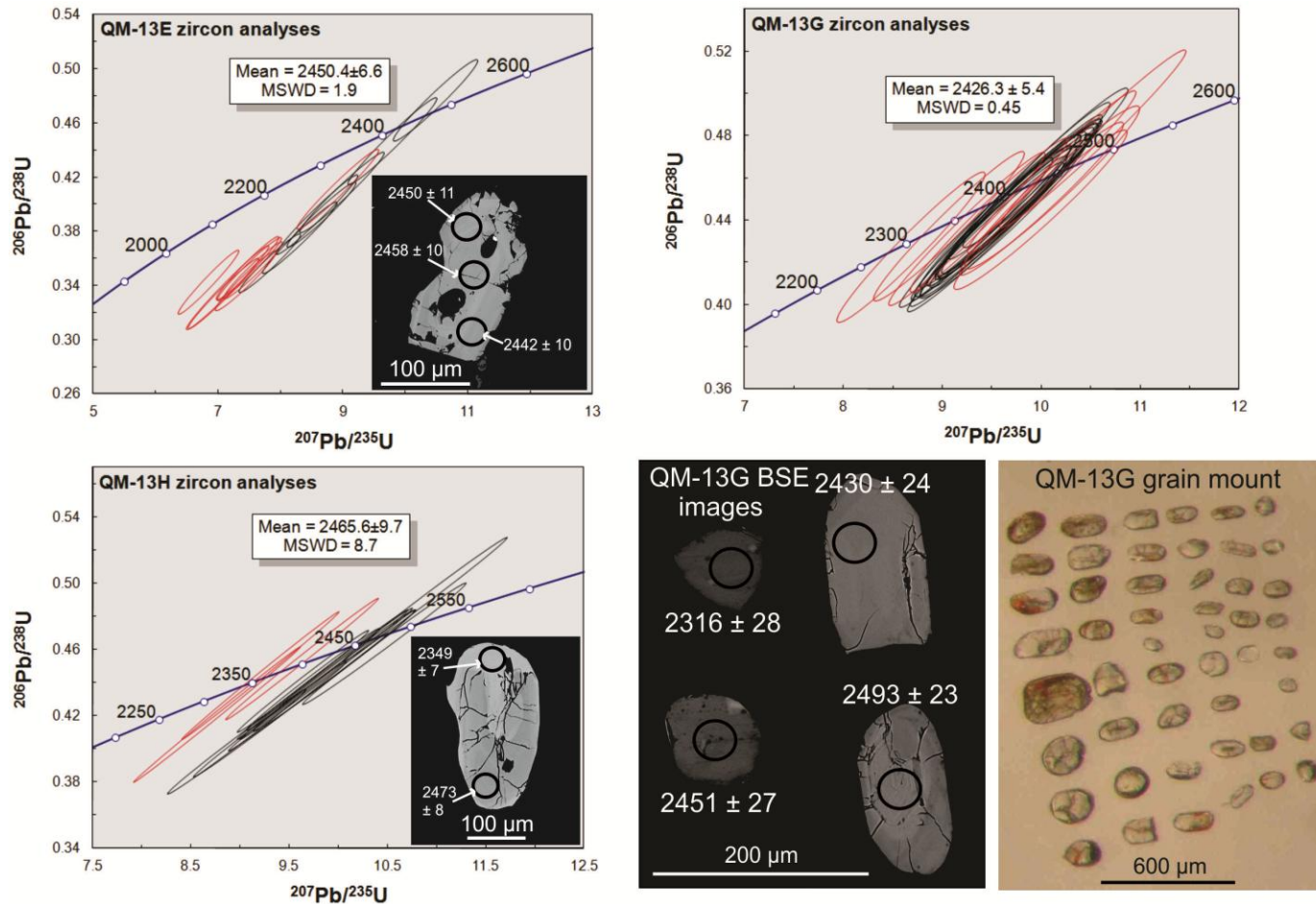


Figure 3-9 (2 of 2): Location QM-13 geochronology summary (continued). Concordia plots and select BSE images of zircon grains from samples QM-13E, QM-13G, and QM-13H are shown, as well as a zircon grain mount photograph from sample QM-13G. Analyses shown as black ellipses are used in calculating the approximate crystallization ages of these granitoid gneisses quoted in the diagrams. Younger ages from sample QM-13H are from recrystallized areas of zircon grains, as shown in the BSE image. Older analyses from sample QM-13G are from oscillatory zoned cores of zircon grains, and are interpreted as being inherited. Younger analyses in sample QM-13G are from irregularly shaped, unzoned zircon grains and are likely due to Pb loss or recrystallization during metamorphism.



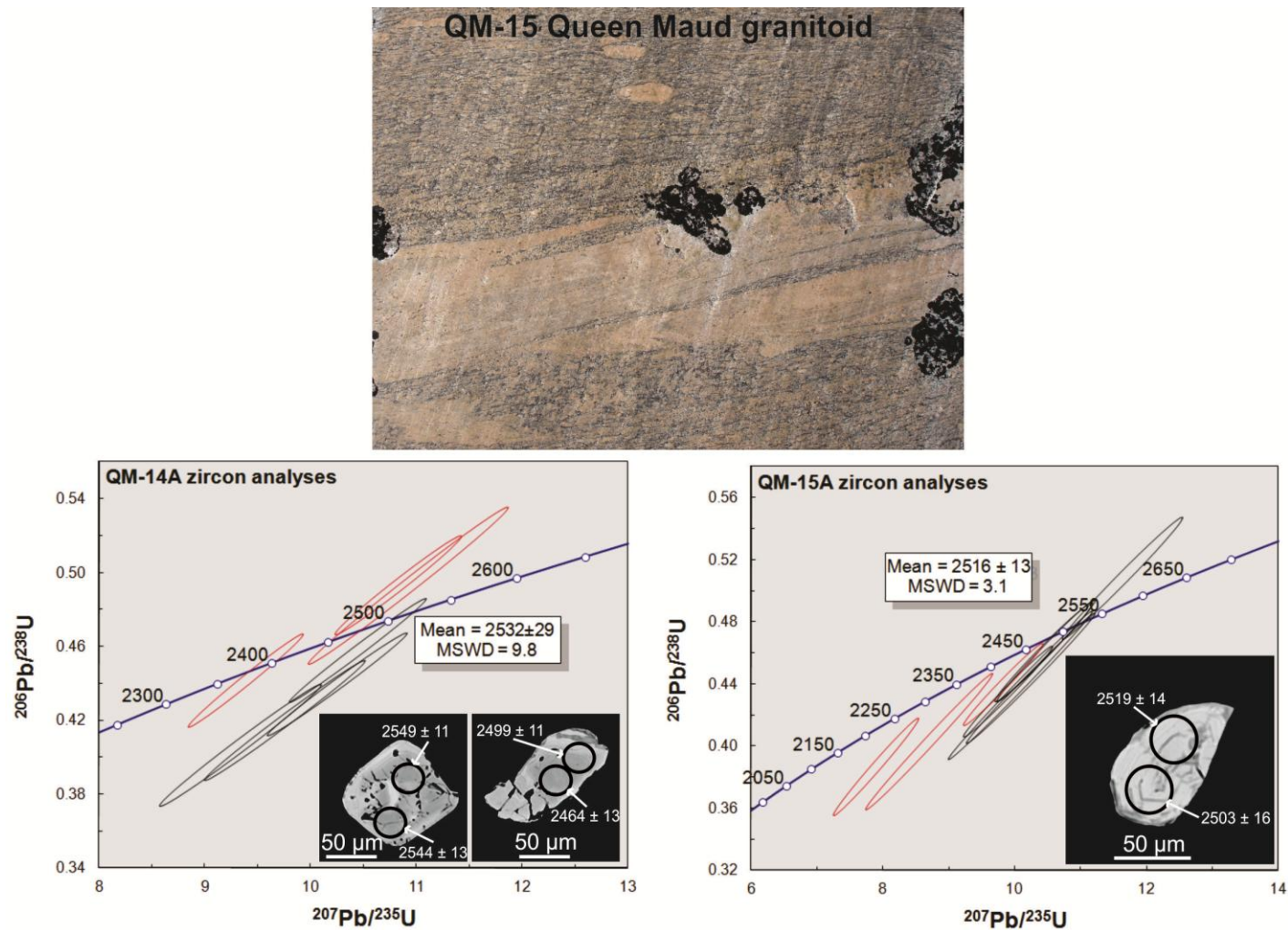


Figure 3-10: Locations QM-14 and QM-15 geochronology summary. Outcrop photograph from location QM-15 illustrating ‘typical’ look of Queen Maud granitoid rocks is shown. Concordia plots and select BSE images of zircon grains from samples QM-14A and QM-15A are shown. Analyses shown as black ellipses are used in calculating the approximate crystallization ages of these granitoid gneisses quoted in the diagrams.



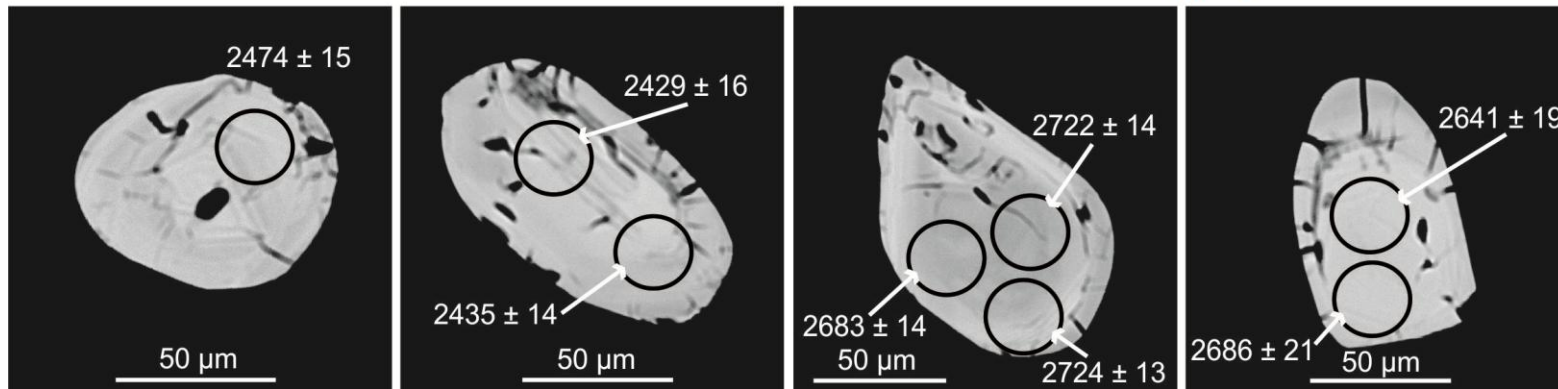
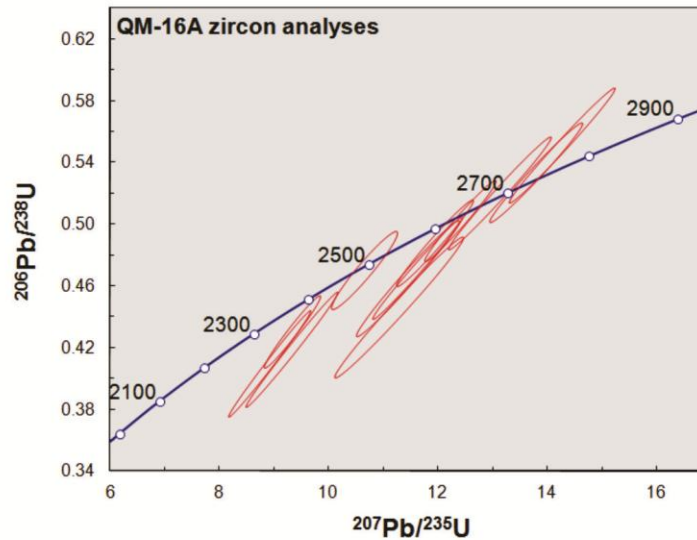


Figure 3-11: Location QM-16 geochronology summary. Outcrop photograph from location QM-16 showing appearance of granitoids at this location. Lithologically, these rocks are similar to the rocks from location QM-15, despite the highly contrasting U-Pb systematics. Concordia plot and select BSE images of zircon grains from sample QM-16A are shown. The younger cluster of analyses, between ~2.50 and 2.45 Ga, are thought to reflect the crystallization age of this granitoid gneiss, as evidenced by the fact that some of these analyses are from oscillatory zoned areas of zircon grains. The older cluster of ages, at around 2.7 Ga are also from oscillatory zoned zircons, but are thought to be inherited grains.

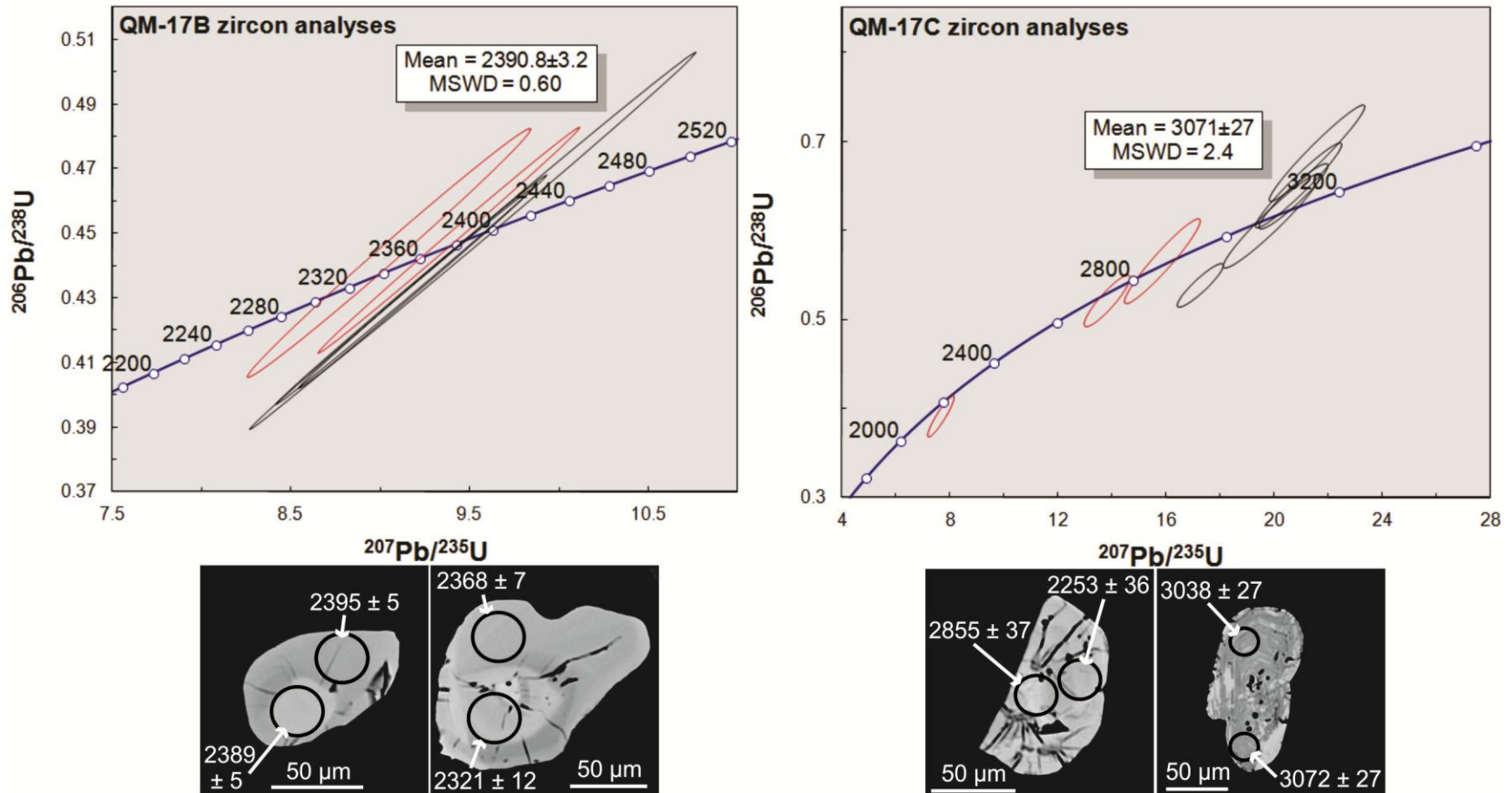


Figure 3-12: Location QM-17 geochronology summary. Concordia plots and select BSE images of zircon grains from samples QM-17B and QM-17C are shown. Analyses shown as black ellipses are used in calculating the ages quoted in the diagrams. Sample QM-17B was collected from a mafic dyke; zircon grains are irregularly shaped and lack oscillatory zoning. Hence, 2390.8 Ma is interpreted to reflect the timing of metamorphism at this location. Analyses from the cluster of ages defining the weighted mean  $^{207}\text{Pb}/^{206}\text{Pb}$  age of 3071 Ma in sample QM-17C are from oscillatory zoned ages of zircon grains, and thus, this is interpreted as the crystallization age of this granitoid gneiss. Younger analyses are due to Pb loss and recrystallization during Archean and Paleoproterozoic metamorphism.

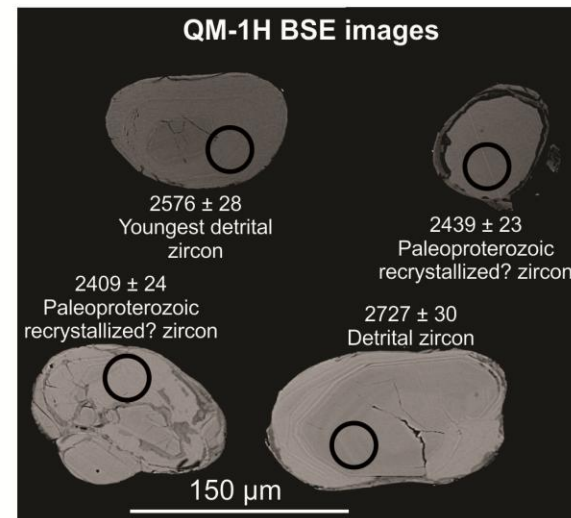
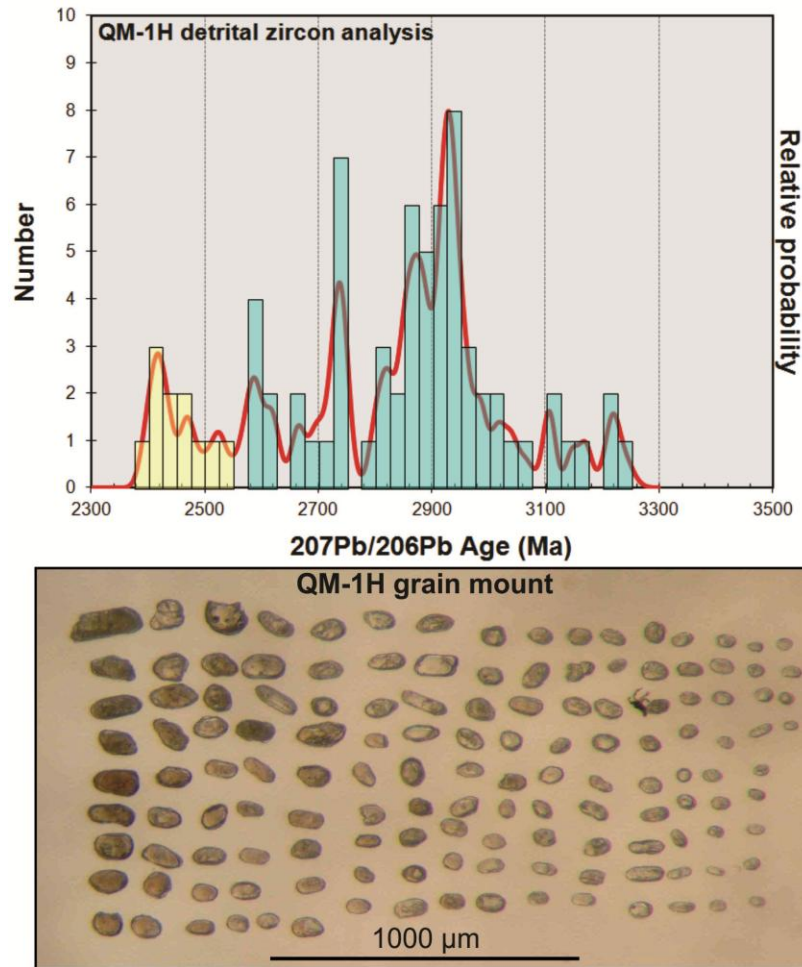


Figure 3-13: QM-1H detrital zircon analysis summary. Probability density plot, select BSE images, and zircon grain mount photograph are shown. Bins highlighted in blue on the probability density plot are from zircon grains that are clearly detrital on the basis of the presence of oscillatory zoning. The youngest of these grains is shown in BSE image and is dated at 2576 Ma. Analyses highlighted yellow on the probability density plot are those from zircon grains that may be detrital or related to post-depositional metamorphism, based on their lacking clearly defined oscillatory zoning.

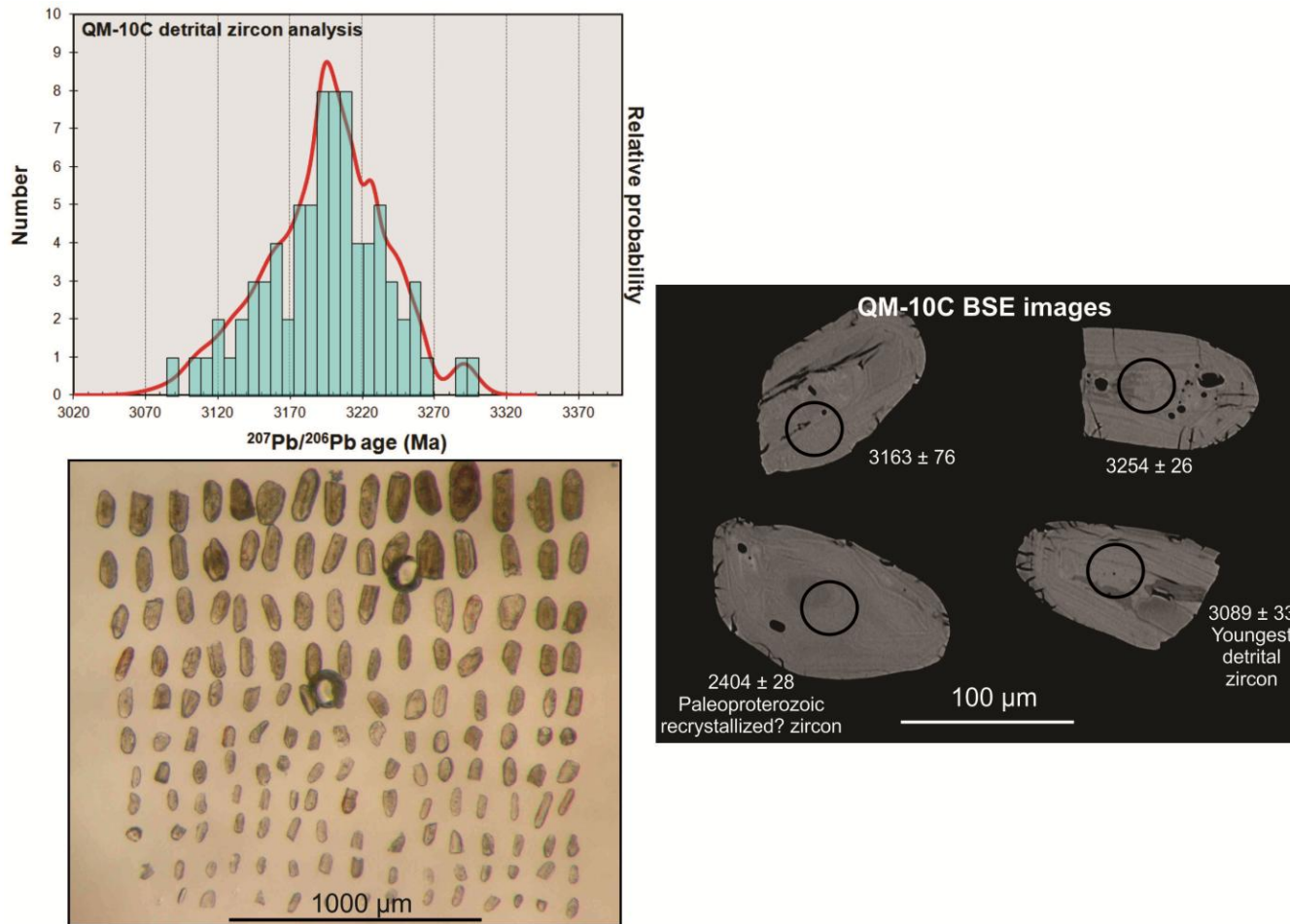


Figure 3-14: QM-10C detrital zircon analysis summary. Probability density plot, select BSE images, and zircon grain mount photograph are shown. Bins highlighted in blue on the probability density plot are from zircon grains that are clearly detrital on the basis of the presence of oscillatory zoning. The youngest of these grains is shown in BSE image and is dated at 3089 Ma. Several analyses, not shown in the probability density plot provide ages younger than 3089 Ma; however, these analyses are from zircon grains that lack clearly defined oscillatory zoning, and likely recrystallized or underwent Pb loss during post-depositional metamorphism.

## CHAPTER 4 – Geothermobarometry

In understanding the evolution of metamorphic terranes it is important to establish peak pressures and temperatures of metamorphism, as these conditions can provide insight into the tectonic setting in which the metamorphism occurred. In some cases, one can establish accurate P-T conditions simply by identifying the metamorphic minerals present in a given sample. More commonly though, mineral assemblages only provide a general P-T range, and one must conduct quantitative geothermobarometric calculations in order to establish more accurate conditions of metamorphism. Based on mineralogy, it has long been established that much of the Queen Maud block is metamorphosed at granulite-facies (Fraser, 1964; Heywood, 1961). However, this chapter presents the results of quantitative geothermobarometric calculations from seven samples collected from the Queen Maud block.

### 4.1 – Methodology

#### 4.1.1 – Net-transfer and Fe-Mg exchange geothermobarometry

Of the sixty samples collected only seven were found to have mineral assemblages appropriate for net-transfer and Fe-Mg exchange geothermobarometry. Seven independent mineral reactions were used to calculate P-T conditions for those samples. Temperature conditions were calculated using three Fe-Mg exchange reactions: the Grt-Opx, Grt-Cpx, and Grt-Crd reactions. Pressure conditions were calculated using four continuous net-transfer reactions: the Grt-Sil-Qtz-Plag (GASP), Grt-Crd-Sil-Qtz, Grt-Plag-Opx-Qtz, and Grt-Plag-Cpx-Qtz geobarometers.

Abbreviation	#	Reaction
Grt-Opx	1	$2\text{Mg}_3\text{Al}_2\text{Si}_3\text{O}_{12} + 3\text{Fe}_2\text{Si}_2\text{O}_6 = 2\text{Fe}_3\text{Al}_2\text{Si}_3\text{O}_{12} + 3\text{Mg}_2\text{Si}_2\text{O}_6$ Pyrope            Ferrosillite    Almandine    Enstatite
Grt-Cpx	2	$\text{Mg}_3\text{Al}_2\text{Si}_3\text{O}_{12} + 3\text{FeCaSi}_2\text{O}_6 = \text{Fe}_3\text{Al}_2\text{Si}_3\text{O}_{12} + 3\text{MgCaSi}_2\text{O}_6$ Pyrope            Hedenbergite    Almandine    Diopside
Grt-Crd	3	$2\text{Fe}_3\text{Al}_2\text{Si}_3\text{O}_{12} + 3\text{Mg}_2\text{Al}_4\text{Si}_5\text{O}_{18} = 2\text{Mg}_3\text{Al}_2\text{Si}_3\text{O}_{12} + 3\text{Fe}_2\text{Al}_4\text{Si}_5\text{O}_{18}$ Almandine            Cordierite            Pyrope            Fe-Cordierite
Grt-Plag-Opx-Qtz	4	$\text{Ca}_3\text{Al}_2\text{Si}_3\text{O}_{12} + 2\text{Mg}_3\text{Al}_2\text{Si}_3\text{O}_{12} + 3\text{SiO}_2 = 3\text{CaAl}_2\text{Si}_2\text{O}_8 + 3\text{Mg}_2\text{Si}_2\text{O}_6$ Grossular            Pyrope            Quartz            Anorthite            Enstatite
Grt-Plag-Cpx-Qtz	5	$\text{Mg}_3\text{Al}_2\text{Si}_3\text{O}_{12} + 2\text{Ca}_3\text{Al}_2\text{Si}_3\text{O}_{12} + 3\text{SiO}_2 = 3\text{CaAl}_2\text{Si}_2\text{O}_8 + 3\text{MgCaSi}_2\text{O}_6$ Pyrope            Grossular            Quartz            Anorthite            Diopside
Grt-Crd-Sil	6	$3\text{Mg}_2\text{Al}_4\text{Si}_5\text{O}_{18} = 2\text{Mg}_3\text{Al}_2\text{Si}_3\text{O}_{12} + 4\text{Al}_2\text{SiO}_5 + 5\text{SiO}_2$ Cordierite            Pyrope            Sillimanite    Quartz
GASP	7	$3\text{CaAl}_2\text{Si}_2\text{O}_8 = \text{Ca}_3\text{Al}_2\text{Si}_3\text{O}_{12} + 2\text{Al}_2\text{SiO}_5 + \text{SiO}_2$ Anorthite            Grossular            Sillimanite    Quartz



For each mineral phase analysed, three grains were targeted for analysis in each thin-section. Grain selection is an important process in calculating P-T conditions in granulite-facies rocks due to the effects of re-equilibration during retrograde metamorphism (Frost and Chacko, 1989). As large of grains as possible should be analysed in order to obtain the chemical composition of mineral cores, not rims which are relatively more susceptible to re-equilibration and secondary growth on the retrograde path. Mineral grains such as orthopyroxene and garnet, which are involved in Fe-Mg exchange reactions should, insofar as possible, not be in contact with one another or with other ferromagnesian phases, as this facilitates the re-equilibration process.

After appropriate mineral grains were located, their identity was confirmed through qualitative energy dispersive spectroscopy (EDS). 5-10 spots per grain were then selected for quantitative analysis. Spot locations were typically chosen in a core-to-rim or rim-to-rim traverse across the grain, avoiding fractures, inclusions, and zones of alteration. These radial traverses were conducted to determine if mineral grains exhibited any compositional zoning.

In order to obtain the mineral composition data needed for the P-T calculations, mineral grains were quantitatively analysed using wavelength dispersive spectroscopy (WDS) on the Department's JEOL 8900 Electron Probe Microanalyser (EPMA). An accelerating voltage of 15 kV, a current of 15 nA, and a beam diameter of 3-4  $\mu\text{m}$  was used for these analyses. The elements targeted for analysis and the crystals used for measurement of those elements are listed below. Standardization of elements was done using in-house mineral standards and standards obtained from the Smithsonian Institution and other sources (Jarosewich et al., 1980) (Table 4-1).

A ZAF correction was applied to the data in order to correct for the atomic number effect, x-ray absorption, and fluorescence. Each data point was evaluated in order to determine if the target mineral was in fact analysed or if inclusions or cracks were accidentally targeted. The data from each sample was then assessed to determine if the mineral grains contain significant zoning profiles. Where this was the case, analyses that were thought to be most representative of mineral core compositions were averaged. Using these averaged compositions (Table 4-3), calculations of P-T conditions were conducted using winTWQ 2.3 (Berman, 2007), which is an updated version of the internally consistent thermodynamic dataset developed by Berman (1988; 1991).



<b>Crystal Type</b>	PET	TAP	PETH	TAPJ	LIFH
<b>Element</b>	Ti Cr	Na Mg	Ca K	Si Al	Fe Mn

Table 4-1: Standards used in EPMA

<b>Element</b>	<b>Garnet</b>	<b>Feldspar</b>	<b>Pyroxene</b>	<b>Cordierite</b>
<b>Si</b>	Gore Mtn Garnet	UA Orthoclase	Wakefield Diopside	UA Orthoclase
<b>Ti</b>	Rutile	Rutile	Rutile	Rutile
<b>Al</b>	Gore Mtn Garnet	Alaska Anorthite	Gore Mtn Garnet	UA Kyanite
<b>Cr</b>	Stillwater Chromite	Stillwater Chromite	Stillwater Chromite	Stillwater Chromite
<b>Fe</b>	Gore Mtn Garnet	Gore Mtn Garnet*	Gore Mtn Garnet	Gore Mtn Garnet
<b>Mn</b>	Franklin Willemite	Franklin Willemite	Franklin Willemite	Franklin Willemite
<b>Mg</b>	Kakanui Pyrope	Kakanui Pyrope	Kakanui Pyrope	Kakanui Pyrope
<b>Ca</b>	Wakefield Diopside	Oregon Plagioclase Alaska Anorthite	Wakefield Diopside	Oregon Plagioclase
<b>Na</b>	UA Albite	UA Albite	UA Albite	UA Albite
<b>K</b>	UA Orthoclase	UA Orthoclase	UA Orthoclase	UA Orthoclase
<b>Ba</b>		UA Barite		

\*Fe concentrations for some feldspar analyses were determined using a fayalite mineral standard.

#### 4.1.2 – Reintegrated feldspar thermometry

Because of the possible effects of re-equilibration during slow cooling of granulite-facies rocks, the temperature provided by Fe-Mg exchange reactions (reactions 1-3) may not accurately represent the peak temperatures of metamorphism. For this reason, reintegrated feldspar thermometry was conducted on two samples containing alkali feldspar with perthitic exsolution textures. In principle, reintegrated feldspar thermometry can be used to retrieve the temperature at which inter-grain exchange of feldspar components between discrete plagioclase and alkali feldspar grains ceased and the mobility of feldspar components was restricted to intra-grain movement in the formation of plagioclase exsolution lamellae within host alkali feldspar grains. Although the temperatures estimated via reintegrated feldspar thermometry still represent minimum estimates of peak metamorphic temperatures, this type of thermometry is generally less susceptible to the effects of re-equilibration than conventional thermometry (e.g., Frost and Chacko, 1989).

In order to estimate the modal abundance of host K-feldspar and plagioclase lamellae, several representative BSE images for each grain targeted were obtained. These images contain as few fractures and inclusions as possible so that the relative abundance of host and lamellae could best be estimated. The relative abundances were estimated using the ImageJ software program. The ImageJ program was developed by Wayne

Rasband at the United States National Institute of Health; the program is available for free download at <http://rsb.info.nih.gov/ij/>. This program analyses each pixel of an image and allows one to select a cut-off of which shade of pixel represents K-feldspar host, and which represents plagioclase lamellae. This method provides a much more accurate estimate of modal percentage than simply making visual estimates.

Three mineral grains per sample were quantitatively analysed using WDS analysis on the Department's JEOL 8900 EMPA. A total of 5 spots within the K-feldspar host and 5 spots in the plagioclase lamellae from each grain were analysed. The averaged compositions of host and lamellae (Table 4-3) were combined with modal estimates of host-lamellae proportions to obtain the reintegrated composition of the alkali feldspar grains prior to exsolution. Temperatures were calculated using the feldspar solution models developed by Elkins and Grove (1990) and by Fuhrman and Lindsley (1988); and were represented graphically using the SOLVCALC 2.0 program (Wen and Nekvasil, 1994).

## 4.2 – Results

P-T estimates derived from Fe-Mg exchange and net-transfer mineral equilibria, and from reintegrated feldspar thermometry are presented and discussed in this section. The results from each of the seven samples are discussed individually in the present chapter and synthesized along with geochronological data in Chapter 5. Photographs of petrographic thin-sections are shown in Figure 4-1 and BSE images of K-feldspar grains analysed for reintegrated feldspar thermometry in Figure 4-2. The mineral composition data are summarized in Tables 4-2 and 4-3. P-T plots showing the position of mineral equilibria applicable to each sample are shown in Figure 4-3, whereas ternary diagrams and temperature conditions based on reintegrated feldspar thermometry are shown in Figure 4-4.

Samples QM-1C, QM-1F, QM-1G, and QM-1I were all collected from the same outcrop location, whereas samples QM-7D, QM-10D, and QM-15C were collected from different locations, moving progressively eastward in the QMB (Figure 2-1).

### QM-1C

Sample QM-1C was collected from the centre of a metamorphosed and weakly deformed fine-grained mafic dyke that clearly cross-cuts the dominant metamorphic fabric of the host paragneiss (Figure 2-2g). This rock exhibits an upper amphibolite- to

lower granulite-facies mineral assemblage of plagioclase, clinopyroxene, hornblende, garnet, and quartz (Figure 4-1a). Garnet and quartz grains are locally present within quartz-rich segregations, whereas clinopyroxene, hornblende, and plagioclase are present throughout the specimen. Mineral grains average 0.5 mm across and form a distinct granoblastic texture. Alteration of mineral grains is minimal, and there is no textural evidence for disequilibrium in this sample. Furthermore, no significant compositional zonation of individual grains was revealed during microprobe analysis, and clinopyroxene grains within quartz-rich segregations do not differ in composition from grains outside of the segregations. For these reasons the mineral assemblage observed is thought to be in a state of equilibrium.

The Grt-Cpx thermometer and the Grt-Plag-Cpx-Qtz barometer were used to determine the P-T conditions of equilibration of this sample. Figure 4-3a illustrates equilibration conditions for this sample of approximately 720°C and 7.5 kbar. Due to the very fine grained nature and close proximity of garnet and clinopyroxene grains it is possible that some degree of Fe-Mg exchange occurred during cooling and therefore, the calculated temperature should be considered a minimum estimate of peak metamorphic temperature.

In Chapter 2 it was discussed that an M1 metamorphic event formed the dominant gneissosity of the host rock and an M2 event formed the mineral assemblage observed in this mafic dyke. Therefore, the minimum temperature conditions of 720°C and pressure conditions of 7.5 kbar, preserved in sample QM-1C are those of the M2 event, which, based on the dating of metamorphic zircons from this sample, occurred at ~1.93 Ga (Chapter 3).

#### QM-1F

This sample is a fine- to medium-grained, highly deformed mafic gneiss. This lithology has a deformational fabric that is cross-cut by the dyke from which QM-1C was collected. Sample QM-1F is composed of plagioclase, clinopyroxene, garnet, hornblende, and orthopyroxene (Figure 4-1c/d). The average grain size is approximately 1 mm. Texturally this sample appears to be in equilibrium, and there is no significant compositional variation between different grains of a particular mineral, nor is there any significant compositional zoning within grains. These observations are consistent with the interpretation that the mineral assemblage in the sample is in chemical equilibrium.

The Grt-Cpx and Grt-Opx thermometers as well as the Grt-Plag-Cpx-Qtz and Grt-Plag-Opx-Qtz barometers were used in calculating P-T conditions of approximately 7.2-8.5 kbar and 750-775°C (Figure 4-3b). It is possible that Fe-Mg exchange between garnet and clinopyroxene, as well as garnet and orthopyroxene continued during cooling, and that the temperature calculated should be considered a minimum temperature of peak metamorphism. However, it is worth noting that the temperatures indicated by both the Grt-Cpx and Grt-Opx thermometers are nearly identical, which suggests either that the calculated temperatures are in fact representative of peak temperature conditions, or that the two thermometers have similar closure temperatures. Due to the lack of quartz observed in this sample, the pressures indicated by the two geobarometers represent maximum pressures of equilibration, rather than the true pressure (Mukhopadhyay et al., 1992).

Whether the P-T conditions of 7.2-8.5 kbar and 750-775°C represent the conditions of metamorphism during M1 or M2 is uncertain. Furthermore, the possibility exists that partial re-equilibration of the mineral assemblage occurred during M2 metamorphism and that the P-T conditions preserved are somewhere between the granulite-facies conditions of M1, preserved in sample QM-1I, and the upper amphibolite- to lower granulite-facies conditions of M2, preserved in sample QM-1C.

#### QM-1G

Sample QM-1G is a coarse-grained ultramafic inclusion found within the mafic gneiss from which QM-1F was collected. This sample is composed primarily of hornblende, plagioclase, orthopyroxene and garnet, as well as trace amounts of biotite (Figure 4-1b; 2-2b). Large garnet porphyroblasts greater than 1cm across are enveloped by distinct reaction rims composed plagioclase, garnet, and orthopyroxene. Not surprisingly for garnet grains displaying resorption textures such as these, calcium and magnesium content decrease and iron and manganese content increase towards the rims of grains. Furthermore, the anorthite component in plagioclase is highly variable, with some grains containing ~80% anorthite and others with ~60% anorthite. These observations suggest a degree of disequilibrium present in this sample.

The Grt-Opx thermometer and Grt-Plag-Opx-Qtz barometer were used to calculate P-T conditions for this sample. Depending on whether garnet cores or rims and either the high Ca or low Ca plagioclase grains are used in calculations, an extremely wide range of P-T conditions are calculated. When garnet cores and the low Ca

plagioclase are used, P-T conditions of 9.8 kbar and 940°C are calculated. At the other extreme end, when garnet rims and Ca-rich plagioclase are used, P-T conditions of 7.6 kbar and 780°C are calculated. Due to the absence of quartz in this specimen, the quoted pressures should be considered maximum pressures of metamorphism.

Based on textural observations and compositional variations of mineral grains, it is difficult to interpret wide range in P-T conditions recorded by this specimen. One possibility is that the high P-T conditions of 940°C and 9.8 kbar indicated by garnet core compositions reflect an early high-grade event. This event may have taken place before this ultramafic xenolith became entrained in its mafic host rock. The P-T conditions indicated by garnet rim compositions are comparable with those recorded by other samples from this location. Therefore, the conditions of 7.6 kbar and 780°C may be those of garnet resorption, which could have occurred during M1 or M2 metamorphism.

#### QM-II

Sample QM-II is a strongly banded semi-pelitic paragneiss comprising part of the host rock of this outcrop. The sample is composed of biotite, K-feldspar, garnet, orthopyroxene, plagioclase, quartz, and sillimanite (Figure 4-1e). Grain size is variable, from about 2mm to less than 1 mm. Interestingly, sillimanite is not widespread throughout the sample, but is present only locally as inclusions in garnet or near the margins of some garnet grains. This may be due to changes in bulk composition associated with depositional variations—more specifically, changes in the abundance of clay minerals. K-feldspar is present locally in leucosomes, formed during partial melting. Orthopyroxene grains are partially altered to chlorite and other phyllosilicate mineral phases (Figure 4-1f). Despite the interpretation that variations in bulk composition exist within this sample there is no significant compositional variations between the individual mineral grains in this sample.

The Grt-Opx thermometer and the Grt-Plag-Opx-Qtz and GASP barometers were used to calculate P-T conditions for this sample. Conditions around 7.5-8.8 kbar and 625-720°C were calculated based on these reactions (Figure 4-3c). Once again, it is possible that some degree of Fe-Mg re-equilibration occurred during cooling or later metamorphic events and that the temperatures quoted may be significantly lower than true peak temperatures of metamorphism. The RCLC program of Pattison et al. (2003) yields P-T conditions of 820°C and 8.5 kbar for sample QM-II. This program corrects for retrograde

Fe-Mg exchange between garnet and orthopyroxene based on Al solubility in orthopyroxene.

In order to better constrain the peak temperature of metamorphism of this sample, re-integrated feldspar thermometry was conducted on K-feldspar grains exhibiting perthitic exsolution. The modal percentage of K-feldspar host and plagioclase lamellae, (Figure 4-4a) as well as the composition of minerals exhibit very little variation between mineral grains. For this reason all analyses were averaged and temperatures of approximately 825°C and 800°C were calculated, based on the Elkins and Grove (1990) and the Fuhrman and Lindsley (1988) solution models, respectively (Figure 4-4, based of a pressure of 8 kbar). With ~825°C as a more accurate representation of peak temperature conditions, the pressures of metamorphism are increased to between 8 and 10 kbar.

Given that there are no compositional or textural indications of disequilibrium—aside from the partial alteration of orthopyroxene—it is possible that the P-T conditions of 825°C and 8-10 kbar are approximately those of equilibration for these sample. The P-T conditions for this rock are significantly higher than those recorded in sample QM-1C, and therefore likely record a different metamorphic event. The most likely event recorded in this sample is M1 metamorphism, which is associated with the main gneissosity forming event.

#### QM-7D

This sample is a weakly foliated semi-pelitic rock found as an enclave in granodiorite. It is composed of plagioclase, K-feldspar, biotite, orthopyroxene, garnet, quartz, and magnetite (Figure 4-1g/h). Subhedral garnet and orthopyroxene porphyroblasts up to 0.5 cm across are common whereas biotite, plagioclase, K-feldspar, and magnetite grains are less than 1 mm across. Orthopyroxene grains are locally altered to chlorite along grain boundaries and within fractures. Aside from this minor alteration there is no textural evidence for disequilibrium in this sample.

The Grt-Opx thermometer and Grt-Plag-Opx-Qtz barometer were used to measure P-T conditions of 770°C and 5.9 kbar in this sample (Figure 4-3d). The large grain sizes of garnet and orthopyroxene, as well as the fact that they occur as isolated porphyroblasts adds credence to the possibility that 770°C is close to the true temperature of peak metamorphic conditions.

The pressure conditions of 5.9 kbar are significantly lower than the pressures of M1 metamorphism indicated by samples collected from location QM-1 and QM-10 to the



west and east of location QM-7. It is possible that this sample was re-equilibrated during M2 metamorphism. Alternatively, assuming the P-T conditions of 770°C and 5.9 kbar are representative of peak metamorphic conditions associated with M1, then the difference in pressure between this and nearby locations may be due to differential thickening, or differential uplift/erosion in the QMB.

QM-10D

This sample was collected from a pelitic layer in an outcrop containing a lithologically diverse suite of layered gneiss. Minerals present in this sample are biotite, garnet, cordierite, sillimanite, plagioclase, orthopyroxene, and quartz (Figure 4-1i). Unfortunately, due to the extremely fragile nature of the hand specimen a thin-section containing orthopyroxene could not be obtained. The average grain size of this rock is highly variable, with biotite grains being less than 0.1 mm across and garnet grains as large as 1 cm across. Minerals in this sample occur in distinct clusters, not evenly spread throughout the specimen. Texturally this specimen appears equilibrated, and there is little compositional variation between mineral grains. The rims of garnet and plagioclase grains differ in composition slightly from the cores of these grains. Compositions most representative of mineral cores were used in calculating P-T conditions.

The Grt-Crd thermometer and the Grt-Crd-Sil-Qtz and GASP barometers were used to calculate P-T conditions of 6.3-7.6 kbar and 700-800°C in this specimen (Figure 4-3e). The low pressure-temperature conditions are based on the intersection between the reaction curves of the GASP barometer and Grt-Crd thermometer. Kohn and Spear (1991), state that when Ca contents in garnet are relatively low, as is the case for this sample, the uncertainty of pressures indicated by the GASP barometer increases. Therefore, it is more likely that the higher P conditions of 7.6 kbar, as indicated by the Grt-Crd-Sil-Qtz barometer, are more representative of peak P conditions. It is possible that Fe-Mg exchange between garnet and cordierite occurred during cooling and that the temperature conditions of 700°C indicated by the Grt-Crd thermometer should be considered a minimum.

No lithologic or mineralogic evidence for multiple metamorphic events is observed at this location. It is possible that the P-T conditions of >700°C and 7.6 kbar recorded by sample QM-10D are representative of the P-T conditions associated with M1 metamorphism at this location.

QM-15C

Sample QM-15C was collected from an outcrop dominated by granitic and granodioritic gneisses. It was collected from a metasedimentary raft found within the granitic rocks. This sample contains K-feldspar, cordierite, biotite, garnet, sillimanite, plagioclase, and quartz (Figure 4-1j/k). K-feldspar grains exhibit well-defined perthitic exsolution textures. Microprobe analysis revealed a relatively high degree of variation in Ca content in individual garnet grains; furthermore, perthitic K-feldspar grains exhibit a wide range in textures, reintegrated composition, and the relative abundance of K-feldspar host and plagioclase lamellae. These compositional and textural variations suggest either disequilibrium or polyphase metamorphism in the area.

The Grt-Crd thermometer and the Grt-Crd-Sil-Qtz and GASP barometers were applied to this sample. When relatively low Ca garnet was used to calculate P-T conditions a very narrow range of P-T conditions near 6.8 kbar and 700°C are recorded. When high Ca garnet is used, as shown in Figure 4-3f and Table 4-3, a much wider range in pressure conditions between 6.4-8.4 kbar is recorded. As was the case for sample QM-10D, the low Ca content of garnet results in a high degree of uncertainty in the GASP barometer. Therefore, the pressure of approximately 6.5 kbar indicated by the Grt-Crd-Sil-Qtz barometer is considered more representative of peak metamorphic pressure.

In order to better constrain the peak temperature of metamorphism of this sample, re-integrated feldspar thermometry was conducted on K-feldspar grains exhibiting perthitic exsolution. As mentioned, the reintegrated composition and textural appearance of K-feldspar grains is variable (Figure 4-2b/c). For this reason, each individual grain as well as the overall average was plotted on ternary feldspar plots. Despite the range in composition, the temperature indicated by individual grains varies little. Using the Elkins and Grove (1990) and Fuhrman and Lindsley (1988) solution models, the models indicate minimum temperatures of initial exsolution of approximately 825°C and 800°C respectively (Figure 4-4, based of a pressure of 7.5 kbar).

Based on re-integrated feldspar thermometry and the Grt-Crd-Sil-Qtz barometer, pressures and temperatures of metamorphism of approximately 825°C and 6.8 kbar are recorded in sample QM-15C. Despite the relatively high degree of textural and compositional heterogeneities observed in this sample, these P-T conditions are comparable to those of M1 metamorphism in other areas of the QMB.

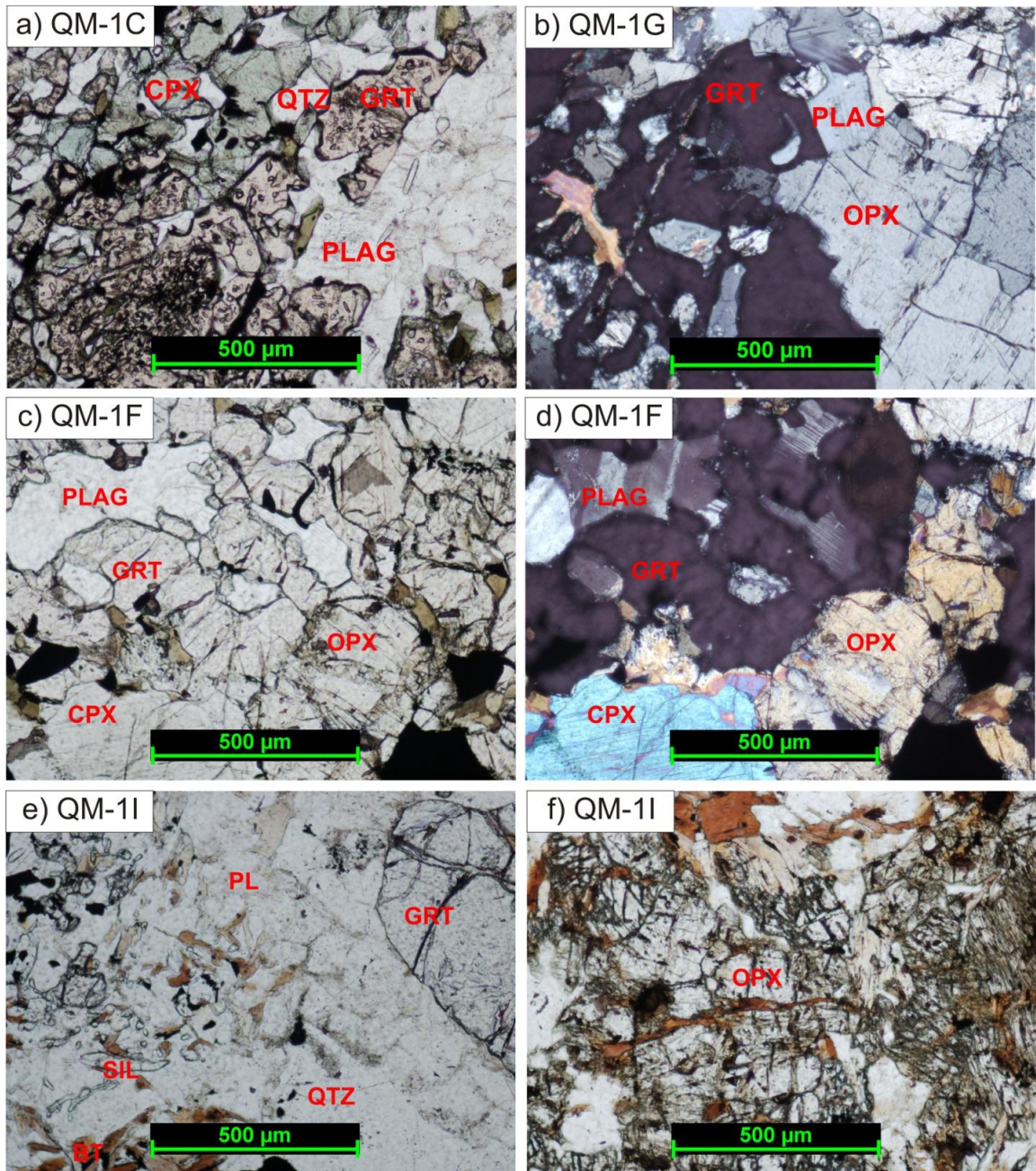


Figure 4-1 (1 of 2): Photographs of petrographic thin-sections showing metamorphic mineral assemblages and textures of each sample analysed. See text for explanation.



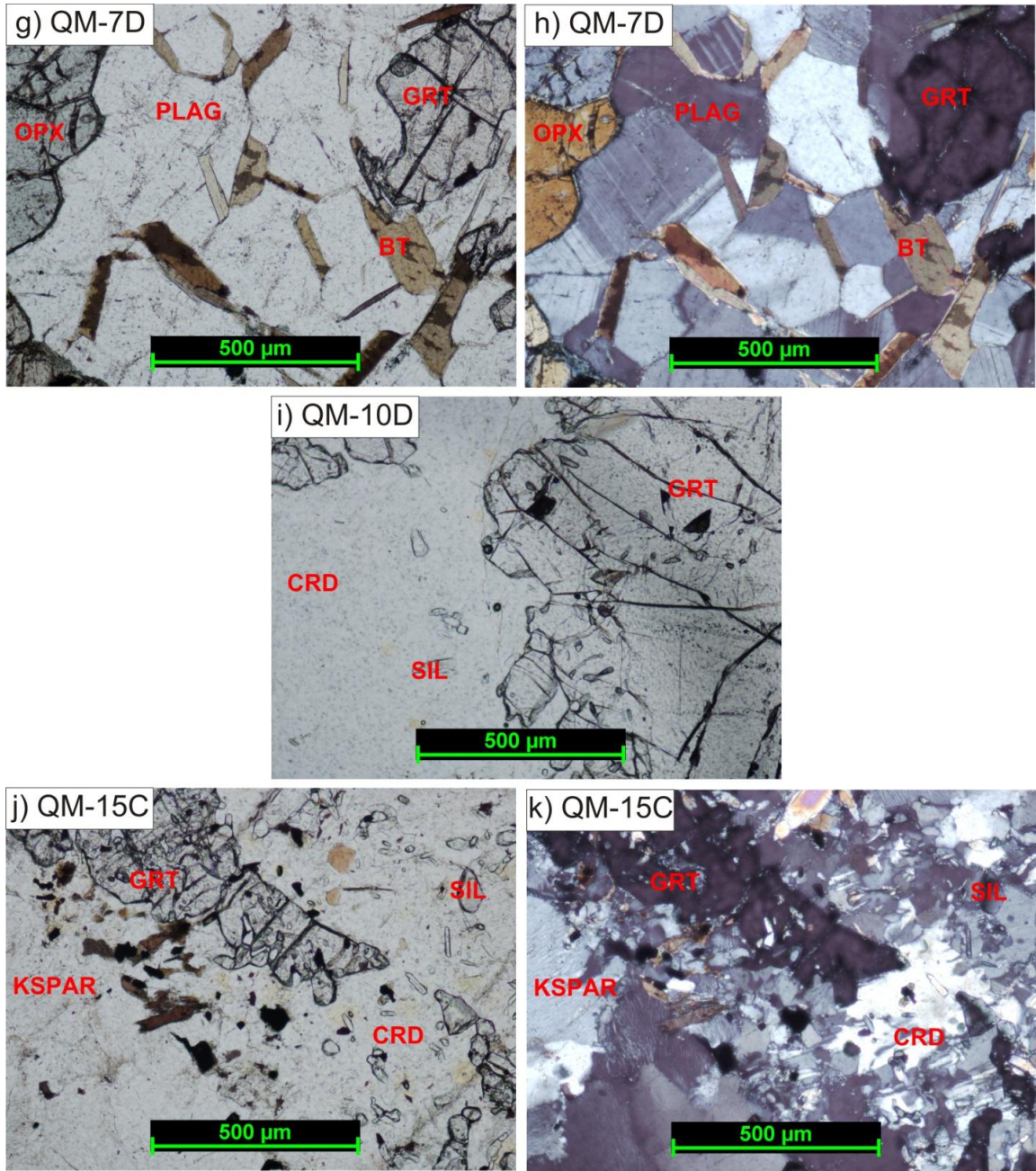


Figure 4-1 (2 of 2): Photographs of petrographic thin-sections showing metamorphic mineral assemblages and textures of each sample analysed (continued). See text for explanation.

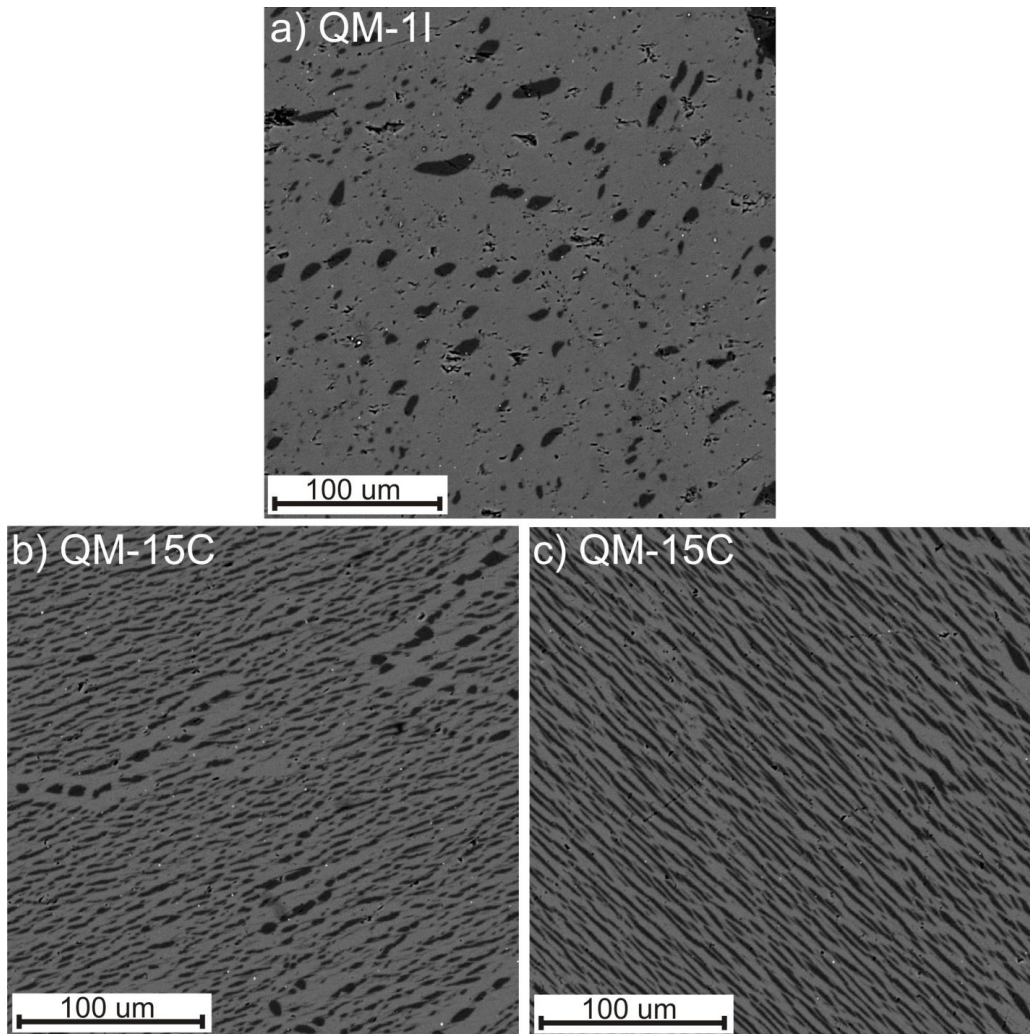


Figure 4-2: BSE images showing perthitic exsolution in K-feldspar grains analysed for re-integrated feldspar thermometry. Note the variable appearance of exsolution textures in sample QM-15C.

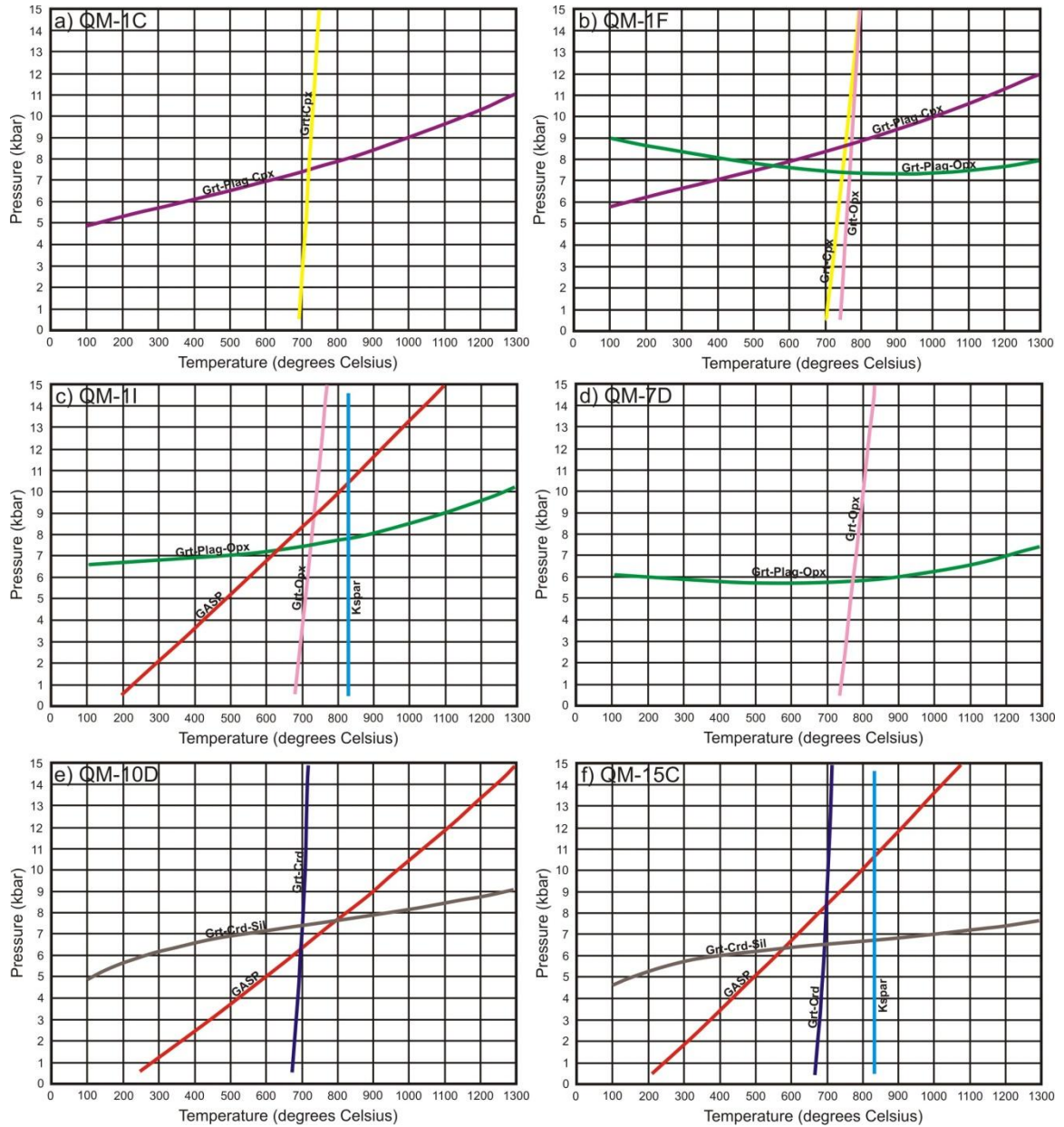


Figure 4-3: P-T graphs for six of seven samples analysed for geothermobarometric conditions. See text for explanation.



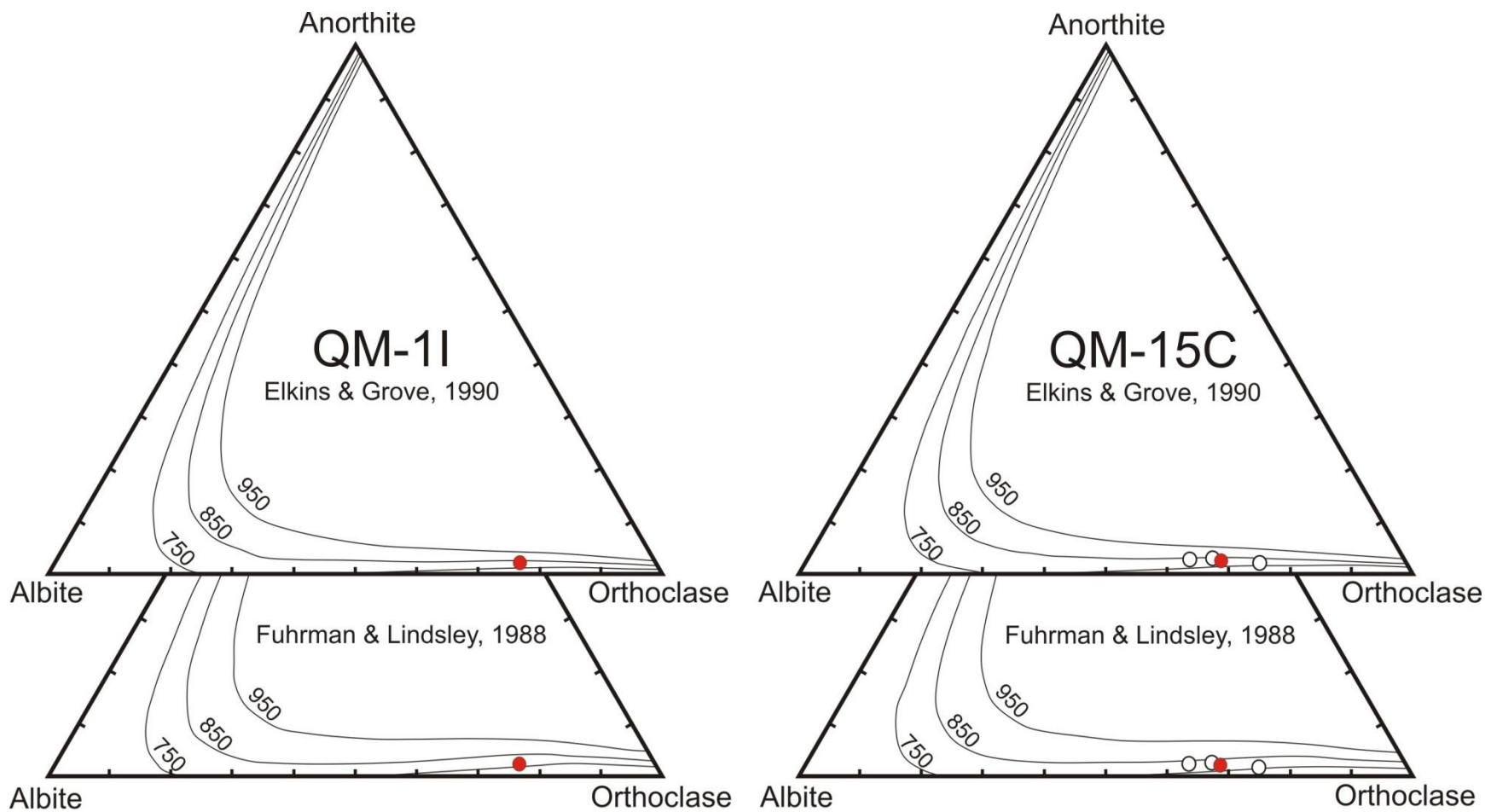


Figure 4-4: Ternary feldspar plots showing minimum temperatures provided by re-integrated feldspar thermometry using both the Elkins and Grove (1990), as well as the Fuhrman and Lindsley (1988) solution models. Red dots are overall re-integrated mineral compositions and white dots are average compositions from individual grains. Isotherms are labelled in degrees Celsius. Isotherms for sample QM-11 are calculated based on a pressure of 8 kbar, and for QM-15C a pressure of 7.5 kbar.

Table 4-2 (1 of 2): Mineral composition averages used in net-transfer and Fe-Mg exchange thermobarometry

<b>Garnet</b>						
	<b>QM-1C</b>	<b>QM-1F</b>	<b>QM-1I</b>	<b>QM-7D</b>	<b>QM-10D</b>	<b>QM-15C</b>
	<b>n=8</b>	<b>n=8</b>	<b>n=9</b>	<b>n=6</b>	<b>n=9</b>	<b>n=9</b>
SiO <sub>2</sub>	38.24	38.25	39.10	38.00	39.55	38.59
TiO <sub>2</sub>	0.04	0.04	0.01	0.02	0.01	0.01
Al <sub>2</sub> O <sub>3</sub>	21.19	21.48	22.03	21.42	22.44	22.06
Cr <sub>2</sub> O <sub>3</sub>	0.01	0.01	0.02	0.10	0.02	0.02
FeO	27.85	28.45	27.65	32.67	26.55	29.93
MnO	3.05	1.27	0.62	2.26	0.80	0.88
MgO	3.31	4.20	9.22	3.96	10.80	8.45
CaO	7.86	7.48	1.99	2.93	0.86	0.50
Na <sub>2</sub> O	0.01	0.01	0.02	0.03	0.02	0.02
K <sub>2</sub> O	0.00	0.00	0.00	0.00	0.00	0.02
Total	101.56	101.21	100.65	101.39	101.05	100.48
Si	2.9943	2.9857	2.9935	2.9937	2.9899	2.9846
Ti	0.0025	0.0025	0.0003	0.0009	0.0005	0.0006
Al	1.9559	1.9765	1.9881	1.9887	1.9997	2.0110
Cr	0.0004	0.0009	0.0015	0.0064	0.0009	0.0010
Fe	1.8240	1.8574	1.7707	2.1527	1.6786	1.9363
Mn	0.2021	0.0841	0.0399	0.1509	0.0514	0.0576
Mg	0.3859	0.4891	1.0529	0.4646	1.2172	0.9739
Ca	0.6592	0.6256	0.1630	0.2475	0.0694	0.0411
Na	0.0022	0.0021	0.0026	0.0044	0.0031	0.0035
K	0.0001	0.0001	0.0004	0.0003	0.0001	0.0021
Total	8.0265	8.0242	8.0128	8.0101	8.0109	8.0117
Grossular	0.2122	0.2047	0.0539	0.0821	0.0230	0.0136
Pyrope	0.1268	0.1600	0.3479	0.1541	0.4035	0.3237
Almandine	0.5956	0.6077	0.5850	0.7138	0.5565	0.6435
Spessartine	0.0654	0.0275	0.0132	0.0500	0.0170	0.0192
<b>Plagioclase</b>						
	<b>QM-1C</b>	<b>QM-1F</b>	<b>QM-1I</b>	<b>QM-7D</b>	<b>QM-10D</b>	<b>QM-15C</b>
	<b>n=9</b>	<b>n=6</b>	<b>n=4</b>	<b>n=8</b>	<b>n=12</b>	<b>n=5</b>
SiO <sub>2</sub>	56.88	49.78	59.64	59.76	62.63	64.58
TiO <sub>2</sub>	0.00	0.01	0.04	0.01	0.02	0.01
Al <sub>2</sub> O <sub>3</sub>	28.42	32.83	24.90	25.79	23.91	22.16
Cr <sub>2</sub> O <sub>3</sub>	0.01	0.01	0.01	0.01	0.01	0.02
FeO	0.15	0.13	0.13	0.16	0.19	0.07
MnO	0.00	0.01	0.01	0.01	0.01	0.02
MgO	0.01	0.01	0.01	0.01	0.01	0.01
CaO	9.96	15.11	6.52	7.31	5.04	2.93
Na <sub>2</sub> O	5.95	2.94	7.74	7.21	8.71	10.03
K <sub>2</sub> O	0.12	0.05	0.28	0.15	0.09	0.14
Total	101.52	100.87	99.28	100.42	100.62	99.97
Si	2.5184	2.2520	2.6776	2.6530	2.7582	2.8476
Ti	0.0000	0.0002	0.0012	0.0003	0.0006	0.0003
Al	1.4832	1.7509	1.3180	1.3492	1.2410	1.1519
Cr	0.0004	0.0004	0.0003	0.0004	0.0005	0.0006
Fe	0.0055	0.0048	0.0050	0.0058	0.0071	0.0028
Mn	0.0002	0.0004	0.0004	0.0005	0.0003	0.0006
Mg	0.0007	0.0008	0.0007	0.0004	0.0008	0.0006
Ca	0.4727	0.7326	0.3136	0.3476	0.2376	0.1385
Na	0.5103	0.2577	0.6748	0.6210	0.7435	0.8577
K	0.0070	0.0026	0.0162	0.0087	0.0053	0.0077
Total	4.9985	5.0023	5.0077	4.9869	4.9949	5.0085
Anorthite	0.4774	0.7378	0.3120	0.3556	0.2409	0.1380
Albite	0.5155	0.2595	0.6722	0.6354	0.7537	0.8544
Orthoclase	0.0071	0.0027	0.0158	0.0089	0.0054	0.0077

Table 4-2 (2 of 2): Mineral composition averages used in net-transfer and Fe-Mg exchange thermobarometry (continued)

<b>Clinopyroxene</b>			<b>Orthopyroxene</b>				<b>Cordierite</b>		
<b>Sample</b>	<b>QM-1C</b>	<b>QM-1F</b>	<b>Sample</b>	<b>QM-1F</b>	<b>QM-1I</b>	<b>QM-7D</b>	<b>Sample</b>	<b>QM=10D</b>	<b>QM-15C</b>
	<b>n=9</b>	<b>n=9</b>		<b>n=7</b>	<b>n=8</b>	<b>n=8</b>		<b>n=5</b>	<b>n=10</b>
SiO <sub>2</sub>	52.13	50.80	SiO <sub>2</sub>	51.03	51.40	50.13	SiO <sub>2</sub>	49.76	48.53
TiO <sub>2</sub>	0.12	0.30	TiO <sub>2</sub>	0.07	0.08	0.05	TiO <sub>2</sub>	0.01	0.01
Al <sub>2</sub> O <sub>3</sub>	1.37	2.64	Al <sub>2</sub> O <sub>3</sub>	1.22	3.57	1.52	Al <sub>2</sub> O <sub>3</sub>	33.72	33.11
Cr <sub>2</sub> O <sub>3</sub>	0.01	0.02	Cr <sub>2</sub> O <sub>3</sub>	0.03	0.09	0.04	Cr <sub>2</sub> O <sub>3</sub>	0.01	0.01
FeO	13.17	12.87	FeO	31.48	22.88	35.04	FeO	3.53	4.73
MnO	0.40	0.23	MnO	0.55	0.19	0.90	MnO	0.05	0.02
MgO	11.08	10.88	MgO	15.65	21.43	12.67	MgO	11.13	10.16
CaO	22.62	21.49	CaO	0.69	0.09	0.36	CaO	0.00	0.01
Na <sub>2</sub> O	0.29	0.43	Na <sub>2</sub> O	0.02	0.02	0.02	Na <sub>2</sub> O	0.08	0.09
K <sub>2</sub> O	0.01	0.02	K <sub>2</sub> O	0.00	0.01	0.00	K <sub>2</sub> O	0.00	0.00
Total	101.19	99.67	Total	100.73	99.76	100.73	Total	98.28	96.69
Si	1.9639	1.9369	Si	1.9726	1.9188	1.9732	Si	5.0085	4.9955
Ti	0.0034	0.0086	Ti	0.0019	0.0022	0.0015	Ti	0.0007	0.0011
Al	0.0609	0.1187	Al	0.0555	0.1572	0.0705	Al	4.0007	4.0169
Cr	0.0002	0.0006	Cr	0.0008	0.0027	0.0013	Cr	0.0011	0.0012
Fe	0.4151	0.4105	Fe	1.0177	0.7145	1.1535	Fe	0.2969	0.4076
Mn	0.0128	0.0073	Mn	0.0180	0.0062	0.0300	Mn	0.0040	0.0020
Mg	0.6221	0.6183	Mg	0.9016	1.1929	0.7435	Mg	1.6699	1.5595
Ca	0.9130	0.8779	Ca	0.0286	0.0036	0.0152	Ca	0.0005	0.0011
Na	0.0212	0.0315	Na	0.0012	0.0017	0.0013	Na	0.0149	0.0183
K	0.0006	0.0010	K	0.0001	0.0003	0.0001	K	0.0003	0.0004
Total	4.0131	4.0112	Total	3.9981	4.0000	3.9902	Total	10.9975	11.0038
Al <sub>M1</sub>	0.0411	0.0751	X <sub>Mg</sub>	0.4508	0.5965	0.3717	X <sub>Mg</sub>	0.8473	0.7920
X <sub>Mg</sub>	0.5998	0.6010	X <sub>Fe</sub>	0.5089	0.3573	0.5767	X <sub>Fe</sub>	0.1506	0.2070
X <sub>Fe</sub>	0.4002	0.3990	X <sub>Al</sub>	0.0139	0.0393	0.0176			
Mg <sub>M1</sub>	0.5730	0.5504							
Fe <sub>M1</sub>	0.3824	0.3654							
Al <sub>M1</sub>	0.0411	0.0751							
Ti <sub>M1</sub>	0.0034	0.0086							
Ca <sub>M2</sub>	0.9130	0.8779							
Mg <sub>M2</sub>	0.0395	0.0545							
Fe <sub>M2</sub>	0.0263	0.0362							
Na <sub>M2</sub>	0.0212	0.0315							

Table 4-3: Averaged K-feldspar host and plagioclase lamellae compositions used in reintegrated feldspar thermometry.

Sample	K-Feldspar Host					Plagioclase Lamellae				
	QM-11 Average n=14	QM-15C a n=5	QM-15C b n=5	QM-15C c n=5	QM-15C Average n=15	QM-11 Average n=14	QM-15C a n=5	QM-15C b n=5	QM-15C c n=5	QM-15C Average n=15
SiO <sub>2</sub>	64.54	64.42	64.46	64.85	64.58	63.19	65.81	65.99	66.01	65.94
Al <sub>2</sub> O <sub>3</sub>	19.18	19.18	19.01	19.04	19.07	23.60	21.96	21.45	21.94	21.78
FeO	0.01	0.00	0.02	0.02	0.01	0.01	0.02	0.02	0.02	0.02
BaO	0.07	0.03	0.04	0.06	0.04	0.04	0.04	0.04	0.04	0.04
CaO	0.08	0.02	0.01	0.01	0.01	4.16	2.18	1.56	2.20	1.98
Na <sub>2</sub> O	1.64	1.05	0.99	1.04	1.03	9.03	10.65	9.90	10.55	10.37
K <sub>2</sub> O	14.18	15.29	15.26	15.13	15.23	0.61	0.14	1.66	0.22	0.67
Total	99.70	99.98	99.80	100.15	99.98	100.64	100.79	100.62	100.98	100.80
Si	2.9718	2.9694	2.9762	2.9804	2.9753	2.7815	2.8736	2.8964	2.8770	2.8823
Al	1.0410	1.0420	1.0344	1.0314	1.0359	1.2245	1.1302	1.1096	1.1266	1.1221
Fe	0.0004	0.0002	0.0009	0.0006	0.0005	0.0004	0.0007	0.0006	0.0006	0.0006
Ba	0.0012	0.0004	0.0007	0.0012	0.0008	0.0008	0.0006	0.0008	0.0007	0.0007
Ca	0.0039	0.0010	0.0005	0.0004	0.0006	0.1964	0.1020	0.0734	0.1028	0.0927
Na	0.1460	0.0935	0.0888	0.0927	0.0917	0.7711	0.9016	0.8424	0.8918	0.8786
K	0.8330	0.8994	0.8990	0.8872	0.8952	0.0343	0.0077	0.0929	0.0122	0.0376
Total	4.9974	5.0059	5.0006	4.9939	5.0001	5.0089	5.0165	5.0160	5.0117	5.0147
X <sub>Ca</sub>	0.0040	0.0010	0.0005	0.0004	0.0006	0.1963	0.1009	0.0729	0.1021	0.0920
X <sub>Na</sub>	0.1486	0.0940	0.0898	0.0945	0.0928	0.7699	0.8915	0.8365	0.8858	0.8713
X <sub>K</sub>	0.8474	0.9050	0.9097	0.9051	0.9066	0.0338	0.0076	0.0906	0.0121	0.0368
Mod. Vol %	90.0	82.4	66.2	74.0	74.2	10.0	17.6	33.8	26.0	25.8
Mod. Wt %	89.7	82.1	65.7	73.5	73.7	10.3	17.9	34.3	26.5	26.3

	Reintegrated Feldspar Composition (%)				
	QM-11 Average	QM-15C a	QM-15C b	QM-15C c	QM-15C Average
Anorthite	0.0245	0.0196	0.0261	0.0283	0.0255
Albite	0.2147	0.2427	0.3536	0.3113	0.3042
Orthoclase	0.7609	0.7377	0.6203	0.6604	0.6703

## **CHAPTER 5 – Evolution of the Queen Maud Block**

Petrographic and field observations, as well as the geochronological and geothermobarometric data presented in the preceding three chapters enhance the understanding of the tectonic evolution of the QMB. These new data, as well as work conducted in earlier studies are synthesized in this chapter. In Section 5.1, I present a new lithological and geochronological map of the northern QMB. Section 5.2 summarizes the metamorphic history of the QMB, including the timing and P-T conditions of metamorphism. Section 5.3 is an overview of previous tectonic models that have been proposed for the QMB and northwestern Laurentia, whereas Section 5.4 presents a revised model based the new data obtained in the present study.

### **5.1 – A geological map of the Queen Maud block**

Throughout the course of field reconnaissance as well as geochronological study, it became apparent that the geology of the northern QMB is not accurately depicted in existing geological maps. The revised geological map presented here (Figure 5-1) is drawn at a scale of approximately 1:2,000,000. In spite of its being drawn at a smaller scale than previous maps, it more accurately represents the lithology and geochronology of the northern QMB area.

Seven distinct map units cover the area from 96° to 104° west and 67° to 68° north. Three of these map units exist outside of the QMB, including the Paleozoic platform cover, the Paleoproterozoic Thelon tectonic zone, and the Rae domain (Units 1, 2, and 5 respectively). The remaining four map units combine to form the QMB. Contacts between map units are discussed individually, but in general are based on aeromagnetic signatures or contacts defined by previous authors. Due to the small scale at which this map is drawn, these contacts should be considered approximate. Map units are described in order of increasing age throughout this section.

Rocks of the eastern and western QMB contrast sharply with one another, as described throughout this section. For this reason, the western QMB, which is dominated by Mesoarchean and Neoproterozoic gneisses, is referred to as the Perry River belt (PRB). The eastern QMB, which is dominated by Paleoproterozoic rocks including the Queen Maud granitoids and the Sherman supracrustal rocks, is termed the Paalliq belt. The contact between the two belts is aeromagnetically expressed as a change from the higher and more uniform magnetic signature of the Paalliq belt, to the generally lower and more irregular signature of the PRB (Geological Survey of Canada, 1982).

The PRB is named for Perry River, one of the largest rivers in the QMB area and one of several that run through the PRB. Perry River has traditionally been one of the most utilized corridors in the area and until 1968, permanent residents lived at a small outpost near the Perry River (Goldring et al., 2011). The Paalliq belt is named for one of the largest rivers in the eastern QMB. This river (also known as McNaughton River) flows into and out of McNaughton Lake, the largest lake in the QMB area. The area surrounding Paalliq and Paalliup Tahirjua (McNaughton Lake) is an important archaeological site (Goldring et al., 2011).

Unit 1: Paleozoic platform cover

Unit one consists of dominantly flat-lying Paleozoic sedimentary rocks unconformably overlying the Archean and Proterozoic rocks comprising the shield. Contacts between this unit and surrounding shield areas are based on earlier geological maps (e.g., Wheeler et al., 1996).

Unit 2: Paleoproterozoic Thelon tectonic zone

The Thelon tectonic zone (TTZ) is composed of amphibolite- to granulite-facies migmatitic granitoids, mafic and quartzofeldspathic gneisses, and several other minor units (James, 1989). Mineral assemblages and P-T data from the TTZ indicate the area is metamorphosed at high T, low P conditions (James, 1989; Thompson, 1989). P-T conditions reported for the central TTZ are 650°C-675°C and 6-7 kbar (James, 1989). Zones of high-strain, caused by dip-slip as well as strike-slip shearing are present in the TTZ (Hanmer et al., 1992).

Sample QM-6B is a porphyritic granodiorite gneiss collected from near the eastern edge of the TTZ and is dated at 2.01 Ga. This age is consistent with those from previous studies that found that the majority of plutonic rocks in the TTZ are Paleoproterozoic in age, dated between 2.01 and 1.91 Ga (van Breemen and Henderson, 1988; van Breemen et al., 1987a; van Breemen et al., 1987b). Granitoid rocks post-dating 1.95 Ga are unstrained, whereas older granitoids are deformed (van Breemen and Henderson, 1988; van Breemen et al., 1987a).

In addition to the 2.01-1.91 Ga granitoids dominating the TTZ, there is cryptic evidence for an older generation of magmatic rocks. Xenocrystic zircon grains from a granitoid rock have been dated between 2.4 and 2.2 Ga (van Breemen et al., 1987b) and the present study identified a xenocrystic zircon dated at 2.35 Ga in sample QM-6B.



Rocks of these ages have been found further south as well, in the Taltson magmatic zone (Bostock and van Breemen, 1994; Hartlaub et al., 2007; McNicoll et al., 2000). The TTZ also preserves Paleoproterozoic metasedimentary rocks, known as the Mary Frances sediments, that were deposited between 2.2 and 2.0 Ga (Henderson and van Breemen, 1992). Rare outcroppings of ca. 2.6 Ga plutonic rocks have been identified in the western TTZ (Henderson and van Breemen, 1992; van Breemen et al., 1987a).

The contact between the TTZ and the QMB is taken from existing geological maps and is based on the contrast between the high magnetic signature of the TTZ relative to the crustal block immediately to the east (e.g., Wheeler et al., 1996; Geological Survey of Canada, 2010).

*Unit 3: Paleoproterozoic metasedimentary and metavolcanic gneiss (Sherman Group)*

This unit consists primarily of metasedimentary and metavolcanic migmatites and gneisses belonging to the Sherman Group. This map unit was first identified and described by Schultz et al. (2007) and Schultz (2007). Metasedimentary rocks vary in composition from psammitic to semi-pelitic and are generally migmatized. Metavolcanic rocks are predominantly mafic in bulk composition. Minor granitic, pegmatitic, and mafic rocks intrude these supracrustal rocks. Structural fabrics are generally steeply dipping and trend in a N to NE direction (Heywood, 1961). Orthopyroxene and cordierite-garnet-K-feldspar assemblages are widespread, indicating that these rocks are metamorphosed at granulite-facies (Heywood, 1961; Schultz et al., 2007). Schultz et al. (2007) determined the timing of this granulite-facies metamorphism at approximately 2.39 Ga, based on dating of monazite grains in semi-pelitic gneisses.

The Sherman group is thought to have been deposited between 2.45 and 2.39 Ga as constrained, respectively, by the youngest detrital zircon recovered from semi-pelitic gneisses and the age of granulite-facies metamorphism recorded by these same gneisses (Schultz et al., 2007). Metasedimentary rocks in this unit are dominated by 2.50-2.45 Ga detritus thought to be sourced from the Queen Maud granitoids (Unit 4) which bound either side of this sedimentary basin (Schultz et al., 2007).

This unit coincides with a prominent low aeromagnetic anomaly dubbed the ‘central magnetic low’ by Schultz et al. (2007). The contacts between this and adjacent units are drawn according to the extent of this low magnetic anomaly. The western contact of this unit also coincides with a distinct 010° trending high-strain zone thought to be a regional-scale shear zone. Mineral lineations within this high-strain zone are sub-

horizontal, suggesting that the most recent displacement along this shear-zone was strike-slip. The present study identified what is interpreted to be syn-tectonic alkali feldspar granite sheets, dated at 2426 Ma, within this shear zone (Sample QM-13G).

Unit 4: Paleoproterozoic granitic gneiss (Queen Maud granitoids)

Unit four is dominated by the orangey-pink weathering bimodal mafic-felsic igneous suite referred to as the Queen Maud granitoids. This unit was first identified by Schultz et al. (2007), and further investigated as part of this study. Granitoid gneisses and migmatites within this map unit vary in composition from tonalitic to alkali feldspar granitic. Locally, these metagranitoids contain large K-feldspar porphyroclasts, which likely originated as igneous megacrysts; however, igneous textures such as these are commonly obscured due to metamorphic recrystallization. Abundant dark grey mafic inclusions are present throughout these granitoids. Minor mafic and pegmatitic dykes are present, as well as yet rarer metasedimentary enclaves. Structural fabrics and degree of strain are highly variable but typically a N to NE trend of steeply dipping gneissosity is observed (Heywood, 1961). Within the map area, the unit is metamorphosed at granulite-facies conditions as evidenced by the widespread occurrence of orthopyroxene in mafic and granitic lithologies. The timing of this metamorphism is dated ca. 2.36-2.39 Ga (This study; Schultz et al., 2007)

The initial work in the area conducted by Schultz et al (2007) provides ages for the majority of granitoids from this map unit between 2.50 and 2.46 Ga. U-Pb dating of zircon grains from samples QM-13A, QM-13D, and QM-16A collected for the present study exhibit crystallization ages consistent with the Queen Maud granitoid suite. Interestingly, sample QM-15A is dated at  $2516 \pm 13$  and sample QM-13E is dated at  $2450.4 \pm 6.6$  Ma. Although the precise age of sample QM-14A is poorly constrained, it is dated at  $2532 \pm 29$  Ma. These results indicate the Queen Maud granitoid suite may include rocks older and younger than previously thought, and expand the age range of this suite to approximately 2.52-2.45 Ga. Mafic inclusions from within the Queen Maud granitoids have also been dated and are found to be broadly coeval with the granitoid rocks, providing ages between 2.47-2.50 Ga (Sample QM-13H; Schultz, 2007).

Neoarchean granitoids that crystallized between 2.6 and 2.7 Ga have also been recognized in this map unit, but are relatively rare compared with the 2.52-2.45 Ga Queen Maud granitoids (Schultz et al., 2007). Furthermore, sample QM-16A contains a population of ~2.7 Ga zircon ages, thought to be xenocrystic. The Queen Maud and

Neoproterozoic granitoids have similar Nd depleted mantle model ages (mostly between 2.8 and 3.0 Ga) which suggests that both granitoid suites are derived from similar late Mesoarchean source rocks (Schultz et al., 2007).

This map unit coincides with Schultz et al.'s (2007) eastern and western magnetic highs. The eastern most contact is defined by a prominent mylonite zone and constrains the Queen Maud granitoids within the QMB (Schultz et al., 2007). The western most contact is aeromagnetically defined along a change from generally higher magnetic signature of the Paleoproterozoic granitoids in this unit to the generally lower and more irregular signature of the dominantly Archean rocks in the adjacent unit 7.

#### Unit 5: Rae domain

Although the area of the Rae domain that directly borders the QMB has been little studied, an abundance of recent research has been published from several hundred kilometres to the east of the QMB, in the area referred to as the Committee Bay belt. This area is dominated by a variety of Neoproterozoic granitoids and greenstone belts with subordinate Paleoproterozoic granitoids and supracrustal sequences (Skulski et al., 2003). In the map area, the Rae domain is very similar in appearance to Unit 4 (the Queen Maud granitoids) to the west (Schultz et al., 2007). The fundamental difference, however, is the fact that none of the Paleoproterozoic Queen Maud granitoids have been documented in this area. Rather, the area is dominated by Neoproterozoic granitoids.

The oldest Nd model ages from the Committee Bay belt are 3.1-2.9 Ga in age and are found in the area immediately adjacent to the QMB (Schultz, 2007). Farther east, directly to the south of Boothia Peninsula, model ages are 2.95-2.75 Ga (Peterson et al., 2010). Although model ages indicate the presence of late Mesoarchean rocks in the area, no rocks of this age have been directly dated in the Committee Bay belt. The oldest rocks in this area are a belt of Neoproterozoic supracrustal rocks referred to as the Prince Albert Group. A felsic tuff in this group has been dated at 2.73 Ga (Skulski et al., 2003). Further constraining the age of deposition of the Prince Albert Group is the youngest detrital zircon of 2.72 Ga and an unconformably overlying tuff dated at 2.71 Ga (Skulski et al., 2003). In addition to ca. 2.7 Ga granitoids, extensive plutonic rocks dated between 2.61-2.58 are documented in the Committee Bay belt (Skulski et al., 2003). Skulski et al. (2003) report a second period of sedimentary deposition from 2.69-2.58 Ga. The westernmost Committee Bay belt, adjacent to the QMB, contains an overlying Paleoproterozoic sedimentary basin referred to as the Amer Group. The timing of deposition of the lower

assemblages in this group are poorly constrained, but post-date 2.6 Ga and pre-date 2.1 Ga (Rainbird et al., 2010). It is possible that the lower Amer Group assemblages correlate with the Sherman Group, but until the timing of deposition of the Amer Group is better constrained, this remains entirely speculative. Trans-Hudson aged granitoids dated ca. 1.82 Ga are also encountered throughout the Committee Bay belt (Skulski et al., 2003).

The metamorphic history of the eastern Committee Bay belt has been examined in detail (Berman et al., 2005; 2010; Carson et al., 2004). These studies have found that the area has undergone several metamorphic events. Textural evidence indicates a thermal event associated with 2.61-2.58 Ga plutonism took place (Berman et al., 2005). Monazite dating and thermobarometric calculations indicate a metamorphic event occurred ca. 2.35 Ga, with peak P-T conditions of 560°C and 4.2 kbar, and an additional event at ca. 1.84 Ga, with associated P-T conditions of 570°C and 5.9 kbar (Berman et al., 2005).

#### Unit 6: Neoproterozoic granitic gneiss

This map unit consists primarily of upper amphibolite- to granulite-facies granitoid rocks exhibiting moderately well-developed gneissic textures and also contains abundant unmetamorphosed mafic dykes. The gneisses vary in composition from tonalitic to granitic. The cross-cutting mafic dykes consistently trend 355°, are 20-30 meters wide, and exhibit well preserved chilled margins.

These pluton-shaped granitoid bodies crystallized around 2.7 Ga, as indicated by the dating of samples QM-4B and QM-5B. This coincides with the age of Neoproterozoic tonalite-trondhjemite-granodiorite rocks found throughout much of the Rae domain and in other areas of the QMB. The mafic dykes remain undated; however their trend and undeformed nature suggest they may belong to the 1.27 Ga Mackenzie dyke swarm (LeCheminant and Heaman, 1989).

The extent of the granitic bodies and the contacts separating them from the surrounding Unit 7 are based on Fraser's (1964) original geological map of the area. The fundamental difference in appearance between this map unit and Unit 7 is that this unit is more lithologically homogenous with less well developed gneissosity, whereas Unit 7 is more lithologically diverse with a relatively strongly developed gneissosity.

#### Unit 7: Mesoproterozoic to Neoproterozoic mixed gneiss

Unit 7 is a lithologically diverse unit consisting primarily of highly deformed gneisses of variable bulk composition. This unit is by far the most heterolithic of all the map units drawn. Although metagranitoids dominate this unit, metavolcanic and metasedimentary gneisses and migmatites are present throughout the area. Cross-cutting pegmatite and mafic dykes are common and trend a variety of directions. Undeformed and unmetamorphosed granitic and mafic plutons of considerably younger age locally intrude these gneisses, but have not been drawn due to the scale of this map. Structural fabrics are highly variable, though in general trend NNE-SSW and are steeply dipping. Regional metamorphism in this area is dated at around 2.36 Ga, with ongoing monazite growth through to 2.1 Ga (Section 5.2).

U-Pb dating of zircon grains from samples QM-2C, QM-2D, QM-7C, QM-10A, QM-10B, and QM-17C reveal that much of the unit is composed of early Mesoarchean granitoid gneisses with emplacement ages from 3.2-3.1 Ga. Other granitoids within this map unit are dated at around 2.7 Ga (McCormick, 1992; Chacko, unpublished data). These Neoproterozoic rocks are similar in age to those that dominate Unit 6 and much of the Rae domain. Sm-Nd isotopic analysis of several samples collected south of the map area provide Nd model ages between 3.6 and 3.1 Ga (Theriault et al., 1994).

Detrital zircon analysis of two metasedimentary samples indicates that several generations of supracrustal rocks may be present in this map unit. The youngest detrital zircon, and therefore the maximum depositional age of sample QM-1H is dated at 2576 Ma. Other supracrustal rocks identified at this location are mafic in bulk composition or metamorphosed iron formations (Figure 2-2c; 2-2d; 2-2e). These lithologies are common in Neoproterozoic greenstone belts found throughout Laurentia. In contrast, the youngest detrital zircon from sample QM-10C is dated at 3089 Ma, suggesting that this semi-pelite belongs to a different sedimentary assemblage that may have been deposited at a different time. Other supracrustal rocks at this location are peculiar in terms of mineralogy and bulk composition. An orthopyroxenite with exceptionally large grains, up to 10cm in length, was identified (Figure 2-2f), as well as rocks of pelitic bulk composition with exceptionally large, sapphire-blue cordierite grains (Sample QM-10D).

Subordinate to the Archean granitic and supracrustal rocks present throughout the unit are several generations of Paleoproterozoic magmatic rocks. Undeformed mafic and granitic plutons (samples QM-8A & QM-8B) are both dated at approximately 2.32 Ga. A minimum age of 2.21 Ga was acquired from a cross-cutting and deformed pegmatite dyke (sample QM-9D) and another minimum age, from a cross-cutting and metamorphosed



mafic dyke, is 2.10 Ga (sample QM-1C). Additional undated mafic and pegmatite dykes of variable mineralogy and orientation are present throughout this map unit.

## **5.2 – Metamorphic history of the Queen Maud block**

In Chapter 2, textural evidence was presented for no less than three metamorphic events having affected the QMB. Geochronology and geothermobarometric calculations presented in Chapter 3 and 4 provide further insight into the metamorphism of the area. In this section the timing and P-T conditions associated with M1 and M2 metamorphism are presented, as well as the timing of additional metamorphic events. The metamorphic events to affect the QMB are discussed in chronological order.

### 5.2.1 – Archean metamorphism

Despite the abundance of Archean rocks, particularly in the western QMB, there is very little evidence for Archean metamorphism. The only geochronological data indicating any metamorphic activity at this time comes from samples QM-4B, QM-5B, QM-10A, and QM-17C. These granitoids are thought to have crystallized at various times throughout the Archean, however also provide several younger Neoproterozoic U-Pb ages. These ages may be the result of metamorphic events that took place during the Archean. Alternatively, they may simply be the result of Pb loss from magmatic zircon grains during Paleoproterozoic metamorphism.

It is possible that several metamorphic events did occur throughout the Archean; most likely during tectonism associated with the intrusion of the 3.2-3.1 Ga granitoid rocks dated from Unit 7, and again during intrusion of the ca. 2.7 Ga granitoids present throughout the QMB. Additional metamorphism may have occurred ca. 2.6 Ga; a metamorphic event at this time was inferred in the Committee Bay belt several hundred kilometres to the east of the QMB (Berman et al., 2005).

### 5.2.2 – Metamorphism: ca. 2.52-2.45 Ga

A population of  $^{207}\text{Pb}/^{206}\text{Pb}$  monazite ages from sample QM-10C is dated at 2.46 Ga, concurrent with intrusion of the 2.52-2.45 Ga Queen Maud granitoids. In Chapter 3 it was argued that this monazite population is metamorphic in origin. Metasedimentary rocks from the Sherman Basin also record monazite ages in this range, although Schultz et al. (2007) interpreted these grains as being inherited monazite cores.

Figure 5-3 shows the distribution of 2.52-2.45 Ga monazite ages as being restricted to the eastern and central QMB, similar to the distribution of the Queen Maud granitoids. The spatial distribution in the occurrence of these ages lends credence to the interpretation that they are the result of metamorphism associated with intrusion of the Queen Maud granitoids.

Unfortunately, the metamorphic conditions associated with this metamorphism could not be determined. Sample QM-15C is a granulite-facies pelitic rock collected from the same outcrop where sample QM-15A was collected (a granitoid rock interpreted to have been emplaced at  $2516 \pm 13$  Ma). Thermobarometric calculations for sample QM-15C reveals P-T conditions of 825°C and 6.8 kbar, which is consistent with the conditions associated with 2.39-2.35 Ga regional M1 metamorphism. Thus, the mineral assemblage that would have formed during granitoid intrusion and contact metamorphism was likely re-equilibrated during regional M1 metamorphism.

### 5.2.3 – Metamorphism: ca. 2.43-2.42 Ga

Samples QM-9C and QM-13G both contain 2.43-2.42 Ga age populations, and both locations contain very highly strained zones characterized by the development of straight gneiss. Sample QM-9C is a garnet-biotite psammitic migmatite, whereas QM-13G is an alkali feldspar granite that is thought to have intruded syn-tectonically (at 2.426 Ga) with strike-slip shearing. Based on modal mineralogy, the composition of sample QM-13G is consistent with that of a magma derived from partial melting of continental crust. If 2.426 Ga is indeed the crystallization age of sample QM-13G, rather than a metamorphic age, then evidently minor amounts of crustal melting occurred at this time. The shear zone in which sample QM-13G was collected is visible as a sharp change in aeromagnetic signature, and extends 010° for several hundred kilometres. A similarly trending fault zone was mapped near location QM-9 by Heywood (1961).

Schultz (2007) report a monazite age of 2.43 Ga from sample ST-4a, which was collected from a Grt-Bt leucosome injected parallel to layering within a high-strain zone. ST-4a was collected from roughly 50 km south along strike from the shear-zone at location QM-13. Berman et al. (2005) cite data acquired at the University of Massachusetts wherein a 2.41 Ga age population is preserved in monazite grains in a sample collected from the southeastern QMB.

Though geochronological evidence for metamorphism and crustal melting at 2.43-2.42 Ga is rare, these ages appear to be restricted to areas where ~010° trending

high-strain shear zones have developed. This suggests that metamorphism at this time is a local phenomenon that may have occurred in response to regional-scale strike-slip shearing of the QMB at 2.43-2.42 Ga. I speculate on the causes of this tectonism in Section 5.4.

5.2.4 – Regional metamorphism: 2.39-2.35 Ga Arrowsmith Orogeny

The widespread nature of U-Pb dates in both zircon and monazite between 2.39 and 2.35 Ga indicate significant regional metamorphism of the QMB at this time. Figure 5-3 illustrates the distribution of these metamorphic ages across the entire QMB. This period of widespread zircon and monazite growth likely represents the approximate timing of the M1 granulite-facies metamorphic event identified in field work and evaluated for its P-T conditions. It is also likely that the dominant metamorphic fabrics throughout the QMB formed at this time. The extent and severity of this tectono-metamorphic event has overprinted nearly all evidence for earlier metamorphic events in the area. The timing of this regional metamorphism is concurrent with the timing of the Arrowsmith Orogeny, evidence for which has been found throughout much of the western Churchill Province (e.g., Berman et al., 2005; Hartlaub et al., 2007; McNicoll et al., 2000; Schultz et al., 2007)

The probability density plots shown in Figure 5-2 highlight the significance of this period of monazite growth in the QMB. In addition to monazite growth, a cluster of  $^{207}\text{Pb}/^{206}\text{Pb}$  ages from zircon analyses from sample QM-17B, a highly deformed mafic dyke, are dated around 2.39 Ga. Zircon grains from this sample have rounded edges and irregular shapes, consistent with the morphology of those grown during metamorphism (Corfu et al., 2003). Furthermore, analyses of overgrowth rims of zircon grains in samples QM-2C and a sample collected from near Perry River, exhibit  $^{207}\text{Pb}/^{206}\text{Pb}$  ages between 2.35 and 2.37 Ga (Chacko, unpublished data). Schultz et al. (2007) also report numerous U-Pb monazite ages around 2.39 Ga from the eastern QMB.

In Chapter 4, the case was made that samples QM-11, QM-10D, and QM-15C most accurately preserve the P-T conditions associated with M1 metamorphism. The approximate temperatures of equilibration of these three samples are 825°C and 8-10 kbar, >700°C and 7.6 kbar, and 825°C and 6.8 kbar, respectively. Geothermobarometric analysis from a sample collected from the Sherman sedimentary basin (ST-1a) in the eastern QMB indicates P-T conditions of approximately 780°C and 6.2 kbar using the Grt-Crd-Sil-Qtz geobarometer and the Grt-Crd geothermometer (Chacko, unpublished

data). The P-T conditions recorded for M1 metamorphism in the QMB are well into granulite-facies and consistent with a burial depth of 25-30 km and an elevated geothermal gradient of 35-40 °C/km. It is worth noting the steady decrease in metamorphic pressures moving eastward in the QMB, as shown in Figure 5-3; this is discussed further in Section 5.4.

I propose that deformation associated with 2.39-2.35 Ga metamorphism formed the dominant metamorphic fabrics observed throughout the QMB. Schultz et al. (2007) state that monazite grains dated at 2.39 Ga are situated within melt leucosomes, and interpreted this to mean that the timing of monazite growth also dated the timing of leucosome formation. Although no obvious textural relationship between monazite grains and metamorphic fabric was observed in samples collected for this study, the principal direction of the metamorphic fabrics is consistent throughout the QMB, suggesting they formed during a single event. Samples QM-8A and QM-8B, a gabbro and granite respectively, are both dated at approximately 2.32 Ga. These rocks exhibit no evidence for having been deformed or metamorphosed. This suggests, but does not prove (due to the possibility that strain partitioning allowed these rocks to escape deformation), that the penetrative deformation associated with the Arrowsmith Orogeny had ceased by 2.32 Ga in the northern QMB.

#### 5.2.5 – Post Arrowsmith metamorphism: 2.35-2.10 Ga

The metamorphic history of the QMB during the 250 million years after the Arrowsmith Orogeny is complicated and enigmatic. The dating of several magmatic rocks from the western QMB indicates multiple Post-Arrowsmith magmatic events in this area. Gabbroic and granitic samples, QM-8A and QM-8B, are both dated at approximately 2.32 Ga and minimum ages of a pegmatite dyke and mafic dyke are 2.21 and 2.10 Ga, respectively (samples QM-9D and QM-1C).

The probability density plots of monazite ages shown in Figure 5-2 reveal a range of ages spanning the interval from ~2.35-2.10 Ga. Interpreting this spread of ages is difficult as there are several potential causes. Catlos et al. (2002) and Parrish (1990) describe several sources of uncertainty in in-situ monazite dating, including Pb loss due to a prolonged period above the closure temperature of monazite (>900 °C (Cherniak, 2000; Cherniak et al., 2004)), dissolution/reprecipitation or recrystallization along the retrograde path, analyses of overlapping age domains, and episodic monazite growth.

Additionally, such an array of ages could simply represent a discordia line, where initial growth occurred at 2.35 Ga or earlier, and a Pb loss event occurred at 2.10 Ga or younger.

Several considerations must be made in regards to the 2.35-2.10 Ga spreading of monazite ages. It is observed that this age population is restricted to samples collected from the western-most QMB (Figure 5-3)—the same area that records the highest P-T conditions associated with 2.39-2.35 Ga regional metamorphism. Although this area does record high temperature conditions (up to ~825°C), peak temperatures do not exceed the closure temperature of monazite, and therefore it is unlikely that Pb loss by diffusion occurred in this area.

A possibility for this spread of ages is that it may be due to the influences of metamorphism associated with episodic magmatism between 2.35 and 2.10 Ga. One possible effect is multiple episodes of monazite growth, which could lead to domains with different ages within a single monazite grain. The probability density plots in Figure 5-2 show that monazite ages do not evenly span the interval between 2.35 and 2.10 Ga, but rather occur in several distinct peaks at approximately 2.33-2.30, 2.23, 2.20, 2.15, and 2.10 Ga. Moreover, on the basis of BSE image analysis, the case was made that in sample QM-1A the spread of ages may in part be the result of analytical spots sampling more than one age domain, which would produce meaningless intermediate ages.

Although interpretation of the post-Arrowsmith metamorphic history of the western QMB is difficult, the currently available evidence suggests that multiple metamorphic events associated with minor magmatic pulses occurred between 2.35 and 2.10 Ga. Such a series of events may be responsible for the array of monazite ages from 2.35-2.10 Ga documented in the western QMB.

#### 5.2.6 – Thelon Orogeny: 2.01-1.91 Ga

The TTZ is a curvilinear belt of magmatic and metamorphic rocks that crystallized and were metamorphosed between 2.01 and 1.91 Ga (e.g., Hoffman, 1988). Two samples collected for the present study preserve U-Pb ages within this 2.01-1.91 Ga time window. One of these samples is a porphyritic granodiorite gneiss collected from the eastern most TTZ that crystallized at 2.01 Ga (Sample QM-6B). The only sample from outside the TTZ that provides Thelon aged dates is the cross-cutting mafic dyke identified at location QM-1, in the western most QMB (Sample QM-1C). Zircon grains from this sample, interpreted as being metamorphic in origin, yield an age of 1.93 Ga. Thus, 1.93 Ga is interpreted as the approximate age of M2 metamorphism described in Chapter 2.

This mafic-dyke contains a weakly developed foliation, indicating that minor deformation may be associated with this metamorphism at this location.

Quantitative thermobarometric calculations conducted on sample QM-1C provide minimum P-T conditions of approximately 720°C and 7.5 kbar. The metamorphic temperatures associated with M2 are slightly lower than those of M1 metamorphism, which in this area are ~825°C (Sample QM-1I). The fact that M2 temperatures are significantly lower than M1 temperatures may account for the observation that no other samples from this location document ages around 1.93 Ga.

East of location QM-1, there are no documented Thelon aged metamorphic or magmatic dates. As mentioned in Chapter 2, there is no petrologic evidence for M2 metamorphism east of location QM-9, nor is there any significant deformation associated with M2. These observations indicate that Thelon aged tectono-metamorphic activity is restricted to the western-most reaches of the QMB, and affect this area in a relatively minor manner when compared with 2.39-2.35 Ga regional metamorphism.

It has been suggested that the QMB was in fact affected during Thelon orogenesis, and the reason that no evidence of this is preserved is due to high-grade metamorphism during the Arrowsmith Orogeny making the QMB rocks unreactive. There are several lines of evidence that indicate that this is not the case: first, is the fact that numerous monazite ages younger than 2.35 Ga are recorded in rocks from the QMB, which indicates that rocks were indeed reactive after the Arrowsmith Orogeny; second, comes from samples QM-8A and QM-8B, which are an undeformed and unmetamorphosed gabbro and granite, respectively. These rocks both crystallized ca. 2.32 Ga and preserve absolutely no evidence for Thelon-aged deformation or metamorphism.

#### 5.2.7 – The Trans-Hudson Orogen: ca. 1.9-1.8 Ga metamorphism

A single monazite analysis from sample QM-1D yields a  $^{207}\text{Pb}/^{206}\text{Pb}$  age of 1843 ± 21 Ma. A pegmatite dyke collected from the Paalliq belt exhibits a crystallization age overlapping with the Trans-Hudson Orogeny as well (Chacko, unpublished data). The rare and local occurrence of Trans-Hudson aged dates indicates that the area was affected by orogenesis at this time, albeit in a very minor manner. A significant Trans-Hudson Orogen overprint is found in many areas of the Rae domain (e.g., Berman et al., 2005; Orrell et al., 1999), but evidently, not the QMB.



### **5.3 – A review of previous models for the Slave-Churchill relationship**

Prior to developing a revised model for the evolution of the northwestern Canadian Shield, it is worth reviewing earlier models that have been proposed. Hoffman's model (1987) for the evolution of the area is the most widely accepted and postulates that the Slave and Churchill provinces are distinct Archean continental blocks that collided between 2.01 and 1.91 Ga forming the Taltson-Thelon zone. Aspler and Chiarenzelli (1998) expanded on this hypothesis, and proposed that the Slave and Churchill cratons were joined in the Archean, rifted apart between 2.5 and 2.1 Ga, and collided ca. 2.01-1.91 Ga as per Hoffman's model. An alternative model asserts that the Taltson-Thelon zone is an area of intracontinental tectonism and that the Slave and Churchill provinces must have collided at an earlier time (Chacko et al., 2000; De et al., 2000). Schultz et al. (2007) suggested this collision occurred between 2.4 and 2.3 Ga, during the Arrowsmith Orogeny.

#### 5.3.1 – 2.01-1.91 Ga collision of the Slave and Churchill cratons

In Hoffman's model, 2.01-1.91 Ga collision of the Slave and Churchill cratons followed eastward dipping subduction beneath the Churchill Province. Using the India-Asia collision as an analogue, Hoffman suggested that the TTZ represents a deeply eroded Himalayan style mountain belt and the QMB a deeply eroded Tibetan Plateau. Hoffman went on to interpret the Kilohigok Basin (refer to Figure 1-1) as a foreland basin associated with this orogeny, and the Great Slave Lake shear zone as a continental scale strike-slip fault system associated with crustal shortening and collisional indentation. Hoffman's (1987) publication, as well as several later publications, cite a variety of geophysical, geochronological, geochemical, and sedimentological evidence in support of this collisional model.

A strong argument for the presence of a continental suture near the Thelon front was made based on the presence of a paired gravity anomaly between the McDonald and Bathurst faults (Gibb and Thomas, 1977). Gibb (1978) took this proposed suture one step further, suggesting that the conjugate McDonald and Bathurst faults are the result of collisional indentation of the Slave Province into the Churchill Province. However, the timing of formation of this gravity anomaly had not yet been constrained.

The Kilohigok Basin is a sedimentary basin deposited synchronously with orogenesis in the TTZ (Bowring and Grotzinger, 1992; McCormick, 1992). In a collisional model, the Kilohigok Basin can be interpreted as having its beginnings as a

foredeep basin, with later depositional sequences interpreted as foreland basin deposits (Tirrul and Grotzinger, 1990), much like those found in the Western Canadian Sedimentary Basin. An ash layer found in this basin has been dated at 1.97 Ga (Theriault, 1992). It was the discovery of this ash layer and the timing of early movement along the Great Slave Lake shear zone, determined by the dating of a syntectonic granitoid (Hanmer et al., 1992), that led Theriault (1992) to propose that the Slave and Churchill provinces terminally collided at ca. 1.97 Ga.

If a collisional model is indeed correct, one should expect to find variation in the isotopic signatures of granitoids in the Taltson-Thelon magmatic zone. More specifically, granitoid suites that intruded prior to the suggested 1.97 Ga date of collision should exhibit continental arc-like isotopic signatures, while younger suites should exhibit continental crust-like signatures. Theriault (1992) interpreted the early Deskenatlata suite to have formed as a result of subduction of oceanic crust beneath a continent, while the later Slave and Konth suites were interpreted to have been derived by melting of continental crust only. A more thorough geochemical study of the Deskenatlata suite provides conflicting evidence for the origins of these igneous rocks (Chacko et al., 2000; De et al., 2000).

Numerous counter-arguments can and have been made against many of the interpretations outlined above. The presence of a suture at the Thelon Front is debatable, as is using an ash layer and movement along the Great Slave Lake shear zone for dating collision. Furthermore, the metamorphic history of the QMB is not consistent with a 2.01-1.91 Ga Himalayan-type collision of the Slave and Churchill cratons.

One rather obvious shortcoming of interpreting the paired gravity anomaly as being the result of collision is the fact that it is restricted to a relatively small area between the McDonald and Bathurst faults and not present along the entire length of the TTZ. A more recent interpretation of this anomaly suggests that it may have formed as the result of intracratonic indentation between 1.84-1.74 Ga (Henderson et al., 1990). This suggestion was made in light of new evidence from extensive geological, geochronological, and geophysical studies across the Thelon front in the 1980's. Furthermore, the metamorphic and structural changes in this area are Archean, not Proterozoic in age (Thompson and Henderson, 1989), and the ~2.6 Ga plutonic rocks found throughout the Slave Craton are present east of the Thelon front (van Breemen et al., 1987a). All of these observations argue against the presence of a suture at the Thelon front, which was one of the fundamental assumptions that led to Hoffman's collisional

model. It is likely that a suture does exist between the Slave and Churchill provinces, but has been overprinted and obscured by the Paleoproterozoic events that took place in the area.

The inadequacy of using an ash layer in the Kilohigok Basin and movement along the Great Slave Lake shear zone as evidence for collision is that these are model dependent interpretations. The Kilohigok Basin as a foredeep basin is an interpretation; likewise the Great Slave Lake shear zone being related to collision is an interpretation. In fact, these observations do not constrain any plate boundaries in the area; all they indicate is that volcanism, tectonic movement, and sedimentary deposition were occurring at that time, which is undisputed. Most, if not all of these features can also be accounted for in an intra-cratonic tectonic setting (e.g., Chacko et al., 2000)

If Slave-Churchill collision did indeed occur ca. 2.01-1.91 Ga and is analogous to the India-Asia collision one would expect to find evidence for extensive reworking of the QMB at this time, much like is observed presently in the Tibetan Plateau behind the India-Asia collisional zone (e.g., Zhang et al., 2004). Two thorough geochronological studies have revealed minimal evidence for 2.01-1.91 Ga reworking of the QMB (This study; Schultz et al., 2007). While a lack of deformation at this time argues against a *Himalayan-type* collision, one cannot rule out collisional orogenesis entirely, as is evident by the Ural Mountains which is a collisional zone where no Tibetan Plateau-like feature developed behind the main mountain belt. (e.g., Otto and Bailey, 1995).

Another shortcoming of the collisional model is that it does not address the presence of the cryptic episode of tectonism in the Taltson-Thelon zone dated between 2.5 and 2.3 Ga (McNicoll et al., 2000). Since Hoffman proposed his collisional model, evidence for tectonic activity in this time period has been found throughout much of the western Churchill Province.

### 5.3.2 – 2.01-1.91 Ga intracontinental orogenesis

A model for the Taltson-Thelon zone being an area of intracontinental orogenesis was originally proposed in the nineteen-eighties (Thompson et al., 1987; Thompson and Henderson, 1983), but until more recently received little attention as the geological community favoured the collisional model. Chacko et al. (2000) and De et al. (2000), compare the 2.01-1.91 Ga tectonic event dominating the Taltson-Thelon zone to the Tian Shan intracontinental mountain belt in central Asia. The Tian Shan range is a 2500km long, east-west trending orogenic belt associated with the collision of the Indian and

Asian plates but situated 700 to 1000 km's north of the former subduction zone (e.g., Yin et al. 1998). In this model, the Thelon and Taltson zones are compared to the western and eastern Tian Shan ranges, respectively. These two ranges are separated by a series of right lateral strike-slip faults (Yin et al., 1998) which are compared to the Great Slave Lake shear zone. Chacko et al. (2000) interpret the Kilohigok basin as being analogous to the Tarim basin, an intracontinental basin formed in response to the rising of the Tian Shan. Chacko et al. (2000) expand their model to the earliest Paleoproterozoic and propose that the cryptic 2.4-2.3 Ga tectonic event in the Taltson-Thelon zone may be the remnants of an old continental arc. Schultz et al. (2007) suggested that collision of the Slave and Churchill cratons occurred during this time.

The original line of evidence used in support of an intracontinental model for formation of the Talston-Thelon zone was P-T conditions of metamorphism. P-T estimates from the TTZ indicate high-T and low-P metamorphic conditions from roughly 2.0-1.98 Ga (Thompson, 1989). According to the subduction-collision model, with collision occurring ca. 1.97 Ga, one would expect low-T and high-P metamorphic conditions at this time period, as is typical of modern subduction zones (e.g., Maekawa, 1993). Thompson (1989) interpreted the high-T and low-P conditions of the TTZ as having been the result of intracontinental orogenesis.

The principal line of evidence used by Chacko et al. (2000) and De et al. (2000) to support their claim of intracontinental orogenesis are the geochemical variations in early and late plutonic suites from the Taltson magmatic zone. As previously discussed, if the 2.01-1.91 Ga TTZ was formed by collision following subduction, one would expect to find that earlier intrusive rocks originated in a continental arc setting, while later suites should have originated solely from continental sources. Chacko et al. (2000) and De et al. (2000) compared both the major-element composition and the Nd, Pb, and O isotope composition of granitoids from the Taltson magmatic zone with Phanerozoic granitoids from different tectonic settings, and concluded that all the 2.01-1.91 Ga granitoids much more closely resemble granitoids formed in an intracontinental setting than those formed in a continental arc setting. These results conflict with the interpretations of Theriault (1992) in his study of Nd isotopic composition of the Deskenatlata intrusive suite.

Similar to the collisional model, several counter arguments against an intracontinental model can be made. One issue with applying the isotopic studies of Chacko et al. (2000), De et al. (2000), and Theriault (1992) to the question as to the relationship between the Slave and Churchill provinces is that each of these studies

analysed rocks from the Taltson magmatic zone, not the Thelon. Although it is possible that both zones formed in similar tectonic environments as can be inferred from their continuous nature, one need only look at any modern mountain range to see that there can be an enormous variety of tectonic settings within a continuous mountain belt. Chacko et al. (2000) suggested that an active plate margin was present to the west of the Slave Craton, and activity at this location was the driving force behind intracontinental orogenesis in the TTZ. However, Chacko et al. did not establish the precise location of this plate boundary, and thus, could not identify an exact driving mechanism behind their intracontinental model.

The scientific community has yet to reach a consensus on the tectonic setting in which the TTZ formed. Further geochronological and geochemical analyses of rocks from the TTZ are necessary in order to better define this enigmatic mountain belt.

#### **5.4 – A new model for the evolution of northwestern Laurentia**

In this section, the data acquired throughout the course of this study are synthesized in a discussion pertaining to the tectonic evolution of northwestern Laurentia. The data not only provide insight into the long debated question as to the relationship between the Slave and Churchill cratons, but they also illuminate previously unknown aspects regarding the evolution of northwestern Laurentia. The model proposed is summarized in a series of schematic tectonic cross-sections shown in Figure 5-4.

##### 5.4.1 – The Archean

Prior to the present study, a reconnaissance east-west Nd isotope transect conducted in the southern QMB suggested the presence of Mesoarchean and even Paleoproterozoic rocks in the western part of the block (Theriault et al., 1994). Hartlaub et al. (2005; 2004) interpreted the presence of a belt of Meso- to Paleoproterozoic rocks along the western margin of the Rae domain, based on both model ages as well as U-Pb crystallization ages of granitoid rocks.

For the first time, this study presents direct U-Pb ages from a variety of earliest Mesoarchean gneisses in the PRB of the western QMB. The majority of granitoid gneisses in the PRB are dated from 3.2-3.1 Ga, and intruded by less abundant Neoproterozoic granitoids dated ca. 2.7 Ga. Supracrustal rocks in the PRB may have been deposited at various times. One detrital zircon study provides a maximum depositional age of 3.09 Ga

for a semi-pelite, whereas a second provides a maximum depositional age of 2.58 Ga for a quartzite.

The Archean history of the PRB compares and contrasts to the Archean history of other areas in the Rae domain in several ways. The most notable contrast is the abundance of Mesoarchean crust in the PRB, and the general absence of these ancient rocks elsewhere in the Rae domain. Aside from model ages and xenocrystic zircons, no evidence for Mesoarchean crust has been found east of the PRB. The oldest rocks identified in the Committee Bay belt are supracrustal rocks dated as old as 2.73 Ga (Skulski et al., 2003); whereas the oldest rocks on Boothia peninsula are supracrustals with a maximum depositional age of 2.76 Ga (Hinchey et al., 2007). Model ages from these areas are typically Neoproterozoic, but occasionally as old as 3.0 Ga; furthermore, xenocrystic zircons up to 2.9 Ga are documented (Frisch, 2011; Shultz et al., 2007; Hinchey et al., 2011). Both the PRB as well as other areas of the Rae domain are intruded by voluminous 2.7 Ga granitoids (e.g., Ryan et al., 2009; Rayner et al., 2011; Skulski et al., 2003). Much of the Rae domain is also intruded by granitoids dated at ~2.6 Ga with associated metamorphism at this time (e.g., Berman et al., 2008; Berman et al., 2005; Ryan et al., 2009; Skulski et al., 2003); but plutonic rocks of these ages have not yet been identified in the PRB.

The geological contrasts between the PRB with the Rae domain to the east, particularly in regard to its Mesoarchean history, suggest that this belt may be a distinct cratonic block that later became incorporated into the Rae domain. Nd model ages from the Queen Maud granitoids are comparable to those of Neoproterozoic granitoids from the Rae domain (Schultz et al., 2007), suggesting that the area intruded by the Queen Maud granitoids is reworked Rae, as opposed to reworked PRB. Therefore, the suture between the PRB and the Rae domain is likely near the contact between the PRB and the Paalliq belts, as shown in Figure 5-4.

The timing of incorporation of the PRB into the Rae domain is not entirely clear; however, evidence from the Paleoproterozoic indicates that they were joined by at least 2.46 Ga. Sample QM-10C, a metasedimentary rock collected from within the PRB contains two metamorphic monazite populations, one at 2.46 Ga, and another at 2.37 Ga. The 2.46 Ga population is consistent with the timing of intrusion of the Queen Maud granitoids to the east. If this rock was metamorphosed during intrusion of the Queen Maud granitoids then it follows that the PRB and Rae domain were likely joined at this time. When exactly the PRB was incorporated into the Rae domain is uncertain, but in



light of the evidence cited above, I suggest that the two crustal blocks were joined prior to intrusion of the 2.52-2.45 Ga Queen Maud igneous suite, sometime in the Archean.

Although the PRB is distinct from the Rae craton, it contrasts even more sharply with the Slave Craton to the west. The eastern Slave Craton contains rare exposures of 2.73-2.64 Ga metavolcanic rocks thought to be related to extension (Bleeker et al., 1999; Davis et al., 2003). Although rocks of this age often exhibit Mesoarchean model ages in the Rae domain, they exhibit juvenile isotopic signatures in the Slave (Davis and Hegner, 1992; Thorpe et al., 1992). These ~2.7 Ga rocks are overlain by abundant metasedimentary rocks dated between 2.7 and 2.6 Ga (van der Velden and Cook, 2002 and references therein). Voluminous 2.63-2.58 Ga granitoid plutonic rocks intrude the eastern Slave, and this time is one of significant deformation and metamorphism in the area (van der Velden and Cook, 2002). Although relatively understudied, the northeastern Slave, directly adjacent to the PRB, appears to be similar to the rest of the eastern Slave Craton. The area is dominated by Neoproterozoic rocks dated between 2.7 and 2.6 Ga and was metamorphosed at approximately 2.6 Ga (Bevier and Gebert, 1991; Culshaw and van Breemen, 1990; Hebel, 1999).

The contrasts between the PRB and Slave in terms of their Archean history suggest that these two blocks must have been joined sometime in the Neoproterozoic or later. Creating difficulty in interpreting the relationship between these two Archean blocks is the fact that the precise boundary between them is obscured by the Paleoproterozoic TTZ. It is uncertain whether the TTZ is built upon PRB, Slave, or perhaps its own distinct crust; however, rare outcroppings of ca. 2.6 Ga plutonic rocks have been identified in the western TTZ (Henderson and van Breemen, 1992; van Breemen et al., 1987a). The presence of these granitoids led Henderson and van Breemen (1992) to suggest that Slave crust is present western TTZ, and thus the TTZ may be partially built on the Slave craton.

Williams et al. (1991) proposed that the Slave and Churchill provinces formed part of a continuous supercontinent, termed Kenorland, in the Neoproterozoic. Aspler and Chiarenzelli (1998) elaborated on this idea and suggested break-up of Kenorland occurred between 2.5 and 2.1 Ga. The discussion that follows does not preclude the presence of a continuous Slave and Churchill continent in the Neoproterozoic, but does require that prior to 2.43 Ga the Slave and Churchill provinces were separated by an ocean basin of unknown size. The details of any earlier relationship between the two provinces are uncertain.

5.4.2 – Pre-collisional tectono-magmatism: 2.52-2.45 Ga

The Paalliq belt (eastern QMB) was the site of intrusion of a voluminous bimodal igneous suite from 2.52-2.45 Ga (this study; Schultz, 2007; Schultz et al., 2007). The oldest granitoids dated from this suite are samples QM-14A, imprecisely dated at  $2532 \pm 29$  Ma, and QM-15A, dated at  $2516 \pm 13$  Ma, whereas the youngest are samples ST-7, dated at  $2457 \pm 24$  Ma (Schultz et al., 2007), and QM-13E, dated at  $2450.4 \pm 6.6$  Ma. This intrusion was accompanied by, or perhaps shortly followed by, deposition of the Sherman sedimentary rocks (Schultz et al., 2007). Similar aged granitoids are found as far north as Boothia Peninsula (Frisch and Hunt, 1993), indicating that rocks of these ages occur in a linear belt that extends NNE-SSW for as much as 1000 km. During this time period, metamorphism of the Paalliq belt and some areas of the PRB occurred.

As has been mentioned, the bimodal nature of the 2.52-2.45 Ga Queen Maud mafic-felsic igneous suite as well as the low Th/Nb and high Ti and V contents of the mafic component of this suite lead Schultz (2007) to interpret intrusion in a continental rift setting. These mafic rocks are dated between 2.50 and 2.48 Ga (Schultz, 2007). Alternatively, the Queen Maud suite has also been interpreted as having intruded in a back-arc basin setting (Perhsson, 2011 pers. comm.). The fact that only five mafic samples from the Queen Maud suite have been geochemically analysed leaves room for debate regarding the origins of this bimodal igneous suite, however, the current geochemical dataset are more indicative of a rift setting than an arc setting.

In the following section it will be discussed that geochronological and quantitative geothermobarometric data are consistent with the 2.43-2.35 Ga collision of the Slave and Churchill cratons. In relation to this model, a continental arc related origin for the Queen Maud granitoid suite would be preferred, as one could easily say that 2.52-2.45 Ga arc magmatism preceded collision of the Slave and Churchill cratons. However, such an interpretation violates the geochemical data from the mafic component of this suite. If indeed the Queen Maud suite is related to rifting, then there is a marked absence of pre-collision, arc related igneous rocks near to the boundary of the Slave and Churchill cratons. It is possible that these rocks exist but simply have not been found. However, with the abundance of geochronological data now available from the QMB, this is unlikely.

An alternate possibility is that the period over which the Queen Maud igneous rocks crystallized is one of evolving tectonic environment. Based on the oldest and youngest granitoids dated from this suite, these granites crystallized over a period of at

least 66 million years, as long as the entire Cenozoic. It is possible that the early phase of Queen Maud magmatism, including crystallization of 2.50-2.48 Ga mafic rocks, occurred in a continental rift setting, and that younger granitoids crystallized in a continental arc setting that preceded collision of the Slave and Churchill cratons. More detailed study of the early and late phases of Queen Maud magmatism are needed to test the hypothesis that the Paalliq belt was an area of evolving tectonic environment between 2.52 and 2.45 Ga.

5.4.3 – Slave-Churchill collision and convergence: 2.43-2.35 Ga

As has been mentioned in Sections 5.1 and 5.2, several magmatic and metamorphic age dates around 2.43-2.42 Ga are recorded in rocks from the QMB. The most prominent and significant of these are from an alkali feldspar granite sheet interpreted to have intruded syntectonically with the formation of a regional-scale strike-slip shear zone at the western contact of the Sherman basin. Another set of ~2.42 Ga ages are from monazite grains interpreted as being metamorphic in origin are found in a psammite collected roughly 100 km west of this shear zone, within a high-strain zone and near to a similarly trending fault zone mapped by Heywood (1961). The leucocratic nature of the 2426 Ma magmatic rocks is indicative of their being the product of intra-crustal melting.

Additional 2.43-2.42 Ga ages are recorded in monazite grains from metasedimentary rocks in the eastern QMB and the Boothia mainland area (Berman et al., 2005; Berman et al., 2008; Schultz, 2007). Bethune et al. (2010) identified a prominent peak in 2.41 Ga detrital zircons from a metasedimentary sample collected from the southwestern Rae domain, near to the Taltson magmatic zone and Athabasca Basin.

Evidently, ~2.42 Ga tectonism affected a large area along the western margin of the Rae domain from as far north as Boothia Peninsula, to as far south as the Athabasca Basin area. In the QMB, this time period is characterised by minor metamorphism and intrusion of small quantities of crustally-derived magmas contemporaneous with strike-slip shearing.

I propose that 2.43 Ga marks the initial phases of the Arrowsmith Orogeny and collision of the Slave and Churchill cratons. Initiation of strike-slip shear zones occurred, which formed conduits for later extrusion of continental fragments from the QMB into the southwestern Rae domain. This extrusion is discussed in greater detail below.

In the QMB, the main phase of the Arrowsmith Orogeny is dated from 2.39-2.35 Ga based on U-Pb ages of metamorphic zircon and monazite grains. In the Committee Bay belt, Berman et al. (2005) also identified a period of monazite growth ca. 2.35 Ga. U-Pb ages from Boothia Peninsula, the southwest Rae domain, and the Taltson-Thelon zone overlap with the Arrowsmith Orogeny (Bostock and van Breemen, 1994; Frisch and Hunt, 1993; McNicoll et al., 2000). No dates from this time are reported from the eastern Slave Craton.

Metamorphic pressures associated with this orogeny steadily decrease moving eastward, away from the Slave-Churchill boundary. Specifically, at granulite-facies temperatures (~800°C) there is a decrease in metamorphic pressures from 8-10 kbar at the western margin of the QMB to ~6 kbar in the Paalliq belt, and still a further decrease in both temperature and pressure in the Committee Bay belt to 560°C and ~4.2 kbar (Berman et al., 2005). Numerical modelling of the Tibetan Plateau predicts a similar decrease in crustal thickness moving northward, away from the India-Asia collisional zone (e.g., Jimenez-Munt and Platt, 2006). Thermobarometric data from the QMB also indicate an elevated geothermal gradient of 35-40 °C/km. Similar elevated geothermal gradients are thought to exist within the Tibetan Plateau (e.g., Clark et al., 2005). Furthermore, the dominant NNE-SSW strike of Arrowsmith aged metamorphic fabrics in the QMB indicates east-west compressional forces, also consistent with Slave-Churchill collision.

The spatial distribution of 2.39-2.35 Ga ages (i.e., along the western margin of the Churchill Province), the elevated geothermal gradient, and metamorphic pressures that decrease to the east, are all consistent with what would be expected to occur as a result of Slave-Churchill collision in a style analogous to the Cenozoic India-Asia collision.

Although no direct evidence for tectonism at this time has been documented in the eastern-most Slave craton, cryptic evidence in the form of 2.4 and 2.2 Ga xenocrystic zircons has been documented in the TTZ (van Breemen et al., 1987b). If the TTZ is built partially on Slave crust, as suggested by Hendersen and van Breemen (1992), then the presence of these xenocrystic zircons indicates the area may have been affected by the Arrowsmith Orogeny. Further work on rocks from the TTZ may uncover more evidence for reworking of the eastern-most Slave craton during 2.43-2.35 Ga Slave-Churchill collision and convergence.

This model is comparable to Hoffman's (1987) collisional model wherein the QMB represents a deeply eroded Tibetan Plateau-like setting, and the Slave Craton is analogous to the Indian sub-continent. The fundamental difference between the proposed model and Hoffman's is the timing of collision. Hoffman suggested that a Himalayan style collision occurred from 2.01-1.91 Ga, whereas this model suggests a Himalayan style collision occurred from 2.43-2.35 Ga. Slave-Churchill collision around this time was first proposed by Schultz et al. (2007).

This collision is thought to have caused the indentation of the Slave Craton into the Churchill Craton, as shown in Figure 5-5a. This collision also resulted in the extrusion of continental fragments from the QMB into the southwestern Rae domain as a result of movement along regional scale strike-slip faults that initially formed ca. 2.43 Ga (Figure 5-5a). Hartlaub et al. (2005) established the presence of early Mesoarchean crust in the southwestern Rae domain, and suggested that these ancient rocks are present in a narrow belt along the western margin of the Rae. In the model presented here, these Mesoarchean rocks are thought to have migrated from the QMB area, southward into the southwest Rae domain, in order to accommodate the compressional forces caused by Slave-Churchill collision. Such processes have been extensively documented in the India-Asia collision zone where continental fragments have been extruded from Tibet into Southeast Asia (Figure 5-5b; Royden et al., 2008).

#### 5.4.4 – Post-collision magmatism: 2.32 Ga

Undeformed and unmetamorphosed mafic and highly potassic felsic igneous rocks dated at 2.32 Ga have been identified in the QMB. Similarly aged granitoids have been identified to the south, in the Uranium City area; collectively, the 2.33-2.29 Ga granitoids in this area are referred to as the North Shore plutons (Hartlaub et al., 2007). Based on petrological and geochemical characteristics, Hartlaub et al. (2007) interpreted the locally deformed North Shore plutons as having formed in a syn- to post-collisional setting, possibly during a period of post-orogenic extension.

I propose that the undeformed 2.32 Ga mafic and felsic igneous rocks identified in the QMB (samples QM-8A and QM-8B) may have also intruded in a post-orogenic, extensional environment. This interpretation is based on the undeformed and unmetamorphosed nature of these rocks, which suggests they intruded after Slave-Churchill convergence ceased. Furthermore, the high potassium contents of the felsic igneous rocks, based on modal mineralogy, are also consistent with intrusion in such an

environment (Dewey, 1988). Geochemical analysis of these 2.32 Ga plutons can further test the hypothesis that they formed in a post-collisional environment.

#### 5.4.5 – Continental rifting ca. 2.3-2.1 Ga

In Section 5.2, it was argued that the spreading of monazite ages from 2.3-2.1 Ga in the western QMB is the result of multiple thermal perturbations associated with episodic magmatic intrusions. The presence of mafic dykes with minimum ages of 2.1 Ga suggests this may have been a time of continental rifting in the western QMB.

Furthermore, the presence of metasedimentary rocks, the Mary Frances sediments, deposited between 2.2 and 2.0 Ga within the TTZ provides evidence for this proposed rifting (Henderson and van Breemen, 1992).

Other authors have also suggested this time period was one of continental break-up in the Rae domain and Slave Province. Aspler and Chiarenzelli (1998) and Rainbird et al. (2010) cite the abundance of early Paleoproterozoic sedimentary successions, such as the Amer, Ketyet River, Penrhyn, and Piling groups, as evidence for Paleoproterozoic rifting in the Rae domain. LeCheminant et al. (1996) state that the presence of the Malley and MacKay swarms, dated at 2.23 and 2.21 Ga respectively, may be related to rifting and break-up along the eastern and southern margins of the Slave Craton. Additional Paleoproterozoic mafic dyke swarms in the Slave Craton include the 2.19 Ga Dogrib swarm and the 2.11 Ga Indin swarm (Buchan et al., 2009 and references therein).

A lack of evidence for tectonism or magmatism at this time in the eastern QMB suggests that rifting was focussed in the western QMB, nearest to the suture between the Slave and Churchill cratons. It is not surprising that rifting was focussed in this area when one considers that sutures are often the focus of later tectonic events. Take for instance the Appalachian Orogeny, which resulted from collision of the North American and African continents (e.g., Vauchez et al., 1987). The area near the suture between the African and North American plates later became the focus for rifting and the subsequent opening of the Atlantic Ocean. Whether 2.3-2.1 Ga rifting of the Slave and Churchill cratons area led to the opening of an ocean basin, or if extension remained in a continental regime, is uncertain.

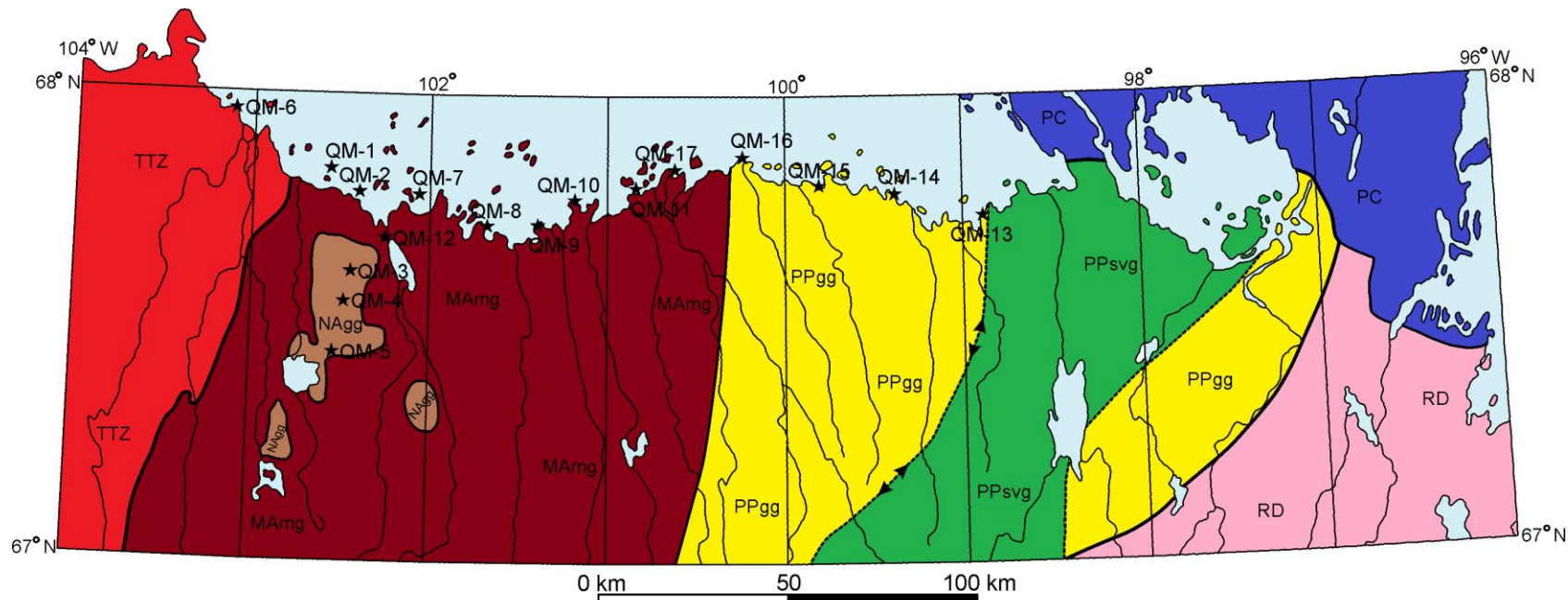
#### 5.4.6 – Thelon Orogeny: 2.01-1.91 Ga

Models for the tectonic origins of the Thelon Orogeny were discussed in detail in Section 5.3. At present, it is uncertain whether the 2.01-1.91 Ga Thelon orogeny is



collisional or intracontinental. The tectonic setting of the Thelon Orogeny depends on whether 2.3-2.1 Ga rifting led to the opening of an ocean basin or not, as discussed in the previous section.

Regardless of whether the TTZ marks the location of a plate boundary at ca. 2.01-1.91 Ga, the data obtained in the present study argue against the QMB being a Tibetan-style plateau during that orogenic event, as per Hoffman's (1987) suggestion. More specifically, the lack of significant metamorphism and deformation over most of the extent of the QMB in that time period is distinctly unlike the present-day Tibetan Plateau, where geophysical data indicate extensive mid-crustal reworking over a broad area of the plateau (e.g., Unsworth et al., 2005). That being said, less spectacular forms of collision remain a possibility. Additional geochronological and geochemical work on rocks from the TTZ are needed in order to better understand the evolution and origins of this belt.



**Legend**





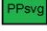






- |   |  |
|---|--|
|  <b>Unit 1:</b> Platform Cover  |  Lithologic contact                        |
|  <b>Unit 2:</b> Thelon Tectonic Zone   |  Fault contact (Unknown displacement)     |
|  <b>Unit 3:</b> Paleoproterozoic metasedimentary and metavolcanic gneiss (Sherman Group) |  Fault contact (Strike-slip displacement) |
|  <b>Unit 4:</b> Paleoproterozoic granitic gneiss (Queen Maud Granitoids)                 |  Boundaries of Queen Maud block           |
|  <b>Unit 5:</b> Rae Domain   |  |
|  <b>Unit 6:</b> Neoproterozoic granitic gneiss   |  |
|  <b>Unit 7:</b> Mesoarchean to Neoproterozoic mixed gneiss                               |  |

Figure 5-1: Geological map of the northern Queen Maud block. The eastern QMB, including units 3 and 4, is referred to as the Paalliq belt, whereas the western QMB, including units 6 and 7, is referred to as the Perry River belt. See text for unit descriptions.

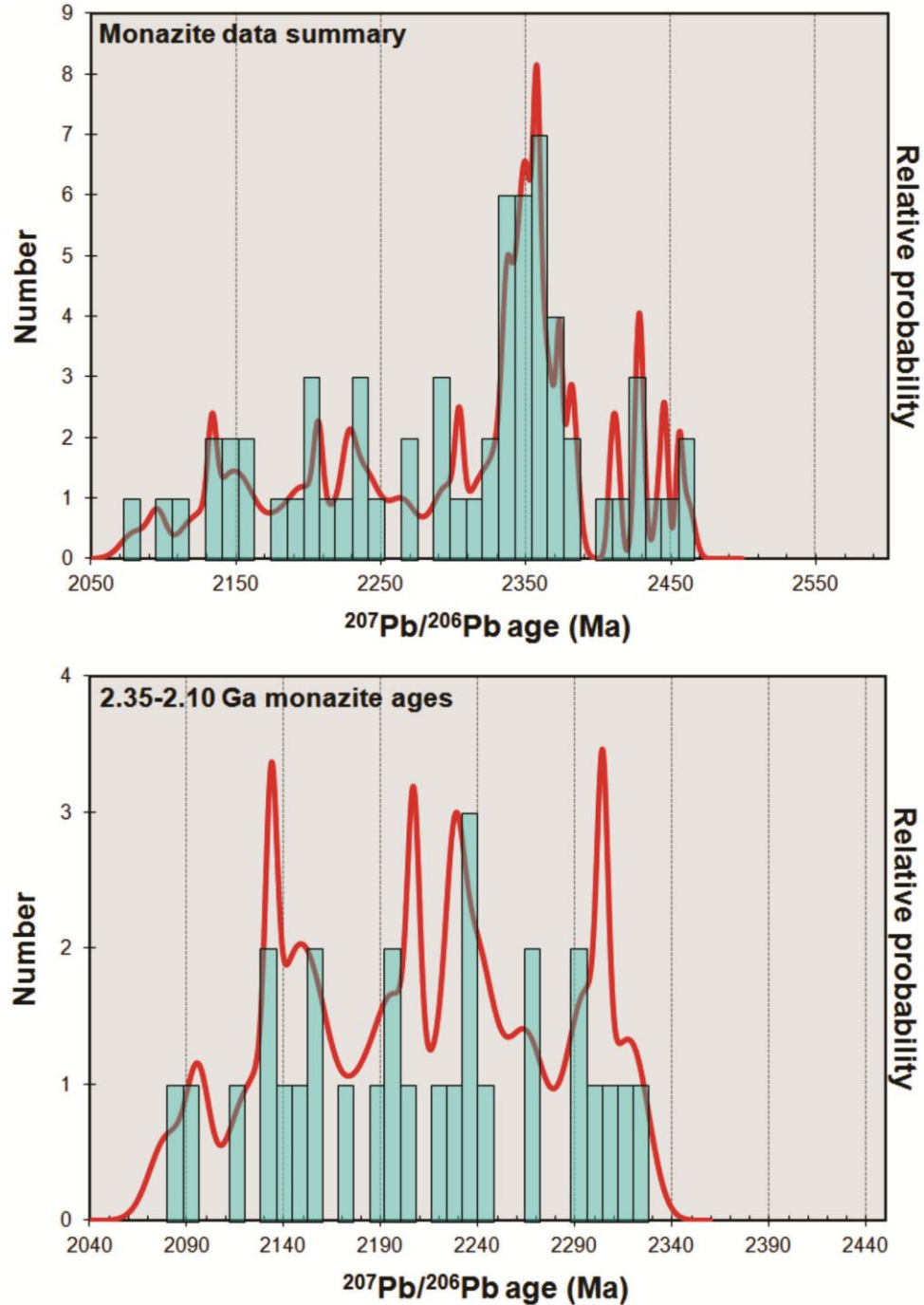


Figure 5-2: Summarized results of in-situ LA-MC-ICP-MS dating of monazite grains. The monazite data summary consists of all 63 analyses within 5% discordance (analyses from sample QM-9D not included). Note the prominent peak at approximately 2.36 Ga; this represents the timing of regional granulite facies metamorphism. A relatively small number of analyses preserve evidence for 2.52-2.45 and 2.43-2.42 Ga metamorphism. Analyses preserving evidence for 2.35-2.10 Ga metamorphism are summarized in their own probability density plot. A 5% discordance and a 2325 Ma cutoff were applied when creating this plot. Note that the data are not evenly distributed across this time period, but occur as several distinct peaks; this provides evidence for multiple episodes of monazite growth throughout this time period.

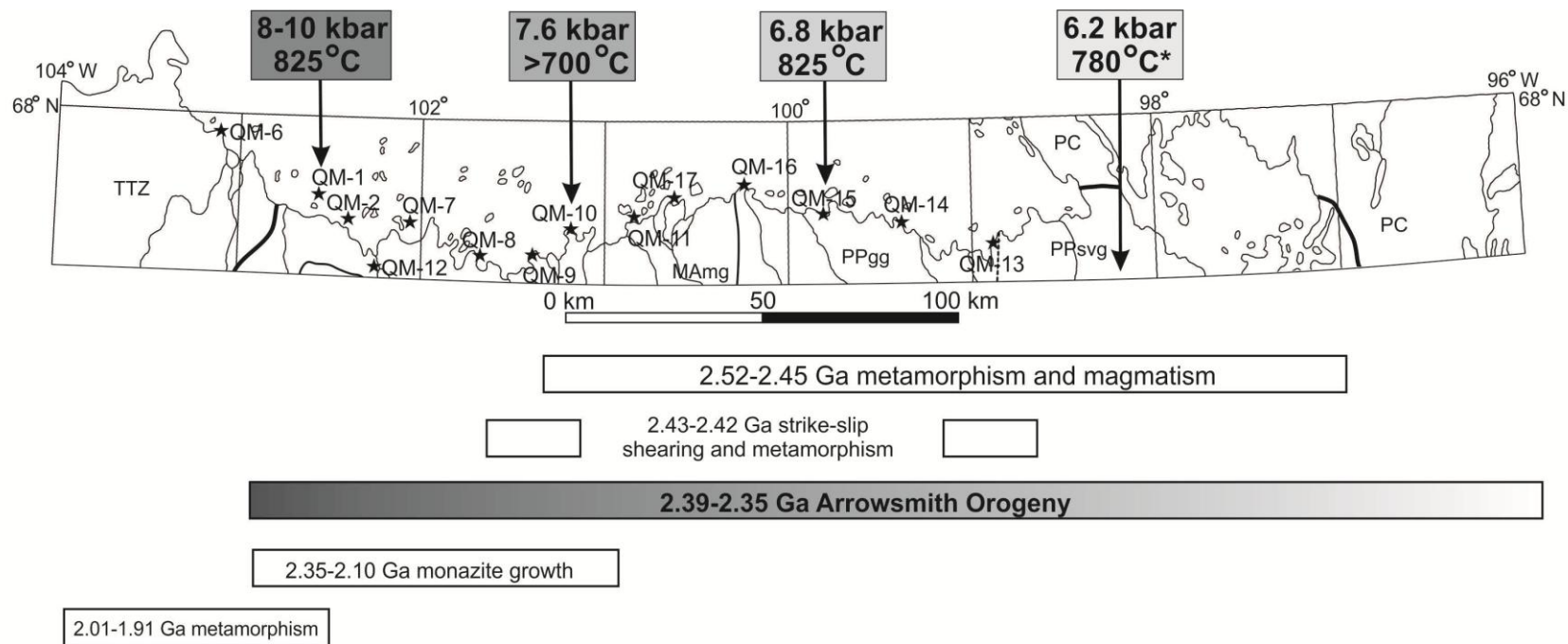
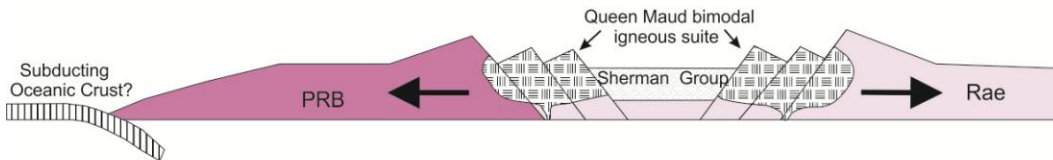


Figure 5-3: Map showing the spatial distribution of five of the tectono-metamorphic events discussed in the text. 2.52-2.45 Ga metamorphism and magmatism is restricted to the eastern QMB. Evidence for 2.43-2.42 Ga metamorphism and strike-slip shearing is present locally at locations QM-9 and QM-13. Evidence for the 2.39-2.35 Ga Arrowsmith Orogeny is documented throughout and to the east of the QMB. The quoted P-T conditions are those associated with the Arrowsmith Orogeny; note the general decrease in peak pressure conditions moving eastward in the QMB. Episodic monazite growth from 2.35-2.10 Ga is restricted to samples collected from the western QMB. Geochronological evidence for the Thelon Orogeny is present within the TTZ and only as far east as location QM-1. Refer to Figure 5-1 for lithologic unit legend. (\* = Chacko, unpublished data, sample ST-3a.)

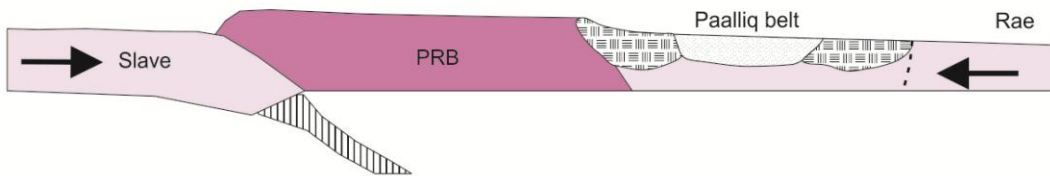
A) >2.52 Ga - Joined Perry River belt and Rae domain



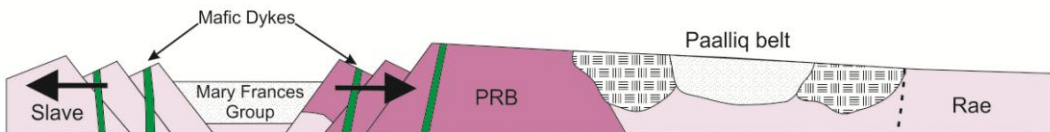
B) 2.52-2.45 Ga - Intrusion of the Queen Maud granitoids and deposition of Sherman Group. Assumed subduction west of PRB



C) 2.43-2.35 Ga - Collision of Slave and Churchill cratons resulting in Arrowsmith Orogeny



D) 2.3-2.1 Ga - Rifting of the western PRB and eastern Slave resulting in mafic magmatism and deposition of Mary Frances group



E) 2.01-1.91 Ga - Reactivation along the Slave-PRB suture resulting in Thelon Orogeny



Figure 5-4: Schematic cross-sections illustrating the Paleoproterozoic tectonic evolution of the QMB area. See text for discussion.



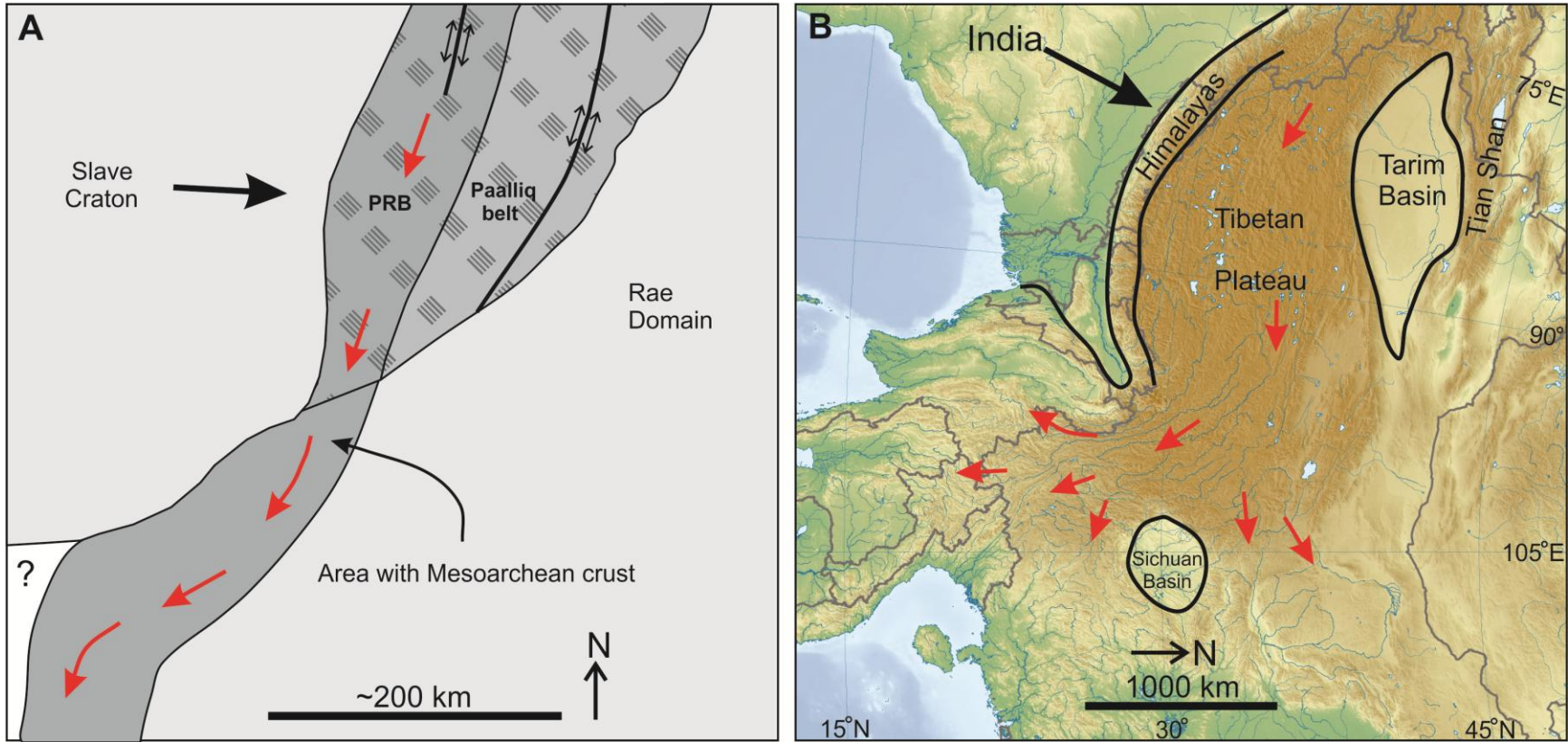


Figure 5-5: Maps comparing 2.43-2.35 Ga collision of the Slave and Churchill cratons with the Cenozoic collision of India and Asia. Red arrows show direction of extrusion of crust from behind collisional zones. A) Simplified tectonic map of northwestern Laurentia highlighting eastward indentation of the Slave Craton into the Churchill and the resulting extrusion of Mesoarchean crust from the QMB southward into the southwestern Rae domain. Small black arrows show the approximate location of strike-slip faults that formed ca. 2.43-2.42 Ga. Hatched area is present day Queen Maud block, including the Perry River belt (PRB) and Paalliq belt. (Modified from Hartlaub et al., 2007) B) Topographic map of southern Asia (brown=high elevation, green=low elevation) showing similar patterns of extrusion (modified from Royden et al., 2008).



## CHAPTER 6 – Conclusion

In Chapter 1, it was stated that the two fundamental goals of this thesis were to investigate the geology of the northwestern and central QMB at a reconnaissance scale and to further the understanding of the metamorphic history of the QMB. Inasmuch as possible for a two year Master's thesis, these two goals were achieved. Tangential to attaining these goals, an alternate model for the tectonic evolution of northwestern Laurentia was proposed. In this concluding chapter the results of the present study are summarized and possibilities for further research proposed.

### 6.1 – Summary

On the basis of field-work conducted in a 200 km long east-to-west transect along the southern coast of the Queen Maud Gulf, U-Pb dating of zircons from 17 samples collected during this field-work, two detrital zircon studies, and the earlier work conducted by Shultz et al. (2007) and Schultz (2007), the Queen Maud block can be divided into two distinct crustal belts: the western Perry River belt and the eastern Paalliq belt. The Perry River belt contains both earliest Mesoarchean and Neoproterozoic granitoid gneisses that were emplaced ca. 3.2-3.1 Ga and 2.7 Ga. Supracrustal rocks in the Perry River belt likely belong to multiple depositional sequences. The youngest detrital zircons from two different metasedimentary samples are dated at 3089 and 2576 Ma. The Paalliq belt is dominated by the Paleoproterozoic Queen Maud granitoids, which crystallized ca. 2.52-2.45 Ga, but also includes subordinate mafic rocks and the Sherman supracrustal sequence, which was previously established to have been deposited between 2.45 and 2.39 Ga (Schultz et al., 2007). The Paalliq belt was formed on Neoproterozoic crust of the Rae domain, whereas the Perry River belt is a distinct and older cratonic block. Metamorphism of the Perry River belt, concurrent with the timing of intrusion of the Queen Maud granitoids, places a minimum age constraint on incorporation of the Perry River belt into the Rae domain at 2.46 Ga.

Based on U-Pb zircon dating of five samples, U-Pb monazite dating of ten samples, and geothermobarometric calculations of seven samples, it is evident that the earliest Paleoproterozoic was a time of active tectonic evolution in the Queen Maud block. Following intrusion of the 2.52-2.45 Ga Queen Maud bimodal mafic-felsic igneous suite, initial collision of the Slave and Churchill cratons is thought to have occurred at ~2.43 Ga. At this time, local metamorphism and crustal melting occurred within N-S trending high-strain strike-slip shear zones. The main phase of convergence of

the Slave and Churchill cratons occurred during the Arrowsmith Orogeny, between 2.39-2.35 Ga, at which time the Queen Maud block was metamorphosed at granulite facies. Peak P-T conditions during this orogeny decrease from 825°C and 8-10 kbar in the western-most Queen Maud block, to >700°C and 7.6 kbar, and 825°C and 6.8 kbar approximately 50 and 100 km to the east, respectively. Post-Arrowsmith mafic and felsic magmatism occurred ca. 2.32 Ga, possibly in response to post-collisional crustal extension. Between 2.3 and 2.1 Ga mafic magmatism and monazite growth occurred in the western 100 km of the Queen Maud block, possibly as a result of continental rifting. The effects of the 2.01-1.91 Ga Thelon Orogeny are manifested only in the western-most Queen Maud block where a cross-cutting mafic dyke records 1.93 Ga metamorphism at minimum P-T conditions of 720°C and 7.5 kbar.

## **6.2 – Further Research**

Throughout the present study, both new discoveries and rather speculative interpretations were made. Additional work on rocks from the QMB will further the understanding of these new discoveries and test some of the hypotheses made.

Despite the present study and previous work conducted by Schultz, the QMB area lacks modern, detailed geological maps. Foremost among the recommendations for further research is to conduct detailed geological mapping of the QMB. Such mapping would be invaluable in furthering the understanding the geology of the QMB, as well as for economic purposes. Unfortunately, a project of this scope represents a logistically complex and costly undertaking.

A more realistic follow-up study would be to perform detailed geochronological and geochemical analysis on the mafic rocks collected during field work conducted for the present study. In a general sense, such a study will add an additional layer of depth to the understanding of the QMB, by defining the history of mafic magmatism in the area. More specifically, the proposed model that the Slave and Churchill provinces collided at 2.43-2.35 Ga can be tested if mafic dykes from the western QMB and eastern Slave craton are compared. The hypothesis that rifting of the western QMB occurred between 2.3 and 2.1 Ga can also be tested. Such a study would be of sufficient scope for a Master's thesis and would be cost effective, as no additional field-work would be required.

Also in regards to the time period between 2.3 and 2.1 Ga, is the fact that monazite growth during this time is not entirely understood. Although a strong argument

was made for the presence of multiple age domains in monazite grains dated between 2.3 and 2.1 Ga, this proposition remains debatable. Age domain mapping by electron probe microanalysis of monazite grains from this time period is necessary in order to further test this hypothesis.

A project of relatively minor scope would be to further analyse the 2.32 Ga mafic and granitic rocks identified in the QMB. Geochemical and isotopic analysis of these rocks will test the hypothesis that they formed in a post-collision extensional environment. Testing of these rocks will also have implications for the hypothesis that the period between 2.45 and 2.2 Ga is one of global tectonic and magmatic quiescence (e.g., Condie et al., 2009). Such testing of the granitic sample, QM-8B was underway at the time of writing.

One of the most interesting discoveries made throughout the course of geochronological study was the presence of earliest Mesoarchean granitic gneisses of the Perry River belt. Also, the youngest detrital zircon from a metasedimentary sample is dated at 3089 Ma. It is possible that this rock was deposited in the earliest Mesoarchean, atop recently formed granitic crust. Detailed investigation of these rocks, which would require additional field work and sample collection, will provide insight into crust formation during a part of Earth's earliest history.

Another investigation, which would also require further field work, is to extend the geological study of the area further west, across the TTZ and into the northeastern Slave Craton. Although in general, the Slave Craton and TTZ are relatively well studied, the remote northeastern corner of the Slave and northern TTZ are not. A reconnaissance style geochronological transect across this area will no doubt make new and surprising discoveries, much as the present study has done, but will also address some of the topics discussed in the preceding chapters.

### **6.3 – Final Remarks**

One of the over-riding topics that drove this research was the question as to the relationship between the Slave and Churchill cratons, and the origins of the Thelon tectonic zone. Although the nature of the Thelon Orogeny remains uncertain, the ever growing body of literature from northwestern Laurentia, including this study, continues to provide insight into the origins of this enigmatic belt. Both of the models proposed for the TTZ, those being a collisional and an intracontinental model, have been built upon modern analogues from Asia. Explaining ancient processes using modern analogues is a

method that stems from the principal of uniformitarianism, wherein the present is the key to the past. Such is the paradigm of geology that was founded by great historical figures such as Sir Charles Lyell and James Hutton (Hutton, 1788; Lyell, 1830). As geology matures as a science it becomes increasingly apparent that such a principal is not always true. The past was in fact different than the present in many regards. Perhaps some processes that occurred in the Paleoproterozoic are not the same as are occurring now and perhaps tectonic events like the Thelon orogeny do not have modern equivalents. As our understanding and scientific paradigm evolves, further insight into early Earth processes will be gained; until then, as always, the present remains the key to the past.

In the opening statements made in Chapter, 1 it was stated that this thesis investigates the physical frontier of the Canadian Arctic as well as the topical frontier of early crust formation and stabilisation. Although this thesis was highly focussed in relation to such broad topics, it does, in some small way, make contributions to improving our understanding of these vast fields of inquiry. The contribution that this thesis has made in Arctic studies is a reflection of mankind's growing interest in this region. Not only do studies such as these assert Canada's claims of sovereignty over its Arctic region, but they also open the door for further investment in an economically deprived area. As resource bases in more accessible areas of Canada continue to be depleted we will be forced to look further north to secure the economic well-being of future generations. Though academic in focus, this study will inform future generations seeking ways to provide for mankind's needs. The need for humankind to ensure our survival is rivalled only by our curiosity and thirst for knowledge. In studying the Paleoproterozoic assembly of a small corner of Laurentia, this thesis enhances our understanding of the evolution of our planet.

## References

- Ashton, K.E., Heaman, L.M., Lewry, J.F., Hartlaub, R.P., and Shi, R., 1999, Age and origin of the Jan Lake Complex; a glimpse at the buried Archean craton of the Trans-Hudson Orogen: *Canadian Journal of Earth Sciences*, v. 36, p. 185-208.
- Aspler, L.B., and Chiarenzelli, J.R., 1998, Two Neoproterozoic supercontinents? Evidence from the Paleoproterozoic: *Sedimentary Geology*, v. 120, p. 75-104.
- Berman, R.G., 1988, Internally-consistent thermodynamic data for minerals in the system  $\text{Na}_2\text{O}-\text{K}_2\text{O}-\text{CaO}-\text{MgO}-\text{FeO}-\text{Fe}_2\text{O}_3-\text{Al}_2\text{O}_3-\text{SiO}_2-\text{TiO}_2-\text{H}_2\text{O}-\text{CO}_2$ : *Journal of Petrology*, v. 29, p. 445-522.
- Berman, R.G., 1991, Thermobarometry using multi-equilibrium calculations: a new technique with petrological applications: *Canadian Mineralogist*, v. 29, p. 833-855.
- Berman, R.G., 2007, winTWQ (version 2.3): a software package for performing internally-consistent thermobarometric calculations: Geological Survey of Canada, Open File 5462, (ed. 2.34); 41 p.
- Berman, R.G., Sanborn-Barrie, M., Stern, R.A., and Carson, C.J., 2005, Tectonometamorphism at ca. 2.35 and 2.85 Ga in the Rae Domain, western Churchill Province, Nunavut, Canada; insights from structural, metamorphic and in-situ geochronological analysis of the southwestern Committee Bay Belt: *Canadian Mineralogist*, v. 43, p. 409-442.
- Berman, R.G., Davis, W.J., and Pehrsson, S., 2007, Collisional Snowbird tectonic zone resurrected: Growth of Laurentia during the 1.9 Ga accretionary phase of the Hudsonian Orogeny: *Geology*, v. 35, p. 911-914.
- Berman, R.G., Ryan, J.J., Davis, W.J., and Nadeau, L., 2008, Preliminary results of linked in situ SHRIMP dating and thermobarometry of the Boothia mainland area, north-central Rae Province, Nunavut: Geological Survey of Canada, Current Research 2008-2, 13 p.
- Berton, P., 1988, *The Arctic Grail: The quest for the Northwest Passage and the North Pole*, Pierre Berton Enterprises Ltd. 672 p.
- Bethune, K.M., Hunter, R.C., Ashton, K.E., 2010. Age and provenance of the Paleoproterozoic Thluicho Lake Group based on detrital zircon U–Pb SHRIMP geochronology: new insights into the protracted tectonic evolution of the southwestern Rae Province, Canadian Shield. *Precambrian Research* 182, p. 83-100.
- Bevier, M.L., and Gebert, J.S., 1991, U-Pb geochronology of the Hope Bay – Elu Inlet area, Bathurst Block, northeastern Slave Structural Province, Northwest Territories: *Canadian Journal of Earth Sciences*, v. 28, p. 1925-1930.
- Bleeker, W., and Hall, B., 2007, The Slave Craton: Geology and metallogenic evolution: *in* Goodfellow, W.D., ed., *Mineral Deposits of Canada: A Synthesis of Major Deposit-Types, District Metallogeny, the Evolution of Geological Provinces, and Exploration*

## References

- Methods: Geological Association of Canada, Mineral Deposits Division, Special Publication No. 5, p. 849-879.
- Bleeker, W., Ketchum, J.W.F., Jackson, V.A., and Villeneuve, M.E., 1999, The Central Slave Basement Complex, Part 1: its structural topology and autochthonous cover: *Canadian Journal of Earth Sciences*, v. 36, p. 1083-1109.
- Bostock, H.H., and van Breemen, O., 1994, Ages of detrital and metamorphic zircons and monazites from a pre-Taltson magmatic zone basin at the western margin of the Rae Province: *Canadian Journal of Earth Sciences*, v. 31, p. 1353-1364.
- Bowring, S.A., and Grotzinger, J.P., 1992, Implications on new chronostratigraphy for tectonic evolution of Wopmay Orogen, Northwest Canadian Shield: *American Journal of Science*, v. 292, p. 1-20.
- Buchan, K.L., LeCheminant, A.N., and van Breemen, O., 2009, Paleomagnetism and U-Pb geochronology of the Lac de Gras diabase dyke swarm, Slave Province, Canada: implications for the relative drift of Slave and Superior provinces in the Paleoproterozoic: *Canadian Journal of Earth Sciences*, v. 46, p. 361-379.
- Canada-Nunavut Geoscience Office, 2008, Nunavut minerals database (NUMIN): Available online at: [http://www.nunavutgeoscience.ca/cngo/geoscience\\_e.html](http://www.nunavutgeoscience.ca/cngo/geoscience_e.html).
- Canadian Pipeline Environment Committee, 2004, The pipeline industry and the Migratory Birds Convention Act: Canadian Energy Pipeline Association, <http://www.cepa.com>
- Carson, C.J., Berman, R.G., Stern, R.A., Sanborn-Barrie, M., Skulski, T., and Sandeman, H.A.I., 2004, Age constraints on the Paleoproterozoic tectonometamorphic history of the Committee Bay region, western Churchill Province, Canada: evidence from zircon and in-situ monazite SHRIMP geochronology: *Canadian Journal of Earth Sciences*, v. 41, p. 1049-1076.
- Catlos, E.J., Gilley, L.D., and Harrison, T.M., 2002, Interpretation of monazite ages obtained via in situ analysis: *Chemical Geology*, v. 188, p. 193-215.
- Chacko, T., De, S.K., Creaser, R.A., and Muehlenbachs, K., 2000, Tectonic setting of the Taltson magmatic zone at 1.9-2.0 Ga; a granitoid-based perspective: *Canadian Journal of Earth Sciences*, v. 37, p. 1597-1609.
- Cherniak, D.J., 2000, Diffusion in accessory minerals: zircon, titanite, apatite, monazite, and xenotime: *Reviews in Mineralogy and Geochemistry*, v. 72, p. 827-869.
- Cherniak, D.J., Watson, E.B., Grove, M., and Harrison, T.M., 2004, Pb diffusion in monazite: A combined RBS/SIMS study: *Geochimica et Cosmochimica Acta*, v. 68, p. 829-840.
- Clark, M.K., House, M.A., Royden, L.H., Whipple, K.X., Burchfiel, B.C., Zhang, X., Tang, W., 2005. Late Cenozoic uplift of southeastern Tibet. *Geology*, v. 33, p. 525-528.



## References

- Condie, K.C., O'Neill, C.O., and Aster, R.C., 2009, Evidence and implications for a widespread magmatic shutdown for 250 My on Earth: *Earth and Planetary Letters*, no. 282, p. 294-298.
- Corfu, F., Hanchar, J.M., Hoskin, P.W.O., and Kinny, P., 2003, Atlas of zircon textures: *Reviews in Mineralogy and Geochemistry*, v. 53, p. 469-500.
- Culshaw, N., and van Breeman, O., 1990, A zoned low P-high T complex at the level of anatexis—structural and plutonic patterns in metasediments of the Archean Yellowknife Supergroup, near Bathurst Inlet, N.W.T., Canada: *Precambrian Research*, v. 48, p. 1-20.
- Davidson, G.I., and Gandhi, S.S., 1989, Unconformity-related U-Au mineralization in the middle Proterozoic Thelon Sandstone, Boomerang Lake prospect, Northwest Territories, Canada: *Economic Geology*, v. 84, p. 143-157.
- Davis, W.J., and Hegner, E., 1992, Neodymium isotopic evidence for the tectonic assembly of Late Archean crust in the Slave Province, northwest Canada: *Contributions to Mineralogy and Petrology*, v. 111, p. 493-504.
- Davis, W.J., Rainbird, R.H., Aspler, L.B., and Chiarenzelli, J.R., 2005, Detrital zircon geochronology of the Paleoproterozoic Hurwitz and Kiyuk groups, western Churchill Province, Nunavut: *Geological Survey of Canada, Current Research 2005-F1*, 13 p.
- De, S.K., Chacko, T., Creaser, R.A., Muehlenbachs, K., 2000, Geochemical and Nd-Pb-O isotope systematic of granites from the Taltson magmatic zone, NE Alberta: implications for early Proterozoic tectonics in western Laurentia: *Precambrian Research*, v. 102, p. 221-249.
- de Kemp, E. A., Gilbert, C., James, D. T., Geological Survey of Canada, Canada-Nunavut Geoscience Office, 2006, *Geology of Nunavut: Geological Survey of Canada, "A" Series Map no. 1860A*.
- Dewey, J.F., 1988, Extensional collapse of orogens: *Tectonics*, v. 7, p. 1123-1139.
- Didiuk, A.B., and Ferguson, R.S., 2005, Land cover mapping of the Queen Maud Gulf Migratory Bird Sanctuary, Nunavut: *Canadian Wildlife Services, Occasional Paper 111*.
- Elkins, L.T., and Grove, T.L., 1990, Ternary feldspar experiments and thermodynamic models: *American Mineralogist*, v. 75, p. 544-559.
- Fraser, J.A., 1964, Geological notes on northeastern District of Mackenzie, Northwest Territories: *Geological Survey of Canada Paper 63-40*, 20 p.
- Fraser, J.A., 1978, Metamorphism in the Churchill Province, District of MacKenzie, *in* Fraser, J.A., and Heywood, W.W., eds., *Metamorphism in the Canadian Shield: Geological Survey of Canada Paper 78-10*, p. 195-202.
- Frisch, T., 2011, *Geology, Precambrian geology of northern Boothia Peninsula and Somerset Island, Nunavut: Geological Survey of Canada, Open File 6051, scale 1:250 000*.

## References

- Frisch, T., and Hunt, P.A., 1993, Reconnaissance U-Pb geochronology of the crystalline core of the Boothia Uplift, District of Franklin, Northwest Territories: *in* Radiogenic Age and Isotopic Studies, Report 7, Geological Survey of Canada, Paper 93-2, p. 3-22.
- Frost, B.R., Chacko, T., 1989. The granulite uncertainty principle: limitations on thermobarometry in granulites. *Journal of Geology*, v. 97, p. 435-450.
- Fuhrman, M.L., and Lindsley, D.H., 1988, Ternary-feldspar modeling and thermometry: *American Mineralogist*, v. 73, p. 201-215.
- Geological Survey of Canada, 1982, Magnetic anomaly map, Thelon River, Northwest Territories: Geological Survey of Canada, National Earth Science Series, Magnetic Anomaly Map NQ-12-13-14-AM.
- Geological Survey of Canada, 2010, Canadian Aeromagnetic Data Base, Airborne Geophysics Section, GSC - Central Canada Division, Geological Survey of Canada, Earth Sciences Sector, Natural Resources Canada.
- Gibb, R.A., 1978, Slave-Churchill collision tectonics: *Nature*, v. 271, p. 50-52.
- Gibb, R.A., and Halliday, D.W., 1974, Gravity measurements in southern District of Keewatin and southeastern District of Mackenzie, N.W.T.: Earth Physics Branch, Gravity Map Series, no. 124-131.
- Gibb, R.A., and Halliday, D.W., 1975, Gravity Measurements in northern District of Keewatin and parts of District of Mackenzie and District of Franklin, N.W.T.: Earth Physics Branch, Gravity Map Series, no. 139-148.
- Gibb, R.A., and Thomas, M.D., 1977, The Thelon Front: a cryptic suture in the Canadian Shield?: *Tectonophysics*, v. 38, p. 211-222.
- Goldring, P., Harris, J., and Brandon, N., 2011, NTI CA IIBA Phase 1 – Cultural heritage resources report & inventory – Queen Maud Gulf migratory bird sanctuary: Nunavut Tunngavik Inc., 337 p. Available at <http://www.tunngavik.com>
- Hanmer, S., and Needham, T., 1988, Great Slave Lake shear zone meets Thelon Tectonic Zone, District of Mackenzie, N.W.T.; *in* Current Research, Part C, Geological Survey of Canada, Paper 88-1C, p. 33-49.
- Hanmer, S., Bowring, S.A., van Breemen, O., and Parrish, R., 1992, Great Slave Lake shear zone, NW Canada: mylonite record of Early Proterozoic continental convergence, collision and indentation: *Journal of Structural Geology*, v. 14, p. 757-773.
- Hartlaub, R.P., 2004, Archean and Proterozoic evolution of the Beaverlodge Belt, Churchill craton, Canada: Unpublished PhD Thesis, University of Alberta, 189 p.
- Hartlaub, R.P., Heaman, L.M., Chacko, T., Ashton, K.E., and Creaser, R.A., 2004, The Archean Murmac Bay Group: evidence for a giant Archean rift in the Rae Province, Canada: *Precambrian Research*, v. 131, p. 345-372.

## References

- Hartlaub, R.P., Chacko, T., Heaman, L.M., Creaser, R.A., Ashton, K.E., and Simonetti, A., 2005, Ancient (Meso- to Paleoproterozoic) crust in the Rae province, Canada: Evidence from Sm-Nd and U-Pb constraints: *Precambrian Research*, v. 141, p. 137-153.
- Hartlaub, R.P., Heaman, L.M., Chacko, T., and Ashton, K.E., 2007, Circa 2.3 Ga magmatism of the Arrowsmith Orogeny, Uranium City region, western Churchill Craton, Canada: *Journal of Geology*, v. 115, p. 181-195.
- Hebel, M. U., 1999, U-Pb geochronology and lithochemistry of the Hope Bay Greenstone Belt, Slave Structural Province, Northwest Territories, Canada: Unpublished M.Sc. Thesis, University of British Columbia.
- Henderson, J.B., and van Breemen, O., 1992, U Pb ages from an Archean orthogneiss and a Proterozoic metasedimentary gneiss of the Thelon Tectonic Zone, District of Mackenzie, Northwest Territories: *in Radiogenic Age and Isotopic Studies, Report 5*, Geological Survey of Canada, Paper 91-2, p. 25-33.
- Henderson, J.B., McGrath, P.H., Theriault, R.J., and van Breemen, O., 1990, Intracratonic indentation of the Archean Slave province into the Early Proterozoic Thelon tectonic zone of the Churchill province, northwestern Canadian Shield: *Canadian Journal of Earth Sciences*, v. 27, p. 1699-1713.
- Heywood, W.W., 1961, Geological notes, Northern District of Keewatin: Geological Survey of Canada Paper 61-18, 9 p.
- Heywood, W.W., and Schau, M., 1978, A subdivision of the northern Churchill structural province: *in Current Research, Part A: Geological Survey of Canada Paper 78-1A*, p. 139-143.
- Hinchey, A.M., Ryan, J.J., Davis, W.J., Nadeau, L., and James, D.T., 2007, Detrital zircon geochronology of the Archean volcano-sedimentary sequence of the Barclay belt and the Paleoproterozoic sequence of the Northern Chantrey group, Boothia mainland area, Kitikmeot region, Nunavut: Geological Survey of Canada, Current Research 2007-C1, 19 p.
- Hinchey, A.M., Davis, W.J., Ryan, J.J., and Nadeau, L., 2011, Neoproterozoic high-potassium granites of the Boothia mainland area, Rae domain, Churchill Province: U-Pb zircon and Sm-Nd whole rock isotopic constraints: *Canadian Journal of Earth Science*, v. 48, p. 247-249.
- Hoffman, P.F., 1987, Continental transform tectonics: Great Slave Lake shear zone (ca. 1.9 Ga) Northwest Canada: *Geology*, v. 15, p. 785-788.
- Hoffman, P.F., 1988, United plates of America: the birth of a craton. Early Proterozoic assembly and growth of Laurentia: *Annual Review of Earth and Planetary Sciences*, v. 16, p. 543-603.
- Hoffman, P.F., 1989, Precambrian geology and tectonic history of North America: *in Bally A.W., and Palmer, A.R., eds., The geology of North America – An overview: Boulder, Colorado, Geological Society of America, Geology of North America*, v. A, p. 447-552.

## References

- Hoffman, P.F., 1990, Subdivision of the Churchill Province and extent of the Trans-Hudson Orogen *in* Lewry, J.F. and Stauffer, M.R., eds., The Early Proterozoic Trans-Hudson Orogen of North America: Geological Association of Canada, Special Paper 37, p. 15-39.
- Hoffman, P.F., Bowring, S.A., Buchwaldt, R., and Hildebrand, R.S., 2011, Birthdate for the Coronation paleocean: age of initial rifting in Wopmay orogen, Canada: *Canadian Journal of Earth Sciences*, v. 48, p. 281-293.
- Hornal, R.W., and Boyd, J.B., 1972, Gravity measurements in the Slave and Bear structural provinces, Northwest Territories: Earth Physics Branch, Gravity Map Series, no. 89-95.
- Hutton, J., 1788, Theory of the Earth; or an investigation of the laws observable in the composition, dissolution, and restoration of land upon the Globe: *Transactions of the Royal Society of Edinburgh*, v. 1, p. 209-304.
- Jackson, G.D., and Berman, R.G., 2000, Precambrian metamorphic and tectonic evolution of northern Baffin Island, Nunavut, Canada: *The Canadian Mineralogist*, v. 38, p. 399-421.
- James, D.T., 1986, Geology of the Moraine Lake area District of Mackenzie; Part 2: a transect across part of the Thelon tectonic zone: *in* Current Research, Part A, Geological Survey of Canada, Paper 86-1A, p. 417-421.
- James, D.T., 1989, Geology of the Thelon Tectonic Zone in the Moraine Lake area, District of Mackenzie, Northwest Territories: The definition and significance of lithologic, structural, and metamorphic changes across the boundary between the Slave and Churchill Provinces: Unpublished Ph.D. Thesis, Queen's University, Kingston, Ontario.
- Jarosewich, E., Nelen, J.A., and Norberg, J.A., 1980, Reference samples for electron microprobe analysis: *Geostandards Newsletter*, v. 4, p. 43-47.
- Jimenez-Munt, I., Platt, J.P., 2006. Influence of mantle dynamics on the topographic evolution of the Tibetan Plateau: results from numerical modeling. *Tectonics*, v. 25.
- Kitsul, V.I., Glebovitsky, V.A., Vapnik, Y.A., Frisch, T., 2000, Gneisses from the granulite terrane of the central Boothia uplift, Arctic Canada: *The Canadian Mineralogist*, v. 38, p. 443-454.
- Kohn, M.J., and Spear, F.S., 1991, Error propagation for barometers: 2. Application to rocks: *American Mineralogist*, v. 76, p. 138-147.
- Koziol, A.M., and Newton, R.C., 1988, Redetermination of the anorthite breakdown reaction and improvement of the plagioclase-garnet- $\text{Al}_2\text{SiO}_5$ -quartz geobarometer: *American Mineralogist*, v. 73, p. 216-223.

## References

- LeCheminant, A.N., and Heaman, L.M., 1989, Mackenzie igneous events, Canada: Middle Proterozoic hotspot magmatism associated with ocean opening: *Earth and Planetary Science Letter*, v. 96, p. 38-48.
- LeCheminant, A.N., and Roddick, J.C., 1991, U-Pb zircon evidence for widespread 2.6 Ga felsic magmatism in the central District of Keewatin, N.W.T.; *in* Radiogenic Age and Isotopic Studies: Report 4, Geological Survey of Canada, Paper 90-2, p. 91-99.
- LeCheminant, A.N., Heaman, L.M., van Breemen, O., Ernst, R.E., Baragar, W.R.A., and Buchan, K.L., 1996, Mafic magmatism, mantle roots, and kimberlites in the Slave Craton: Geological Survey of Canada, Open File 3228, p. 161-169.
- Lowdon, J.A., 1960, Age determinations by the Geological Survey of Canada, Report 1, Isotopic ages: Geological Survey of Canada, Paper 60-17.
- Lowdon, J.A., Stockwell, C.H., Tipper, H.W. and Wanless, R.K., 1963, Age determinations and geological studies (Including isotopic ages – Report 3): Geological Survey of Canada, Paper 62-17.
- Ludwig, K.R., 2003, Isoplot/Ex, A geochronological toolkit for Microsoft Excel, Version 3.0: Berkeley Geochronology Center Special Publication 4, 70 p.
- Lyell, C., 1830, Principles of geology, being an attempt to explain the former changes of the Earth's surface, by reference to causes now in operation, Vol 1: London, John Murray.
- Maekawa, H., Shozul, M., Ishii, T., Fryer, P., and Pearce, J.A., 1993, Blueschist metamorphism in an active subduction zone: *Nature*, v. 364, p. 520-523.
- Mahan, K.H., and Williams, M.L., 2005, Reconstruction of a large deep-crustal terrane: Implications for the Snowbird Tectonic Zone and early growth of Laurentia: *Geology*, v. 33, p. 385-388.
- McCormick, D. S., 1992, Evolution of an early Proterozoic alluvially-dominated foreland basin, Burnside Formation, Kilohigok Basin, N.W.T., Canada: Unpublished PhD Thesis, Massachusetts Institute of Technology, 547 p.
- McDonough, M.R., McNicoll, V.J., Schetselaar, E.M., and Grover, T.W., Geochronological and kinematic constraints on crustal shortening and escape in a two-sided oblique-slip collisional and magmatic orogen, Paleoproterozoic Taltson magmatic zone, northeastern Alberta: *Canadian Journal of Earth Sciences*, v. 37, p. 1549-1573.
- McNicoll, V.J., Theriault, R.J., and McDonough, M.R., 2000, Taltson basement gneissic rocks; U-Pb and Nd isotopic constraints on the basement to the Paleoproterozoic Taltson Magmatic Zone, northeastern Alberta: *Canadian Journal of Earth Sciences*, v. 37, p. 1575-1596.
- Migratory Birds Convention Act, 1994, Department of Justice, Canada: <http://laws.justice.gc.ca/en/M-7.01/index.html>.

## References

- Mukhopadhyay, B., and Holdaway, M.J., 1994, Cordierite-garnet-sillimanite-quartz equilibrium: I. New experimental calibration in the system FeO-Al<sub>2</sub>O<sub>3</sub>-SiO<sub>2</sub>-H<sub>2</sub>O and certain P-T-X<sub>H<sub>2</sub>O</sub> relations: *Contributions to Mineralogy and Petrology*, v. 116, p. 462-472.
- Mukhopadhyay, A., Bhattacharya, A., and Mohanty, L., 1994: Geobarometers involving clinopyroxene, garnet, plagioclase, ilmenite, rutile, sphene and quartz: estimation of pressure in quartz-absent assemblages: *Contributions to Mineralogy and Petrology*, v. 110, p. 346-354.
- Orrell, S.E., Bickford, M.E., and Lewry, J.F., 1999, Crustal evolution and age of thermotectonic reworking in the western hinterland of the Trans-Hudson orogen, northern Saskatchewan: *Precambrian Research*, v. 95, p. 187-223.
- Otto, S.C., and Bailey, R.J., 1995, Tectonic evolution of the northern Ural Orogen: *Journal of the Geological Society*, v. 152, p. 903-906.
- Palmer, S.E., Kyser, T.K., and Hiatt, E.E., 2004, Provenance of the Proterozoic Thelon Basin, Nunavut, Canada, from detrital zircon geochronology and detrital quartz oxygen isotopes: *Precambrian Research*, v. 129, p. 115-140.
- Parrish, R.R., 1990, U-Pb dating of monazite and its applications to geological problems: *Canadian Journal of Earth Sciences*, v. 27, p. 1431-1450.
- Pattison, D.R.M., and Newton, R.C., 1989, Reversed experimental calibration of the garnet-clinopyroxene Fe-Mg exchange thermometer: *Contributions to Mineralogy and Petrology*, v. 101, p. 87-103.
- Pattison, D.R.M., Chacko, T., Farquhar, J., and McFarlane, C.R.M., 2003, Temperatures of granulite-facies metamorphism: constraints from experimental phase equilibria and thermobarometry corrected for retrograde exchange: *Journal of Petrology*, v. 44, p. 867-900.
- Peterson, T.D., van Breeman, O., Sandeman, H., and Cousens, B., 2002, Proterozoic (1.85-1.75 Ga) igneous suites of the Western Churchill Province: granitoid and untrapotassic magmatism in a reworked Archean hinterland: *Precambrian Research*, v. 119, p. 73-100.
- Peterson, T.D., Pehrsson, S., Skulski, T., and Sandeman, H., 2010, Compilation of Sm-Nd isotope analyses of igneous suites, Western Churchill Province: Geological Survey of Canada, Open File 6439, 18 p.
- Powell, R., and Holland, T.J.B., 1988, An internally consistent dataset with uncertainties and correlations: 3. Applications to geobarometry, worked examples and a computer program: *Journal of Metamorphic Geology*, v. 6, p. 173-204.
- Rainbird, R.H., Hadlari, T., Apler, L.B., Donaldson, J.A., LeCheminant, A.N., and Peterson, T.D., 2003, Sequence stratigraphy and evolution of the Paleoproterozoic intracontinental Baker Lake and Thelon basins, western Churchill Province, Nunavut, Canada: *Precambrian Research*, v. 125, p. 21-53.



## References

- Rainbird, R.H., Davis, W.J., Pehrsson, S.J., Wodicka, N., Rayner, N., and Skulski, T., 2010, Early Paleoproterozoic supracrustal assemblages of the Rae domain, Nunavut, Canada: Intracratonic basin development during supercontinent break-up and assembly: *Precambrian Research*, v. 181, p. 167-186.
- Rayner, N., Chakungal, J., and Sanborn-Barrie, M., 2011, New U-Pb geochronological results from plutonic and sedimentary rocks of Southampton Island, Nunavut: *Geological Survey of Canada, Current Research 2011-5*, 20 p.
- Ross, G.M., Parrish, R.R., Villeneuve, M.E., and Bowring, S.A., 1991, Geophysics and geochronology of the crystalline basement of the Alberta Basin, western Canada: *Canadian Journal of Earth Sciences*, v. 28, p. 512-522.
- Royden, L.H., Burchfiel, B.C., and van der Hilst, R.D., 2008, The geological evolution of the Tibetan Plateau: *Science*, v. 321, p. 1054-1058.
- Ryan J.J., Nadeau, L., Hinchey, A.M., James, D.T., Sandeman, H.A., Schetselaar, E.M., Davis, W.J., and Berman, R.G., 2009, Bedrock geology of the Boothia mainland area (Pelly Bay-Rae Strait-Spence Bay map areas), Kitikmeot region, Nunavut: *Geological Survey of Canada, Current Research 2009-1*, 18 p.
- Schultz, M.E.J., 2007, The Queen Maud block, Nunavut – Genesis of a large felsic igneous province in the earliest Paleoproterozoic and implications for Laurentian geotectonic models, Unpublished M.Sc. Thesis, University of Alberta, 71 p.
- Schultz, M.E.J., Chacko, T., Heaman, L.M., Sandeman, H.A., Simonetti, A., and Creaser, R.A., 2007, Queen Maud Block: A newly recognized Paleoproterozoic (2.4-2.5 Ga) terrane in northwest Laurentia: *Geology*, v. 35, p. 707-710.
- Sen, S.K., and Bhattacharya, A., 1984, An orthopyroxene-garnet thermometer and its application to the Madras charnockites: *Contributions to Mineralogy and Petrology*, v. 88, p. 64-71.
- Simonetti, A., Heaman, L.M., Hartlaub, R.P., Creaser, R.A., MacHattie, T.G., and Bohm, C., 2005, U-Pb zircon dating by laser ablation-MC-ICP-MS using a new multiple ion counting Faraday collector array; *Journal of Analytical Atomic Spectrometry*, v. 20, p. 677-686.
- Simonetti, A., Heaman, L.M., Chacko, T., and Banerjee, N.A., 2006, In situ petrographic thin-section U-Pb dating of zircon, monazite, and titanite using laser ablation-MC-ICP-MS; *International Journal of Mass Spectrometry* v. 253, p. 87-97
- Skulski, T., Sandeman, H., Sanborn-Barrie, M., Hyde, T., Johnstone, S., Panagapko, D., and Byrne, D., 2002, Contrasting crustal domains in the Committee Bay belt, Walker Lake-Arrowsmith River area, central Nunavut: *in Current Research, Geological Survey of Canada, Paper 2002-C11*, 11p.
- Skulski, T., Sandeman, H., Sanborn-Barrie, M., MacHattie, T., Young, M., Carson, C., Berman, R., Brown, J., Rayner, N., Panagapko, D., Byrne, D., and Deyell, C., 2003, Bedrock geology of the Ellice Hills map area and new constraints on the regional geology

## References

of the Committee Bay area, Nunavut: *in* Current Research, Geological Survey of Canada, Paper 2003-C22, 11 p.

Stern, R.A., Bodorkos, S., Kamo, S.L., Hickman, A.H., and Corfu, F., 2009, Measurement of SIMS instrumental mass fractionation of Pb isotopes during zircon dating: *Geostandards and Geoanalytical Research*, v. 33, p. 145–168.

Stockwell, C.H., 1961, Structural provinces, orogenies, and time classifications of rocks of the Precambrian Shield: *in* Lowden, J.A., eds., *Age Determinations by the Geological Survey of Canada: Geological Survey of Canada, Paper 61-17*, p. 108-118.

Theriault, R.J., 1992, Nd isotopic evolution of the Taltson magmatic zone, Northwest Territories, Canada: insights into Early Proterozoic accretion along the western margin of the Churchill province: *Journal of Geology*, v. 100, p. 465-475.

Theriault, R.J., Henderson, J.B., and Roscoe, S.M., 1994, Nd isotopic evidence for early to mid-Archean crust from high grade gneisses in the Queen Maud block and south of the McDonald fault, western Churchill Province, Northwest Territories: *in* Radiogenic Age and Isotopic Studies: Report 8; Geological Survey of Canada, Current Research 1994-F, p. 37-42.

Thompson, A.B., 1976, Mineral reactions in pelitic rocks: II. Calculations of some P-T-X(Fe-Mg) phase relations: *American Journal of Science*, v. 276, p. 425-454.

Thompson, P.H., 1989, An empirical model for metamorphic evolution of the Archean Slave Province and adjacent Thelon Tectonic Zone, north-western Canadian Shield: *Geological Society of London, Special Publications*, v. 43, p. 245-263.

Thompson, P.H., and Henderson, J.B., 1983, Polymetamorphism in the Healy Lake map area – implications for the Thelon tectonic zone: *in* Current activities forum, Program with Abstracts, Geological Survey of Canada, Paper 83-8, p. 2.

Thompson, P.H., Henderson, J.B., and Firth R.A., 1987, The Thelon Front – the transition between the Slave Structural Province and Thelon Tectonic Zone, NW Canadian Shield: *Geological Association of Canada, Program with Abstracts*, v. 12, p. 96.

Thorpe, R., Cummings, G.L., and Mortenson, J., 1992, A significant Pb isotopic boundary in the Slave Province and its probable relationship to ancient basement in the western Slave Province, *in* Project Summaries, Canada – Northwest Territories Mineral Development Agreement 1987-1991: Geological Survey of Canada, Open File 2484, p. 179-184.

Tirrul, R., Grotzinger, J.P., 1990, Early Proterozoic collisional orogeny along the northern Thelon tectonic zone, Northwest Territories, Canada: evidence from the foreland: *Tectonics*, v. 9, p. 1015-1036.

Unsworth, M. J., Jones, A. G., Wei, W., Marquis, G., Gokarn, S. G., and Spratt, J. E., 2005, Crustal rheology of the Himalaya and southern Tibet inferred from magnetotelluric data: *Nature*, v. 438, p 78-31.

## References

- van Breeman, O., and Henderson, J.B., 1988, U-Pb Zircon and monazite ages from the eastern Slave Province and Thelon Tectonic Zone, Artillery Lake area, N.W.T.; *in* Radiogenic Age and Isotopic Studies: Report 2, Geological Survey of Canada, Paper 88-2, p. 73-83.
- van Breemen, O., Thompson, P.H., Hunt, P.A., and Culshaw, N., 1987a, U-Pb zircon and monazite geochronology from the Thelon Tectonic Zone, District of MacKenzie, *in* Radiogenic Age and Isotopic Studies, Report 1: Geological Survey of Canada, Paper 87-2, p. 81-93.
- van Breemen, O., Henderson, J.B., Loveridge, W.D., and Thompson, P.H., 1987b, U-Pb zircon and monazite geochronology and zircon morphology of granulites and granite from the Thelon Tectonic Zone, Healy Lake and Artillery Lake map-areas, N.W.T.: Geological Survey of Canada, Paper 87-1A, p. 783-801.
- van Breemen, O., Bostock, H.H., and Loveridge, W.D., 1991, Geochronology of granites along the margin of the northern Taltson Magmatic Zone and western Rae Province, Northwest Territories, *in* Radiogenic Age and Isotopic Studies, Report 5: Geological Survey of Canada, Paper 91-2, p. 17-24.
- van der Velden, A.J., and Cook, F.A., 2002, Products of 2.65-2.58 ga orogenesis in the Slave Province correlated with Slave – Northern Cordillera Lithospheric Evolution (SNORCLE) seismic reflection patterns: Canadian Journal of Earth Sciences, v. 38, p. 1189-1200.
- Vauchez, A., Kessler, S.F., Lecorche, J.-P., and Villeneuve, M., 1987, Southward extrusion tectonics during the Carboniferous Africa-North America collision: Tectonophysics, v. 142, p. 317-322.
- Wanless, R.K., Stevens, R.D., Lachance, G.R. and Rimsaite, J.Y.H., 1965, Age determinations and geological studies, Part 1 - Isotopic ages, Report 5: Geological Survey of Canada, Paper 64-17, Part A.
- Wanless, R.K., Stevens, R.D., Lachance, G.R. and Rimsaite, J.Y.H., 1966, Age determinations and geological studies, K-Ar isotopic ages, Report 6: Geological Survey of Canada, Paper 65-17.
- Wanless, R.K., Stevens, R.D., Lachance, G.R. and Edmonds, C.M., 1968, Age determinations and geological studies, K-Ar isotopic ages, Report 8: Geological Survey of Canada, Paper 67-2.
- Wen, W., and Nekvasil, H., 1994, SOLVCALC: An interactive graphics program package for calculating the ternary feldspar solvus and for two-feldspar geothermometry: Computers & Geosciences, v. 20, p. 1025-1040.
- Wheeler, J.O., Hoffman, P.F., Card, K.D., Davidson, A., Sanford, B.V., Okulitch, A.V., and Roest, W.R., 1996, Geological map of Canada: Geological Survey of Canada, "A" Series Map 1860A, 2 sheets.

## References

- Williams, H., Hoffman, P.F., Lewry, J.F., Monger, J.W.H., and Rivers, T., 1991, Anatomy of North America: thematic geologic portrayals of the continent: *Tectonophysics*, v. 187, p. 117-134.
- Wilson, J.T., 1968, Static or mobile earth: the current scientific revolution: *Proceedings of the American Philosophical Society*, v. 112, p. 309-320.
- Wright, G.M., 1967, Geology of the southeastern barren grounds, parts of the District of MacKenzie and Keewatin: *Geological Survey of Canada, Memoir 350*.
- Yin, A., Nie, P., Craig, P., and Harrison, T.M., 1998, Late Cenozoic tectonic evolution of the southern Chinese Tian Shan: *Tectonics*, v. 17, p. 1-27.
- Zhang, P., Shen, Z., Wang, M., Gan, W., Burgmann, R., Molnar, P., Wang Q., Nui, Z., Sun, J., Wu, J., Hanrong, S., and Xinzhao, Y., 2004, Continuous deformation of the Tibetan Plateau from global positioning system data: *Geology*, v. 32, p. 809-812.

## APPENDIX A – Geological Notes

Included herein are edited field notes as well as descriptions of rock samples based on hand sample and thin-section observations. The main purpose for including these notes as an appendix is to present the contextual understanding of each of the rock samples collected for the benefit of any future researchers accessing the sample suite. Table A-1 lists the location of the 17 outcrops studied. Figure A-1 is a map showing these locations.

Site #	Latitude (N)	Longitude (W)	Geographic Reference
QM-1	67° 49.872'	102° 33.006'	Kettle Island
QM-2	67° 47.055'	102° 22.346'	Island on west end of Chester Bay
QM-3	67° 38.129'	102° 28.867'	Inland, 20km west of Perry River
QM-4	67° 33.557'	102° 31.967'	Inland, 20km west of Perry River
QM-5	67° 26.932'	102° 33.680'	Inland, 20km west of Perry River
QM-6	67° 58.929'	102° 08.450'	Island on east end of Gernon Bay
QM-7	67° 47.108'	102° 03.289'	Island on east end of Chester Bay
QM-8	67° 43.482'	101° 42.434'	Peninsula on west coast of Ogden Bay
QM-9	67° 43.459'	101° 25.036'	Peninsula on east coast of Ogden bay
QM-10	67° 47.082'	101° 12.863'	Peninsula 5km west of McTavish Point
QM-11	67° 46.338'	100° 55.946'	Island 5km east of McTavish Point
QM-12	67° 41.898'	102° 12.817'	Near Perry River outlet
QM-13	67° 44.772'	98° 53.140'	Island 3km west of Stewart Point
QM-14	67° 47.517'	99° 23.547'	30km west of Stewart Point
QM-15	67° 48.776'	99° 49.443'	Island 50km west of Stewart Point
QM-16	67° 52.576'	100° 15.374'	Island 20km east of Johnson Point
QM-17	67° 51.009'	100° 39.126'	Johnson Point

Table A-1: Latitude and longitude coordinates for each of the 17 sites studied, as well as a geographical reference point.

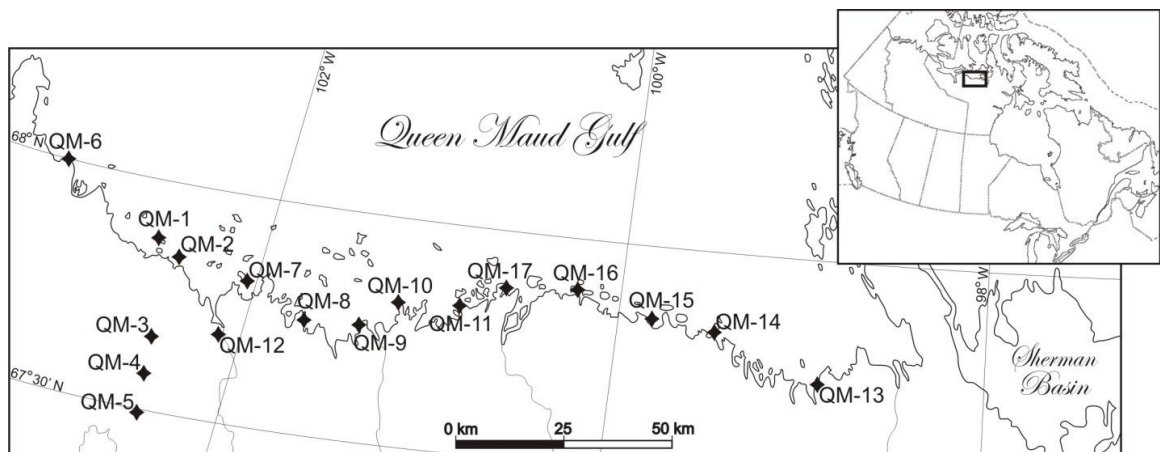


Figure A-1: Map of Queen Maud Gulf showing locations of the 17 outcrops studied. Inset map shows location of the main map.

**Mineral Abbreviations\***

Act	Actinolite	Kspar	Alkali Feldspar
Bt	Biotite	Mt	Magnetite
Cal	Calcite	Musc	Muscovite
Chl	Chlorite	Opx	Orthopyroxene
Cpx	Clinopyroxene	Plag	Plagioclase
Crd	Cordierite	Py	Pyrite
Ep	Epidote	Qtz	Quartz
Grt	Garnet	Sil	Sillimanite
Hbl	Hornblende	Sp	Spinel

\*Mineral modifiers in rock names are listed in order of increasing abundance

**QM-1**

This outcrop is dominated by a suite of lithologically diverse gneisses. These gneisses are cross-cut by a mafic dyke as well as a several smaller granitic pegmatite dykes.

The host gneisses include a metasedimentary package, a mafic gneiss, and metagranitoids. The grey weathering metasedimentary rocks include a 1m thick quartzite and a several meters thick garnet rich pelitic to semi-pelitic paragneiss. A 50 cm thick rusty weathering layer of iron formation is present as well. The dark weathering mafic gneiss contains ultramafic enclaves containing abundant Hbl and Grt. The large Grt porphyroblasts exhibit symplectite textures. The meta-granitoids are primarily granitic in composition and locally contain mafic enclaves.

The package as a whole is variably strained. Gneissosity is generally wavy, but in local zones of higher strain it is straight. Gneissosity measurements are: 105/60, 130/70, 148/65. Deformation of outcrop makes discerning relative age of gneisses impossible.

The cross-cutting mafic dyke clearly truncates the gneissosity of the host rock (Figure A-2). It contains numerous granitic veins which are lightly folded. The mafic dyke is strained, though not to the same degree as the gneissic host rock. A chill margin is preserved in the dyke: average grain size in center of dyke is approximately 1 mm, while at margins is microscopic. The dyke is approximately 11 m wide and trends 330°.

Several granitic pegmatite dykes cross-cut the host gneisses in this area. These dykes are moderately strained, as evidenced by elongate quartz grains and boudinage. The largest pegmatite dyke varies in width from about 30 cm to 1 m and trends approximately 320°. Other dykes found were roughly 10 cm or less in width.

**Samples**

QM-1A

Bt-Opx granitic gneiss

Medium grained, greasy brown weathering, moderately gneissic granite. 2 mm average grain size. Very weakly magnetic. Sample is composed of 75% Plag/Qtz/Kspar, 25% Opx/Bt/Mt.

Appendix A – Geological Notes

- QM-1B      Bt-Opx granitic gneiss  
Duplicate of QM-1A. Smaller grain size and more highly strained.
- QM-1C      Mafic dyke (centre, deformed)  
Dark colored, medium grained, weakly strained mafic dyke. Average grain size is 1-2 mm. Sample collected from coarse grained interior of mafic dyke. Minerals form a granoblastic texture. Minerals present in order of decreasing abundance are: Plag, Hbl, Cpx, opaques, Opx, Qtz, and Grt. Qtz and Grt are restricted to leucosomes.
- QM-1D      Mafic dyke/host gneiss (from contact)  
Collected from contact between cross-cutting mafic dyke and host gneiss. 50% of rock is fine grained dark colored mafic dyke from the chilled margin. 50% of rock is semipelitic gneiss. Mafic dyke exhibits a granoblastic texture and is composed of Plag, Hbl, Cpx, Opx, and opaques in order of decreasing abundance. Host rock is composed of Qtz, Kspar, with minor Grt. The host rock is much coarser grained than the mafic dyke, and is quite altered containing various fine grained micaceous minerals.
- QM-1E      Granitic pegmatite  
Very coarse grained, pink colored, deformed and metamorphosed cross-cutting pegmatite dyke. Sample composed of nearly 100% Qtz/Plag/Kspar. Trace Bt and Grt present. Kspar phenocrysts up to 2 cm across are common. Average grain size of Qtz/Plag is 0.5 cm.
- QM-1F      Opx-Hbl-Grt-Cpx mafic gneiss  
Fine grained dark colored mafic gneiss. 1 mm average grain size. Minerals present in decreasing abundance: Plag, Cpx, Grt, Hbl, Opx, Opaques.
- QM-1G      Ultramafic enclave (hosted by mafic gneiss)  
Dark green, very coarse grained, ultramafic enclave from within mafic gneiss. 1.5 cm Grt porphyroblasts comprise 20% of specimen. Symplectite rims composed of Plag and Opx surround Grt porphyroblasts. Minerals present in decreasing abundance: Hbl, Plag, Opx, Grt, Bt, Cal. Serpentine alteration present locally.
- QM-1H      Crd-Sp-Opx-Grt-Bt quartzite  
Brownish weathering, banded, highly strained quartzite. Average grain size is 1-2 mm. Sample composed of 95% Qtz and 5% Bt/Grt/Opx/Sp/Crd.



- QM-1I            Sil-Opx-Grt-Kspar-Bt semi-pelitic gneiss  
Coarse grained, grey weathering, gneissic semi-pelite. 60% Plag/Qtz/Kspar, 40% Bt/Grt/Opx/Sil, trace Sp present in centre of Grt grains. 3 mm garnet porphyroblasts present, 1 mm average grain size. Opx extremely altered to Chl. Kspar present in leucosomes.
- QM-1J            Sil-Opx-Grt-Kspar-Bt semi-pelitic gneiss  
Duplicate of QM-1I.

## QM-2

This site is dominated by strongly gneissic and migmatized granitoids that are intruded by two mafic dykes. The two dykes are clearly of different generations. One is older, highly deformed and conformable to gneissosity in granitoid host rock; the other is younger, very lightly strained, and clearly cross-cuts the gneissosity of the host granitoid gneiss as well as the older mafic dyke.

The host granitoid migmatite is composed of dark grey granodioritic to tonalitic bands and lighter granitic bands. These bands are 1-10 cm wide and are highly folded. The more felsic granites intrude, and therefore post-date the darker granodiorites. Gneissosity, though highly variable, trends approximately 050/62. Younger pegmatitic dykes up to ten cm wide cross-cut the previously described host rocks.

The older of the two mafic dykes is anywhere from 3 m wide to less than 30 cm wide. It is boudinaged and conformable with the gneissosity in the host rock. This dyke trends approximately 70°.

The younger mafic dyke cross-cuts the gneissosity of the host rocks as well as the previously described, older dyke (Figure A-2). It is very lightly deformed, at least 16 m wide, and trends approximately 345°. A chilled margin is visible along the one exposed side of the dyke.

## **Samples**

- QM-2A            Mafic dyke (younger)  
Dark colored, very lightly strained (as evidenced by recrystallized Cpx and granoblastic texture), medium grained mafic dyke. Average grain size is 2 mm. Composed of 50% Plag, 50% Hbl/Cpx. Trace Mt and Py present. Hbl and Opaque minerals are intergrown, possibly indicative of retrogressed Opx.
- QM-2B            Mafic dyke (older)  
Dark colored, highly deformed, fine grained mafic dyke. Serpentinized veinlets up to 2 mm wide are present but rare. Sample is otherwise massive, though dyke as a whole is strongly boudinaged and conformable with the gneissosity of host granodiorite. Average grain size is 0.5 mm. Sample is composed of 60% Plag, 40% Bt, Hbl, Cpx, Opx. Thin section is beautifully homogeneous.
- QM-2C            Act-Bt-Opx granodioritic gneiss  
Grey weathering, medium grained gneissic granodiorite. Average grain size is 2-3 mm. Composed of 90% Qtz/Plag/Kspar, 10% Opx/Bt/Act/Mt. Act/Bt/Mt

are retrograde products of Opx as evidenced by pseudomorphing. Discrete, planar zones of potassic alteration up to 5 mm wide occur along fractures.

QM-2D Act-Bt granitic gneiss  
Pinkish grey weathering, coarse grained gneissic granite. Average grain size is 3 mm. Composed of 75% Qtz/Plag/Kspar, 25% Bt/Act/Opaques. Well defined gneissic bands are up to 1 cm thick. Act possibly replacing Opx.

### QM-3

This lichen covered outcrop is dominated by metagranodiorite with a moderately well developed gneissosity. A 16 m wide, undeformed, cross-cutting mafic dyke with a well defined chill margin intrudes the host granodiorite. This dyke trends 355° and is at least several kilometres long. Gneissosity in the granodiorite is highly variable though typically trends 285/60.

### **Samples**

QM-3A Bt-Opx granodioritic gneiss  
Weakly gneissic, medium grained, grey weathering granodiorite. Average grain size is 2 mm, though commonly as large as 4 mm. Composed of 90% Qtz/Plag/Kspar, 10% Bt/Mt/Opx/Hbl. Opx is largely retrogressed to Bt/Mt.

QM-3B Mafic dyke (undeformed)  
Dark weathering, medium grained, undeformed mafic dyke. 2 mm average grain size. Minerals present in order of decreasing abundance are: Plag, Cpx, Mt, Py. Plag present in euhedral laths, while Cpx is largely altered to Hbl, Bt, and Chl. This undeformed mafic dyke is thought to be a Mackenzie dyke.

### QM-4

This lichen covered outcrop is dominated by a metagranite with a moderately well developed gneissosity. A large, undeformed, cross-cutting mafic dyke with well defined chill margins trends 355° for at least several kilometres and is about 33 m wide.

### **Samples**

QM-4A Bt-Act-Opx granitic gneiss  
Duplicate of QM-4B.

QM-4B Bt-Act-Opx granitic gneiss  
Light colored, medium grained, well foliated granite. Average grain size is 2-3 mm. 90% Plag/Qtz/Kspar, 10% Opx/Act/Bt/Mt. Act present in reaction rims around Opx grains.

QM-4C Mafic Dyke (undeformed)  
Dark weathering, medium grained, undeformed mafic dyke. 2 mm average grain size. Minerals present in order of decreasing abundance are: Plag, Cpx, and Mt.

**QM-5**

This lichen covered outcrop is dominated by a metagranite with a moderately well developed gneissosity. A large, undeformed, cross-cutting mafic dyke with well defined chill margins trends 355° for at least several kilometres and is about 20 m wide (Figure A-2). A second dyke is visible from the air slightly to the west of the first dyke. This dyke parallels the one visited and is slightly narrower, about 10 m wide.

**Samples**

QM-5A Mafic Dyke (undeformed)

Dark weathering, medium grained, undeformed mafic dyke. 2 mm average grain size. Minerals present in order of decreasing abundance are: Plag, Cpx, and Mt. Plag present in euhedral laths, while Cpx is largely altered to Hbl, Bt, and Chl. This undeformed mafic dyke is thought to be a Mackenzie dyke.

QM-5B Bt-Opx-Hbl granitic gneiss

Pinkish weathering, coarse grained, gneissic granite. Average grain size is 3 mm. 80% Plag/Qtz/Kspar, 20% Bt/Mt/Opx/Hbl. Locally slightly greasy greenish weathering. Abundant zircon grains present.

**QM-6**

Outcrop is composed almost entirely of a grey weathering, metamorphosed, and strongly gneissic granite (Figure A-2). Common mafic to ultramafic inclusions, not more than 20 cm wide, are present within the granite. Also present in minor quantities are younger, more alkaline, cross cutting phases. Gneissosity in granite is locally folded and generally trends 320/60. Granite is locally porphyritic.

**Samples**

QM-6A Cpx-Bt-Hbl granitic gneiss

Duplicate of QM-6b.

QM-6B Cpx-Bt-Hbl granitic gneiss

Grey weathering, coarse grained, strongly magnetic, gneissic granite. 3 mm average grain size. Plag phenocrysts up to 1 cm are present. Gneissic bands typically 0.5 cm thick. 65% Plag/Qtz/Kspar, 35% Hbl/Bt/Cpx/Mt

**QM-7**

The dominant lithology present in this outcrop is metagranodiorite. Minor quantities of more mafic and more felsic granitoids are present locally. Occasional Grt bearing semi-pelite inclusions are present within the granodiorite. Minor cross-cutting pegmatitic phases are present. An extremely high strain mylonite zone cuts through these granitoids.

The high strain zone is horizontally lineated and characterized by several anastomosing bands as thick as 1 m across (Figure A-2). The overall trend of these zones is approximately

040/70. Upper greenschist- to lower amphibolite-facies mineral assemblages dominate this high strain zone, while elsewhere in the outcrop, granulite assemblages are present.

**Samples**

- QM-7A     Cpx-Bt-Opx granodioritic gneiss  
Light grey weathering, coarse grained, moderately strained gneissic granodiorite. 3 mm average grain size. 85% Qtz/Plag/Kspar, 15% Bt/Mt/Opx/Cpx.
- QM-7B     Greenschist mylonite (oriented sample)  
This mafic bulk composition sample is fine grained, mylonitized, and dark grey colored with white bands. 80% of rock is dark grey, fine grained mass of Act/Bt/Chl/Ep. 20% of rock is light colored, fine grained, quartzofeldspathic bands up to 5 mm thick containing Qtz/Plag/Cal.
- QM-7C     Bt-Hbl tonalitic gneiss  
Medium grained, dark grey, strongly gneissic tonalite. Average grain size is 2 mm. 70% Plag/Qtz/Kspar, 30% Hbl/Bt. Minor zones of potassic alteration up to 5 mm thick along fracture zones.
- QM-7D     Grt-Opx-Bt semi-pelitic gneiss  
Dark colored semi-pelite found as an enclave in granodiorite. Garnet porphyroblasts up to 5 mm are present. Minerals present in order of decreasing abundance: Plag/Bt/Opx/Grt/Mt/Qtz. Chlorite reaction rims surround Opx.

**QM-8**

The primary lithology found at this location is a massive, undeformed gabbroic pluton at least several km's squared in size. The pluton is intruded by three distinct rock types, granitic pegmatite dykes, basaltic dykes, and granite.

The basaltic dykes cross-cut and are therefore younger than the pegmatitic dykes. Both sets of dykes are not more than 30 cm across and are very minor. A massive, amorphous, intrusive granite body was found cross-cutting the gabbro and contains angular enclaves of the gabbro (Figure A-2). Like the gabbro, this granite is entirely undeformed.

**Samples**

- QM-8A     Gabbro (undeformed)  
Coarse grained, dark green, gabbro. 3 mm average grain size. 40% Plag, 60% Bt/Hbl/Cpx. Trace Qtz and Opx present locally. Plag grains are subhedral. Wormy intergrown textures in Plag grains are preserved.
- QM-8B     Bt-Hbl granite (undeformed)  
Pink weathering, coarse grained massive granite. Average grain size approximately 3 mm. K-spar phenocrysts up to 6mm long present. 70% Qtz/Plag/Kspar, 30% Hbl/Bt. Intergrowth textures in Kspar grains are preserved.

### **QM-9**

This location contains lithologically varied, strongly gneissic host rock cross-cut by a large mafic dyke as well as several small pegmatitic dykes. There is obvious evidence for at least 2 phases of deformation preserved in this outcrop. D1 is the gneissosity forming event which includes isoclinal folds at the decimetre scale, axial planar to dominant gneissosity. Evidence for D2 is a large scale (more than 10 m across) closed fold, wherein the gneissosity has been folded (Figure A-2). Outside the folded area rocks are highly deformed as straight gneiss.

The host gneisses are granitic and contain variable amounts of Grt and Opx, suggesting a sedimentary origin and granulite-facies metamorphism. Where these granitoids are devoid of garnet, there are abundant mafic bands. Outside of the D2 fold, gneissosity consistently trends around 155/80.

The mafic dyke is around 40 m wide and trends about 080°. The dyke exhibits minor deformation and a clearly defined chilled margin.

Within the D2 fold a pegmatitic dyke of variable thickness, but not more than 1 m wide is present. This dyke clearly cross cuts the gneissosity, but itself is folded by D2. This indicates that the pegmatitic dyke post dates D1, but intruded prior to D2. The plunge of this D2 fold is 216-65.

### **Samples**

- QM-9A      Mafic dyke (centre)  
Medium grained, dark colored mafic rock. Average grain size is 1 mm. Collected from centre of mafic dyke where grain size was coarsest. Minerals present in decreasing abundance are Plag, Cpx, Mt, and trace Grt. Cpx is granoblastic and heavily altered to Hbl and Chl. Exsolution structures visible in larger Cpx porphyroclasts.
- QM-9B      Mafic dyke (chill margin)  
Fine grained, dark colored mafic rock. Average grain size is <0.5 mm. Only Plag is identifiable in hand sample. Collected from chill margin of dyke.
- QM-9C      Grt-Bt psammitic migmatite  
Grey weathering, coarse grained, migmatitic psammite. Average grain size is 3 mm. Migmatitic bands are 0.5 cm thick. 90% Qtz, Plag, K-spar, 10% Bt/Grt. Sample is non-magnetic.
- QM-9D      Granitic pegmatite  
Pink colored, coarse grained granitic pegmatite. Sample contains 99% felsic minerals, and only 1% Bt. Average grain size is 0.5 cm. Pegmatite dyke cross-cuts gneissosity in host rocks, but is folded about F2.

### **QM-10**

This outcrop contains a variety of gneissic rocks. It is dominated by 2 distinct phases of granitoid rocks. Additional ultramafic and pelitic sheets are present in relatively rare abundance. Minor 10-100 cm wide cross-cutting mafic dykes are present.

The two lithologies of granitoid are a brownish grey weathering Bt-Hbl-Opx-Cpx granitic gneiss, and a pink weathering Opx-Bt granitic gneiss. The Opx-Bt bearing granitoid is present as sheets intruding the Bt-Hbl-Opx-Cpx granitoid. A third granitoid rock occurs as 5-10 cm wide dykelets intruding the Bt-Hbl-Opx-Cpx granitoid. These dykelets are highly felsic in composition, and are distinct from other granites present.

Local sheets of coarse grained (up to 5cm) orthopyroxenite (or possibly orthoamphibole) are present. Additionally, Grt, Crd, and Opx bearing pelitic to semipelitic sheets are present. The exact relationship between these rocks and the more abundant granitoids could not be determined in the field.

### **Samples**

- QM-10A Bt-Hbl-Opx-Cpx granitic gneiss  
Greasy grey weathering, medium grained, strongly gneissic granite. Average grain size is 2 mm. Sample composed of 70% Plag/Qtz/Kspar, 30% Cpx/Opx/Hbl/Mt/Bt. Gneissic bands are 0.5 cm thick.
- QM-10B Opx-Bt granitic gneiss  
Pink weathering, moderately strained coarse grained granite. 95% felsic minerals, 5% Bt/Mt/Opx. Average grain size 3 mm. Sample contains a moderately well developed foliation as defined by aligned Bt grains.
- QM-10C Opx-Bt-Crd semi-pelitic gneiss  
Grey brown weathering strongly gneissic semipelite. Sample composed of 70% Qtz/Crd. 30% Bt/Opx. Trace Grt present in hand sample but not thin-section. Average grain size is 3 mm.
- QM-10D Sil-Crd-Opx-Grt-Bt pelitic gneiss  
Sample is very coarse grained with mineral grains in excess of 1 cm across. Opx grains are euhedral, brown to black in color and slightly larger than 1 cm across. Crd grains are brilliant blue in color, are anhedral, and also slightly larger than 1 cm across. Grt is grains are about 2-3 mm across. Grt grains are orangey red in color and often form aggregates exceeding 1 cm across. Bt grains are fine grained, nearly black in color, and form similar aggregates. Together Bt, Opx, Crd, and Grt comprise about 70% of the sample. The remaining 30% of the sample is light in color very fine grained and composed primarily of Plag with minor Qtz and Sil.
- QM-10E Opx-Bt granite dykelet  
Pink weathering, medium grained granite dykelet. Average grain size is 2 mm. Sample composed of 99% Qtz/Kspar/Plag, 1% Bt/Opx.

### **QM-11**

This outcrop is strongly gneissic and composed of two distinct lithologies. These lithologies are a Bt bearing pink weathering medium grained granite and dark weathering mafic

inclusions and dykes (Figure 2-A). The granite dominates the area and comprises more than 80% of the exposed rocks. The mafic inclusions and dykes are gabbroic and contain Hbl, Cpx, Plag, and locally Opx; they are oddly shaped and highly strained. All of the mafic inclusions and dykes appear to have identical compositions.

This outcrop is highly strained as evidenced by well developed gneissosity and often very elongated mafic inclusions. Fold closures are present locally. These folds are roughly 1 m across.

### **Samples**

QM-11A     Bt granitic gneiss  
Pink weathering, coarse grained granitic gneiss. Average grain size is 3 mm.  
Composed of 70% felsic minerals and 30% Bt/Mt. Trace Opx present.

QM-11B     Mafic inclusion  
Dark colored, medium grained mafic inclusion. Plag comprises 40% of sample, Cpx/Hbl comprise 60%. Trace Py and Mt present; sample is weakly magnetic.  
Average grain size is 1 mm.

### **QM-12**

This outcrop consists of a massive, undeformed gabbro dyke intruding into a highly deformed felsic gneiss host rock. The grain size of the gabbro is on average, roughly 3mm, and there is no visible internal deformation. No chill margin is visible along the contact of the intrusion. An aerial view reveals that this large intrusive body is dyke shaped, about 100 m wide, and at least several kilometres long (Figure A-2). Minor basaltic dykes about 10 cm wide cross-cut the gabbro.

While the exact contact between the gabbro and the gneissic host rock is not exposed, there is less than one meter of covered area between the two units. It appears from this that the gabbro cross-cuts the gneissosity of this felsic host rock. The felsic host rock was not examined in detail as this was a somewhat impromptu stop while refuelling the helicopter. It appears as though the gneiss is very similar to that described at location QM-2.

### **Samples**

QM-12A     Massive gabbro  
Dark colored, coarse grained, undeformed gabbro. Average grain size is roughly 3 mm. 40% Plag, 60% Cpx/Opx/Bt/Mt present. Plagioclase grains are euhedral.

### **QM-13**

The outcrop is dominated by an assortment of granitoid rocks with mafic inclusions and is located on a prominent magnetic lineament and what was previously mapped as a fault of unknown displacement. This fault zone is traceable along a noticeable topographic depression several hundred meters wide and trending NNE-SSW for several kilometres (Figure A-2). Locally, this outcrop contains the highest strained rocks found during field reconnaissance (Figure A-2). Across strike this outcrop exhibits variation in the degree of strain. In highly strained zones the rocks form 'straight gneiss', wherein the gneissic banding is continuous and parallel. In lower strain zones the gneissic banding is folded and highly distorted. Measurements



of the direction of gneissosity within these high strain zones are: 022/70, 030/80, and 024/70. Mineral lineations within zones of high strain are horizontal suggesting that displacement along this fault is strike-slip.

Lithologically, the outcrop is dominated by granodiorite containing mafic enclaves. Younger granitic to alkali feldspar granite sheets up to 2 m wide are common, and cross-cut the gneissosity of the granodiorite outside of the high strain zones. Within the high strain zones however, these granitic sheets are highly deformed and parallel to the direction of gneissosity. Based on these observations it is determined that the granitic sheets intruded after the granodiorite but before shearing.

### Samples

- QM-13A Bt-Opx-Hbl granodioritic gneiss  
Greasy grey weathering, moderately gneissic granodiorite. 85% Qtz/Plag/Kspar, 15% Hbl, Opx, Bt, and Mt. Average grain size is approximately 2 mm. Sample is similar in appearance to other granodiorite samples collected at this outcrop, but is unique in that it is more felsic.
- QM-13B Mafic enclave  
Dark colored mafic enclave from granodiorite consisting of 60% Plag, 40% Bt/Hbl/Opx/Mt, and trace Py. Average grain size is about 2 mm.
- QM-13C Hbl granite  
Weakly lineated, pink weathering granite. Sample is composed of 95% Kspar/Qtz/Plag, and 5% Hbl/Mt. Average grain size is 1-2 mm, though local larger Kspar phenocrysts up to 1 cm are present.
- QM-13D Cpx-Bt-Hbl straight gneiss (oriented sample)  
Sample consists of alternating compositional bands composed of either Qtz/Plag/Kspar or Hbl/Bt/Cpx/Mt/Plag. Bands are 1 to 5 cm thick and continuous in outcrop for substantial distances (several meters). Grain size in felsic bands is 3.5 mm and in mafic bands 1 mm. Sample is granodioritic in composition.
- QM-13E Hbl-Bt-Cpx-Opx granodioritic gneiss  
Greasy dark grey weathering strongly gneissic granodiorite. Average grain size is roughly 2 mm and gneissic bands are about 5 mm thick. Sample consists of 70% Plag/Qtz/Kspar, and 30% Opx/Cpx/Bt/Hbl/Mt. Identical in composition to QM-13F, but containing a more strongly developed gneissosity.
- QM-13F Hbl-Bt-Cpx-Opx granodioritic gneiss  
Duplicate of QM-13E, with less well developed gneissosity.
- QM-13G Alkali-feldspar granite  
Strongly horizontally lineated, pink weathering alkali-feldspar granite. Sample

is composed of 99% Kspar/Qtz, and 1% Bt/Hbl/Mt. Qtz grains are about 0.5 mm wide and up to 5 mm long.

**QM-13H**     Mafic enclave

Dark colored mafic enclave from within granodiorite. Sample composed of 60% Plag, 40% Hbl/Bt, and trace Mt. A strong lineation is present in the sample as defined by elongated Hbl grains. Hbl grains are roughly 3 mm across, and up to 1 cm long.

**QM-14**

There are three phases of granitoid present at this outcrop. First, and by far the most abundant, is a pink weathering Bt bearing granite. This lithology comprises roughly 90% of the outcrop. Found as 10 cm to >1 m enclaves within the granite are dark grey weathering, more mafic, Hbl-Bt tonalite inclusions (Figure A-2). Locally present are minor, roughly 10 cm wide cross-cutting pegmatitic dykes.

The tonalite is very highly strained as defined by its well developed gneissosity. The granite is strained, though not to the same degree as the tonalite. The pegmatitic dykes cross-cut the foliation in both units and appear unstrained.

**Samples**

**QM-14A**     Bt granitic gneiss

Pink colored, coarse grained, moderately gneissic granite. Average grain size is 3 mm. Sample is composed of 95% felsic minerals and 5% Bt/Mt.

**QM-14B**     Opx-Bt tonalitic gneiss

Dark greasy grey weathering, strongly gneissic tonalite. Average grain size is 2 mm. Sample composed of 70% Qtz/Plag, 30% Bt/Opx, trace Mt present. Tonalite occurs as enclaves in granite.

**QM-15**

This outcrop is dominated by intercalated dark weathering Opx and Bt bearing granite and light weathering Bt bearing granodiorite. The granite is more abundant than the granodiorite, comprising about 70% of the outcrop. Rare Kspar phenocrysts up to about 5 cm across are present in the granite. The granodiorite postdates and intrudes the granite. Mafic enclaves are present, but not abundant in the granodiorite. A two-mica granite is present in trace quantities throughout the outcrop and intrudes the other granitoids.

Present in minor abundance is a zone of Grt and Bt rich quartzofeldspathic migmatite. The contact between the igneous and metasedimentary rocks appears to be plutonic. It is interpreted that the garnet bearing zone is a raft within the granitoids. All rock types found at this location are strongly deformed and gneissosity is highly variable throughout.

**Samples**

**QM-15A**     Opx-Bt granitic gneiss

Dark pinkish weathering. Average grain size is approximately 2 mm.

Plag/Qtz/Kspar comprise roughly 70% of sample, while Bt/Mt/Opx comprise 30%. A well developed gneissosity is present in the sample.

- QM-15B Musc-Bt granitic gneiss  
Extremely felsic light grey weathering Musc-Bt bearing granite. Qtz/Plag/Kspar comprise more than 90% of sample, while Bt-Musc comprises less than 10%. Average grain size is approximately 1 mm.
- QM-15C Sil-Crd-Bt-Grt-Kspar pelitic migmatite  
Brown weathering, pinkish grey on fresh surface. Sample is strongly compositionally banded. Light bands consist mainly of Kspar, Qtz, Crd, and Sil and comprise about 80% of the sample. Dark bands consist of Grt and Bt and comprise the remaining 20%. Bands are up to 1 cm thick, though this is an extreme case, as they are typically a few mm. Average grain size of Grt, Bt, Qtz, Crd, and Sil is roughly 1 mm. Kspar grains are found as large as 5 mm.
- QM-15D Sil-Crd-Bt-Grt-Kspar pelitic migmatite  
Duplicate of QM-15c, slightly coarser grained.

### **QM-16**

This outcrop consists of a pink weathering weakly deformed granite laden with dark colored angular to rounded mafic inclusions anywhere from a few cm across to more than 2 m across (Figure A-2). A possible hypothesis for formation of this outcrop is the mingling of felsic and mafic magmas. Large (maximum 5cm) Kspar phenocrysts are present within granite. This outcrop is approximately 80% granite, and 20% mafic inclusions.

### **Samples**

- QM-16A Hbl-Opx-Bt granite  
Sample is pink weathering. Average grain size is about 4 mm. Reaction rims surround Opx. These reaction rims contain Bt and Mt. Hbl, Opx, Bt, Mt comprise roughly 30% of sample while Qtz, Plag, K-spar comprise 70%. Sample is weakly strained as defined by elongate mafic blebs containing Opx, Bt, and Mt. Kspar phenocrysts up to 1 cm present in this sample.
- QM-16B Mafic inclusion  
The dark colored mafic inclusions consist of Plag, Cpx, and Hbl in roughly equal proportions. Average grain size is approximately 0.5 mm. Hbl appears to be present in reaction rims surrounding Cpx.

### **QM-17**

This outcrop is dominated by a greasy brownish weathering, strongly gneissic granodiorite to tonalite. Gneissosity parallel granitic veins intrude the granodiorite. These veins are fairly abundant and are no more than 10 cm thick. Outcrop is roughly 80% granodiorite and 20% granite. Both phases are highly deformed.

Several highly boudinaged, cross-cutting mafic dykes are present in the granitoid phases (Figure A-2). These dykes are 2-10 m thick and trend approximately 45°. A later, cross-cutting, undeformed granitic pegmatite dyke about 30 cm wide is present within the charnokite.

**Samples**

QM-17A Mafic dyke (deformed)

Mafic dyke is dark weathering and amphibolitic in composition. In decreasing abundance minerals present are: Plag, Cpx, Opx, Mt, and Hbl. Average grain size in this sample is 2 mm. This sample is a textbook mafic granulite.

QM-17B Mafic dyke (deformed)

Identical in appearance and composition to the previously described sample, but collected from a different dyke.

QM-17C Opx-Bt granodioritic gneiss

Greasy brownish weathering, strongly gneissic meta-granitoid. Average grain size is approximately 1 mm. Qtz/Plag/Kspar comprise about 80% of the sample while Bt/Opx/Mt comprise 20%. Discontinuous gneissic bands are approximately 0.5 cm thick.

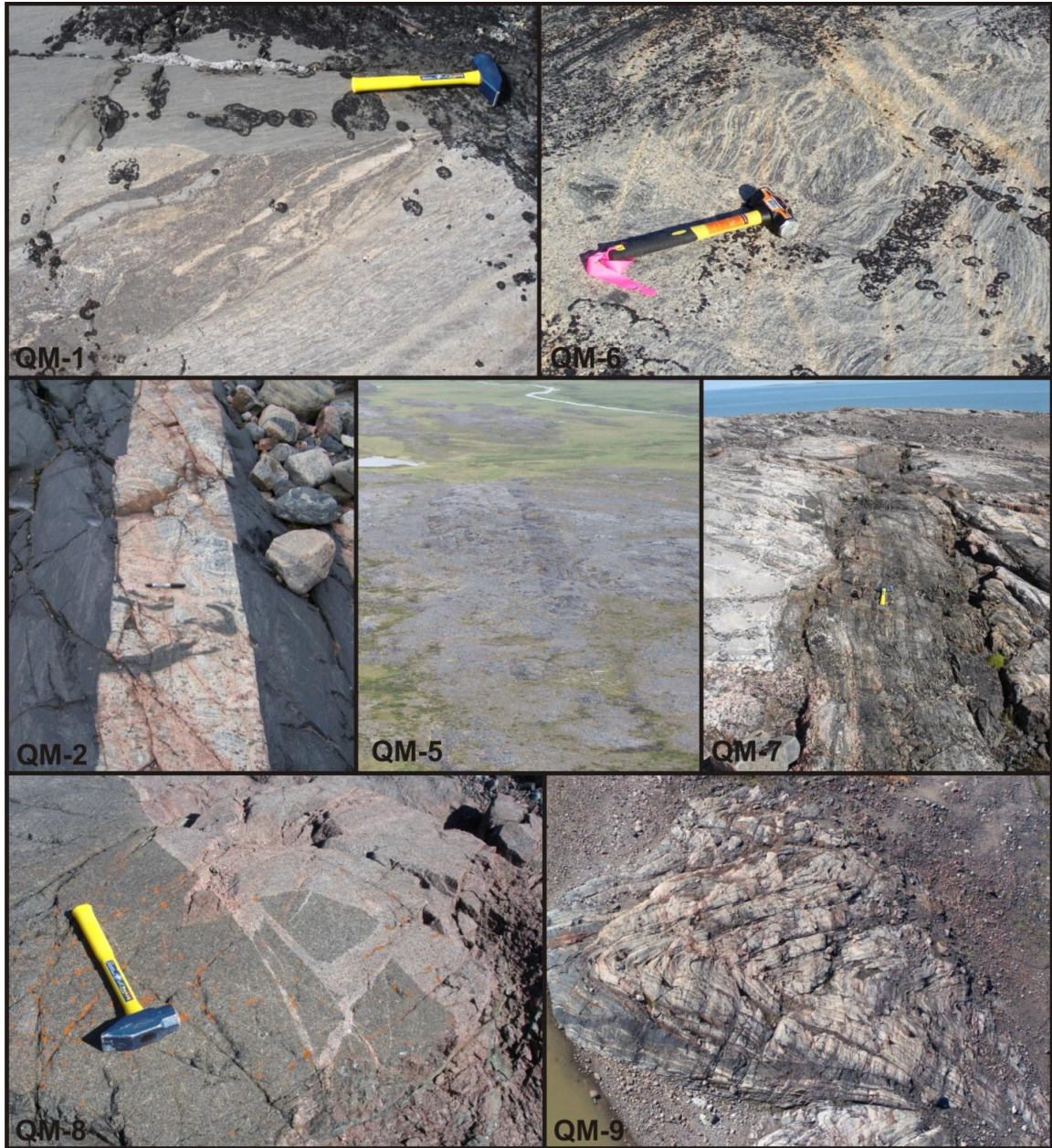


Figure A-2: Photographs from outcrops. QM-1: Cross cutting mafic dyke, and host semi-pelitic paragneiss. QM-2: Two generations of mafic rocks and host granitoid gneiss. QM-5: NNW trending mafic dyke seen from air. QM-6: Granitic gneiss. QM-7: High strain zone trending 040/70. QM-8: Undeformed gabbro, and younger undeformed granite. QM-9: Southwest plunging D2 fold seen from air.



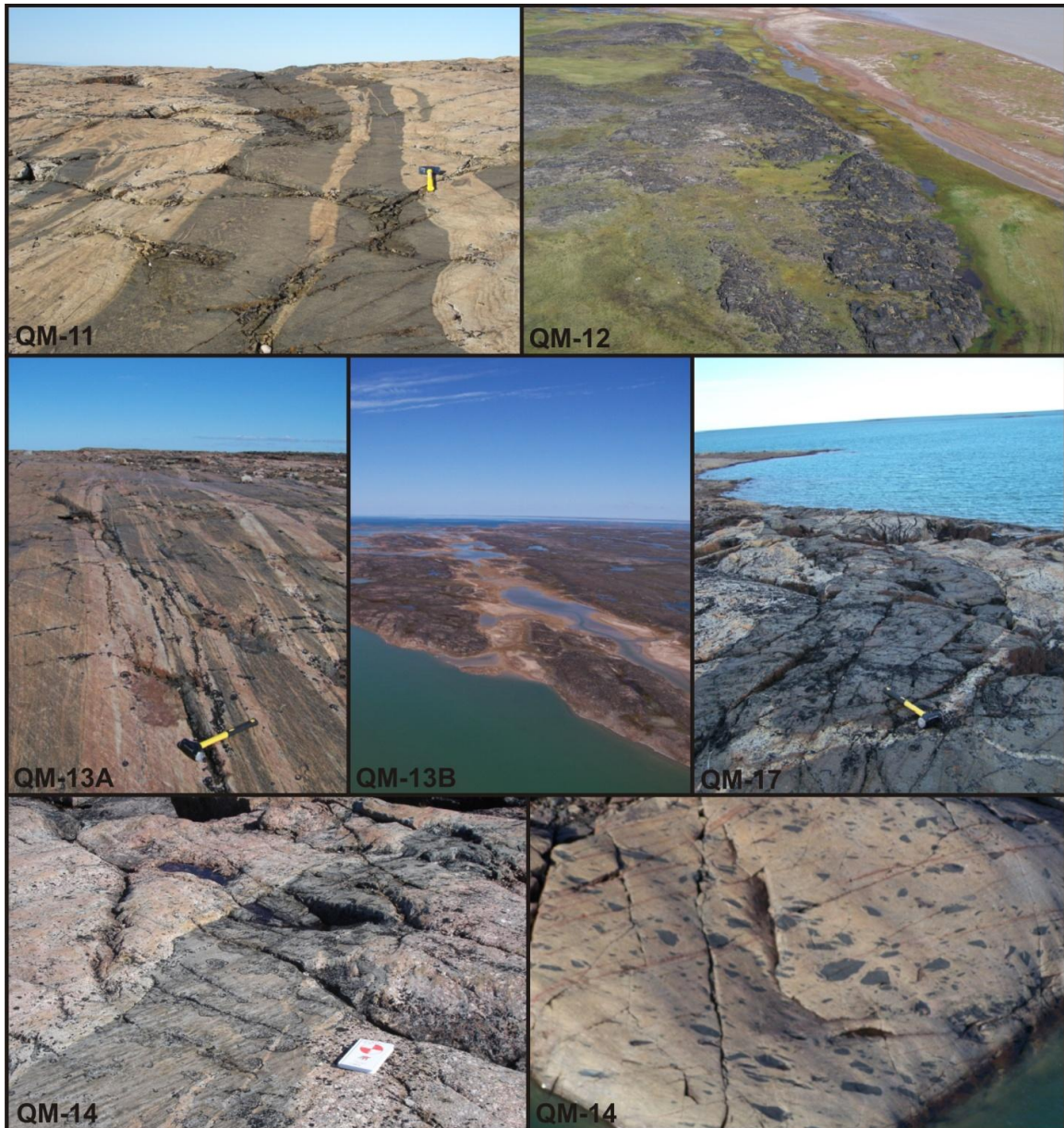


Figure A-2 (continued): **QM-11:** Deformed mafic dyke in host granite. **QM-12:** Massive, intrusive gabbro dyke trending NW seen from air. **QM-13A:** NNE trending straight gneiss formed in high strain zone. **QM-13B:** Topographic depression formed along high strain zone shown in QM-13A, seen from air. **QM-14:** OPX bearing granodioritic enclave in host granite. **QM-16:** Extremely abundant mafic inclusions within host granite, seen from air. **QM-17:** Deformed mafic dyke within host OPX bearing granodiorite.

## APPENDIX B – U-Pb Geochronological Data

In-situ LA-MC-ICP-MS U-Pb dating of monazite grains from rocks collected from the Queen Maud block

Analysis	Spot Size µm	<sup>206</sup> Pb (cps)	<sup>204</sup> Pb (cps)	<sup>207</sup> Pb/ <sup>206</sup> Pb	±2σ	<sup>207</sup> Pb/ <sup>235</sup> U	±2σ	<sup>206</sup> Pb/ <sup>238</sup> U	±2σ	ρ	Model Ages (Ma)						% Disc.
											<sup>207</sup> Pb/ <sup>206</sup> Pb	±2σ	<sup>207</sup> Pb/ <sup>235</sup> U	±2σ	<sup>206</sup> Pb/ <sup>238</sup> U	±2σ	
QM1A-1A	16	342429	46	0.13516	0.00274	7.91514	0.66354	0.42471	0.03455	0.970	2166	18	2221	73	2282	154	-6.3
QM1A-1B	16	363965	1054	0.18005	0.00750	12.93187	0.95925	0.52093	0.03197	0.827	2653	35	2675	68	2703	134	-2.3
QM1A-1C	16	449931	35	0.13243	0.00273	7.37730	0.86151	0.40401	0.04644	0.984	2130	18	2158	99	2187	210	-3.2
QM1A-1D	16	231021	165	0.14311	0.00327	8.71881	0.48527	0.44187	0.02243	0.912	2265	20	2309	49	2359	100	-5.0
QM1A-1E	16	316590	149	0.14150	0.00324	8.18478	0.66543	0.41952	0.03272	0.959	2246	20	2252	71	2258	147	-0.7
QM1A-2A	16	404939	37	0.13920	0.00287	8.27170	0.63189	0.43097	0.03170	0.963	2217	18	2261	67	2310	141	-5.0
QM1A-2B	16	799494	45	0.13355	0.00270	7.17763	0.52775	0.38981	0.02756	0.962	2145	18	2134	64	2122	127	1.3
QM1A-2C	16	672603	32	0.13140	0.00268	6.73158	0.48124	0.37155	0.02546	0.958	2117	18	2077	61	2037	119	4.4
QM1A-4A	16	527438	47	0.13336	0.00271	6.51038	0.35842	0.35407	0.01811	0.929	2143	18	2047	47	1954	86	10.2
QM1A-4B	16	429124	51	0.12930	0.00268	6.07683	0.34859	0.34087	0.01823	0.932	2088	18	1987	49	1891	87	10.9
QM1A-4C	16	429286	25	0.12959	0.00268	6.29557	0.37396	0.35233	0.01962	0.937	2092	18	2018	51	1946	93	8.1
QM1D-1C	12	455484	41	0.13765	0.00287	7.35671	0.48562	0.38761	0.02428	0.949	2198	18	2156	57	2112	112	4.6
QM1D-2A	12	175659	43	0.13591	0.00300	7.51839	0.43123	0.40121	0.02124	0.923	2176	19	2175	50	2175	97	0.1
QM1D-2B	12	162929	46	0.14068	0.00314	7.86462	0.44864	0.40544	0.02128	0.920	2236	19	2216	50	2194	97	2.2
QM1D-2C	12	148288	44	0.11269	0.00267	4.83662	0.33016	0.31129	0.01993	0.938	1843	21	1791	56	1747	97	6.0
QM1D-2D	12	185731	28	0.13554	0.00330	6.54179	0.47842	0.35005	0.02414	0.943	2171	21	2052	62	1935	114	12.6
QM1D-2E	12	167003	50	0.14306	0.00302	8.06874	0.48688	0.40906	0.02312	0.937	2265	18	2239	53	2211	105	2.8
QM1D-3A	12	570683	53	0.14245	0.00288	7.63345	0.60416	0.38864	0.02974	0.967	2257	17	2189	69	2116	137	7.3
QM1D-3B	12	678730	52	0.14587	0.00300	7.73251	0.47337	0.38447	0.02217	0.942	2298	18	2200	54	2097	102	10.2
QM1D-3C	12	602673	48	0.14529	0.00307	8.00213	0.55186	0.39946	0.02622	0.952	2291	18	2231	60	2167	120	6.4
QM1D-4A	12	637794	31	0.12870	0.00272	6.74674	0.58145	0.38020	0.03177	0.969	2080	19	2079	73	2077	147	0.2
QM1D-4B	12	517310	148	0.12994	0.00278	6.14401	0.42991	0.34293	0.02285	0.952	2097	19	1997	59	1901	109	10.8
QM1D-4C	12	1076438	41	0.13481	0.00275	6.39985	0.41434	0.34430	0.02116	0.949	2162	18	2032	55	1907	101	13.6
QM1D-4D	12	772438	99	0.13444	0.00297	7.22889	0.54443	0.38998	0.02808	0.956	2157	19	2140	65	2123	129	1.9
QM1D-6A	12	986106	37	0.14261	0.00297	7.27968	0.44838	0.37023	0.02146	0.941	2259	18	2146	54	2030	100	11.8
QM1D-6B	12	960315	42	0.14216	0.00291	7.35391	0.42509	0.37518	0.02028	0.935	2254	18	2155	50	2054	94	10.4
QM1I-1A	12	594470	80	0.13541	0.00086	8.03343	0.71609	0.43029	0.03826	0.997	2169	6	2235	77	2307	170	-7.6
QM1I-1B	12	943365	91	0.14028	0.00083	8.97797	0.79203	0.46416	0.04086	0.998	2231	5	2336	78	2458	177	-12.3
QM1I-1C	12	650969	83	0.13597	0.00078	8.05883	0.35244	0.42986	0.01864	0.991	2176	5	2238	39	2305	83	-7.0
QM1I-2A	12	1865077	122	0.13418	0.00147	6.88697	0.41439	0.37225	0.02202	0.983	2153	10	2097	52	2040	103	6.1
QM1I-2B	12	1597760	125	0.12985	0.00175	6.54201	0.29587	0.36539	0.01577	0.954	2096	12	2052	39	2008	74	4.9
QM1I-3A	12	1649583	114	0.14005	0.00146	7.61266	0.37752	0.39423	0.01911	0.978	2228	9	2186	44	2142	88	4.5
QM1I-3B	12	1196236	146	0.13836	0.00097	7.56285	0.39502	0.39643	0.02052	0.991	2207	6	2180	46	2153	94	2.9
QM1I-3C	12	1890927	92	0.15032	0.00113	8.95550	0.66564	0.43209	0.03195	0.995	2350	6	2333	66	2315	142	1.7
QM7A-1A	12	938139	82	0.15270	0.00309	8.78185	0.57954	0.41709	0.02620	0.952	2376	17	2316	58	2247	118	6.4
QM7A-1B	12	1069081	116	0.15163	0.00302	9.86930	0.75869	0.47206	0.03505	0.966	2364	17	2423	69	2493	152	-6.5
QM7A-1C	12	1036989	104	0.15143	0.00306	8.99659	0.50548	0.43090	0.02260	0.933	2362	17	2338	50	2310	101	2.6
QM7A-2A	12	210782	80	0.14815	0.00319	8.87860	0.57073	0.43465	0.02633	0.942	2325	18	2326	57	2327	117	-0.1
QM7A-3A	12	457886	53	0.15117	0.00306	8.74671	0.62586	0.41964	0.02880	0.959	2359	17	2312	63	2259	129	5.0
QM7A-3B	12	385960	73	0.15083	0.00305	8.80290	0.50355	0.42328	0.02265	0.935	2355	17	2318	51	2275	102	4.0
QM7A-3C	12	476375	68	0.15171	0.00313	8.42322	0.66089	0.40269	0.03049	0.965	2365	18	2278	69	2181	139	9.2
QM7A-4A	12	684072	62	0.15246	0.00307	9.09331	0.60132	0.43258	0.02724	0.952	2374	17	2347	59	2317	121	2.8
QM7A-4B	12	494136	51	0.15189	0.00306	8.98506	0.66515	0.42902	0.03056	0.962	2367	17	2336	65	2301	136	3.3
QM7A-4C	12	392595	35	0.15013	0.00317	8.78153	0.51359	0.42423	0.02314	0.933	2347	18	2316	52	2280	104	3.4



In-situ Monazites (continued)

Analysis	Spot Size μm	<sup>206</sup> Pb (cps)	<sup>204</sup> Pb (cps)	<sup>207</sup> Pb/ <sup>206</sup> Pb	±2σ	<sup>207</sup> Pb/ <sup>235</sup> U	±2σ	<sup>206</sup> Pb/ <sup>238</sup> U	±2σ	ρ	Model Ages (Ma)						% Disc.
											<sup>207</sup> Pb/ <sup>206</sup> Pb	±2σ	<sup>207</sup> Pb/ <sup>235</sup> U	±2σ	<sup>206</sup> Pb/ <sup>238</sup> U	±2σ	
QM7A-5A	12	447339	35	0.15111	0.00307	8.51024	0.44262	0.40847	0.01956	0.921	2358	17	2287	46	2208	89	7.5
QM7A-5B	12	382487	37	0.15142	0.00308	8.55424	0.61565	0.40973	0.02828	0.959	2362	17	2292	63	2214	128	7.4
QM7A-6B	12	1535848	85	0.15021	0.00311	9.86091	0.87966	0.47612	0.04132	0.973	2348	18	2422	79	2510	178	-8.3
QM7D-2A	12	435942	180	0.14071	0.00312	7.76439	0.55668	0.40022	0.02729	0.951	2236	19	2204	63	2170	124	3.5
QM7D-2B	12	812246	136	0.14779	0.00298	9.01460	0.73463	0.44237	0.03493	0.969	2321	17	2339	72	2361	154	-2.1
QM7D-2C	12	332123	107	0.14577	0.00292	8.63187	0.71543	0.42948	0.03454	0.970	2297	17	2300	73	2303	154	-0.3
QM7D-3A	12	211430	101	0.15027	0.00306	8.73141	0.53033	0.42142	0.02412	0.942	2349	17	2310	54	2267	108	4.1
QM7D-3B	12	287506	97	0.14750	0.00327	9.08267	0.63410	0.44660	0.02957	0.948	2317	19	2346	62	2380	130	-3.2
QM7D-4A	12	202777	105	0.15105	0.00327	8.62419	0.49595	0.41409	0.02206	0.926	2358	19	2299	51	2234	100	6.2
QM7D-5A	12	329099	98	0.13445	0.00286	7.10838	0.55468	0.38346	0.02879	0.962	2157	19	2125	67	2092	133	3.5
QM7D-5B	12	423128	106	0.13557	0.00282	7.09684	0.48058	0.37965	0.02447	0.952	2171	18	2124	59	2075	113	5.2
QM7D-5C	12	388816	145	0.13339	0.00286	7.11181	0.50508	0.38668	0.02618	0.953	2143	19	2126	61	2107	121	2.0
QM9C-2A	12	1347427	65	0.15605	0.00097	9.75230	0.78999	0.45326	0.03661	0.997	2413	5	2412	72	2410	160	0.2
QM9C-2B	12	1102667	39	0.15711	0.00087	9.19446	0.63160	0.42445	0.02906	0.997	2425	5	2358	61	2281	130	7.1
QM9C-2C	12	1063498	42	0.15738	0.00088	9.32426	0.66464	0.42969	0.03053	0.997	2428	5	2370	63	2304	136	6.0
QM9C-5A	12	1776280	41	0.15969	0.00125	9.19606	0.84530	0.41766	0.03825	0.996	2452	7	2358	81	2250	172	9.8
QM9C-5B	12	1310401	41	0.15756	0.00114	9.93703	0.76765	0.45740	0.03518	0.996	2430	6	2429	69	2428	154	0.1
QM9C-5C	12	977285	32	0.15745	0.00099	9.58407	0.66011	0.44147	0.03028	0.996	2428	5	2396	61	2357	134	3.5
QM9C-9A	12	1908017	59	0.15508	0.00127	8.42907	0.64586	0.39420	0.03003	0.994	2403	7	2278	67	2142	137	12.7
QM9C-9B	12	1084286	25	0.14639	0.00094	8.63354	0.59410	0.42774	0.02930	0.996	2304	6	2300	61	2296	131	0.4
QM9C-9C	12	1015120	41	0.14461	0.00079	7.77665	0.55975	0.39003	0.02799	0.997	2283	5	2206	63	2123	129	8.2
QM9C-9D	12	1367335	33	0.15341	0.00137	9.02877	0.62126	0.42685	0.02912	0.992	2384	8	2341	61	2292	130	4.6
QM9C-10A	12	1438612	55	0.15737	0.00112	9.78334	0.67191	0.45087	0.03080	0.995	2428	6	2415	61	2399	135	1.4
QM9C-10B	12	1349230	46	0.13813	0.00083	7.34919	0.47809	0.38588	0.02499	0.996	2204	5	2155	57	2104	115	5.3
QM9C-10C	12	2266715	66	0.15758	0.00120	9.00877	0.61565	0.41462	0.02816	0.994	2430	6	2339	61	2236	127	9.4
QM9C-10D	12	1102681	27	0.15314	0.00103	9.51726	0.64488	0.45073	0.03039	0.995	2381	6	2389	60	2398	134	-0.9
QM9C-10E	12	1049802	35	0.13266	0.00088	6.89368	0.44305	0.37688	0.02409	0.995	2134	6	2098	55	2062	112	3.9
QM9C-12A	12	1303907	50	0.15645	0.00113	10.59249	0.99163	0.49104	0.04583	0.997	2418	6	2488	83	2575	195	-7.9
QM9C-12B	12	1124370	48	0.15259	0.00101	10.46413	0.98206	0.49738	0.04656	0.998	2375	6	2477	83	2603	197	-11.7
QM9C-12C	12	1261417	49	0.15496	0.00107	10.57384	0.97122	0.49488	0.04533	0.997	2401	6	2486	82	2592	193	-9.6
QM9C-13A	12	1964788	77	0.15570	0.00096	9.83927	0.81128	0.45831	0.03768	0.997	2410	5	2420	73	2432	164	-1.1
QM9C-13B	12	1063151	63	0.14919	0.00096	8.87863	0.60315	0.43162	0.02919	0.995	2337	6	2326	60	2313	130	1.2
QM9C-13C	12	1183131	81	0.14789	0.00119	10.07542	0.91686	0.49410	0.04479	0.996	2322	7	2442	81	2588	190	-14.0
QM9D-2A	16	39049	15	0.13006	0.00217	6.76087	0.36325	0.37703	0.01925	0.951	2099	29	2081	46	2062	90	2.0
QM9D-2B	16	25204	13	0.12713	0.00255	6.70528	0.37292	0.38252	0.01985	0.933	2059	35	2073	48	2088	92	-1.7
QM9D-2C	16	32766	4	0.13202	0.00257	7.75421	0.50769	0.42600	0.02663	0.955	2125	34	2203	57	2288	119	-9.1
QM9D-2D	16	34076	12	0.12954	0.00359	7.40466	0.59004	0.41458	0.03098	0.938	2092	49	2162	69	2236	140	-8.2
QM9D-3A	16	40882	19	0.12882	0.00373	6.88482	0.38228	0.38762	0.01837	0.854	2082	51	2097	48	2112	85	-1.7
QM9D-3B	16	45002	11	0.13823	0.00141	7.87565	0.57804	0.41321	0.03003	0.990	2205	18	2217	64	2230	136	-1.3
QM9D-4A	16	105774	10	0.12376	0.00110	6.29612	0.34859	0.36898	0.02017	0.987	2011	16	2018	47	2025	94	-0.8
QM9D-4B	16	86157	20	0.12083	0.00184	5.85331	0.45576	0.35133	0.02683	0.981	1969	27	1954	65	1941	127	1.6
QM9D-4C	16	81786	13	0.12475	0.00177	5.92497	0.39020	0.34448	0.02215	0.976	2025	25	1965	56	1908	105	6.7
QM10B-1A	12	150320	136	0.14966	0.00309	9.24334	0.88743	0.44794	0.04200	0.977	2342	18	2362	84	2386	184	-2.3
QM10B-1B	12	129504	127	0.15020	0.00305	9.47719	0.81541	0.45764	0.03826	0.972	2348	17	2385	76	2429	167	-4.1
QM10B-1C	12	147307	121	0.15029	0.00309	9.21767	0.46057	0.44482	0.02025	0.911	2349	18	2360	45	2372	90	-1.2

In-situ Monazites (continued)

Analysis	Spot Size μm	<sup>206</sup> Pb (cps)	<sup>204</sup> Pb (cps)	<sup>207</sup> Pb/ <sup>206</sup> Pb	±2σ	<sup>207</sup> Pb/ <sup>235</sup> U	±2σ	<sup>206</sup> Pb/ <sup>238</sup> U	±2σ	ρ	Model Ages (Ma)						% Disc.
											<sup>207</sup> Pb/ <sup>206</sup> Pb	±2σ	<sup>207</sup> Pb/ <sup>235</sup> U	±2σ	<sup>206</sup> Pb/ <sup>238</sup> U	±2σ	
QM10B-1D	12	149998	138	0.15061	0.00306	9.82382	0.64107	0.47307	0.02933	0.950	2353	17	2418	58	2497	127	-7.4
QM10B-2A	12	96615	127	0.14567	0.00337	8.36352	0.65204	0.41642	0.03101	0.955	2296	20	2271	68	2244	140	2.7
QM10B-2B	12	149192	145	0.14455	0.00298	7.84899	0.48526	0.39383	0.02296	0.943	2282	18	2214	54	2141	105	7.3
QM10B-2C	12	119024	126	0.13781	0.00331	7.40988	0.63637	0.38996	0.03215	0.960	2200	21	2162	74	2123	147	4.1
QM10B-2D	12	89476	135	0.14367	0.00338	8.87560	0.57099	0.44806	0.02683	0.931	2272	20	2325	57	2387	118	-6.0
QM10B-3A	12	56311	116	0.14058	0.00395	7.68592	0.50447	0.39654	0.02353	0.904	2234	24	2195	57	2153	108	4.3
QM10B-3B	12	23721	103	0.13051	0.00894	7.59610	0.80540	0.42213	0.03416	0.763	2105	60	2184	91	2270	153	-9.3
QM10B-3C	12	13845	119	0.10046	0.01861	6.10808	1.20182	0.44095	0.02927	0.337	1633	172	1991	159	2355	130	-53.0
QM10B-3D	12	52623	88	0.14418	0.00394	7.81699	0.53403	0.39322	0.02462	0.916	2278	24	2210	60	2138	113	7.2
QM10B-4A	12	58715	87	0.14505	0.00364	8.06474	0.50245	0.40323	0.02300	0.915	2288	22	2238	55	2184	105	5.4
QM10B-4B	12	101004	83	0.14965	0.00324	8.93454	0.49985	0.43300	0.02234	0.922	2342	19	2331	50	2319	100	1.2
QM10B-4C	12	47665	83	0.14504	0.00399	8.31635	0.49473	0.41586	0.02193	0.886	2288	24	2266	53	2242	99	2.4
QM10B-5A	12	199840	82	0.15098	0.00306	8.61932	0.51931	0.41405	0.02349	0.942	2357	17	2299	53	2233	106	6.2
QM10B-5B	12	132610	84	0.14964	0.00315	8.99247	0.58983	0.43583	0.02707	0.947	2342	18	2337	58	2332	120	0.5
QM10B-5C	12	133831	105	0.14895	0.00349	8.31600	0.81782	0.40494	0.03868	0.971	2334	20	2266	85	2192	175	7.2
QM10C-4A	12	208108	89	0.15104	0.00078	9.65583	0.38778	0.46366	0.01847	0.992	2358	4	2403	36	2456	81	-5.0
QM10C-4B	12	290141	100	0.15178	0.00072	10.11510	0.54988	0.48333	0.02617	0.996	2366	4	2445	49	2542	113	-9.0
QM10C-4C	12	343912	105	0.15105	0.00088	9.31955	0.27895	0.44747	0.01314	0.981	2358	5	2370	27	2384	58	-1.3
QM10C-8A	12	1653060	107	0.15912	0.00087	10.01460	0.71373	0.45645	0.03244	0.997	2446	5	2436	64	2424	142	1.1
QM10C-8B	12	552209	107	0.15244	0.00071	9.33082	0.60119	0.44394	0.02853	0.997	2373	4	2371	57	2368	126	0.3
QM10C-9A	12	3291316	224	0.16217	0.00095	9.86716	0.38530	0.44128	0.01704	0.989	2478	5	2422	35	2356	76	5.9
QM10C-9B	12	2758712	150	0.16004	0.00090	10.34069	0.45475	0.46863	0.02044	0.992	2456	5	2466	40	2478	89	-1.1
QM10C-9C	12	2778432	159	0.16060	0.00167	10.15472	0.54416	0.45857	0.02410	0.981	2462	9	2449	48	2433	106	1.4
QM10C-9D	12	1961423	140	0.15998	0.00084	9.66441	0.58120	0.43812	0.02625	0.996	2455	4	2403	54	2342	117	5.5
QM10C-9E	12	2239783	160	0.15881	0.00121	9.88028	0.55638	0.45123	0.02517	0.991	2443	6	2424	51	2401	111	2.1
QM10C-9F	12	2908449	165	0.16233	0.00137	9.92713	0.53492	0.44354	0.02360	0.988	2480	7	2428	49	2366	105	5.5
QM10C-9G	12	2279728	160	0.15729	0.00151	12.03462	0.77152	0.55491	0.03518	0.989	2427	8	2607	58	2846	144	-21.4
QM10C-9H	12	1968865	180	0.15775	0.00121	11.30135	1.02222	0.51959	0.04683	0.996	2432	7	2548	81	2697	196	-13.4
QM10D-1A	12	390710	68	0.15117	0.00307	9.82313	0.67396	0.47129	0.03089	0.955	2359	17	2418	61	2489	134	-6.6
QM10D-1B	12	286595	44	0.15129	0.00307	9.07880	0.51258	0.43522	0.02293	0.933	2361	17	2346	50	2329	102	1.6
QM10D-1C	12	220507	38	0.13693	0.00320	7.72627	0.60049	0.40924	0.03033	0.954	2189	20	2200	68	2211	137	-1.2
QM10D-1D	12	412606	73	0.15231	0.00306	9.96587	0.73845	0.47455	0.03385	0.963	2372	17	2432	66	2503	146	-6.7
QM10D-1E	12	315211	35	0.15007	0.00307	9.03421	0.44317	0.43661	0.01947	0.909	2347	17	2341	44	2335	87	0.6
QM10D-1F	12	685107	50	0.15103	0.00311	8.73645	0.57655	0.41955	0.02631	0.950	2358	18	2311	58	2258	118	5.0
QM10D-2A	12	305859	36	0.15059	0.00306	9.84030	0.61033	0.47393	0.02777	0.945	2353	17	2420	56	2501	120	-7.6
QM10D-2B	12	268210	42	0.15209	0.00314	10.25997	0.83859	0.48927	0.03869	0.968	2370	18	2459	73	2568	165	-10.1
QM10D-2C	12	399652	88	0.15239	0.00309	10.32942	0.69211	0.49160	0.03139	0.953	2373	17	2465	60	2578	134	-10.5
QM10D-4A	12	581648	60	0.15257	0.00305	9.86201	1.01615	0.46882	0.04739	0.981	2375	17	2422	91	2478	205	-5.3
QM10D-4B	12	363115	61	0.14958	0.00303	9.29311	0.63766	0.45060	0.02954	0.955	2341	17	2367	61	2398	130	-2.9
QM10D-4C	12	614483	49	0.15267	0.00311	10.09193	0.69391	0.47943	0.03149	0.955	2376	17	2443	62	2525	136	-7.6
QM10D-4D	12	383159	45	0.14964	0.00301	9.30694	0.56750	0.45107	0.02596	0.944	2342	17	2369	54	2400	114	-3.0
QM10D-5A	12	598521	107	0.15180	0.00314	9.04756	0.51402	0.43228	0.02288	0.931	2366	18	2343	51	2316	102	2.5

In-situ LA-MC-ICP-MS U-Pb dating of zircon grains from rocks collected from the Queen Maud block

Analysis	Spot Size µm	<sup>206</sup> Pb (cps)	<sup>204</sup> Pb (cps)	<sup>207</sup> Pb/ <sup>206</sup> Pb	±2σ	<sup>207</sup> Pb/ <sup>235</sup> U	±2σ	<sup>206</sup> Pb/ <sup>238</sup> U	±2σ	ρ	Model Ages (Ma)						% Disc.
											<sup>207</sup> Pb/ <sup>206</sup> Pb	±2σ	<sup>207</sup> Pb/ <sup>235</sup> U	±2σ	<sup>206</sup> Pb/ <sup>238</sup> U	±2σ	
QM2C-1A	30	934034	87	0.24449	0.00355	20.48097	1.69590	0.60755	0.04953	0.985	3149	12	3114	77	3060	196	3.6
QM2C-1B	30	1141791	101	0.23571	0.00314	19.35160	1.35512	0.59544	0.04093	0.982	3091	11	3060	65	3011	163	3.2
QM2C-2A	30	1231272	144	0.25016	0.00291	20.06116	1.43700	0.58161	0.04111	0.987	3186	9	3094	67	2955	165	9.0
QM2C-3A	30	741136	57	0.24980	0.00284	20.34261	1.47046	0.59062	0.04216	0.988	3184	9	3108	68	2992	169	7.5
QM2C-3B	30	1980414	161	0.24263	0.00313	16.85159	1.34299	0.50372	0.03961	0.987	3137	10	2926	74	2630	168	19.7
QM2C-6A	30	837615	380	0.25795	0.00308	25.72379	2.10847	0.72327	0.05865	0.989	3234	9	3336	77	3508	216	-11.0
QM2C-7A	30	746192	269	0.22742	0.00276	12.99988	0.87953	0.41459	0.02759	0.984	3034	10	2680	62	2236	125	31.0
QM2C-7C	30	1886983	84	0.23019	0.00306	17.07845	1.10346	0.53809	0.03402	0.979	3053	11	2939	60	2775	141	11.2
QM2C-10A	30	1439423	41	0.25408	0.00284	20.94471	1.05472	0.59788	0.02935	0.975	3210	9	3136	48	3021	117	7.4
QM2C-11A	30	680707	38	0.24878	0.00270	18.33066	0.89604	0.53439	0.02547	0.975	3177	9	3007	46	2760	106	16.1
QM2C-11D	30	781742	25	0.25134	0.00274	16.95425	1.19789	0.48924	0.03415	0.988	3193	9	2932	66	2567	146	23.7
QM2C-11E	30	1490891	23	0.15193	0.00165	7.45372	0.41387	0.35583	0.01938	0.981	2368	9	2167	49	1962	91	19.8
QM2C-11F	30	870972	63	0.15159	0.00168	8.17432	0.46551	0.39108	0.02185	0.981	2364	9	2251	50	2128	100	11.7
QM2C-11B	30	1671188	34	0.15163	0.00164	7.62668	0.49669	0.36479	0.02343	0.986	2364	9	2188	57	2005	110	17.7
QM2C-11C	30	1786236	34	0.15157	0.00165	7.76821	0.40565	0.37170	0.01898	0.978	2364	9	2205	46	2037	89	16.1
QM2D-1A	30	608717	35	0.25102	0.00297	19.09309	1.19507	0.55165	0.03391	0.982	3191	9	3047	59	2832	139	13.9
QM2D-2A	30	633397	8	0.25591	0.00255	22.14500	1.15236	0.62760	0.03206	0.982	3222	8	3190	49	3140	126	3.2
QM2D-2B	30	910904	14	0.14668	0.00164	8.65902	0.53685	0.42816	0.02611	0.984	2308	10	2303	55	2297	117	0.5
QM2D-3A	30	705272	48	0.25088	0.00251	20.21706	1.34614	0.58446	0.03847	0.989	3190	8	3102	62	2967	155	8.7
QM2D-3B	30	708783	157	0.23716	0.00267	19.76713	1.15261	0.60451	0.03458	0.981	3101	9	3080	55	3048	137	2.1
QM2D-7A	30	767646	17	0.14789	0.00149	8.83747	0.48289	0.43341	0.02328	0.983	2322	9	2321	49	2321	104	0.0
QM2D-7B	30	272676	4	0.14739	0.00148	8.21497	0.49334	0.40425	0.02393	0.986	2316	9	2255	53	2189	109	6.5
QM2D-9A	30	458356	16	0.25602	0.00258	22.66131	1.68445	0.64197	0.04728	0.991	3222	8	3213	70	3197	183	1.0
QM2D-9B	30	1024236	24	0.15709	0.00164	9.69865	0.77303	0.44779	0.03538	0.991	2425	9	2407	71	2385	156	1.9
QM2D-10A	30	914456	7	0.25340	0.00260	21.12660	1.08024	0.60467	0.03029	0.980	3206	8	3144	48	3049	121	6.2
QM2D-11A	30	539767	75	0.24310	0.00248	20.37793	1.17257	0.60795	0.03443	0.984	3140	8	3109	54	3062	137	3.1
QM4B 1A	30	104011	51	0.18566	0.00209	13.46020	0.75615	0.52582	0.02894	0.980	2704	9	2712	52	2724	121	-0.9
QM4B 1B	30	85947	57	0.18442	0.00211	13.40131	0.78640	0.52702	0.03033	0.981	2693	9	2708	54	2729	127	-1.6
QM4B 1C	30	106179	56	0.17633	0.00326	11.89416	0.61360	0.48923	0.02356	0.934	2619	15	2596	47	2567	101	2.4
QM4B 2A	30	58383	54	0.18455	0.00220	11.90307	0.66074	0.46779	0.02536	0.977	2694	10	2597	51	2474	110	9.8
QM4B 2B	30	125205	56	0.14916	0.00169	8.79561	0.66885	0.42766	0.03216	0.989	2336	10	2317	67	2295	144	2.1
QM4B 3A	30	511322	130	0.15772	0.00196	10.03864	0.58665	0.46163	0.02636	0.977	2431	11	2438	53	2447	115	-0.8
QM4B 4A	30	51384	56	0.18863	0.00243	15.48036	0.84188	0.59519	0.03145	0.972	2730	11	2845	51	3010	126	-12.9
QM4B 5A	30	44716	55	0.17003	0.00217	11.03521	0.56652	0.47072	0.02341	0.969	2558	11	2526	47	2487	102	3.4
QM4B 5B	30	67346	57	0.17951	0.00223	12.41638	0.64276	0.50165	0.02521	0.971	2648	10	2636	48	2621	107	1.3
QM4B 6A	30	1152728	657	0.24046	0.00289	17.74108	2.83982	0.53510	0.08541	0.997	3123	10	2976	143	2763	349	14.1
QM5B-1A	30	82196	19	0.17487	0.00345	11.22873	0.53171	0.46570	0.02005	0.909	2605	33	2542	43	2465	88	6.5
QM5B-1B	30	1224446	41	0.15863	0.00296	9.48179	0.77942	0.43351	0.03470	0.974	2441	32	2386	73	2322	154	5.8
QM5B-2A	30	51954	15	0.18238	0.00352	12.71380	0.63250	0.50558	0.02318	0.922	2675	32	2659	46	2638	98	1.7
QM5B-2B	30	87181	15	0.18407	0.00350	12.93167	0.70354	0.50953	0.02597	0.937	2690	31	2675	50	2655	110	1.6
QM5B-3A	30	49293	13	0.16153	0.00322	9.78646	0.56801	0.43940	0.02395	0.939	2472	34	2415	52	2348	106	6.0
QM5B-3B	30	41566	10	0.17626	0.00344	11.41564	0.74894	0.46972	0.02942	0.955	2618	32	2558	59	2482	128	6.2
QM5B-4A	30	77419	9	0.18372	0.00343	12.97842	0.63373	0.51234	0.02312	0.924	2687	31	2678	45	2667	98	0.9
QM5B-4B	30	36553	9	0.18257	0.00365	12.84125	0.68655	0.51012	0.02530	0.928	2676	33	2668	49	2657	107	0.9
QM5B-5A	30	301350	13	0.18823	0.00347	13.30624	0.91257	0.51271	0.03387	0.963	2727	30	2702	63	2668	143	2.6

In-situ Zircons (Continued)

Analysis	Spot Size µm	<sup>206</sup> Pb (cps)	<sup>204</sup> Pb (cps)	<sup>207</sup> Pb/ <sup>206</sup> Pb	±2σ	<sup>207</sup> Pb/ <sup>235</sup> U	±2σ	<sup>206</sup> Pb/ <sup>238</sup> U	±2σ	ρ	Model Ages (Ma)						% Disc.
											<sup>207</sup> Pb/ <sup>206</sup> Pb	±2σ	<sup>207</sup> Pb/ <sup>235</sup> U	±2σ	<sup>206</sup> Pb/ <sup>238</sup> U	±2σ	
QM5B-5B	30	71077	13	0.18494	0.00350	12.71090	0.59601	0.49848	0.02138	0.915	2698	31	2658	43	2607	91	4.1
QM5B-6A	30	54596	5	0.18178	0.00347	13.07415	0.71695	0.52164	0.02681	0.937	2669	32	2685	50	2706	113	-1.7
QM5B-7A	30	63244	3	0.18526	0.00355	13.70048	1.01612	0.53635	0.03843	0.966	2701	31	2729	68	2768	159	-3.1
QM5B-7B	30	1004953	18	0.18789	0.00345	13.87788	0.84989	0.53569	0.03129	0.954	2724	30	2741	56	2765	130	-1.9
QM5B-8A	30	73216	15	0.18377	0.00352	11.57301	0.57793	0.45675	0.02106	0.923	2687	32	2570	46	2425	93	11.7
QM5B-8B	30	32171	16	0.17618	0.00407	10.84575	0.74397	0.44647	0.02884	0.942	2617	38	2510	62	2380	127	10.8
QM5B-9A	30	46615	11	0.18549	0.00369	12.52572	0.63112	0.48977	0.02267	0.919	2703	33	2645	46	2570	97	6.0
QM5B-9B	30	56897	4	0.18705	0.00354	13.50034	1.01073	0.52345	0.03792	0.968	2716	31	2715	68	2714	158	0.1
QM5B-10A	30	69373	10	0.18659	0.00351	12.82966	0.65462	0.49868	0.02365	0.930	2712	31	2667	47	2608	101	4.7
QM6B-1A	30	2111590	140	0.12265	0.00233	5.84653	0.32944	0.34573	0.01834	0.941	1995	34	1953	48	1914	87	4.7
QM6B-1B	30	1762112	104	0.12112	0.00225	5.49217	0.36610	0.32886	0.02105	0.960	1973	33	1899	56	1833	101	8.1
QM6B-3A	30	1002274	58	0.12362	0.00104	5.67475	0.46719	0.33295	0.02727	0.995	2009	15	1928	69	1853	131	9.0
QM6B-5A	30	24933	33	0.12922	0.00279	6.32575	0.48889	0.35505	0.02635	0.960	2087	38	2022	66	1959	124	7.1
QM6B-6A	30	1277821	392	0.11652	0.00241	4.85507	0.30818	0.30219	0.01814	0.945	1904	37	1794	52	1702	89	12.0
QM6B-7A	30	6825	24	0.15009	0.00459	7.89535	0.51739	0.38153	0.02211	0.884	2347	52	2219	57	2083	102	13.1
QM6B-7B	30	476068	215	0.13089	0.00251	6.39303	0.46223	0.35424	0.02470	0.964	2110	34	2031	62	1955	117	8.5
QM6B-7C	30	415676	114	0.12761	0.00242	6.41738	0.30654	0.36474	0.01599	0.918	2065	33	2035	41	2005	75	3.4
QM6B-8B	30	1192918	73	0.12555	0.00119	5.92482	0.35617	0.34225	0.02032	0.988	2037	17	1965	51	1898	97	7.9
QM6B-10A	30	13546	14	0.12035	0.00172	6.21303	0.28942	0.37442	0.01660	0.952	1961	26	2006	40	2050	77	-5.3
QM6B-10B	30	342830	68	0.12396	0.00104	6.39387	0.44249	0.37409	0.02570	0.993	2014	15	2031	59	2049	119	-2.0
QM6B-11A	30	9300	14	0.12312	0.00230	7.02115	0.43633	0.41361	0.02451	0.954	2002	33	2114	54	2231	111	-13.6
QM6B-11B	30	244349	34	0.12385	0.00112	6.40831	0.23279	0.37528	0.01320	0.968	2012	16	2033	31	2054	62	-2.4
QM7C-1A	30	2304230	130	0.23141	0.00267	16.34984	1.37152	0.51243	0.04258	0.991	3062	18	2897	77	2667	179	15.7
QM7C-3A	30	1450784	28	0.23724	0.00271	19.86310	1.10201	0.60724	0.03297	0.979	3102	18	3085	52	3059	131	1.7
QM7C-4A	30	1286565	32	0.22765	0.00260	16.41535	1.24119	0.52298	0.03909	0.989	3036	18	2901	70	2712	163	13.0
QM7C-6A	30	2490320	14996	0.27685	0.01376	17.68535	1.83263	0.46330	0.04213	0.878	3345	78	2973	95	2454	183	31.9
QM7C-6B	30	1254271	556	0.16007	0.00215	8.61032	0.47756	0.39013	0.02100	0.970	2456	23	2298	49	2123	97	15.9
QM7C-6C	30	1641965	195	0.21966	0.00265	12.98496	0.92395	0.42874	0.03006	0.985	2978	19	2679	65	2300	134	27.0
QM7C-6D	30	1880258	30	0.22366	0.00297	15.45860	0.76587	0.50128	0.02393	0.963	3007	21	2844	46	2619	102	15.7
QM7C-7A	30	1891062	1362	0.22419	0.00325	13.28725	0.73059	0.42985	0.02280	0.965	3011	23	2700	51	2305	102	27.8
QM7C-7B	30	1472783	678	0.23810	0.00314	18.48379	1.18648	0.56302	0.03537	0.979	3107	21	3015	60	2879	144	9.1
QM7C-8A	30	1799895	53	0.22869	0.00273	16.69003	0.95500	0.52931	0.02962	0.978	3043	19	2917	53	2739	124	12.3
QM8B-2A	30	106032	23	0.14718	0.00175	6.75701	0.43431	0.33297	0.02103	0.983	2313	10	2080	55	1853	101	22.9
QM8B-2B	30	107900	24	0.14828	0.00177	6.94063	0.38032	0.33949	0.01816	0.976	2326	10	2104	48	1884	87	21.9
QM8B-5A	30	87114	32	0.14713	0.00176	7.17401	0.42339	0.35365	0.02044	0.979	2313	10	2133	51	1952	97	18.1
QM8B-7A	30	129432	86	0.15291	0.00219	8.05030	0.46810	0.38183	0.02152	0.969	2379	12	2237	51	2085	100	14.4
QM8B-7B	30	127325	45	0.14938	0.00197	7.50721	0.43248	0.36449	0.02044	0.974	2339	11	2174	50	2003	96	16.7
QM8B-9A	30	2098693	72	0.22222	0.00343	14.32153	1.04487	0.46741	0.03333	0.977	2997	12	2771	67	2472	145	21.0
QM8B-10A	30	212621	53	0.14793	0.00175	6.68581	0.37502	0.32778	0.01797	0.977	2322	10	2071	48	1828	87	24.4
QM8B-10B	30	349427	89	0.14831	0.00175	6.68200	0.33777	0.32677	0.01606	0.972	2327	10	2070	44	1823	78	24.8
QM8B-13A	30	660798	327	0.15300	0.00183	8.41932	0.52665	0.39910	0.02450	0.982	2380	10	2277	55	2165	112	10.6
QM8B-15A	30	166031	34	0.14735	0.00174	7.10273	0.44887	0.34960	0.02170	0.982	2315	10	2124	55	1933	103	19.1
QM8B-16A	30	421652	88	0.14777	0.00175	7.57996	0.46743	0.37202	0.02251	0.981	2320	10	2182	54	2039	105	14.1
QM8B-16B	30	1194335	132	0.14870	0.00173	7.99908	0.48555	0.39014	0.02324	0.981	2331	10	2231	53	2124	107	10.4
QM8B-16C	30	450149	42	0.14685	0.00173	7.52511	0.46734	0.37165	0.02266	0.982	2310	10	2176	54	2037	106	13.7

In-situ Zircons (Continued)

Analysis	Spot Size µm	<sup>206</sup> Pb (cps)	<sup>204</sup> Pb (cps)	<sup>207</sup> Pb/ <sup>206</sup> Pb	±2σ	<sup>207</sup> Pb/ <sup>235</sup> U	±2σ	<sup>206</sup> Pb/ <sup>238</sup> U	±2σ	ρ	Model Ages (Ma)						% Disc.
											<sup>207</sup> Pb/ <sup>206</sup> Pb	±2σ	<sup>207</sup> Pb/ <sup>235</sup> U	±2σ	<sup>206</sup> Pb/ <sup>238</sup> U	±2σ	
QM8B-17A	30	214892	33	0.14700	0.00171	7.94658	0.56015	0.39208	0.02726	0.986	2311	10	2225	62	2132	125	9.1
QM8B-1A1	30	239736	18	0.14620	0.00176	8.83232	0.51509	0.43814	0.02500	0.979	2302	21	2321	52	2342	111	-2.1
QM8B-1B1	30	123086	41	0.15065	0.00238	9.37164	0.46887	0.45118	0.02141	0.949	2353	27	2375	45	2400	94	-2.4
QM8B-2A1	30	145607	8	0.14749	0.00169	8.79946	0.49300	0.43270	0.02373	0.979	2317	20	2317	50	2318	106	0.0
QM8B-3A1	30	465576	23	0.14848	0.00166	9.11182	0.46760	0.44506	0.02229	0.976	2329	19	2349	46	2373	99	-2.3
QM8B-4A1	30	58313	12	0.14736	0.00184	8.70094	0.38537	0.42824	0.01820	0.959	2316	21	2307	40	2298	82	0.9
QM8B-4B1	30	49740	3	0.14574	0.00206	8.06649	0.39360	0.40142	0.01875	0.957	2297	24	2238	43	2176	86	6.2
QM8B-4C1	30	45037	5	0.14566	0.00207	8.65819	0.37095	0.43111	0.01742	0.943	2296	24	2303	38	2311	78	-0.8
QM8B-5A1	30	211950	30	0.14534	0.00301	8.36960	0.43381	0.41765	0.01985	0.917	2292	36	2272	46	2250	90	2.2
QM8B-6A1	30	72027	47	0.14598	0.00195	8.43107	0.55236	0.41889	0.02686	0.979	2299	23	2279	58	2255	121	2.3
QM8B-6B1	30	175729	18	0.14885	0.00177	8.23563	0.53584	0.40129	0.02567	0.983	2333	20	2257	57	2175	117	8.0
QM8B-6C1	30	179357	17	0.14896	0.00171	8.94270	0.49232	0.43542	0.02344	0.978	2334	20	2332	49	2330	104	0.2
QM8B-7A1	30	559377	23	0.14579	0.00169	9.74749	0.50465	0.48492	0.02447	0.975	2297	20	2411	47	2549	105	-13.3
QM8B-7B1	30	787014	12	0.14815	0.00166	10.05193	0.54649	0.49208	0.02618	0.978	2325	19	2440	49	2580	112	-13.3
QM8B-7C1	30	489335	42	0.14890	0.00167	9.52035	0.45637	0.46374	0.02161	0.972	2333	19	2390	43	2456	94	-6.3
QM8B-8A1	30	65826	12	0.14623	0.00174	8.50080	0.43261	0.42161	0.02086	0.972	2302	20	2286	45	2268	94	1.8
QM8B-8B1	30	68543	10	0.14748	0.00178	8.37465	0.52270	0.41184	0.02522	0.981	2317	21	2272	55	2223	114	4.8
QM8B-9A1	30	415246	37	0.14882	0.00170	8.62989	0.69363	0.42057	0.03346	0.990	2332	20	2300	71	2263	150	3.5
QM8B-9B1	30	155320	17	0.14813	0.00174	8.62252	0.43724	0.42216	0.02083	0.973	2324	20	2299	45	2270	94	2.8
QM8B-10A1	30	768311	69	0.14538	0.00172	8.09947	0.42904	0.40407	0.02086	0.975	2292	20	2242	47	2188	95	5.4
QM9C-11A	30	1222175	85	0.25237	0.00312	23.79891	1.26145	0.68394	0.03525	0.972	3200	10	3260	50	3359	134	-6.4
QM9C-14A	30	1856098	59	0.25251	0.00394	21.61304	1.02320	0.62077	0.02774	0.944	3201	12	3166	45	3113	109	3.4
QM10A-1A	30	765367	36	0.21729	0.00311	15.06832	0.97227	0.50295	0.03164	0.975	2961	23	2820	60	2626	134	13.7
QM10A-1B	30	181232	17	0.19039	0.00284	12.14685	0.66071	0.46272	0.02420	0.962	2746	25	2616	50	2452	106	12.9
QM10A-1E	30	149965	12	0.24717	0.00353	19.76010	1.03245	0.57982	0.02914	0.962	3167	23	3080	49	2948	118	8.6
QM10A-1F	30	314469	13	0.25016	0.00340	19.73306	0.83958	0.57210	0.02307	0.948	3186	22	3078	40	2916	94	10.5
QM10A-2A	30	223643	6	0.18354	0.00248	11.45944	0.58482	0.45282	0.02229	0.964	2685	22	2561	47	2408	98	12.4
QM10A-2B	30	602076	13	0.24341	0.00336	19.63661	1.03922	0.58508	0.02989	0.965	3142	22	3074	50	2969	120	6.9
QM10A-2C	30	281934	7	0.19778	0.00287	13.05502	0.63677	0.47873	0.02229	0.955	2808	24	2684	45	2522	96	12.3
QM10A-2D	30	563732	14	0.24638	0.00340	20.37709	1.26504	0.59984	0.03630	0.975	3162	22	3109	58	3029	145	5.2
QM10A-2E	30	332788	6	0.24559	0.00331	18.59561	1.78406	0.54916	0.05217	0.990	3157	21	3021	88	2822	213	13.1
QM10A-3A	30	383953	12	0.24417	0.00329	20.56075	1.06161	0.61071	0.03044	0.965	3147	21	3118	49	3073	121	3.0
QM10A-3B	30	404071	10	0.24488	0.00333	21.10999	1.40107	0.62521	0.04062	0.979	3152	22	3144	62	3131	159	0.9
QM10B-1A	30	2337406	108	0.23649	0.00171	19.66681	1.30072	0.60315	0.03965	0.994	3096	11	3075	62	3043	158	2.2
QM10B-2A	30	1792196	333	0.24779	0.00131	18.16737	1.74924	0.53175	0.05112	0.998	3171	8	2999	89	2749	212	16.3
QM10B-2B	30	802889	163	0.23917	0.00145	19.62665	1.40353	0.59516	0.04241	0.996	3114	10	3073	67	3010	169	4.2
QM10B-2C	30	1732012	234	0.23690	0.00209	16.41232	1.14287	0.50246	0.03471	0.992	3099	14	2901	65	2624	147	18.6
QM10B-3A	30	1902957	374	0.22593	0.00169	15.89969	1.15600	0.51040	0.03691	0.995	3023	12	2871	67	2658	156	14.7
QM13A-1A	30	127887	26	0.15676	0.00080	9.21748	0.60013	0.42646	0.02768	0.997	2421	9	2360	58	2290	124	6.4
QM13A-1B	30	261330	19	0.15915	0.00079	10.13630	0.73153	0.46192	0.03326	0.998	2447	8	2447	65	2448	145	-0.1
QM13A-1C	30	188006	11	0.16038	0.00075	9.51032	0.60370	0.43007	0.02723	0.997	2460	8	2389	57	2306	122	7.4
QM13A-1D	30	185688	8	0.16018	0.00078	9.30997	0.57119	0.42154	0.02578	0.997	2458	8	2369	55	2267	116	9.2
QM13A-2A	30	139057	20	0.15572	0.00126	8.98288	0.56864	0.41837	0.02627	0.992	2410	14	2336	56	2253	118	7.7
QM13D-1A	30	1629149	36	0.15601	0.00187	8.60582	0.36121	0.40007	0.01609	0.958	2413	10	2297	37	2169	74	11.9
QM13D-2A	30	549926	30	0.15604	0.00212	8.95034	0.40353	0.41602	0.01789	0.954	2413	12	2333	40	2242	81	8.4

In-situ Zircons (Continued)

Analysis	Spot Size µm	<sup>206</sup> Pb (cps)	<sup>204</sup> Pb (cps)	<sup>207</sup> Pb/ <sup>206</sup> Pb	±2σ	<sup>207</sup> Pb/ <sup>235</sup> U	±2σ	<sup>206</sup> Pb/ <sup>238</sup> U	±2σ	ρ	Model Ages (Ma)						% Disc.
											<sup>207</sup> Pb/ <sup>206</sup> Pb	±2σ	<sup>207</sup> Pb/ <sup>235</sup> U	±2σ	<sup>206</sup> Pb/ <sup>238</sup> U	±2σ	
QM13D-3A	30	150267	19	0.14108	0.00174	6.84966	0.42286	0.35213	0.02130	0.980	2241	11	2092	53	1945	101	15.3
QM13D-3B	30	634378	18	0.15744	0.00181	9.47253	0.60418	0.43636	0.02737	0.984	2428	10	2385	57	2334	122	4.6
QM13D-3C	30	358226	309	0.15949	0.00256	9.77697	0.53905	0.44460	0.02345	0.957	2450	14	2414	50	2371	104	3.9
QM13D-6A	30	178512	28	0.16127	0.00195	9.73669	0.70259	0.43789	0.03115	0.986	2469	10	2410	64	2341	138	6.2
QM13D-9A	30	27871	15	0.14786	0.00199	8.08924	0.32354	0.39680	0.01495	0.942	2321	12	2241	36	2154	69	8.5
QM13D-9B	30	26429	8	0.15149	0.00220	8.30239	0.37241	0.39749	0.01687	0.946	2363	12	2265	40	2157	77	10.2
QM13E-2A	30	332201	35	0.15337	0.00208	7.15376	0.54453	0.33830	0.02534	0.984	2384	12	2131	66	1878	121	24.4
QM13E-4A	30	192157	27	0.15746	0.00204	8.92239	0.53747	0.41098	0.02418	0.977	2429	11	2330	54	2219	110	10.2
QM13E-4B	30	189410	15	0.16069	0.00201	8.31351	0.48728	0.37523	0.02149	0.977	2463	11	2266	52	2054	100	19.4
QM13E-4C	30	146053	19	0.15923	0.00196	7.82680	0.40522	0.35650	0.01793	0.971	2447	10	2211	46	1966	85	22.8
QM13E-5A	30	401581	42	0.15460	0.00192	7.50712	0.42178	0.35218	0.01930	0.975	2397	11	2174	49	1945	91	21.8
QM13E-5B	30	307076	23	0.15364	0.00195	7.47291	0.41367	0.35277	0.01901	0.973	2387	11	2170	48	1948	90	21.3
QM13E-6A	30	504577	35	0.16006	0.00197	8.65677	0.44832	0.39225	0.01973	0.971	2456	10	2303	46	2133	91	15.4
QM13E-6B	30	299067	35	0.15868	0.00194	8.58450	0.53938	0.39236	0.02418	0.981	2442	10	2295	56	2134	111	14.8
QM13E-6C	30	699041	67	0.15945	0.00207	8.98294	0.55009	0.40859	0.02445	0.977	2450	11	2336	54	2208	111	11.6
QM13E-7A	30	65564	10	0.15387	0.00203	7.08969	0.46267	0.33417	0.02136	0.979	2389	11	2123	56	1859	102	25.5
QM13E-7B	30	232535	29	0.15617	0.00193	7.55967	0.38444	0.35108	0.01732	0.970	2415	10	2180	45	1940	82	22.7
QM13E-7C	30	83074	22	0.15731	0.00211	7.44671	0.39930	0.34333	0.01783	0.968	2427	11	2167	47	1903	85	24.9
QM13E-8A	30	571740	24	0.15899	0.00194	9.78874	0.58433	0.44652	0.02609	0.979	2445	10	2415	54	2380	115	3.2
QM13E-8B	30	216899	26	0.14524	0.00184	6.85021	0.39753	0.34208	0.01937	0.976	2291	11	2092	50	1897	92	19.8
QM13E-10A	30	406643	32	0.15946	0.00195	10.47965	0.55353	0.47665	0.02449	0.973	2450	10	2478	48	2513	106	-3.1
QM13H-1A	30	132247	58	0.15863	0.00083	9.64069	0.54909	0.44079	0.02500	0.996	2441	9	2401	51	2354	111	4.2
QM13H-2A	30	98334	70	0.16381	0.00099	10.47131	0.67917	0.46361	0.02994	0.996	2495	10	2477	58	2455	131	1.9
QM13H-3A	30	156329	80	0.16148	0.00105	9.96049	0.67171	0.44737	0.03003	0.995	2471	11	2431	60	2384	132	4.2
QM13H-3B	30	139880	63	0.16040	0.00082	9.84113	0.70874	0.44497	0.03197	0.997	2460	9	2420	64	2373	141	4.2
QM13H-4A	30	464998	71	0.15029	0.00065	9.20947	0.65613	0.44443	0.03160	0.998	2349	7	2359	63	2370	140	-1.1
QM13H-4B	30	131800	71	0.16164	0.00078	9.83432	0.78139	0.44127	0.03500	0.998	2473	8	2419	71	2356	155	5.6
QM13H-4C	30	511984	103	0.15106	0.00062	8.76492	0.69707	0.42083	0.03342	0.999	2358	7	2314	70	2264	150	4.7
QM13H-4D	30	86808	72	0.16086	0.00097	8.96887	0.57612	0.40439	0.02586	0.996	2465	10	2335	57	2189	118	13.2
QM13H-5A	30	148819	69	0.16160	0.00087	9.30489	0.63654	0.41761	0.02848	0.997	2472	9	2369	61	2250	128	10.7
QM13H-5B	30	159864	72	0.16077	0.00081	9.87478	0.71813	0.44546	0.03232	0.998	2464	9	2423	65	2375	143	4.3
QM13H-6A	30	118130	50	0.15991	0.00095	9.73991	0.55569	0.44174	0.02507	0.995	2455	10	2410	51	2358	111	4.7
QM13H-7A	30	487207	92	0.15383	0.00076	9.63234	0.63675	0.45413	0.02994	0.997	2389	8	2400	59	2414	131	-1.2
QM13H-7B	30	140147	60	0.16098	0.00080	10.87998	0.68418	0.49018	0.03073	0.997	2466	8	2513	57	2571	132	-5.2
QM14A-1A	30	552540	25	0.15935	0.00105	10.82935	0.48761	0.49289	0.02195	0.989	2449	11	2509	41	2583	94	-6.7
QM14A-1B	30	155903	15	0.16075	0.00123	10.92289	0.77564	0.49282	0.03479	0.994	2464	13	2517	64	2583	149	-5.9
QM14A-2A	30	295536	1	0.15422	0.00099	9.38896	0.44427	0.44155	0.02070	0.991	2393	11	2377	43	2358	92	1.8
QM14A-2B	30	1035620	41	0.16548	0.00101	10.44375	0.52883	0.45773	0.02301	0.993	2512	10	2475	46	2430	101	4.0
QM14A-3A	30	189060	73	0.16660	0.00142	9.33595	0.62365	0.40642	0.02693	0.992	2524	14	2372	59	2199	122	15.2
QM14A-4A	30	190847	87	0.16858	0.00127	9.75682	0.62288	0.41977	0.02661	0.993	2544	13	2412	57	2259	120	13.2
QM14A-4B	30	221627	42	0.16914	0.00109	10.25016	0.53913	0.43952	0.02294	0.992	2549	11	2458	48	2348	102	9.4
QM14A-5A	30	910512	763	0.14892	0.00234	5.85916	0.36233	0.28536	0.01707	0.967	2334	27	1955	52	1618	85	34.6
QM15A-1A	30	369207	32	0.16654	0.00130	10.08432	0.89858	0.43916	0.03898	0.996	2523	13	2443	79	2347	172	8.3
QM15A-2A	30	423531	123	0.15673	0.00150	8.70433	0.78523	0.40280	0.03613	0.994	2421	16	2308	79	2182	164	11.6
QM15A-2B	30	268765	66	0.14811	0.00140	7.89548	0.52903	0.38664	0.02565	0.990	2324	16	2219	59	2107	118	10.9

In-situ Zircons (Continued)

Analysis	Spot Size μm	<sup>206</sup> Pb (cps)	<sup>204</sup> Pb (cps)	<sup>207</sup> Pb/ <sup>206</sup> Pb	±2σ	<sup>207</sup> Pb/ <sup>235</sup> U	±2σ	<sup>206</sup> Pb/ <sup>238</sup> U	±2σ	ρ	Model Ages (Ma)						% Disc.
											<sup>207</sup> Pb/ <sup>206</sup> Pb	±2σ	<sup>207</sup> Pb/ <sup>235</sup> U	±2σ	<sup>206</sup> Pb/ <sup>238</sup> U	±2σ	
QM15A-4A	30	1098146	87	0.16452	0.00152	10.44318	0.60613	0.46037	0.02638	0.987	2503	16	2475	52	2441	115	2.9
QM15A-4B	30	831279	30	0.16610	0.00134	11.63514	0.74358	0.50803	0.03221	0.992	2519	14	2576	58	2648	136	-6.3
QM15A-5A	30	874242	2357	0.16758	0.00236	10.15551	0.54848	0.43953	0.02292	0.965	2534	24	2449	49	2349	102	8.7
QM15A-6A	30	463444	37	0.16466	0.00135	10.47535	0.61590	0.46141	0.02686	0.990	2504	14	2478	53	2446	117	2.8
QM15A-7A	30	691146	76	0.16748	0.00131	10.24374	0.79675	0.44360	0.03433	0.995	2533	13	2457	70	2367	151	7.8
QM15A-8A	30	900800	82	0.16210	0.00130	9.83031	0.49307	0.43982	0.02178	0.987	2478	13	2419	45	2350	97	6.2
QM15A-8B	30	1146397	420	0.16660	0.00136	9.46764	0.74606	0.41216	0.03230	0.995	2524	14	2384	70	2225	146	14.0
QM15A-9A	30	1024169	91	0.16492	0.00133	9.89914	0.55030	0.43534	0.02394	0.989	2507	14	2425	50	2330	107	8.4
QM16A-1A	30	529157	41	0.15802	0.00129	8.91893	0.61679	0.40935	0.02811	0.993	2435	14	2330	61	2212	127	10.8
QM16A-1B	30	660112	44	0.15753	0.00150	9.33953	0.42495	0.43000	0.01913	0.978	2429	16	2372	41	2306	86	6.0
QM16A-2A	30	1103158	35	0.16462	0.00219	10.66296	0.49201	0.46978	0.02075	0.957	2504	22	2494	42	2483	90	1.0
QM16A-3A	30	104536	480	0.23558	0.00354	16.47266	0.84121	0.50714	0.02475	0.956	3090	24	2905	48	2644	105	17.5
QM16A-4A	30	188761	36	0.18336	0.00155	13.13988	0.76646	0.51974	0.03000	0.989	2683	14	2690	54	2698	126	-0.7
QM16A-4B	30	407154	26	0.18793	0.00145	14.27693	0.79291	0.55097	0.03030	0.990	2724	13	2768	51	2829	125	-4.8
QM16A-4C	30	228130	22	0.18772	0.00165	13.80084	0.69778	0.53321	0.02655	0.985	2722	14	2736	47	2755	111	-1.5
QM16A-5A	30	377790	31	0.17940	0.00151	12.41724	0.53756	0.50199	0.02132	0.981	2647	14	2636	40	2622	91	1.1
QM16A-5B	30	652313	13	0.17882	0.00142	11.62178	0.67261	0.47136	0.02702	0.991	2642	13	2574	53	2490	117	6.9
QM16A-6A	30	980308	35	0.18362	0.00234	11.29466	0.95978	0.44612	0.03748	0.989	2686	21	2548	76	2378	165	13.7
QM16A-6B	30	1601574	242	0.17870	0.00204	11.45119	0.76690	0.46476	0.03067	0.985	2641	19	2561	61	2461	134	8.2
QM16A-7A	30	716215	385	0.16176	0.00141	9.33187	0.68828	0.41841	0.03064	0.993	2474	15	2371	65	2253	138	10.6
QM16A-8A	30	1082782	40	0.17772	0.00162	11.94421	0.56873	0.48744	0.02278	0.981	2632	15	2600	44	2560	98	3.3
QM17B-1A	30	441448	37	0.15382	0.00046	9.17404	0.61822	0.43256	0.02912	0.999	2389	5	2356	60	2317	130	3.6
QM17B-1B	30	138253	31	0.15406	0.00048	9.05750	0.64258	0.42639	0.03022	0.999	2392	5	2344	63	2289	135	5.1
QM17B-2A	30	238867	26	0.15194	0.00059	9.38448	0.59898	0.44796	0.02854	0.998	2368	7	2376	57	2386	126	-0.9
QM17B-2B	30	273360	21	0.14786	0.00107	9.05078	0.64866	0.44396	0.03166	0.995	2321	12	2343	64	2368	140	-2.4
QM17B-3A	30	151292	42	0.15424	0.00066	9.65588	0.90815	0.45404	0.04266	0.999	2393	7	2403	83	2413	186	-1.0
QM17C-2B	20	724042	88	0.19257	0.00420	13.82069	0.69329	0.52052	0.02352	0.901	2764	36	2737	46	2701	99	2.8
QM17C-3A	20	444980	116	0.23634	0.00495	19.88511	1.46878	0.61022	0.04323	0.959	3095	33	3086	69	3071	171	1.0
QM17C-3B	20	674639	84	0.23268	0.00387	17.26171	0.70214	0.53806	0.01997	0.913	3071	27	2949	38	2775	83	11.8
QM17C-4A	20	563655	63	0.20355	0.00458	15.86884	1.14581	0.56541	0.03879	0.950	2855	37	2869	67	2889	158	-1.5
QM17C-4B	20	162136	39	0.14213	0.00295	7.66266	0.40184	0.39101	0.01883	0.918	2253	36	2192	46	2128	87	6.6
QM17C-5A	20	978308	133	0.22792	0.00390	21.57293	1.44268	0.68646	0.04438	0.967	3038	27	3165	63	3369	167	-14.0
QM17C-5B	20	1865987	290	0.23295	0.00395	20.89881	1.29743	0.65065	0.03886	0.962	3072	27	3134	58	3231	150	-6.6
QM17C-6A	20	1527693	364	0.23525	0.00396	20.71644	1.03848	0.63868	0.03015	0.942	3088	27	3125	47	3184	118	-3.9



Grain mount LA-MC-ICP-MS U-Pb dating of zircon grains from rocks collected from the Queen Maud block

Analysis	Spot Size µm	<sup>206</sup> Pb (cps)	<sup>204</sup> Pb (cps)	<sup>207</sup> Pb/ <sup>206</sup> Pb	±2σ	<sup>207</sup> Pb/ <sup>235</sup> U	±2σ	<sup>206</sup> Pb/ <sup>238</sup> U	±2σ	ρ	Model Ages (Ma)						% Disc.
											<sup>207</sup> Pb/ <sup>206</sup> Pb	±2σ	<sup>207</sup> Pb/ <sup>235</sup> U	±2σ	<sup>206</sup> Pb/ <sup>238</sup> U	±2σ	
QM1C-1	30	324226	153	0.11931	0.00101	5.73075	0.22495	0.34838	0.01335	0.97648	1946	15	1936	33	1927	64	1.1
QM1C-2	30	361084	373	0.12688	0.00381	6.38012	0.33133	0.36469	0.01545	0.81584	2055	52	2030	45	2004	73	2.9
QM1C-3	30	2124278	186	0.11956	0.00178	5.32725	0.22863	0.32315	0.01300	0.93759	1950	26	1873	36	1805	63	8.5
QM1C-4	30	233539	161	0.11853	0.00178	3.74218	0.28834	0.22899	0.01731	0.98082	1934	27	1580	60	1329	90	34.6
QM1C-5	30	406609	155	0.11850	0.00094	6.03885	0.25324	0.36962	0.01522	0.98181	1934	14	1981	36	2028	71	-5.7
QM1C-6	30	365034	156	0.11844	0.00090	5.70817	0.19429	0.34954	0.01160	0.97493	1933	13	1933	29	1932	55	0.0
QM1C-7	30	378153	207	0.11893	0.00131	5.58358	0.25277	0.34049	0.01495	0.96987	1940	20	1914	38	1889	71	3.0
QM1C-8	30	1316731	173	0.12096	0.00091	5.28965	0.21598	0.31717	0.01273	0.98283	1970	13	1867	34	1776	62	11.3
QM1C-9	30	216967	168	0.12538	0.00203	6.33048	0.34703	0.36619	0.01918	0.95524	2034	28	2023	47	2011	90	1.3
QM1C-10	30	1115715	251	0.12229	0.00147	5.69092	0.32912	0.33751	0.01909	0.97804	1990	21	1930	49	1875	91	6.7
QM1C-11	30	1481868	501	0.12469	0.00149	6.01581	0.30332	0.34992	0.01714	0.97165	2024	21	1978	43	1934	81	5.2
QM1C-12	30	1044000	190	0.12305	0.00122	5.87924	0.23592	0.34651	0.01347	0.96881	2001	18	1958	34	1918	64	4.8
QM1C-13	30	425511	145	0.11794	0.00091	5.62878	0.26238	0.34615	0.01591	0.98626	1925	14	1921	39	1916	76	0.5
QM1C-14	30	1028975	178	0.12997	0.00103	6.86443	0.30418	0.38305	0.01670	0.98381	2098	14	2094	39	2091	77	0.4
QM1C-15	30	1351922	497	0.12330	0.00237	5.82894	0.32542	0.34286	0.01797	0.93877	2005	34	1951	47	1900	86	6.0
QM1C-16	30	438586	268	0.11692	0.00089	5.64716	0.22815	0.35030	0.01390	0.98222	1910	14	1923	34	1936	66	-1.6
QM1C-17	30	725359	173	0.12513	0.00096	6.94356	0.30167	0.40246	0.01721	0.98441	2031	13	2104	38	2180	79	-8.7
QM1C-18	30	841666	1042	0.12421	0.00134	6.10402	0.26649	0.35642	0.01508	0.96911	2018	19	1991	37	1965	71	3.0
QM1C-19	30	1093506	244	0.12045	0.00095	5.28335	0.20421	0.31812	0.01204	0.97887	1963	14	1866	32	1781	59	10.6
QM1C-20	30	411623	218	0.11757	0.00088	5.60160	0.25835	0.34556	0.01573	0.98682	1920	13	1916	39	1913	75	0.4
QM1C-21	30	472078	207	0.12340	0.00140	6.00162	0.23104	0.35273	0.01297	0.95527	2006	20	1976	33	1948	62	3.4
QM1C-22	30	507971	191	0.11685	0.00091	5.74845	0.28989	0.35678	0.01777	0.98791	1909	14	1939	43	1967	84	-3.5
QM1C-23	30	375344	235	0.11905	0.00125	5.64495	0.16505	0.34391	0.00938	0.93310	1942	19	1923	25	1905	45	2.2
QM1C-24	30	330392	185	0.11895	0.00103	5.33011	0.22090	0.32500	0.01317	0.97810	1940	15	1874	35	1814	64	7.5
QM1C-25	30	292005	187	0.11981	0.00090	5.83769	0.25999	0.35340	0.01551	0.98555	1953	13	1952	38	1951	73	0.1
QM1C-26	30	465350	193	0.11732	0.00092	5.53179	0.23603	0.34197	0.01434	0.98286	1916	14	1906	36	1896	69	1.2
QM1C-27	30	536399	300	0.12880	0.00113	6.73350	0.29217	0.37915	0.01611	0.97948	2082	15	2077	38	2072	75	0.5
QM1C-28	30	379923	221	0.11797	0.00120	5.58892	0.17689	0.34360	0.01030	0.94692	1926	18	1914	27	1904	49	1.3
QM1C-29	30	281983	184	0.11940	0.00106	6.07373	0.37401	0.36893	0.02248	0.98948	1947	16	1986	52	2024	105	-4.6
QM1C-30	30	439111	182	0.11756	0.00093	5.65735	0.32507	0.34901	0.01986	0.99040	1920	14	1925	48	1930	94	-0.6
QM1C-31	30	592191	221	0.12483	0.00107	6.27854	0.30405	0.36480	0.01739	0.98417	2026	15	2015	42	2005	82	1.2
QM1C-32	30	410879	196	0.11895	0.00115	5.71221	0.27301	0.34829	0.01631	0.97951	1940	17	1933	40	1926	77	0.8
QM1C-33	30	503018	178	0.11742	0.00100	5.76111	0.29248	0.35586	0.01781	0.98588	1917	15	1941	43	1962	84	-2.7
QM1C-34	30	377108	178	0.11713	0.00089	5.56656	0.22752	0.34468	0.01384	0.98273	1913	14	1911	35	1909	66	0.2
QM1C-35	30	342475	201	0.11774	0.00094	5.38775	0.22291	0.33189	0.01347	0.98103	1922	14	1883	35	1848	65	4.5
QM1C-36	30	1098006	241	0.11873	0.00216	4.01420	0.45303	0.24521	0.02731	0.98693	1937	32	1637	88	1414	140	30.1
QM1C-37	30	1660742	1085	0.12075	0.00153	5.74799	0.23568	0.34523	0.01347	0.95128	1967	22	1939	35	1912	64	3.3
QM1C-38	30	643905	207	0.13048	0.00108	7.00283	0.23008	0.38926	0.01238	0.96772	2104	14	2112	29	2119	57	-0.8
QM1C-1A*	30	2423566	315	0.12562	0.00275	6.03815	0.31247	0.34860	0.01635	0.90630	2038	39	1981	44	1928	78	6.2
QM1C-2A*	30	2221824	402	0.12852	0.00263	6.38879	0.39750	0.36052	0.02119	0.94457	2078	36	2031	53	1985	100	5.2
QM1C-2B*	30	1481054	335	0.12613	0.00318	6.12980	0.48347	0.35249	0.02634	0.94739	2045	45	1994	67	1946	124	5.6
QM1H-1	30	853774	129	0.20653	0.00301	15.07968	1.49507	0.52955	0.05193	0.98916	2879	23	2820	90	2740	215	5.9
QM1H-2	30	856948	84	0.21459	0.00286	18.61917	1.50040	0.62929	0.05001	0.98627	2941	21	3022	75	3147	195	-8.9
QM1H-4	30	727406	4	0.21360	0.00314	18.43749	2.05401	0.62602	0.06913	0.99126	2933	24	3013	102	3134	268	-8.7
QM1H-5	30	84834	7	0.21151	0.00464	17.27565	1.56171	0.59239	0.05195	0.97008	2917	35	2950	83	2999	207	-3.5

\* Analysis acquired in-situ in petrographic thin-section. All others acquired in grain mount

Grain Mount Zircons (Continued)

Analysis	Spot Size μm	<sup>206</sup> Pb (cps)	<sup>204</sup> Pb (cps)	<sup>207</sup> Pb/ <sup>206</sup> Pb	±2σ	<sup>207</sup> Pb/ <sup>235</sup> U	±2σ	<sup>206</sup> Pb/ <sup>238</sup> U	±2σ	ρ	Model Ages (Ma)						% Disc.
											<sup>207</sup> Pb/ <sup>206</sup> Pb	±2σ	<sup>207</sup> Pb/ <sup>235</sup> U	±2σ	<sup>206</sup> Pb/ <sup>238</sup> U	±2σ	
QM1H-6	30	51331	3	0.18064	0.00749	13.31764	1.24337	0.53471	0.04474	0.89611	2659	67	2702	85	2761	185	-4.7
QM1H-7	30	877460	1	0.15570	0.00223	9.85559	0.95232	0.45910	0.04387	0.98896	2409	24	2421	85	2436	191	-1.3
QM1H-8	30	178615	3	0.18828	0.00345	14.18468	1.30384	0.54639	0.04921	0.97987	2727	30	2762	84	2810	202	-3.8
QM1H-9	30	256487	2	0.21274	0.00362	17.74524	1.64375	0.60496	0.05508	0.98298	2927	27	2976	85	3050	218	-5.3
QM1H-10	30	335658	1	0.22362	0.00371	19.47122	1.73419	0.63152	0.05526	0.98254	3007	26	3065	83	3156	215	-6.3
QM1H-11	30	234858	272	0.24577	0.00445	19.56854	1.88123	0.57746	0.05452	0.98208	3158	28	3070	89	2938	219	8.6
QM1H-12	30	228152	2	0.20411	0.00357	16.53250	1.29191	0.58746	0.04474	0.97460	2859	28	2908	72	2979	179	-5.2
QM1H-13	30	563982	0	0.21691	0.00325	17.68711	1.56570	0.59139	0.05159	0.98555	2958	24	2973	82	2995	206	-1.6
QM1H-14	30	367025	6	0.15167	0.00430	5.44473	0.74452	0.26036	0.03483	0.97824	2365	48	1892	111	1492	176	41.3
QM1H-15	30	68038	0	0.18824	0.00763	15.27173	1.24603	0.58839	0.04167	0.86796	2727	65	2832	75	2983	167	-11.7
QM1H-16	30	375944	22	0.20742	0.00391	19.02394	1.75574	0.66519	0.06009	0.97887	2886	30	3043	85	3287	229	-17.8
QM1H-17	30	316863	0	0.20022	0.00448	16.42319	1.69209	0.59491	0.05983	0.97614	2828	36	2902	94	3009	237	-8.0
QM1H-18	30	551441	24	0.18943	0.00423	15.35514	1.63548	0.58791	0.06123	0.97777	2737	36	2838	97	2981	244	-11.1
QM1H-19	30	502546	316	0.20505	0.00406	18.15472	2.13808	0.64214	0.07455	0.98574	2867	32	2998	107	3197	286	-14.7
QM1H-20	30	280807	51	0.21514	0.00326	18.60557	1.71878	0.62723	0.05716	0.98642	2945	24	3022	85	3139	223	-8.3
QM1H-21	30	772792	41	0.19971	0.00302	14.81081	1.52485	0.53786	0.05478	0.98918	2824	24	2803	93	2775	226	2.1
QM1H-23	30	841174	68	0.19671	0.00276	15.67842	1.60142	0.57807	0.05849	0.99055	2799	23	2857	93	2941	235	-6.3
QM1H-24	30	946288	64	0.20748	0.00279	17.52222	1.66336	0.61252	0.05756	0.98994	2886	22	2964	87	3080	226	-8.5
QM1H-25	30	677097	21	0.23766	0.00334	20.25403	1.71781	0.61808	0.05170	0.98617	3104	22	3104	79	3102	203	0.1
QM1H-26	30	708799	33	0.18467	0.00269	13.72491	1.41938	0.53902	0.05519	0.99001	2695	24	2731	93	2779	227	-3.8
QM1H-27	30	453414	49	0.24781	0.00330	20.76825	1.95850	0.60783	0.05674	0.98995	3171	21	3128	87	3061	224	4.3
QM1H-28	30	371991	47	0.22816	0.00308	19.62792	1.84541	0.62392	0.05805	0.98962	3039	21	3073	87	3126	226	-3.6
QM1H-29	30	545334	19	0.21139	0.00324	17.27374	1.48616	0.59264	0.05017	0.98399	2916	25	2950	79	3000	200	-3.6
QM1H-30	30	312468	43	0.20891	0.00299	15.97094	1.42029	0.55447	0.04867	0.98700	2897	23	2875	82	2844	199	2.3
QM1H-31	30	995164	3	0.22483	0.00306	20.53090	2.04074	0.66230	0.06521	0.99058	3016	22	3117	92	3276	248	-11.0
QM1H-32	30	273791	18	0.19942	0.00418	18.24158	2.04415	0.66344	0.07303	0.98238	2821	34	3003	103	3281	277	-20.8
QM1H-33	30	257574	25	0.21614	0.00315	18.61113	1.60406	0.62452	0.05305	0.98558	2952	23	3022	80	3128	207	-7.5
QM1H-34	30	234610	146	0.20532	0.00334	17.30194	1.68209	0.61117	0.05858	0.98594	2869	26	2952	89	3075	230	-9.0
QM1H-35	30	503728	6	0.20702	0.00472	18.89508	1.53969	0.66197	0.05178	0.95999	2882	37	3036	76	3275	198	-17.4
QM1H-36	30	292362	12	0.21481	0.00294	18.94395	1.59891	0.63962	0.05327	0.98676	2942	22	3039	78	3188	206	-10.6
QM1H-37	30	58669	65	0.25479	0.00592	24.89837	2.18019	0.70875	0.05983	0.96414	3215	36	3304	82	3454	222	-9.6
QM1H-38	30	502720	33	0.20586	0.00305	18.16058	1.59907	0.63981	0.05553	0.98576	2873	24	2998	81	3188	215	-13.9
QM1H-39	30	369919	59	0.24418	0.00353	21.18165	1.98929	0.62913	0.05838	0.98806	3147	23	3147	87	3146	227	0.1
QM1H-40	30	41922	30	0.25851	0.00557	24.17552	1.94528	0.67825	0.05258	0.96342	3238	34	3275	76	3338	199	-4.0
QM1H-41	30	392136	56	0.21219	0.00334	17.48154	1.61887	0.59751	0.05453	0.98543	2922	25	2962	85	3020	216	-4.2
QM1H-42	30	1263997	321	0.16519	0.00290	11.06479	1.04483	0.48581	0.04508	0.98261	2509	29	2529	84	2553	193	-2.1
QM1H-43	30	461474	40	0.21433	0.00289	17.94396	1.78576	0.60721	0.05987	0.99078	2939	22	2987	91	3059	236	-5.1
QM1H-44	30	729954	24	0.22016	0.00317	18.91144	1.49014	0.62299	0.04826	0.98314	2982	23	3037	73	3122	189	-5.9
QM1H-45	30	712232	26	0.20811	0.00294	16.35422	1.50346	0.56994	0.05177	0.98814	2891	23	2898	84	2908	209	-0.7
QM1H-46	30	432516	50	0.20478	0.00385	14.81694	1.24232	0.52477	0.04288	0.97456	2865	30	2804	77	2719	179	6.2
QM1H-48B	30	1794234	59	0.18929	0.00354	12.81649	1.43281	0.49107	0.05413	0.98591	2736	30	2666	100	2575	230	7.1
QM1H-49	30	2049959	113	0.15659	0.00238	9.73128	0.84818	0.45073	0.03868	0.98468	2419	26	2410	77	2399	170	1.0
QM1H-51	30	1723429	41	0.21170	0.00285	17.04940	1.68454	0.58409	0.05717	0.99068	2919	22	2938	91	2965	229	-2.0
QM1H-52	30	1263306	53	0.21428	0.00312	15.80809	1.64008	0.53505	0.05496	0.99010	2938	23	2865	95	2763	227	7.3
QM1H-53	30	2002265	61	0.16075	0.00225	10.13386	0.94574	0.45723	0.04219	0.98869	2464	23	2447	83	2427	184	1.8

Grain Mount Zircons (Continued)

Analysis	Spot Size μm	<sup>206</sup> Pb (cps)	<sup>204</sup> Pb (cps)	<sup>207</sup> Pb/ <sup>206</sup> Pb	±2σ	<sup>207</sup> Pb/ <sup>235</sup> U	±2σ	<sup>206</sup> Pb/ <sup>238</sup> U	±2σ	ρ	Model Ages (Ma)						% Disc.
											<sup>207</sup> Pb/ <sup>206</sup> Pb	±2σ	<sup>207</sup> Pb/ <sup>235</sup> U	±2σ	<sup>206</sup> Pb/ <sup>238</sup> U	±2σ	
QM1H-54	30	1469085	182	0.17342	0.00280	10.89238	1.05063	0.45553	0.04332	0.98588	2591	27	2514	86	2420	189	7.9
QM1H-55	30	1649741	43	0.16420	0.00306	10.24835	0.94342	0.45268	0.04081	0.97929	2499	31	2457	82	2407	179	4.4
QM1H-56	30	1470276	302	0.15796	0.00228	9.76629	0.82332	0.44842	0.03724	0.98519	2434	24	2413	75	2388	164	2.2
QM1H-57	30	807234	48	0.19884	0.00328	15.95458	1.34706	0.58195	0.04819	0.98074	2817	27	2874	78	2957	193	-6.2
QM1H-58	30	945483	51	0.17664	0.00292	11.32149	0.92209	0.46485	0.03707	0.97920	2622	27	2550	73	2461	161	7.4
QM1H-59	30	1328325	39	0.17316	0.00260	11.34745	1.43071	0.47528	0.05950	0.99289	2588	25	2552	111	2507	255	3.8
QM1H-60	30	150016	111	0.18182	0.00389	13.62058	1.25156	0.54331	0.04855	0.97246	2670	35	2724	83	2797	200	-5.9
QM1H-61	30	81467	86	0.23158	0.00435	20.16823	1.67602	0.63163	0.05113	0.97417	3063	30	3099	77	3156	199	-3.8
QM1H-62	30	328527	75	0.20919	0.00340	18.02481	1.54026	0.62493	0.05243	0.98171	2899	26	2991	79	3130	205	-10.0
QM1H-63	30	867954	73	0.19043	0.00264	14.43962	1.24905	0.54995	0.04695	0.98703	2746	23	2779	79	2825	192	-3.6
QM1H-64	30	674477	21	0.21354	0.00308	18.02002	1.77775	0.61203	0.05973	0.98929	2933	23	2991	91	3078	235	-6.2
QM1H-65	30	597524	27	0.15442	0.00215	10.27395	1.00174	0.48254	0.04657	0.98976	2395	23	2460	86	2538	199	-7.2
QM1H-66	30	962936	32	0.20484	0.00313	14.55950	1.27726	0.51550	0.04453	0.98471	2865	25	2787	80	2680	187	7.9
QM1H-67	30	911958	15	0.20286	0.00276	15.67408	1.36351	0.56040	0.04815	0.98771	2849	22	2857	80	2868	196	-0.8
QM1H-69	30	623177	42	0.25530	0.00355	24.62926	2.18667	0.69968	0.06135	0.98768	3218	22	3294	83	3419	229	-8.1
QM1H-70	30	542515	10	0.19367	0.00406	16.79397	1.62471	0.62890	0.05940	0.97624	2774	34	2923	89	3145	233	-17.0
QM1H-71	30	580879	16	0.23041	0.00328	21.23935	1.80642	0.66856	0.05606	0.98593	3055	23	3150	79	3300	211	-10.3
QM1H-72	30	295800	11	0.25707	0.00366	25.39097	2.16468	0.71634	0.06021	0.98592	3229	22	3323	80	3482	222	-10.2
QM1H-73	30	1024428	40	0.16971	0.00273	11.75182	0.95589	0.50222	0.04005	0.98031	2555	27	2585	73	2623	170	-3.3
QM1H-74	30	1137078	17	0.19040	0.00366	14.60822	1.71764	0.55646	0.06455	0.98658	2746	31	2790	106	2852	262	-4.8
QM1H-75	30	547446	63	0.18995	0.00280	15.22755	1.39466	0.58142	0.05256	0.98699	2742	24	2830	84	2955	211	-9.7
QM1H-76	30	812939	86	0.17917	0.00306	10.31267	0.80065	0.41744	0.03162	0.97552	2645	28	2463	69	2249	142	17.7
QM1H-77	30	1105555	26	0.21319	0.00353	17.21616	1.47123	0.58570	0.04910	0.98102	2930	27	2947	79	2972	197	-1.8
QM1H-78	30	703082	12	0.20295	0.00297	16.23063	1.56837	0.58001	0.05540	0.98845	2850	24	2890	88	2949	222	-4.3
QM1H-79	30	576662	2	0.17591	0.00260	12.47737	0.98546	0.51442	0.03991	0.98237	2615	24	2641	72	2675	168	-2.8
QM1H-80	30	539287	1	0.21359	0.00297	18.20727	1.67837	0.61824	0.05634	0.98857	2933	22	3001	85	3103	221	-7.3
QM1H-81	30	265042	85	0.22548	0.00313	19.99674	1.80639	0.64321	0.05741	0.98810	3020	22	3091	84	3202	221	-7.6
QM1H-82	30	581458	71	0.21151	0.00291	17.01069	1.76141	0.58330	0.05987	0.99116	2917	22	2935	95	2962	239	-1.9
QM1H-83	30	425199	1	0.19872	0.00393	14.99119	1.26446	0.54715	0.04487	0.97215	2816	32	2815	77	2813	184	0.1
QM1H-84	30	1310535	18	0.18880	0.00288	13.02706	1.32456	0.50042	0.05031	0.98869	2732	25	2682	92	2616	213	5.2
QM1H-85	30	550946	18	0.21162	0.00341	16.53594	1.92186	0.56672	0.06523	0.99033	2918	26	2908	106	2894	263	1.0
QM1H-86	30	1110486	24	0.17617	0.00250	12.38048	1.08013	0.50969	0.04388	0.98673	2617	23	2634	79	2655	185	-1.8
QM1H-87	30	873373	15	0.17271	0.00458	12.36769	1.18262	0.51937	0.04772	0.96082	2584	44	2633	86	2697	199	-5.3
QM1H-88	30	372113	79	0.20624	0.00466	15.72098	1.61403	0.55284	0.05537	0.97547	2876	36	2860	94	2837	226	1.7
QM1H-89	30	818042	27	0.22063	0.00295	18.18338	1.43973	0.59774	0.04665	0.98561	2985	21	2999	73	3021	186	-1.5
QM1H-90	30	890862	42	0.16667	0.00236	10.90693	0.91121	0.47463	0.03908	0.98549	2524	24	2515	75	2504	169	1.0
QM1H-91	30	1334451	72	0.16869	0.00463	11.60073	0.98380	0.49875	0.04002	0.94625	2545	45	2573	76	2608	170	-3.0
QM1H-92	30	1161163	33	0.20580	0.00323	15.94346	1.40630	0.56187	0.04877	0.98408	2873	25	2873	81	2874	198	-0.1
QM1H-93	30	552454	45	0.18909	0.00266	14.95034	1.52311	0.57344	0.05786	0.99039	2734	23	2812	93	2922	233	-8.5
QM1H-94	30	1413454	48	0.16167	0.00227	10.48962	0.78016	0.47058	0.03437	0.98208	2473	23	2479	67	2486	149	-0.6
QM1H-95	30	872695	23	0.21740	0.00293	18.33260	1.54943	0.61160	0.05103	0.98723	2962	22	3007	78	3076	201	-4.9
QM1H-96	30	2460225	35	0.15726	0.00224	9.45064	1.03529	0.43586	0.04734	0.99153	2426	24	2383	96	2332	209	4.6
QM1H-99	30	1292362	12	0.18644	0.00358	13.12865	1.19166	0.51070	0.04530	0.97733	2711	31	2689	82	2660	190	2.3
QM1H-100	30	813831	15	0.23821	0.00316	20.71320	1.97287	0.63065	0.05948	0.99024	3108	21	3125	88	3152	231	-1.8
QM1H-101	30	1737233	191	0.17188	0.00289	12.63571	1.40665	0.53317	0.05867	0.98850	2576	28	2653	100	2755	242	-8.5

Grain Mount Zircons (Continued)

Analysis	Spot Size µm	<sup>206</sup> Pb (cps)	<sup>204</sup> Pb (cps)	<sup>207</sup> Pb/ <sup>206</sup> Pb	±2σ	<sup>207</sup> Pb/ <sup>235</sup> U	±2σ	<sup>206</sup> Pb/ <sup>238</sup> U	±2σ	ρ	Model Ages (Ma)						% Disc.
											<sup>207</sup> Pb/ <sup>206</sup> Pb	±2σ	<sup>207</sup> Pb/ <sup>235</sup> U	±2σ	<sup>206</sup> Pb/ <sup>238</sup> U	±2σ	
QM1H-102	30	1900744	23	0.18117	0.00245	11.96238	1.06056	0.47888	0.04196	0.98828	2664	22	2601	80	2522	180	6.4
QM1H-103	30	2194600	14	0.15839	0.00221	9.82379	0.82478	0.44982	0.03724	0.98605	2439	23	2418	75	2394	163	2.2
QM1H-105	30	1599900	22	0.15618	0.00221	9.93975	0.95775	0.46159	0.04400	0.98921	2415	24	2429	85	2447	191	-1.6
QM8A-1	30	1139449	93	0.14894	0.00114	9.54786	0.40172	0.46494	0.01924	0.98327	2334	13	2392	38	2461	84	-6.6
QM8A-2	30	720496	102	0.14688	0.00105	8.86725	0.51877	0.43785	0.02543	0.99254	2310	12	2324	52	2341	113	-1.6
QM8A-3	30	730027	95	0.14703	0.00108	8.88875	0.46786	0.43846	0.02285	0.99014	2312	13	2327	47	2344	102	-1.7
QM8A-4	30	690589	79	0.14715	0.00109	8.72757	0.44284	0.43017	0.02159	0.98922	2313	13	2310	45	2306	97	0.3
QM8A-5	30	937148	118	0.14740	0.00112	9.07015	0.31683	0.44630	0.01522	0.97611	2316	13	2345	31	2379	67	-3.2
QM8A-6	30	180525	113	0.14564	0.00122	8.33334	0.26824	0.41499	0.01290	0.96533	2295	14	2268	29	2238	58	3.0
QM8A-7	30	390767	120	0.14703	0.00105	8.76028	0.37694	0.43211	0.01834	0.98611	2312	12	2313	38	2315	82	-0.2
QM8A-8	30	1029202	104	0.14832	0.00111	8.58204	0.33652	0.41965	0.01615	0.98163	2327	13	2295	35	2259	73	3.4
QM8A-9	30	1003833	120	0.14792	0.00111	9.33992	0.66414	0.45794	0.03238	0.99440	2322	13	2372	63	2430	142	-5.6
QM8A-10	30	99246	125	0.14781	0.00166	8.85136	0.36995	0.43431	0.01749	0.96339	2321	19	2323	37	2325	78	-0.2
QM8A-11	30	1599723	193	0.15052	0.00125	9.58226	0.38095	0.46171	0.01795	0.97795	2352	14	2395	36	2447	79	-4.9
QM8A-12	30	323153	148	0.14729	0.00108	9.03701	0.46916	0.44500	0.02287	0.99002	2315	12	2342	46	2373	101	-3.0
QM8A-13	30	1164058	199	0.14880	0.00118	9.53824	0.54231	0.46492	0.02618	0.99022	2332	14	2391	51	2461	114	-6.7
QM8A-14	30	831083	146	0.14778	0.00108	8.53215	0.31429	0.41874	0.01512	0.98006	2320	12	2289	33	2255	68	3.3
QM8A-15	30	946326	177	0.14834	0.00116	8.63976	0.35868	0.42243	0.01722	0.98208	2327	13	2301	37	2271	78	2.8
QM8A-16	30	496963	205	0.14788	0.00113	8.70523	0.29595	0.42696	0.01415	0.97455	2321	13	2308	31	2292	64	1.5
QM8A-17	30	142756	262	0.14717	0.00123	8.39765	0.35332	0.41386	0.01707	0.98020	2313	14	2275	37	2233	77	4.1
QM8A-18	30	353930	234	0.14939	0.00119	8.43791	0.29626	0.40966	0.01401	0.97371	2339	14	2279	31	2213	64	6.3
QM8A-19	30	410364	256	0.14869	0.00122	8.92438	0.25923	0.43530	0.01213	0.95915	2331	14	2330	26	2330	54	0.1
QM8A-20	30	270896	276	0.14904	0.00121	8.74767	0.29778	0.42568	0.01407	0.97121	2335	14	2312	31	2286	63	2.5
QM8A-21	30	520022	285	0.14847	0.00129	8.66413	0.34663	0.42325	0.01653	0.97612	2328	15	2303	36	2275	74	2.7
QM8A-22	30	1257435	254	0.14878	0.00118	8.92435	0.61731	0.43504	0.02989	0.99342	2332	13	2330	61	2328	133	0.2
QM8A-23	30	2159265	270	0.15132	0.00119	8.83811	0.40336	0.42361	0.01905	0.98512	2361	13	2321	41	2277	86	4.2
QM8A-24	30	659971	282	0.14771	0.00109	9.26088	0.33159	0.45473	0.01593	0.97846	2320	13	2364	32	2416	70	-5.0
QM8A-25	30	747046	243	0.14799	0.00114	8.87092	0.40121	0.43474	0.01938	0.98550	2323	13	2325	40	2327	86	-0.2
QM8A-26	30	303837	240	0.14688	0.00110	8.63031	0.28312	0.42616	0.01361	0.97349	2310	13	2300	29	2288	61	1.1
QM10C-1	20	239534	104	0.25598	0.00218	21.45898	0.72151	0.60800	0.01978	0.96739	3222	13	3160	32	3062	79	6.2
QM10C-2	20	1126551	168	0.25793	0.00306	21.47763	0.96969	0.60393	0.02631	0.96489	3234	19	3160	43	3046	105	7.3
QM10C-3	20	374364	141	0.26009	0.00215	22.82475	0.74370	0.63649	0.02006	0.96731	3247	13	3220	31	3175	79	2.8
QM10C-4	20	835841	132	0.25968	0.00361	22.64663	0.87313	0.63250	0.02275	0.93289	3245	22	3212	37	3159	89	3.3
QM10C-5	20	863635	156	0.23317	0.00335	16.32251	0.69930	0.50770	0.02049	0.94195	3074	23	2896	40	2647	87	16.9
QM10C-6	20	1335174	109	0.26971	0.00309	21.75473	0.94308	0.58500	0.02446	0.96455	3304	18	3173	41	2969	99	12.6
QM10C-7	20	267451	67	0.15681	0.00133	9.58403	0.31779	0.44327	0.01421	0.96693	2422	14	2396	30	2365	63	2.8
QM10C-8	20	667811	83	0.25189	0.00257	20.64275	1.07844	0.59437	0.03045	0.98075	3197	16	3122	49	3007	122	7.4
QM10C-9	20	1162593	161	0.26787	0.00341	23.49414	0.87028	0.63612	0.02213	0.93909	3294	20	3248	35	3174	87	4.6
QM10C-10	20	267350	122	0.26241	0.00201	23.55243	0.74531	0.65097	0.01999	0.97023	3261	12	3250	30	3232	78	1.1
QM10C-11	20	736118	114	0.25337	0.00433	19.88218	0.78503	0.56912	0.02026	0.90161	3206	27	3086	37	2904	83	11.7
QM10C-12	20	230272	140	0.25276	0.00254	21.31210	0.84319	0.61154	0.02340	0.96719	3202	16	3153	38	3076	93	4.9
QM10C-13	20	286158	125	0.25286	0.00589	22.22852	1.19980	0.63756	0.03105	0.90218	3203	36	3194	51	3179	121	0.9
QM10C-14	20	333885	157	0.25766	0.00240	22.58464	0.98960	0.63573	0.02722	0.97714	3232	15	3209	42	3172	106	2.4
QM10C-15	20	735018	120	0.26705	0.00276	22.75563	0.80535	0.61802	0.02092	0.95654	3289	16	3217	34	3102	83	7.1
QM10C-16	20	478614	116	0.23971	0.00502	20.19169	1.16008	0.61091	0.03268	0.93117	3118	33	3101	54	3074	129	1.8

Grain Mount Zircons (Continued)

Analysis	Spot Size μm	<sup>206</sup> Pb (cps)	<sup>204</sup> Pb (cps)	<sup>207</sup> Pb/ <sup>206</sup> Pb	±2σ	<sup>207</sup> Pb/ <sup>235</sup> U	±2σ	<sup>206</sup> Pb/ <sup>238</sup> U	±2σ	ρ	Model Ages (Ma)						% Disc.
											<sup>207</sup> Pb/ <sup>206</sup> Pb	±2σ	<sup>207</sup> Pb/ <sup>235</sup> U	±2σ	<sup>206</sup> Pb/ <sup>238</sup> U	±2σ	
QM10C-17	20	564151	101	0.25900	0.00258	21.90885	1.15485	0.61352	0.03176	0.98199	3241	16	3180	50	3084	126	6.1
QM10C-18	20	237527	68	0.25128	0.00229	21.12285	0.97334	0.60968	0.02754	0.98019	3193	14	3144	44	3069	109	4.9
QM10C-19	20	257884	162	0.24550	0.00286	20.75689	1.02047	0.61320	0.02929	0.97160	3156	18	3127	47	3083	116	2.9
QM10C-20	20	255754	115	0.25150	0.00391	19.59252	1.22054	0.56501	0.03409	0.96841	3194	24	3071	58	2887	139	11.9
QM10C-21	20	667321	38	0.25147	0.00409	23.36631	1.54155	0.67391	0.04309	0.96913	3194	25	3242	62	3321	164	-5.1
QM10C-22	20	206388	56	0.24438	0.00266	20.58416	1.07447	0.61090	0.03119	0.97805	3149	17	3119	49	3074	124	3.0
QM10C-23	20	873999	81	0.25116	0.00386	20.71495	1.08863	0.59817	0.03006	0.95639	3192	24	3125	50	3022	120	6.7
QM10C-24	20	691985	34	0.25431	0.00267	22.57889	1.21433	0.64393	0.03396	0.98069	3212	17	3209	51	3204	132	0.3
QM10C-25	20	494931	54	0.24868	0.00269	20.97278	1.10326	0.61166	0.03149	0.97856	3176	17	3137	50	3077	125	3.9
QM10C-26	20	1243591	28	0.25562	0.00223	22.44231	1.26776	0.63676	0.03554	0.98802	3220	14	3203	53	3176	138	1.7
QM10C-27	20	868723	49	0.23802	0.00311	21.52436	1.59271	0.65587	0.04777	0.98424	3107	21	3163	69	3251	183	-5.9
QM10C-28	20	590946	73	0.24156	0.00273	21.09763	1.56866	0.63343	0.04655	0.98839	3130	18	3143	70	3163	181	-1.3
QM10C-29	20	1017876	74	0.25311	0.00227	23.58637	1.54832	0.67586	0.04395	0.99061	3204	14	3251	62	3328	167	-5.0
QM10C-30	20	940532	104	0.24264	0.00361	20.57821	1.02684	0.61510	0.02929	0.95444	3137	23	3119	47	3090	116	1.9
QM10C-31	20	1197431	74	0.24214	0.00268	18.36177	0.87868	0.54999	0.02560	0.97285	3134	17	3009	45	2825	106	12.2
QM10C-32	20	873172	61	0.25405	0.00254	23.46098	1.30688	0.66977	0.03670	0.98380	3210	16	3246	53	3305	140	-3.8
QM10C-33	20	767476	87	0.25788	0.00247	23.35014	1.36159	0.65671	0.03777	0.98638	3234	15	3242	55	3254	145	-0.8
QM10C-34	20	121412	81	0.17069	0.00415	11.71360	0.58536	0.49772	0.02173	0.87348	2564	40	2582	46	2604	93	-1.9
QM10C-35	20	577994	71	0.25110	0.00255	22.20243	1.18644	0.64130	0.03365	0.98180	3192	16	3193	51	3194	141	-0.1
QM10C-36	20	430915	113	0.25643	0.00168	23.92425	1.32444	0.67666	0.03720	0.99297	3225	10	3265	53	3332	131	-4.2
QM10C-37	20	737522	115	0.25463	0.00147	22.23539	0.85286	0.63335	0.02402	0.98857	3214	9	3194	37	3163	94	2.0
QM10C-38	20	900481	127	0.25336	0.00212	21.11908	1.09947	0.60457	0.03107	0.98702	3206	13	3144	49	3048	124	6.2
QM10C-39	20	186312	95	0.25106	0.00135	21.61214	0.72547	0.62434	0.02069	0.98706	3191	8	3166	32	3127	82	2.5
QM10C-40	20	355783	113	0.25676	0.00142	22.03599	1.10932	0.62246	0.03114	0.99392	3227	9	3185	48	3120	123	4.2
QM10C-41	20	436286	171	0.24630	0.00229	20.79051	0.96537	0.61221	0.02785	0.97976	3161	15	3129	44	3079	110	3.3
QM10C-42	20	1282119	338	0.25442	0.00495	22.17490	1.06594	0.63212	0.02779	0.91449	3213	30	3191	46	3158	109	2.1
QM10C-43	20	1297908	219	0.25777	0.00557	21.06652	1.05794	0.59274	0.02687	0.90253	3233	34	3142	48	3001	108	9.0
QM10C-44	20	311627	175	0.25246	0.00248	22.77676	1.00168	0.65434	0.02805	0.97483	3200	15	3217	42	3245	108	-1.8
QM10C-45	20	963891	178	0.25376	0.00352	20.47475	0.92327	0.58518	0.02511	0.95159	3208	22	3114	43	2970	101	9.3
QM10C-46	20	1118381	120	0.24633	0.00255	19.09960	0.63490	0.56234	0.01776	0.95020	3161	16	3047	32	2876	73	11.2
QM10C-47	20	1064357	127	0.23996	0.00192	17.92142	1.05442	0.54166	0.03157	0.99072	3120	13	2986	55	2790	131	13.0
QM10C-48	20	597656	121	0.24911	0.00346	20.53289	0.91869	0.59781	0.02543	0.95059	3179	22	3117	42	3021	102	6.2
QM10C-49	20	1071560	156	0.26022	0.00160	21.00837	0.74884	0.58552	0.02056	0.98505	3248	10	3139	34	2971	83	10.6
QM10C-50	20	2377832	249	0.27608	0.00180	20.70277	1.02862	0.54387	0.02679	0.99137	3341	10	3125	47	2800	111	19.9
QM10C-51	20	630274	109	0.24955	0.00245	20.95130	1.02996	0.60891	0.02933	0.97980	3182	15	3136	47	3066	116	4.6
QM10C-52	20	802805	111	0.25268	0.00271	21.65923	1.26508	0.62170	0.03570	0.98302	3202	17	3169	55	3117	140	3.3
QM10C-53	20	231997	141	0.25172	0.00149	20.80172	0.85458	0.59936	0.02437	0.98954	3196	9	3129	39	3027	97	6.6
QM10C-54	20	1386935	198	0.26101	0.00257	22.01672	1.17532	0.61177	0.03210	0.98284	3253	15	3184	51	3077	127	6.8
QM10C-55	20	344419	26	0.24623	0.00423	18.76391	1.01285	0.55269	0.02828	0.94804	3161	27	3030	51	2836	116	12.7
QM10C-56	20	1807904	51	0.26116	0.00434	20.10524	0.84143	0.55835	0.02145	0.91783	3254	26	3096	40	2860	88	15.0
QM10C-57	20	570232	56	0.24170	0.00463	18.62860	0.78000	0.55898	0.02081	0.88904	3131	30	3023	40	2862	85	10.6
QM10C-58	20	603593	64	0.23536	0.00490	18.69194	0.89126	0.57599	0.02470	0.89948	3089	33	3026	45	2932	100	6.3
QM10C-59	20	880583	102	0.24937	0.00439	20.16343	1.22847	0.58642	0.03420	0.95735	3181	28	3099	57	2975	138	8.1
QM10C-60	20	291425	63	0.25384	0.00424	20.99674	0.99346	0.59991	0.02656	0.93577	3209	26	3138	45	3029	106	7.0
QM10C-61	20	582885	57	0.24512	0.00463	19.83876	1.03906	0.58699	0.02868	0.93285	3154	30	3084	49	2977	115	7.0

Grain Mount Zircons (Continued)

Analysis	Spot Size μm	<sup>206</sup> Pb (cps)	<sup>204</sup> Pb (cps)	<sup>207</sup> Pb/ <sup>206</sup> Pb	±2σ	<sup>207</sup> Pb/ <sup>235</sup> U	±2σ	<sup>206</sup> Pb/ <sup>238</sup> U	±2σ	ρ	Model Ages (Ma)						% Disc.
											<sup>207</sup> Pb/ <sup>206</sup> Pb	±2σ	<sup>207</sup> Pb/ <sup>235</sup> U	±2σ	<sup>206</sup> Pb/ <sup>238</sup> U	±2σ	
QM10C-62	20	793193	83	0.25906	0.00443	21.32915	1.07915	0.59713	0.02843	0.94113	3241	27	3154	48	3018	114	8.6
QM10C-63	20	704817	33	0.25503	0.00447	22.23851	1.21624	0.63244	0.03276	0.94718	3216	27	3194	52	3159	128	2.2
QM10C-64	20	1204835	47	0.26423	0.00475	21.27669	0.91919	0.58401	0.02295	0.90944	3272	28	3151	41	2965	93	11.7
QM10C-65	20	1812164	196	0.25433	0.00561	18.93286	0.87075	0.53990	0.02179	0.87768	3212	34	3038	43	2783	91	16.4
QM10C-66	20	590971	66	0.24183	0.00424	19.09991	0.94290	0.57283	0.02644	0.93487	3132	28	3047	47	2919	107	8.4
QM10C-67	20	991347	77	0.24666	0.00423	19.69982	0.90544	0.57925	0.02471	0.92796	3163	27	3077	43	2946	100	8.6
QM10C-68	20	916391	53	0.25066	0.00441	20.43097	0.93918	0.59115	0.02510	0.92373	3189	28	3112	44	2994	101	7.6
QM10C-69	20	367445	120	0.15521	0.00263	9.03967	0.43793	0.42240	0.01918	0.93706	2404	28	2342	43	2271	86	6.6
QM10C-70	20	1989528	77	0.23386	0.00395	16.76812	0.66131	0.52002	0.01854	0.90390	3079	27	2922	37	2699	78	15.1
QM10C-71	20	929302	80	0.24417	0.00462	19.29026	1.04878	0.57298	0.02920	0.93749	3147	30	3056	51	2920	119	9.0
QM10C-72	20	1602045	120	0.25351	0.00428	20.02888	0.95058	0.57300	0.02542	0.93455	3207	26	3093	45	2920	103	11.1
QM10C-73	20	583753	59	0.25230	0.00423	21.05594	1.44585	0.60528	0.04031	0.96979	3199	26	3141	64	3051	160	5.8
QM10C-74	20	827007	46	0.24360	0.00418	19.88665	0.95539	0.59209	0.02657	0.93412	3144	27	3086	45	2998	107	5.8
QM10C-75	20	1235991	102	0.25004	0.00432	19.19771	1.03020	0.55685	0.02829	0.94673	3185	27	3052	51	2854	116	12.9
QM10C-76	20	474082	154	0.24389	0.00430	19.90027	1.46731	0.59178	0.04237	0.97106	3146	28	3087	69	2997	169	5.9
QM10C-77	20	628062	81	0.24875	0.00414	22.25007	1.00365	0.64873	0.02720	0.92945	3177	26	3195	43	3223	105	-1.9
QM10C-78	20	588972	97	0.25837	0.00434	23.72570	1.70183	0.66601	0.04644	0.97218	3237	26	3257	68	3290	177	-2.1
QM10C-79	20	1196023	66	0.23918	0.00481	20.03413	1.24425	0.60750	0.03570	0.94620	3115	32	3093	58	3060	142	2.2
QM10C-80	20	825320	76	0.24764	0.00453	22.34329	1.86263	0.65436	0.05322	0.97558	3170	29	3199	78	3245	204	-3.0
QM10C-81	20	595347	60	0.25040	0.00477	21.01362	1.33457	0.60864	0.03687	0.95394	3187	30	3139	60	3065	146	4.8
QM10C-82	20	508899	61	0.24980	0.00468	21.20045	1.28110	0.61554	0.03536	0.95076	3183	29	3148	57	3092	140	3.6
QM10C-83	20	1496197	76	0.25367	0.00446	21.99082	1.14861	0.62874	0.03093	0.94173	3208	27	3183	50	3145	121	2.5
QM10C-84	20	1455666	79	0.26056	0.00451	21.08237	1.34040	0.58684	0.03590	0.96231	3250	27	3142	60	2977	144	10.5
QM10C-85	20	1405694	109	0.25108	0.00435	19.58976	0.96010	0.56587	0.02595	0.93554	3192	27	3071	46	2891	106	11.7
QM10C-86	20	1197118	77	0.25626	0.01205	21.02739	4.86046	0.59512	0.13468	0.97908	3224	72	3140	202	3010	523	8.3
QM10C-87	20	2716030	130	0.24722	0.00491	18.17439	0.98060	0.53318	0.02675	0.92991	3167	31	2999	51	2755	112	16.0
QM10C-88	20	1728823	87	0.24902	0.00456	19.84787	0.96414	0.57807	0.02601	0.92632	3179	29	3084	46	2941	105	9.3
QM10C-89	20	678074	93	0.24902	0.00442	21.48589	1.09233	0.62576	0.02981	0.93717	3179	28	3161	48	3133	117	1.8
QM10C-90	20	386645	46	0.25032	0.00414	21.11584	1.11293	0.61179	0.03061	0.94941	3187	26	3144	50	3077	121	4.3
QM10C-91	20	1598916	155	0.25185	0.00432	20.12306	0.87381	0.57951	0.02312	0.91881	3196	27	3097	41	2947	94	9.7
QM10C-92	20	1594047	54	0.25405	0.00430	20.94260	1.26970	0.59788	0.03480	0.96019	3210	27	3136	57	3021	139	7.4
QM10C-93	20	1868597	90	0.26090	0.00480	22.44481	1.14841	0.62393	0.02979	0.93301	3252	29	3203	49	3126	117	4.9
QM10C-94	20	1698156	91	0.26100	0.00433	22.08787	1.16888	0.61377	0.03084	0.94955	3253	26	3188	50	3085	122	6.5
QM10C-95	20	633685	109	0.24667	0.00413	20.75474	1.13898	0.61024	0.03189	0.95234	3164	26	3127	52	3071	126	3.7
QM10C-96	20	1120378	45	0.25815	0.00427	21.80138	1.09169	0.61251	0.02895	0.94375	3235	26	3175	47	3080	115	6.0
QM10C-97	20	741474	119	0.23964	0.00395	19.84902	0.91545	0.60072	0.02588	0.93401	3118	26	3084	44	3033	103	3.4
QM10C-98	20	664191	83	0.25155	0.00437	21.16693	0.92763	0.61027	0.02455	0.91797	3195	27	3146	42	3071	98	4.9
QM10C-99	20	799145	42	0.25259	0.00460	21.47357	1.07365	0.61658	0.02871	0.93136	3201	28	3160	47	3096	113	4.1
QM10C-100	20	2363789	730	0.26399	0.00597	21.14717	1.31148	0.58098	0.03355	0.93104	3271	35	3145	58	2953	135	12.1
QM10C-101	20	991115	26	0.22858	0.00390	18.13432	1.10143	0.57538	0.03354	0.95977	3042	27	2997	57	2930	136	4.6
QM10C-102	20	2851440	139	0.26257	0.00524	21.46763	1.54402	0.59298	0.04098	0.96078	3262	31	3160	67	3002	164	10.0
QM10C-103	20	1363311	169	0.22407	0.00632	16.96845	0.86402	0.54923	0.02329	0.83281	3010	45	2933	48	2822	96	7.7
QM10C-104	20	557933	70	0.24645	0.00428	19.58698	1.06848	0.57641	0.02981	0.94791	3162	27	3071	51	2934	121	9.0
QM10C-105	20	905520	59	0.24688	0.00437	19.57372	0.82638	0.57502	0.02204	0.90780	3165	28	3071	40	2928	90	9.3

Grain Mount Zircons (Continued)

Analysis	Spot Size μm	<sup>206</sup> Pb (cps)	<sup>204</sup> Pb (cps)	<sup>207</sup> Pb/ <sup>206</sup> Pb	±2σ	<sup>207</sup> Pb/ <sup>235</sup> U	±2σ	<sup>206</sup> Pb/ <sup>238</sup> U	±2σ	ρ	Model Ages (Ma)						% Disc.
											<sup>207</sup> Pb/ <sup>206</sup> Pb	±2σ	<sup>207</sup> Pb/ <sup>235</sup> U	±2σ	<sup>206</sup> Pb/ <sup>238</sup> U	±2σ	
QM13G-1	30	764437	192	0.15836	0.00220	10.10453	0.69911	0.46277	0.03137	0.97964	2438	23	2444	62	2452	137	-0.7
QM13G-2	30	343648	155	0.15945	0.00207	10.51947	0.76822	0.47849	0.03439	0.98409	2450	22	2482	66	2521	148	-3.5
QM13G-3	30	178092	133	0.15624	0.00204	9.57185	0.65354	0.44433	0.02978	0.98162	2415	22	2394	61	2370	132	2.2
QM13G-4	30	242478	127	0.15760	0.00222	9.73005	0.65624	0.44778	0.02953	0.97786	2430	24	2410	60	2385	130	2.2
QM13G-5	30	1200359	924	0.16372	0.00224	9.93832	0.69445	0.44026	0.03017	0.98060	2494	23	2429	63	2352	134	6.8
QM13G-6	30	125010	104	0.15715	0.00227	9.64894	0.65969	0.44532	0.02976	0.97745	2425	24	2402	61	2374	131	2.5
QM13G-7	30	2656030	320	0.15538	0.00212	8.73386	0.61638	0.40768	0.02823	0.98117	2406	23	2311	62	2204	128	9.9
QM13G-8	30	330160	125	0.15671	0.00227	10.04080	0.68202	0.46470	0.03084	0.97693	2420	24	2439	61	2460	134	-2.0
QM13G-9	30	363835	238	0.16109	0.00254	10.00011	0.67970	0.45022	0.02977	0.97270	2467	26	2435	61	2396	131	3.4
QM13G-10	30	392104	78	0.15617	0.00203	9.87838	0.66795	0.45875	0.03044	0.98128	2415	22	2423	61	2434	133	-1.0
QM13G-11	30	94470	102	0.15792	0.00230	9.56299	0.64655	0.43920	0.02900	0.97655	2433	24	2394	60	2347	129	4.2
QM13G-12	30	181171	227	0.16095	0.00293	10.10843	0.72312	0.45551	0.03151	0.96711	2466	30	2445	64	2420	138	2.2
QM13G-13	30	297485	155	0.15697	0.00208	9.49068	0.65691	0.43851	0.02979	0.98151	2423	22	2387	62	2344	132	3.9
QM13G-14	30	972280	135	0.16284	0.00289	9.99027	0.71612	0.44495	0.03091	0.96897	2485	30	2434	64	2373	136	5.4
QM13G-15	30	131656	92	0.15390	0.00214	9.24563	0.64302	0.43570	0.02969	0.97982	2390	23	2363	62	2331	132	2.9
QM13G-16	30	113689	89	0.15692	0.00220	9.51435	0.64983	0.43974	0.02940	0.97874	2423	24	2389	61	2349	130	3.6
QM13G-17	30	160604	67	0.15738	0.00218	9.74449	0.67086	0.44905	0.03028	0.97961	2428	23	2411	61	2391	133	1.8
QM13G-18	30	209198	168	0.15722	0.00224	9.77275	0.67881	0.45082	0.03064	0.97864	2426	24	2414	62	2399	135	1.3
QM13G-19	30	199908	104	0.15801	0.00224	9.68460	0.66672	0.44453	0.02995	0.97860	2434	24	2405	61	2371	132	3.1
QM13G-20	30	249689	114	0.15695	0.00212	9.76966	0.68886	0.45144	0.03124	0.98149	2423	23	2413	63	2402	137	1.1
QM13G-21	30	219749	88	0.15751	0.00217	9.79885	0.66426	0.45118	0.02995	0.97912	2429	23	2416	61	2401	132	1.4
QM13G-22	30	39131	48	0.14738	0.00243	8.68278	0.61017	0.42729	0.02919	0.97205	2316	28	2305	62	2293	130	1.1
QM13G-23	30	555493	1431	0.18309	0.00447	11.45527	0.82974	0.45378	0.03095	0.94150	2681	40	2561	65	2412	136	12.0
QM13G-24	30	99779	82	0.15046	0.00240	9.06840	0.62081	0.43712	0.02910	0.97250	2351	27	2345	61	2338	129	0.7
QM13G-25	30	208876	120	0.15535	0.00217	9.47438	0.65294	0.44231	0.02985	0.97926	2406	24	2385	61	2361	132	2.2
QM13G-26	30	137895	68	0.15602	0.00208	9.33983	0.63302	0.43416	0.02885	0.98041	2413	22	2372	60	2324	128	4.4
QM13G-27	30	108718	90	0.15845	0.00213	9.43981	0.64442	0.43209	0.02892	0.98038	2439	23	2382	61	2315	129	6.0
QM13G-28	30	126727	113	0.15790	0.00212	9.46773	0.64792	0.43488	0.02918	0.98052	2433	23	2384	61	2328	130	5.2
QM13G-29	30	187480	143	0.15835	0.00253	9.61841	0.68754	0.44053	0.03069	0.97462	2438	27	2399	64	2353	136	4.2
QM13G-30	30	130273	140	0.15776	0.00236	9.76863	0.66446	0.44909	0.02980	0.97548	2432	25	2413	61	2391	131	2.0



## Appendix C – Official sample collection

The following samples have been submitted to the Department of Earth and Atmospheric Sciences at the University of Alberta for their permanent collection. Hand samples and powdered samples have been submitted for the permanent collection. Powdered samples were crushed in a tungsten carbide mill for three and a half minutes. The samples chosen for this collection are representative of the key rock types present in the western and central Queen Maud block, and those that were most pivotal in defining the geological history outlined in the present study. Rock names and coordinates from where the samples were collected are provided in this list, as well as a brief summary of the quantitative data obtained for each sample. More detailed sample and outcrop descriptions are provided in Appendix A.

Sample Name/Type	Latitude (N)	Longitude (W)	Sample Name	Analytics conducted	Notes
QM-1A Powder	67° 49.872'	102° 33.006'	Bt-Opx granitic gneiss	Sm-Nd	T <sub>DM</sub> 3.2 Ga
QM-1C Hand sample	67° 49.872'	102° 33.006'	Cross-cutting mafic dyke	Mineral separation, U-Pb zircon	Minimum age 2.1 Ga, metamorphosed 1.93 Ga
QM-1H Hand sample	67° 49.872'	102° 33.006'	Quartzite	Mineral separation, detrital zircon analysis	Youngest detrital zircon 2576 Ma
QM-2C Hand sample Powder	67° 47.055'	102° 22.346'	Act-Bt-Opx granodioritic gneiss	In-situ U-Pb zircon, Sm-Nd	U-Pb age 3.205 Ga, T <sub>DM</sub> 3.3 Ga
QM-5B Hand sample Powder	67° 26.932'	102° 33.680'	Bt-Opx-Hbl granitic gneiss	In-situ U-Pb zircon, Sm-Nd	U-Pb age 2.698 Ga, T <sub>DM</sub> 3.4 Ga
QM-6B Hand sample Powder	67° 58.929'	102° 08.450'	Cpx-Bt-Hbl granitic gneiss	In-situ U-Pb zircon, Sm-Nd	U-Pb age 2.009 Ga, T <sub>DM</sub> 2.7 Ga
QM-7C Powder	67° 47.108'	102° 03.289'	Bt-Hbl tonalitic gneiss	Sm-Nd	T <sub>DM</sub> 3.4 Ga
QM-8A Hand sample	67° 43.482'	101° 42.434'	Gabbro	Mineral separation, U-Pb zircon	U-Pb age 2.322 Ga
QM-8B Hand sample	67° 43.482'	101° 42.434'	Bt-Hbl granite	In-situ U-Pb zircon, Sm-Nd	U-Pb age 2.319 Ga, T <sub>DM</sub> 3.1 Ga
QM-9C Hand sample	67° 43.459'	101° 25.036'	Grt-Bt psammitic migmatite	In-situ U-Pb monazite	Metamorphic ages 2.43-2.13 Ga
QM-10A Powder	67° 47.082'	101° 12.863'	Bt-Hbl-Opx-Cpx granitic gneiss	Sm-Nd	T <sub>DM</sub> 3.4 Ga
QM-10C Hand sample	67° 47.082'	101° 12.863'	Opx-Bt-Crd semi-pelitic gneiss	In-situ U-Pb monazite, mineral separation, detrital zircon analysis	Metamorphic ages 2.459, 2.365 Ga, youngest detrital zircon 3089 Ma
QM-13E/F Hand sample Powder	67° 44.772'	98° 53.140'	Hbl-Bt-Cpx-Opx granodioritic gneiss	In-situ U-Pb zircon, Sm-Nd (on QM-13F, a duplicate sample)	U-Pb age 2.450 Ga, T <sub>DM</sub> 2.7 Ga
QM-13G Hand sample	67° 44.772'	98° 53.140'	Alkali feldspar granite	Mineral separation, U-Pb zircon	U-Pb age 2.426 Ga
QM-14A Powder	67° 47.517'	99° 23.547'	Bt granitic gneiss	Sm-Nd	T <sub>DM</sub> 2.7 Ga

QM-15A Powder	67° 48.776'	99° 49.443'	Opx-Bt granitic gneiss	Sm-Nd	T <sub>DM</sub> 2.7 Ga
QM-16A Hand sample Powder	67° 52.576'	100° 15.374'	Hbl-Opx-Bt granite	In-situ U-Pb zircon, Sm-Nd	U-Pb age 2.43-2.50 Ga, T <sub>DM</sub> 3.0 Ga
QM-17C Powder	67° 51.009'	100° 39.126'	Opx-Bt granodioritic gneiss	Sm-Nd	T <sub>DM</sub> 3.3 Ga